BIOMASS PYROLYSIS IN FREE – FALL AND CONICAL SPOUTED – BED REACTORS AND LOW – TEMPERATURE GASIFICATION OF COCONUT SHELL WITH CO_2 AND KOH

Natthaya Punsuwan

A Thesis Submitted in Partial Fulfillment of the Requirements for the

Degree of Doctor of Philosophy in Chemical Engineering

Suranaree University of Technology

Academic Year 2012

กระบวนการไพโรไลซีสของมวลชีวภาพในปฏิกรณ์แบบตกอิสระ และแบบสะเป๊าเตดเบดทรงกรวย และกระบวนการแก๊สซิฟิเคชันอุณหภูมิต่ำของกะลามะพร้าวโดยใช้คาร์บอนไดออกไซด์ และโปแตสเซียมไฮดรอกไซด์

นางสาวณัฐยา พูนสุวรรณ

วิทยานิพนธ์นี้เป็นส่วนหนึ่งของการศึกษาตามหลักสูตรปริญญาวิศวกรรมศาสตรดุษฎีบัณฑิต
สาขาวิชาวิศวกรรมเคมี
มหาวิทยาลัยเทคโนโลยีสุรนารี
ปีการศึกษา 2555

BIOMASS PYROLYSIS IN FREE – FALL AND CONICAL SPOUTED – BED REACTORS AND THE LOW – TEMPERATURE GASIFICATION OF COCONUT SHELL WITH CO_2 AND KOH

Suranaree University of Technology has approved this thesis submitted in partial fulfillment of the requirements for the Degree of Doctor of Philosophy.

Thesis Examining Committee

(Dr. Terasut Sookkumnerd)
Chairperson

(Prof. Dr. Chaiyot Tangsathitkulchai)
Member (Thesis Advisor)

(Assoc. Prof. Dr. Malee Tangsathitkulchai)
Member

(Asst. Prof. Dr. Nakorn Worasuwannarak)
Member

(Asst. Prof. Dr. Atichat Wongkoblap)
Member

(Prof. Dr. Sukit Limpijumnong)
Vice Rector for Academic Affairs

(Assoc. Prof. Flt. Lt. Dr.Kontorn Chamniprasart)
Dean of Institute of Engineering

ณัฐยา พูนสุวรรณ : กระบวนการไพโรไลซีสของมวลชีวภาพในปฏิกรณ์แบบตกอิสระ และแบบสะเป๊าเตดเบดทรงกรวย และกระบวนการแก๊สซิฟิเคชันอุณหภูมิต่ำของกะลามะพร้าวโดยใช้คาร์บอนไดออกไซด์ และโปแตสเซียมไฮดรอกไซด์ (BIOMASS PYROLYSIS IN FREE – FALL AND CONICAL SPOUTED – BED REACTORS AND THE LOW – TEMPERATURE GASIFICATION OF COCONUT SHELL WITH CO_2 AND KOH)
อาจารย์ที่ปรึกษา : ศาสตราจารย์ ดร.ชัยยศ ตั้งสถิตย์กุลชัย, 246 หน้า.

งานวิจัยนี้มีวัตถุประสงค์เพื่อศึกษากระบวนการไพโรไลซีสของมวลชีวภาพในปฏิกรณ์แบบสะเป๊าเตดเบดทรงกรวย และกระบวนการแก๊สซิฟิเคชันอุณหภูมิต่ำของกะลามะพร้าวโดยใช้คาร์บอนไดออกไซด์ และโปแตสเซียมไฮดรอกไซด์ เพื่อให้บรรลุวัตถุประสงค์ งานวิจัยนี้จึงครอบคลุมหัวข้อที่ศึกษาดังนี้ การไพโรไลซีสของมวลชีวภาพในปฏิกรณ์แบบตกอิสระ การศึกษาปัจจัยที่ส่งผลต่อพฤติกรรมอุทกพลศาสตร์ของอากาศกับกะลาปาล์มในระดับห้องปฏิบัติการ และเปรียบเทียบกับผลการจำลองด้วยโปรแกรมสำเร็จรูปพลศาสตร์เชิงคำนวณ (ANSYS CFX 10.0) การไพโรไลซีสของกะลาปาล์มในปฏิกรณ์สะเป๊าเตดเบดทรงกรวย และการศึกษากระบวนการแก๊สซิฟิเคชันที่อุณหภูมิต่ำของกะลามะพร้าวโดยใช้คาร์บอนไดออกไซด์ และโปแตสเซียมไฮดรอกไซด์ในปฏิกรณ์เบดนิ่ง เพื่อวัตถุประสงค์ในการผลิตแก๊สสังเคราะห์ และถ่านกัมมันต์

การศึกษาไพโรไลซีสของมวลชีวภาพในปฏิกรณ์แบบตกอิสระ พบว่าที่สภาวะอุณหภูมิสูงและอนุภาคมีขนาดเล็ก ส่งผลให้ร้อยละผลผลิตของแก๊สเพิ่มขึ้น แต่ร้อยละผลผลิตของของแข็งมีค่าลดลง ผลการศึกษาชี้ให้เห็นว่ากากมันสำปะหลังสลายตัวเป็นสารระเหยได้สูงกว่าเมล็ดในปาล์มและกะลาปาล์ม แต่เกิดเป็นถ่านได้ในปริมาณที่ต่ำกว่า การเพิ่มอัตราการไหลของแก๊สไนโตรเจนในช่วง 100 – 200 ลูกบาศก์เซนติเมตรต่อนาที ทำให้ร้อยละผลผลิตของของเหลวมีค่าเพิ่มขึ้น และทำให้ปริมาณแก๊สผลิตภัณฑ์มีค่าลดลง นอกจากนี้ยังพบว่ากระบวนการไพโรไลซีสของมวลชีวภาพที่ใช้ในการทดลองนี้สามารถอธิบายได้เป็นอย่างดีด้วยแบบจำลองปฏิกิริยาคู่ขนาน

สำหรับการศึกษาพฤติกรรมอุทกพลศาสตร์ในสะเป๊าเตดเบดทรงกรวย พบว่าค่าของความเร็วต่ำสุดที่เกิดสภาวะสะเป๊ามีค่าเพิ่มขึ้นเมื่อเพิ่มความสูงของเบดนิ่งเริ่มต้น เส้นผ่าศูนย์กลางท่อแก๊ส มุมที่ฐานของทรงกรวย และขนาดอนุภาค ทั้งนี้การเพิ่มขนาดอนุภาคทำให้ค่าความดันลดของระบบมีค่าเพิ่มขึ้นที่ทุกๆ ขนาดเส้นผ่าศูนย์กลางท่อแก๊ส และมุมที่ฐานของทรงกรวยที่ใช้ในการทดลอง ในทางตรงกันข้ามค่าความดันลดกลับมีค่าลดลง เมื่อเพิ่มขนาดเส้นผ่าศูนย์กลางท่อแก๊สที่ทุกๆ ค่าความสูงของเบดนิ่งเริ่มต้น ขนาดอนุภาค และมุมที่ฐานของทรงกรวย นอกจากนี้การใช้แบบจำลองเชิงคำนวณศึกษาพฤติกรรมอุทกพลศาสตร์สำหรับสะเป๊าเตดเบด พบว่าแบบจำลองสามารถอธิบาย

ปัจจัยที่ส่งผลต่อการเปลี่ยนแปลงค่าความเร็วต่ำสุดที่เกิดสภาวะสะเป๊าได้ดีเมื่อเทียบกับค่าที่ได้จากการทดลอง

การไพโรไลซีสของกะลาปาล์มในปฏิกรณ์สะเป๊าเตดเบดแบบกะ พบว่าอุณหภูมิ และเวลาเป็นปัจจัยสำคัญที่ส่งผลต่อผลิตภัณฑ์จากการไพโรไลซีส ขณะที่ขนาดอนุภาค และความสูงเริ่มต้นของเบดนิ่งนั้นไม่ส่งผลมากนักต่อผลผลิตผลิตภัณฑ์ของการไพโรไลซีส สภาวะไพโรไลซีสของกะลาปาล์มที่ให้ผลผลิตของผลิตภัณฑ์ของเหลวสูงที่สุดร้อยละ 65 โดยน้ำหนัก คือสภาวะอุณหภูมิ 650 องศาเซลเซียส อัตราการป้อนวัฎดิบ 5 กรัมต่อนาที ขนาดอนุภาค 1.55 มิลลิเมตร และอัตราการไหลของแก๊สไนโตรเจน 9.6 ลิตรต่อนาที ในปฏิกรณ์สะเป๊าเตดเบดแบบต่อเนื่อง

ในส่วนของกระบวนการแก๊สซิฟิเคชันที่อุณหภูมิต่ำของกะลามะพร้าวในปฏิกรณ์แบบเบดนิ่ง พบว่าโปแตสเซียมไฮดรอกไซด์ และขั้นตอนการทำให้เป็นถ่าน เป็นปัจจัยที่มีความสำคัญต่อองค์ประกอบ และปริมาณการเกิดแก๊สผลิตภัณฑ์ ทั้งนี้พบว่าอัตราส่วนโดยน้ำหนักระหว่างโพแตสเซียมไฮดรอกไซด์ต่อวัตถุดิบ อุณหภูมิแก๊สซิฟิเคชัน และขั้นตอนการทำให้เป็นถ่าน เป็นปัจจัยที่มีความสำคัญต่อการพัฒนาความพรุนของถ่านกัมมันต์ โดยสภาวะที่มีความเหมาะสมต่อกระบวนการแก๊สซิฟิเคชัน เพื่อผลิตแก๊สไฮโดรเจนในปริมาณสูง และให้ได้ถ่านกัมมันต์ที่มีพื้นที่ผิวจำเพาะสูง ได้แก่ สภาวะอุณหภูมิ 600 องศาเซล เซียส เป็นเวลา 60 นาที และใช้อัตราส่วนโดยน้ำหนักระหว่างโปแตสเซียมไฮดรอกไซด์ต่อถ่านกะลาปาล์ม เท่ากับ 3.0 โดยที่สภาวะดังกล่าวจะได้แก๊สผลิตภัณฑ์ซึ่งมีองค์ประกอบของแก๊สไฮโดรเจนสูงถึงร้อยละ 27.90 โดยน้ำหนัก และถ่านกัมมันต์ซึ่งมีพื้นที่ผิว 2650 ตารางเมตรต่อกรัม

สาขาวิชาวิศวกรรมเคมี ลายมือชื่อนักศึกษา ณัฐษา พูนสุวรรณ

ปีการศึกษา 2555 ลายมือชื่ออาจารย์ที่ปรึกษา Chaiyot J

NATTHAYA PUNSUWAN : BIOMASS PYROLYSIS IN FREE – FALL AND CONICAL SPOUTED – BED REACTORS AND LOW – TEMPERATURE GASIFICATION OF COCONUT SHELL WITH CO_2 AND KOH. THESIS ADVISOR : PROF. CHAIYOT TANGSATHITKULCHAI, Ph.D., 246 PP.

BIOMASS/ PYROLYSIS/ CONICAL PBOUTED BED/ LOW TEMPERATURE CATALYTIC GASIFCATION

The overall objective of this thesis research was to perform a systematic study on the biomass pyrolysis in a conical spouted bed and study the low temperature gasification of coconut shell with carbon dioxide (CO_2) and potassium hydroxide (KOH). To achieve this aim, the following tasks were included in this work: pyrolysis of biomass using a free fall reactor, studying the hydrodynamic behavior of air – coconut shell under different conditions in a laboratory unit and via the simulation program of CFD (ANSYS CFX 10.0), pyrolysis study of palm shell using a conical spouted bed reactor, and studying the low temperature catalytic gasification of coconut shell for the purpose of combined production of syngas and activated carbon.

The biomass pyrolysis in a free fall reactor showed that higher temperature and smaller particle size increased the gas yield but decreased the char yield. Cassava pulp residue gave more volatiles and less char than palm kernel and palm shell. Increasing of sweeping gas flow rate in the range of 100 – 200 cm^3 N_2/min gave increased liquid yield and less gas yield. Prediction of pyrolysis kinetics by the two – parallel reactions model gave a good fitting with the experimental data for all pyrolysis conditions.

The hydrodynamic study of a conical spouted bed system indicated that the minimum spouting velocity increased with the increase of static bed height, gas inlet diameter, conical base angle, and particle size. The increasing in particle size led to the pressure drop increasing for all air inlet diameters and conical base angles. On the contrary, the pressure drop decreased with the increase of the air inlet diameter for all static bed height, particle size and conical spouted bed geometry. In addition, the minimum spouting velocity predicted from CFD simulation agreed very well with the experimental measurements.

The pyrolysis of palm shell in a batch conical spouted bed reactor showed that pyrolysis temperature and time had a significant effect on the pyrolysis product, while particle size and static bed height had no significant effect on the pyrolysis product yields. The maximum liquid yield of 65 wt% was obtained from palm shell pyrolysis at 650°C, palm shell feed rate of 5 g/min, particle size of 1.55 mm and N_2 flow rate of 9.6 L/min in a continuous spouted bed mode.

The low temperature catalytic gasification of coconut shell in a fixed bed reactor indicated that KOH and carbonization step exerted a significant effect on the composition and amount of gas product. The chemical weight ratio, gasification temperature and carbonization step played an important role on the extent of porosity development of activated carbon. The optimum conditions to obtain high H_2 composition and solid surface area were gasification at 600°C for 60 min with carbonization step and using chemical weight ratio of 3.0. This condition gave the H_2 composition up to 27.90 wt% of gas produced and activated carbon with the specific surface area of 2,650 m^2/g.

School of Chemical Engineering　　Student's Signature Natthaya Punsuwan

Academic Year 2012　　Advisor's Signature Chaiyot

ACKNOWLEDGEMENTS

This dissertation would not have been possible without the assistance and support of many persons around me, to only some of whom it is possible to give particular mention here.

I take this opportunity to express my profound gratitude and deep regards to my advisor Prof. Dr. Chaiyot Tangsathitkulchai, for his exemplary guidance, monitoring and constant encouragement throughout the course of this thesis. I also take this opportunity to express my deep appreciation to Prof. Dr. Takayuki Takarada who is a great supervisor during my oversea research time at the Gunma University, Japan.

I would like to express my deep gratitude and respect to my thesis defense committee for their many valuable comments and suggestions.

I am obliged to staff members of Center for Science and Technology Equipment, Mr. Saran Dokmaikul, Mr. Manop Jornkokkruad and Mr. Thiti Sutthivong for the valuable information provided by them in their respective fields. I am grateful for their cooperation during the period of my assignment.

I am most grateful to Mrs. Amporn Ladnongkun for her kindness, friendship, support and her skillful secretarial work in the School of Chemical Engineering.

I wish to thank my family and friends for their constant encouragement without which this assignment would not have been possible.

I would like to acknowledge the Ministry of Science and Technology of Thailand for the financial support.

Finally, I would like to acknowledge Ubon Ratchathani University for giving me the opportunity to pursue my Ph.D. study.

Natthaya Punsuwan

TABLE OF CONTENTS

Page

CHAPTER

TABLE OF CONTENTS (Continued)

Page

TABLE OF CONTENTS (Continued)

Page

TABLE OF CONTENTS (Continued)

Page

TABLE OF CONTENTS (Continued)

TABLE OF CONTENTS (Continued)

Page

TABLE OF CONTENTS (Continued)

Page

TABLE OF CONTENTS (Continued)

Page

LIST OF TABLES

Table **Page**

LIST OF TABLES (Continued)

Table **Page**

LIST OF TABLES (Continued)

Table **Page**

LIST OF TABLES (Continued)

Table **Page**

LIST OF FIGURES

Figure **Page**

LIST OF FIGURES (Continued)

Figure **Page**

LIST OF FIGURES (Continued)

LIST OF FIGURES (Continued)

Figure **Page**

LIST OF FIGURES (Continued)

Figure **Page**

LIST OF FIGURES (Continued)

Figure **Page**

LIST OF FIGURES (Continued)

Figure **Page**

LIST OF FIGURES (Continued)

Figure **Page**

SYMBOLS AND ABBREVIATIONS

A = frequency or pre-exponential factor [s^{-1}]

Ar = Archimedes number

C_D = drag coefficient

D_B = diameter of top bed surface [m]

d_p = mean solid particle diameter [m]

D_C = spouted bed column diameter [m]

D_o = nozzle inlet diameter of spouted bed [m]

e_{RC} = restitution coefficient of particles

E = activation energy [kJ/mol]

g , $\vec{g}_s$ = gravitational acceleration [9.81 m/s^2]

H_B = height of dense solid bed [m]

H_F = height of bed fountain [m]

H_s = static bed height of particle bed [m]

H_T = total bed height of particle bed [m]

k = pyrolysis rate constant, [s^{-1}]

K_{sf} = solid – fluid momentum exchange coefficient [$kg/m^3.s$]

K_{fs} = fluid – solid momentum exchange coefficient [$kg/m^3.s$]

SYMBOLS AND ABBREVIATIONS (Continued)

M = mass fraction

M_f = final yield of char

n = order of pyrolysis reaction

P = static pressure [N/m^2]

P_s = solid pressure [N/m^2]

R = universal gas constant [mol. K/ kJ]

= weight of residue at time t [g]

Re_P = particle Reynolds number

t = time [s]

T = absolute temperature [K]

V_f = gas volume [m^3]

U = slip velocity [m/s]

U_{ms} = minimum spouting velocity [m/s]

$X_{P,Max}$ = maximum particle packing volume fraction

α = residual weight fraction

α_f = volume fraction of fluid phase

α_s = volume fraction of dispersed phase

β = heating rate [K/min]

γ = conical base angle

SYMBOLS AND ABBREVIATIONS (Continued)

μ = viscosity of fluid [kg/m.s]

ρ_f = densities of fluid [kg/m^3]

ρ_p = densities of solid particle [kg/m^3]

$\overline{\overline{\tau}}_f$ = fluid phase stress – strain tensor

$\overline{\overline{\tau}}_s$ = solid phase stress – strain tensor

$\vec{v}_f$ = velocity of fluid phase [m/s]

$\vec{v}_s$ = velocity of solid phase [m/s]

CHAPTER 1

INTRODUCTION

1.1 Rationale of the Study

Nowadays, the world’s energy markets rely heavily on the fossil fuels (coal, petroleum crude oil, and natural gas) as a source of thermal energy. Since millions of years are required to form fossil fuels in the earth, their reserves are limited and subject to depletion as they are continually consumed. The only natural, renewable carbon resource that is large enough to be used as a substitute for fossil fuels is biomass. Biomass is the general terminology to describe all organic matter such as crops, forestry and organics wastes. The major constituents of biomass consist of cellulose, hemicellulose, lignin, organic extractives, and inorganic materials. The principal biomass resources are: (1) waste and residues from agriculture and forest industries, (2) animal manure from livestock farms, and (3) municipal solid waste.

Thailand is an agriculture country that is rich in agricultural and forestry resources, which provide abundant supply of biomass resources. Agriculture and wood residues around 60 million tons (Thai Net Metering Project, n.d.) are produced each year in Thailand. Among them, the major biomass resources in Thailand are listed in Table 1.1. Normally, these wasted materials are directly fed as fuels in a boiler furnace.

Table 1.1 Annual agricultural biomass products in Thailand, in order of increasing production capacity (Prammanee, and Weerathaworn, 2006)

Biomass	**× 1,000 tons**
Palm shell	490
Palm fiber	565
Coconut shell	596
Corn cobs	1,001
Coconut fiber	1,400
Cassava rhizomes	1,893
Cassava stalks	2,517
Rich husk	8,250
Bagasse	22,908
Rice straw	43,443

The southern region of the country is the major area of oil palm planting and production with some plantation of oil palm being found in the eastern region. The fresh oil-palm fruit and its longitudinal section are shown in Figure 1.1. The fresh fruit bunch (FFB) consists of fruit stems or commonly known as empty fruit bunch (EFB) and its fruits, which contain crude palm oil, fiber, and nuts. The inner portion of the nut can be processed to produce palm kernel oil. EFB, fiber, and nuts shells which constitute approximately 44% of the FFB weight are solid residues left from palm oil mills (Black & Veatch (Thailand) Co., Ltd., 2000). The traditional use of oil palm residues is as a fuel to generate the steam and power for the operating mill. Figure 1.2 shows the utilization of by products from a palm oil mill.

Fiber, shells and empty bunches are generated during processing. Lim (1986) has reported values of 1,853 kg of shells and 1,483 kg of empty bunches per hectare as dry matter. Shells and fibers are normally used internally for power generation while some parts may be sold as fuel or used for road construction. Empty bunches are normally incinerated, after which the potash rich ash is used as fertilizer (Koopmans and Koppejan, 1997).

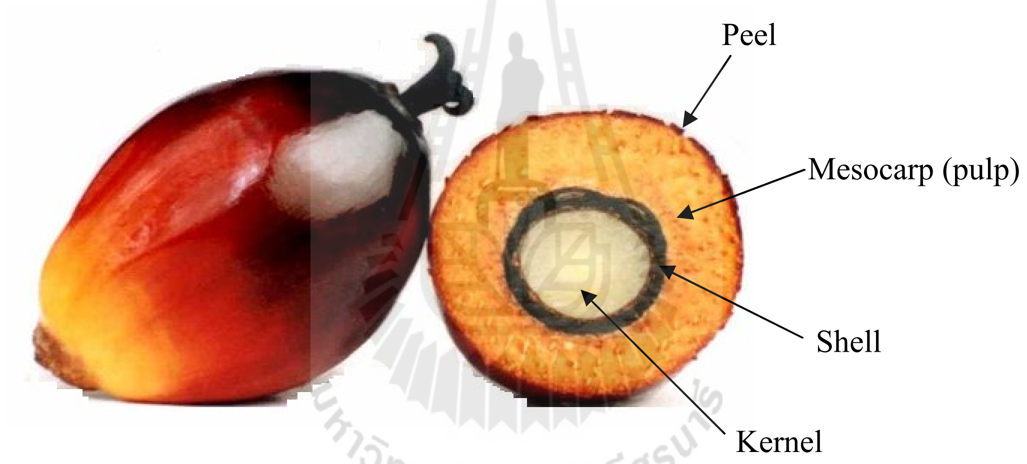

Figure 1.1 Fresh oil-palm fruit and its longitudinal section.

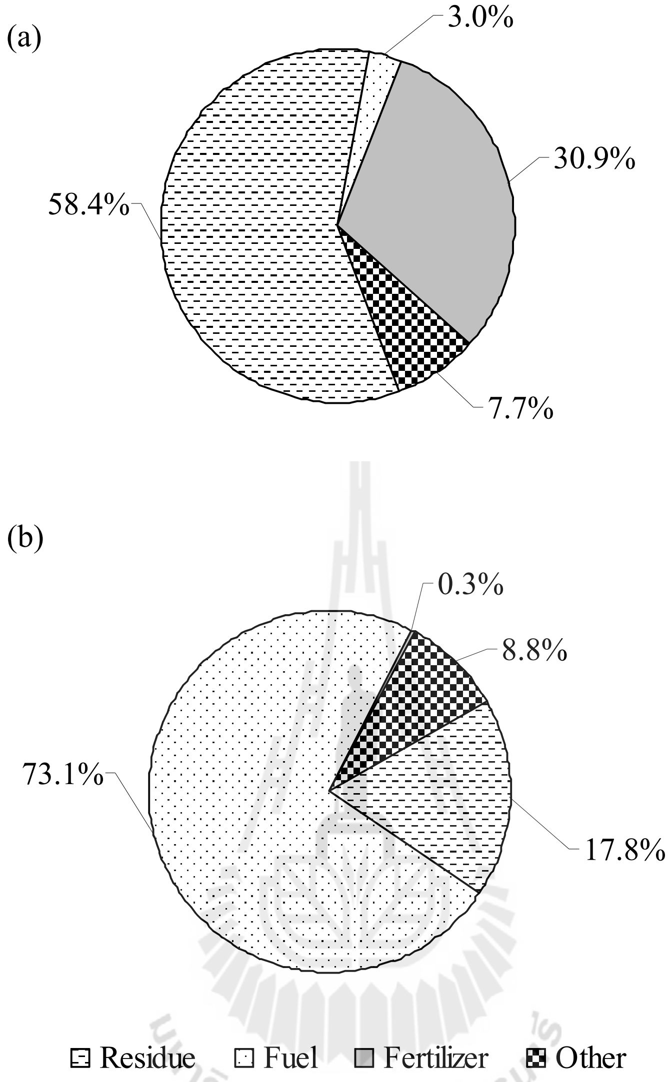

Figure 1.2 The utilization of by products from palm oil mill (a) EFB and (b) fiber and shell from fruit (Department of Alternative Energy Development and Efficiency, 2003).

The other biomass source in the country that should be mentioned is cassava. Cassava is considered as one of the most important economic crops. Cassava roots are utilized in many industries such as native starch, modified starch, monosodium glutamate (MSG), glucose, fructose, sorbitol, and plywood industries. In addition, they are used as the major raw material for the production of bioethanol, and alternative biofuel to be blended with petroleum gasoline. Cassava was introduced into the southern part of Thailand from Malaysia during the year 1786-1840. The main concentration of this crop is now found in the northeast of Thailand, especially in Nakhon Ratchasima province. Cassava has excellent drought tolerance property and can be planted in almost all types of soil. The total production in 2012 is reported to be greater than 23 million tones (Thai Tapioca Development Institute, n.d.). Cassava pulp residue can be utilized to produce ethanol due to its containing cellulose and hemi-cellulose at levels of 24.99 and 6.67% (w/w) respectively (Srinorakutara, Kaewvimol and Saengow, n.d.).

Coconut is the fruit of the coconut palm, *Cocos nucifera*. These plants are believed to be native of Southeast Asia, where they have been cultivated and used in food for centuries. When mature they still contain some water and can be used as seednuts or processed to give oil from the kernel, charcoal from the hard shell and coir from the fibrous husk. The oil and milk derived from it are commonly used in cooking and frying; coconut oil is also widely used in soaps and cosmetics. The clear liquid coconut water within is a refreshing drink. The husks and leaves can be used as material to make a variety of products for furnishing and decorating. The coconut shells are used to make charcoal and activated carbon. Coconut palms are grown in more than 80 countries of the world, with a total world production of 61 million tonnes per year.

At present, several types of processes have been developed for biomass conversion into energy such as fermentation, and thermal decomposition. Thermal decomposition covers the processes of combustion, gasification and pyrolysis in which material feedstocks undergo chemical changes, which are principally driven by the action of heat, to produce various liquid, solid and gaseous end products. Combustion is a simple process to convert biomass into energy. However, combustion of biomass is a cause of air pollution that has contributed to the so called “greenhouse effect”. Another thermal decomposition technology that has been employed to convert biomass into energy is gasification. Gasification process converts a biomass feedstock to a primary gaseous product which can be used either directly as fuel gas or as synthesis gas for further conversion to a liquid fuel or chemical products (e.g. methanol). It offers several advantages over direct combustion of biomass including higher combustion temperature, more efficient and better controlled combustion and lower emissions (Hogen, n.d.). However, the complexity and sensitivity of the process and the high cost for an initial investment are the major disadvantages of gasification process (Turare, n.d.). Of the three thermal conversion processes, it appears that pyrolysis should show promise as a cheap and simple route for converting biomass to useful source of energy.

Pyrolysis is the thermal decomposition that occurs in the absence oxygen. It is always the first step in combustion and gasification processes (Bridgewater, 2004). Biomass pyrolysis products consist of gases (mainly CO_2, H_2, CO, CH_4, C_2H_2, C_2H_4, C_2H_6, and etc.), liquid products (tars, high molecular hydrocarbons and water) and solid products (char) that can be used primarily as a fuel. Apart from being used as fuels, solid product (char) can be further used for activated carbon production and the liquid products as a chemical feed stock to produce many valuable chemical species (Uzun, Pütün and Pütün, 2006). The distribution of pyrolysis products varies and depends on the pyrolysis condition. Flash pyrolysis has gained much attention due to its ability to produce a liquid product with yield up to 80 wt% on the basis of dry biomass (Chiaramontia, Oasmaab and Solantaustab 2007). In particular, the liquid product obtained from the biomass pyrolysis is considered a very promising fuel because it can be easily transported, burnt directly in thermal power stations, injected into conventional petroleum refineries, burnt in gas turbines or upgraded to obtain a light hydrocarbon fuel (Goyal, Seal and Saxena, 2008). For these reasons, considerable research efforts have recently been focused on flash pyrolysis to produce liquid product (bio-oil) with high yield. In addition, several studies have been concentrated on finding the most suitable pyrolysis conditions in many types of pyrolysis reactors, including fixed bed reactors (Islam et al., 2004), packed bed reactors (Yang et al., 2006), fluidized-bed reactors (Kersten et at., 2005), and conical-cylindrical spouted bed reactors (Tsai, Lee and Chang, 2007).

In this work, both a free-fall reactor (or drop tube reactor) and a conical spouted bed reactor, are proposed for the study of biomass flash pyrolysis. The free fall reactor has been widely used in laboratory studies on flash pyrolysis because it provides high heating rate. In addition, the determination of mass balance and residence time in this type of reactor are simple and straightforward. Moreover, the residence time in this type of reactor can be moderately controlled (Lehto, 2007). Further, the single biomass decomposition kinetic parameters can be conveniently examined by using pyrolysis results from the free fall reactor. Flash pyrolysis can also be achieved in a conical spouted bed reactor. The most attractive feature of a conical spouted bed compared to fixed and packed bed reactors are its capability to provide high heat and mass transfer between gas and solid. Also, the conical spouted bed reactor has the following further advantages over conventional spouted beds (cylindrical with conical base). This include simple design because no distributor plate is needed, lower pressure drop, cyclic circulation of the particle making it suitable for sticky or irregular shape particles, high heat and mass transfer between gas and solid (whose circulation is mainly counter-current), and short gas residence time. For these reasons a conical spouted bed is proposed for the study of flash pyrolysis of biomass in the present work.

Nowadays, the success of the design and scaling up of the process equipments depend largely on the ability to predict system performances from models combining hydrodynamic behavior, chemical reaction kinetic, and heat and mass transfer. Since, direct experimental measurement for all of variables is difficult and tedious, thus the simulation program has turned out to be a powerful tool which can provide the complete information for the processes design and scaling – up tasks. Several commercial simulation programs have been developed and used for optimum process design and simulation purposes. One of the well known commercial simulation program is Computational Fluid Dynamic (CFD). This simulation program applies the numerical method and additional algorithms to solve the heat and mass transfer, fluid flow behavior, and other related physical variables. Due to the uniqueness and many variables affecting the spouting phenomenon, it is decided to first apply the CFD simulation to simulate the process for further understanding of its flow characteristics. By using the two-fluid model (TEM) embedded in the commercial CFD simulation package ANSYS CFX 10.0, the spouting hydrodynamics of biomass particles in a conical spouted bed is simulated and compared with the experimental data. In addition, the optimized simulation condition will be used for determining the operating conditions of the conical spouted bed reactor for pyrolysis study. Moreover, in this study it is also decided to develop a simple mathematical model for predicting pyrolysis product yields as well as the product distributions.

As already stated, biomass conversion into energy by thermal decomposition includes the processes of combustion, gasification and pyrolysis. The advantage of gasification process is that it can produce syngas from a wide variety of carbon – containing feedstocks, such as coal, heavy petroleum residues and biomass. Syngas can be burned directly in gas engines, used to produce methanol and hydrogen, or converted via the Fischer – Tropsch process into synthetic fuel. Although the gasification process has the disadvantages of complexity and sensitivity of the process and the high cost for an initial investment, it has been very attractive. Gasification process is widely used on industrial scales to generate electricity and several types of gasifies are currently available for commercial use, e.g., counter – current fixed bed, co – current fixed bed, entrained flow and fluidized bed (National Non – Food Crops Centre, 2011). Since most of conventional gasification processes are operated at a high temperature (> 700^{o}C), increasing attention has been directed toward studying gasification at low temperatures to focus on tar elimination and maximizing the product yields. It is known that the application of catalyst is effective for lowering the gasification temperature. For example, metallic iron is found to be an excellent catalyst for biomass gasification at low temperature for tar elimination and improvement of hydrogen formation (Bimbela, Oliva, Ruiz, García and Arouzo, 2007). In this work, the low temperature CO_2 gasification of coconut shell using potassium hydroxide, as a chemical additive or more specifically as a catalyst, was studied with emphasis on examining the effect of gasification conditions on the yields and properties of gas and solid products (activated carbon). According to Huang et al. (2009), the CO_2 gasification reactivity of char was improved by the addition of metal catalysts in the order of K>Na>Fe>Mg and Lee et al. (2012) reported that potassium hydroxide activation creates carbon surface rich in oxygen functional groups that can give future advantages for electrode application in fuel cells. Formerly, coal has become the major precursor for activated carbon production. Since coal is more available to be used for energy source, biomass is being considered as a suitable precursor for activated carbon production. One of the potential side products from the industries that can be used for producing activated carbon is coconut shell. Due to their high carbon content and hardness, coconut shells are an excellent raw material source to produce activated carbon. Therefore, coconut shell was chosen as an alternative biomass for the study of low – temperature gasification in this work.

1.2 Research Objectives

The aim of this research is to study the pyrolysis of several biomass in a conical spouted bed and coconut shell gasification at low temperature in a fixed – bed reactor with the following specific objectives.

- Investigating the thermal decomposition of biomass during flash pyrolysis in a free-fall reactor to determine the kinetic parameters and characterize the pyrolysis products.

- Investigating the thermal decomposition of biomass for flash pyrolysis in a conical spouted bed reactor and to estimate the kinetic parameters and pyrolysis product yields.

- Applying the commercial simulation program ANSYS CFX 10.0 to study the effect of conical spouted bed geometry and biomass particle size on the hydrodynamic behavior of the unit.

- Investigating the gasification of coconut shell at low temperature in a fixed - bed reactor, using potassium hydroxide as a chemical additive.

1.3 Scope and Limitation of the Study

This study is focused on investigating thermal decomposition of biomass during flash pyrolysis in a conical spouted bed pyrolysis and biomass gasification at low temperature in a fixed – bed reactor. The scope and limitation of the research work is schematically shown in Figure 1.3.

1.3.1 Raw Material Characterization

Biomass precursors (palm shell, palm kernel and cassava pulp residue) are used in this study and are characterized by determining their physical properties, including proximate analysis, ultimate analysis, and particle density.

1.3.2 The Influence of Pyrolysis and Gasification Conditions and Product Characterizations

1.3.2.1 Thermal decomposition of biomass during flash pyrolysis are conducted in a free-fall and a conical spouted bed reactor. The geometry of a conical spouted bed reactor to be used for pyrolysis study will be based on the results from the hydrodynamics study.

1.3.2.2 The effect of pyrolysis parameters such as temperature, particle size, biomass feed rate, biomass type and sweeping gas flow rate (N_2) on the pyrolysis yields are investigated.

1.3.2.3 The effect of gasification parameters such as temperature, chemical weight ratio, holding time and carbonization step are investigated.

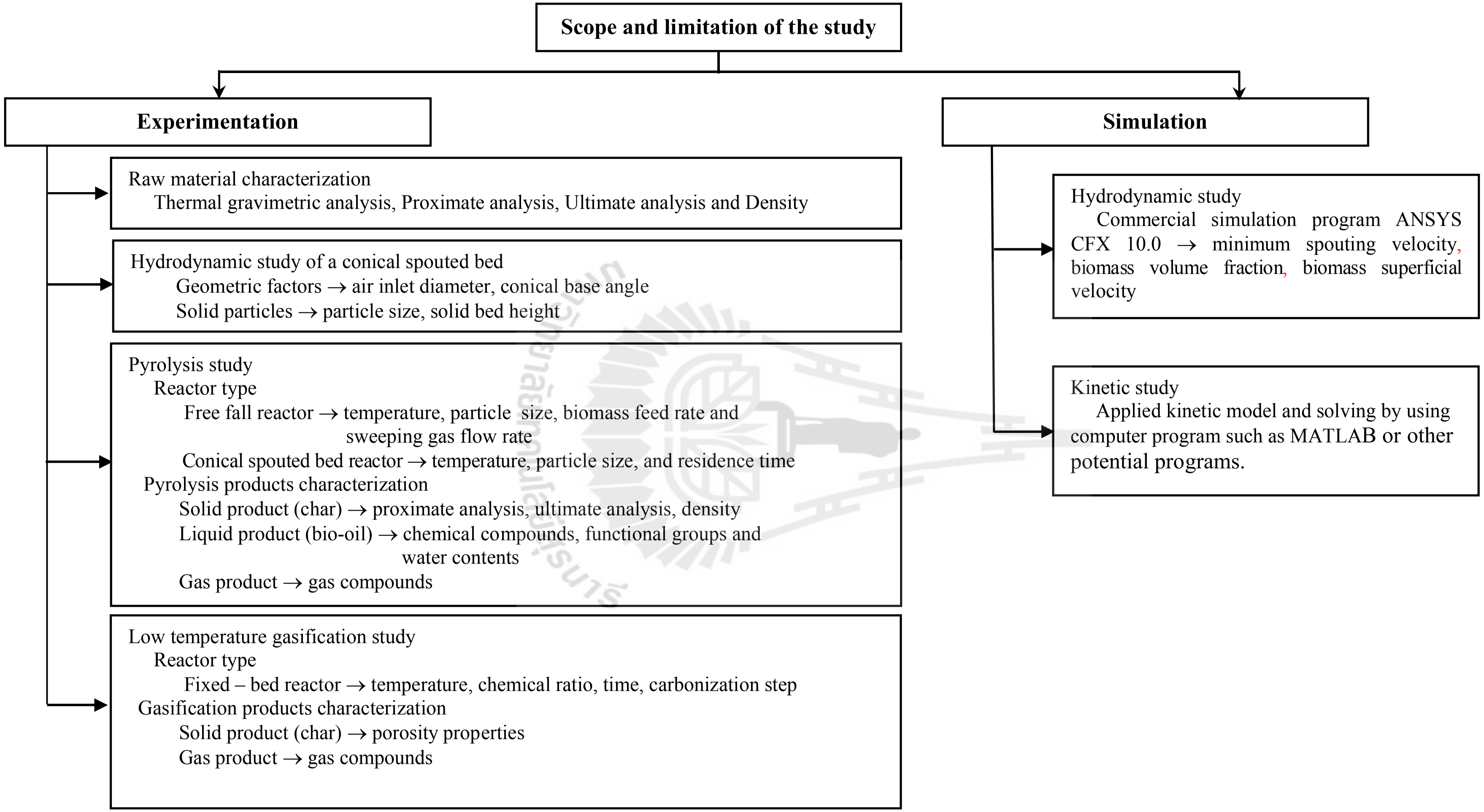

Figure 1.3 Scope and limitation of the research study.

1.3.2.4 Solid product from pyrolysis (char) and gasification (activated carbon) experiments are characterized for porosity properties (specific surface area, pore volume and average pore diameter) and calorific value.

1.3.2.5 Chemical composition of bio-oil products from pyrolysis experiments will be characterized by gas chromatography. Moreover, the functional group of the bio-oil is identified by Fourier Transform Infrared Spectroscopy (FTIR), and water content in the bio-oil is determined by water contents analyzer equipment.

1.3.2.6 Compositions of gas products are determined by gas chromatography method for both of pyrolysis and gasification studies.

1.3.3 Hydrodynamics of Conical Spouted Bed

This part of the experiment is dealt with studying the effect of geometric factors (such as, air inlet diameter, and conical base angle), solid bed height and particle size on the hydrodynamic behavior of a conical spouted bed. Bed pressure drop, bed height and solid circulation pattern is observed and measured as a function of air flow rate.

1.3.4 Simulation Modeling

Simulation modeling of this research work can be divided in to two parts. In the first part, commercial simulation program CFX version 10.0 is used to simulate the hydrodynamics of a conical spouted bed to provide data on the minimum spouting velocity, velocity profiles of air, and bed voidage profile of the biomass and the circulation pattern of biomass particles in the conical spouted bed. The simulation results will be compared with the experimental measurements for model verification. In the second part, the experimental results from biomass pyrolysis in a conical spouted bed reactor are used to propose an improved simple and accurate kinetic description suitable for biomass decomposition behaviors in a conical spouted. Mathematical methods are required to solve the problems and the potential computer program, for example, MATLAB is used as the computation tool.

1.4 References

Bimbela, F., Oliva, M., Ruiz, J., García, L., and Arouzo, J. (2007). Hydrogen production by catalytic steam reforming of acetic acid, a model compound of biomass pyrolysis liquids. **Journal of Analytical and Applied Pyrolysis.** 79: 112 – 120.

Black & Veatch (Thailand) Co., Ltd. (2000). **Thailand Biomass – Based Power Generation and Cogeneration within Small Rural Industries.** Final Report, Supported by National Energy Policy Office. Bangkok.

Bridgwater, V. (2004). **Biomass fast pyrolysis.** Review paper. 8 (2): 21-49.

Chiaramontia, D., Oasmaab, A., and Solantaustab, Y. (2007). Power generation using fast pyrolysis liquids from biomass. **Renewable and Sustainable Energy Reviews.** 11: 1056–1086.

Department of Alternative Energy Development and Efficiency. (2003). **Oil Palm**. Ministry of Enery. Bangkok. (Thai Version)

Goyal, H.B., Seal, D., and Saxena, R.C.(2008). Bio-fuels from thermo chemical conversion of renewable resources: A review. **Renewable and Sustainable Energy Reviews**.12: 504–517.

Hogen, E. (n.d.). **Overview of Canadian Thermochemical Biomass Conversion Activities.** In Advances in Thermochemical Biomass Conversion (Volume 1).

Huang et al. (2009). Effects of metal catalysts on CO_2 gasification reactivity of biomass char. **Biotechnology Advances.** 27(5): 568 – 572.

Islam, M. N., et al. (2005). Pyrolytic oil from fixed bed pyrolysis of municipal solid waste and its characterization. **Renewable Energy.** 30 (3): 413-420.

Kersten, R.A., et at. (2005). Biomass Pyrolysis in a Fluidized Bed Reactor. Part1: Literature Review and Model Simulations. **Ind. Eng. Chem. Res.** 44 (23): 8773–8785.

Koopmans, A., and Koppejan, J. (1997). Agricultural and forest residues generation, utilization and availability. **Wood Energy Conservation Specialists Regional Wood Energy Development Programme in Asia.**

Lee, Y. J., Park, H. W., Park, S., and Song, I. K. (2012). Nono – sized Mn – doped activated carbon aerogel as electrode material for electrochemical capacitor: effect of activation conditions. **J. Nanosci Nanotechnology.** 12(7): 6058 – 64.

Lehto, J. (2007). Determination of kinetic parameters for Finish milled peat in conditions similar reactor and optical measurement techniques. **Fuel.** 85: 1656- 1663.

Lim, K. O. (1986). The energy potential and current utilization of agriculture and logging wastes in Malaysia. **Renewable Energy Review Journal**. 8: 57 – 75.

National Non – Food Crops Centre. (2011). **Review of Technologies for Gasification of Biomass and Wastes, NNFCC 09 – 008.** Available: http://www.nnfcc.co.uk/

Prammanee, P., and Weerathaworn. (2006). **Annual agricultural biomass products in Thailand**. Available: www.biomass-asia-workshop.jp

Srinorakutara, T., Kaewvimol, L., and Saengow, L. (n.d.). Approach of Cassava Waste Pretreatments for Fuel Ethanol Production in Thailand. Biotechnology Department, Thailand Institute of Scientific and Technological Research (TISTR).

Sriroth, K., Lamchaiyaphum B., and Piyachomkwan, K. (2007). Present Situation and Future Potential of Cassava in Thailand. Cassava and Starch Technology Research Unit. Available: http://www.cassava.org

Thai Net Metering Project. Available: http://www.netmeter.org/.

Thai Tapioca Development Institute. (n.d.). Available: http://www.tapiocathai.org/L1.html.

Tsai, W.T., Lee, M.K., and Chang, Y.M. (2007). Fast pyrolysis of rice husk: Product yields and compositions. **Bioresource Technology.** 98: 22–28.

Turare, C. (n.d.). Gasification technology. ARTES Institute. University of Flensburg. **Flensburg. Germany.** Available: http://www.members.tripod.com/~cturare/tro.htm

Uzun, B. B., Pütün, A. E., and Pütün, E. (2006). Fast pyrolysis of soybean cake: Product yields and compositions. **Bioresource Technology.** 97: 569 – 576.

Yang, H., et al. (2006). Mechanism of Palm Oil Waste Pyrolysis in a Packed Bed. **Energy Fuels**. 20 (3): 1321–1328.

CHAPTER 2

LITERATURE REVIEW

2.1 Composition of Biomass

Biomass is a natural polymer complex of cellulose, hemicellulose, and lignin. The major structural chemical components with high molar masses are carbohydrate polymers and oligomers (65 -75%) and lignin (18-35%). Minor low molar mass extraneous materials are mostly organic extractives and inorganic materials (usually 4 – 10%). The weight percent of cellulose, hemicellulose, and lignin varies in different biomass species of wood (Chiaramontia, Oasmaab, and Solantaustab, 2007). The typical lignocellulose contents of some biomass based materials are given in Table 2.1.

2.1.1 Cellulose

Cellulose fibers provide wood strength and comprise 50 wt% of dry wood (Miller, n.d.). Cellulose is a high molecular weight (106 or more) linear polymer of β-(1→4)-D-glucopyranose units in the $4C_1$ conformation (Figure 2.1). Cellulose is insoluble molecule consisting of between 2000 and 14000 glucose units. Cellulose forms long chains that are bonded to each other by a long network of hydrogen bonds (Figure 2.2). Groups of cellulose chains twist in space to make up ribbonlike microfibril sheets, which are the basic construction units for a variety of complex fibers. These microfibrils form composite tubular structures that run along a longitudinal tree axis. The crystalline structure resists thermal decomposition better than hemicelluloses. Amorphous regions in cellulose exist that contain waters of hydration, and free water is present within the wood. This water, when rapidly heated, disrupts the structure by a steam explosion-like process prior to chemical dehydration of the cellulose molecules. Cellulose degradation occurs at 240-350°C (Wooten, Seeman, Hajaligol, 2004)

Table 2.1 Composition of biomass

Type	**Cellulose**	**Hemicellulose**	**Lignin**	**Organic Extractives**	**Ash**
Soft wood(1)	41.0	24.0	28.0	2.0	0.4
Hard wood(1)	39.0	35.0	20.0	3.0	0.3
Pine bark(1)	34.0	16.0	34.0	14.0	2.0
Wheat straw (1)	40.0 40.0(2)	28.0 24.0(2)	17.0 21.0(2)	11.0 8.0(2)	7.0 8.0(2)
Rice husks(1)	30.0	25.0	12.0	18.0	16.0
Peat(1)	10.0	32.0	44.0	11.0	6.0
Poplar wood(2)	22.5	48.1	21.7	5.7	1.0
Beech wood(2)	19.4	47.5	24.0	7.5	1.6
Hazel nut(2)	24.1	27.5	40.7	3.9	1.0
Olivehusks(2)	21.1	22.2	5.0	8.1	3.6
Corn-cobs(2)	31.8	51.2	14.8	1.2	1.0

(1)Chiaramontia et al., 2007 and (2) Maschio, Lucchesi, and Koufopanos, 1994

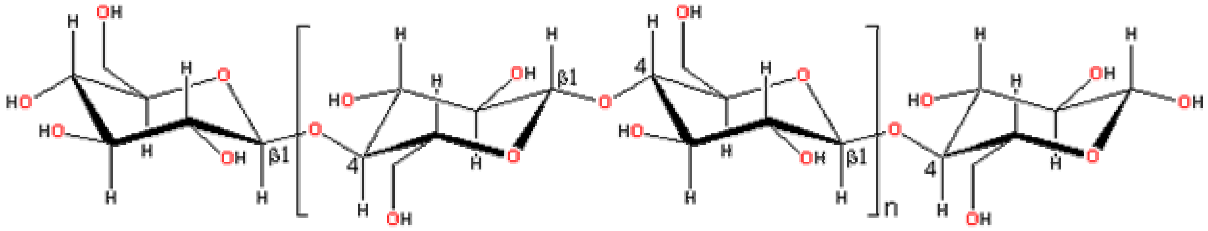

Figure 2.1 Chemical structure of cellulose (Chaplin, n.d.)

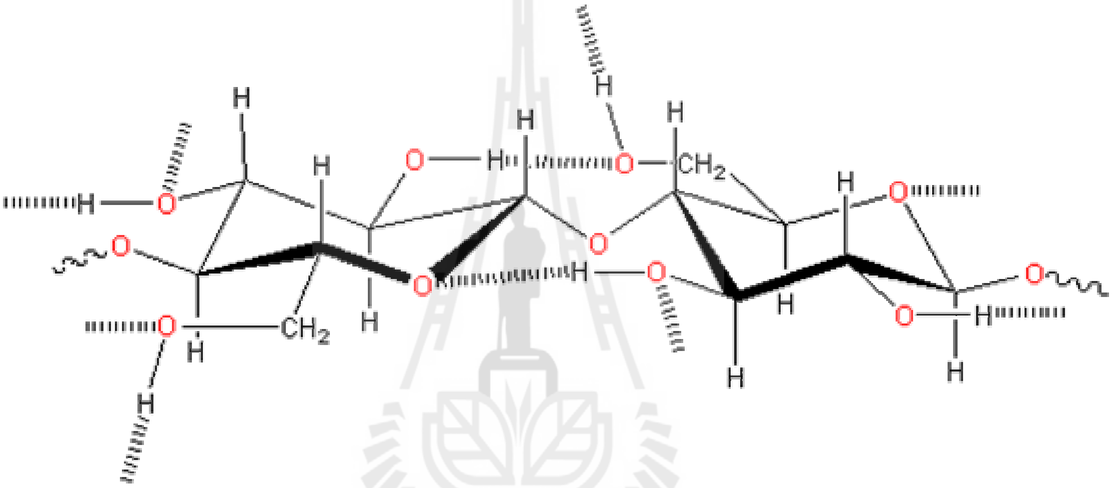

Figure 2.2 Intrachain and interchain hydrogen-bonded bridging (Chaplin, n.d.).

2.1.2 Hemicellulose

A second major wood chemical constituent is hemicellulose, which is also known as polyose. A variety of hemicelluloses usually account for 25%-35% of the mass of dry wood: 28% in softwoods, and 35% in hardwoods (Miller, n.d.). Hemicellulose is a mixture of various polymerized monosaccharides such as glucose, mannose, galactose, xylose, arabinose, 4-O-methyl glucuronic acid and galacturonic acid residues (see Figure 2.3). Hemicelluloses exhibit lower molecular weights than cellulose. The number of repeating saccharide monomers is only ~150, as compared to the number in cellulose of 5000-10000. Cellulose has only glucose in its structure, whereas hemicellouse has a heteropolysaccharide makeup and some contains short side-chain “branches” pendent along the main polymeric chain. Hemicellulose decomposes at temperatures of 200-260°C, giving rise to more volatiles, less tars, and less chars than cellulose (Grønli, Antal, and Va´rhegyi, 1999). The onset of hemicellulose thermal decomposition occurs at lower temperatures than crystalline cellulose. The loss of hemicellulose occurs in slow pyrolysis of wood in the temperature range of 130-194°C, with most of this loss occurring above 180°C (Grønli et al., 1999). However, the relevance of this more rapid decomposition of hemicellulose versus cellulose is not realized during fast pyrolysis, which is completed in few seconds at such a rapid heating rate.

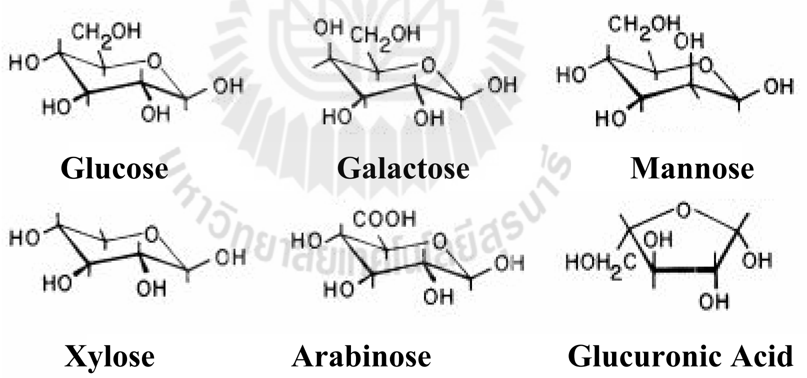
Glucose **Galactose** **Mannose**

Xylose **Arabinose** **Glucuronic Acid**

Figure 2.3 Main component of hemi cellulose (Smith, n.d.)

2.1.3 Lignin

The third major component of wood is lignin, which accounts for 23%-33% of the mass of softwoods and 16%-25% of the mass of hardwoods (Miller, n.d.). It is an amorphous cross-linked resin with no exact structure. It is the main binder for the agglomeration of fibrous cellulosic components and also providing a shield against the rapid microbial or fungal destruction of the cellulosic fibers. Lignin is a three-dimensional, highly branched, polyphenolic substance that consists of an irregular array of variously bonded “hydroxy-” and “methoxy-”substituted phenylpropane units (Miller, n.d.). These three general monomeric phenylpropane units exhibit the p-coumaryl, coniferyl, and sinapyl structures (Figure 2.4). Hardwood and softwood lignin have different structures. “Guaiacyl” lignin, which is found predominantly in softwoods, results from the polymerization of a higher fraction of coniferyl phenylpropane units. “Guaiacyl-syringyl” lignin, which is typically found in many hardwoods, is a copolymer of both the coniferyl and sinapyl phenylpropane units where the fraction of sinapyl units is higher than that in softwood lignins. Lignin has an amorphous structure, which leads to a large number of possible interlinkages between individual units, because the radical reactions are nonselective random condensations. Ether bonds predominate between lignin units, unlike the acetal functions found in cellulose and hemicellulose, but carbon to carbon linkages also exist. Covalent linking also exists between lignin and polysaccharides, which strongly enhances the adhesive bond strength between cellulose fibers and its lignin “potting matrix”. A small section of a lignin polymer is presented in Figure 2.5, illustrating some typical lignin chemical linkages.

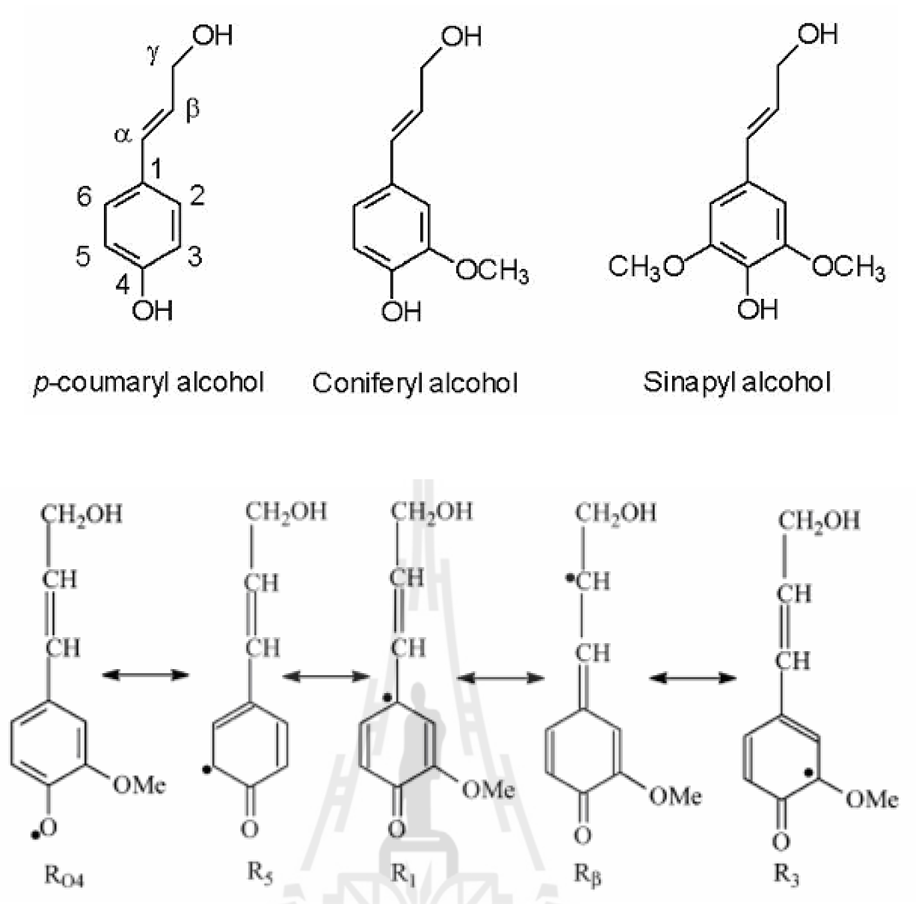

Figure 2.4 p-Coumaryl, coniferyl, and sinapyl structures and resonance hybrid structures of phenoxy radicals produced by the oxidation of coniferyl (Energy Information Admini- stration, n.d.).

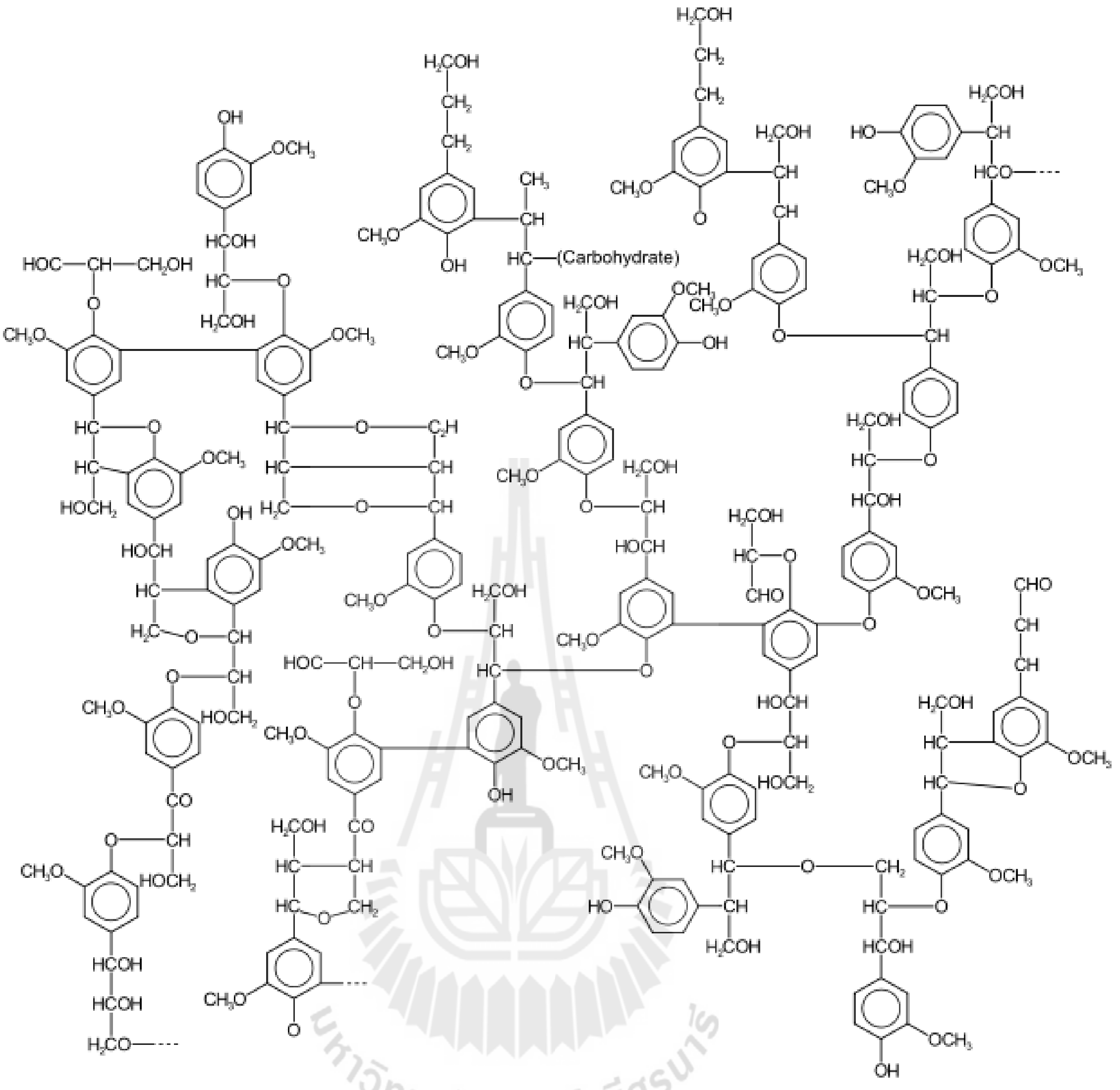

Figure 2.5 Partial structure of a hardwood lignin molecule (Wikipedia The Free Encyclopedia, n.d.).

The physical and chemical properties of lignins differ, depending on the extraction or isolation technology used to isolate them. Because lignin is inevitably modified and partially degraded during isolation, thermal decomposition studies on separated lignin will not necessarily match the pyrolysis behavior of this component when it is present in the original biomass. Yang, Yan, Chen, Lee, and Zheng (2007) found that lignin decomposes when heated at 280-500°C. Lignin pyrolysis yields phenols via the cleavage of ether and carbon linkages. Lignin is more difficult to dehydrate than cellulose or hemicelluloses. Lignin pyrolysis produces more residual char than does the pyrolysis of cellulose. In differential thermal analysis (DTA) studies at slow heating rates, a broad exotherm plateau extending from 290°C to 389°C is observed, followed by a second exotherm, peaking at 420°C and tailing out to beyond 500°C. Lignin decomposition in wood was proposed to begin at 280°C and continues to 450-500°C, with a maximum rate being observed at 350-450°C. The liquid product, which is known as pyroligneous acid, typically consists of ~20% aqueous components and ~15% tar residue, calculated on a dry lignin basis. The aqueous portion is composed of methanol, acetic acid, acetone, and water, whereas the tar residue consists mainly of homologous phenolic compounds. The gaseous products represent 10 wt% of the original lignin and contain methane, ethane, and carbon monoxide.

2.1.4 Inorganic Minerals

Biomass also contains a small mineral content that ends up in the pyrolysis ash. Inorganic minerals generally consist of 0.2% to 1.0% of wood substances (Miller, n.d.) Table 2.2 shows some typical values of the mineral components in biomass, expressed as percentage of the dry matter (DM) in the biomass.

2.1.5 Organic Extractives

Wood extractives represent extremely wide range of classes of organic chemicals. The most important groups that occur naturally in larger amount are the polyphenols and oleoresin (Miller, n.d.). The fifth wood component is composed of organic extractives, constitutes approximately 5% to 30% of extraneous materials (Properties of wood, n.d.). These can be extracted from wood with polar solvents (such as water, methylene chloride, or alcohol) or nonpolar solvents (such as toluene or hexane). Organic extractives include fats, waxes, alkaloids, proteins, phenolics, simple sugars, pectins, mucilages, gums, resins, terpenes, starches, glycosides, saponins, and essential oils. Extractives function as intermediates in metabolism, as energy reserves, and as defenser against microbial and insect attack.

Table 2.2 Typical mineral components of biomass (Energy Information Administration, n.d.)

Element	Percentage of dry matter
Potassium, K	0.1
Sodium, Na	0.015
Phosphorus, P	0.02
Calcium, Ca	0.2
Magnesium, Mg	0.04

2.2 Methods for Converting Biomass to Energy

There are several methods of converting biomass into energy. These methods include combustion, alcohol fermentation, anaerobic digestion, gasification and pyrolysis.

2.2.1 Combustion

Direct combustion of biomass is the most straightforward method of energy production. Mankind has burned wood and other forms of biomass for thousands of years, to keep warm, to cook food, and eventually to forge weapons and other tools. The energy released by direct combustion takes the form of heat, and can be used to directly influence the temperature of a small environment or to power steam-driven turbines to produce electricity. Unfortunately, the combustion of biomass is the cause of a great deal of pollution and has contributed to the so-called "greenhouse effect" and global warming. A relatively new field of research is the development of high energy crops specifically designed to be burned for power generation. Because at most only about 5% of a plant's mass is edible, the potential for large-scale energy production from biomass is relatively great. At the moment, however, growing large amounts of crops is still quite expensive. Thus, other methods of biomass energy production are being pursued with somewhat greater success. These methods include alcohol fermentation, anaerobic fermentation, and pyrolysis.

2.2.2 Fermentation

In alcohol fermentation, the starch in organic matter is converted to sugar by hydrolysis. This sugar is then fermented by yeast (as in the production of beer and wine). The resulting ethanol (also known as ethyl alcohol or grain alcohol) from the fermentation process is distilled that can be used as a substitute for gas gasoline or blended with another fuel. Gasohol, a mixture of gasoline and ethanol, has been used successfully in Brazil and the United States as an alternative to regular gasoline. The drawback of this method of biomass energy conversion is that the process itself requires the use of fossil fuels, and is therefore somewhat inefficient.

2.2.3 Anaerobic Digestion

Anaerobic digestion converts biomass, especially waste products, into methane (a major component of natural gas) and carbon dioxide. The biomass is mixed with water and stored in an airtight tank. This form of biomass energy conversion is attractive because it converts human, animal, and agricultural waste into a gas that is readily used as an energy source. Although the process is quite costly, it is relatively efficient.

2.2.4 Gasification

Gasification is the thermal degradation of carbonaceous material in the presence of an externally supplied oxidizing agent (air, pure oxygen or steam). The main product of gasification is a mixture of gases (producer gas) with the main components being carbon monoxide, hydrogen, carbon dioxide, water, methane and air nitrogen. The gas also contains particles, oxygenated organics and higher-molecular hydrocarbons; the latter two product classes are commonly referred to as tar. The quality of the producer gas depends on the same parameters as in the pyrolysis process.

2.2.5 Pyrolysis

Pyrolyisis involves the heating of biomass in the absence of oxygen. Biomass such as wood or agricultural waste is heated to around 1000^{o}F and allowed to decompose into gas and charcoal (carbon). A major advantage of pyrolysis is that carbon dioxide, one of the main drawbacks to most biomass energy conversion processes, is not produced. A disadvantage, however, is that the biomass must be heated to relatively high temperatures, a process that in and of itself requires significant amounts of energy.

2.3 Pyrolysis Process

Pyrolysis is the thermal decomposition of materials in the absence of oxygen or when significantly less oxygen is present than that required for complete combustion. Pyrolysis is difficult to precisely define, especially when applied to biomass. The general changes that occur during pyrolysis are enumerated below (Chiaramontia et al., 2007).

(1) Heat transfer from a heat source, to increase the temperature inside the fuel.

(2) The initiation of primary pyrolysis reactions at this higher temperature releases volatiles and forms char.

(3) The flow of hot volatiles toward cooler solids results in heat transfer between hot volatiles and cooler unpyrolyzed fuel.

(4) Condensation of some of the volatiles in the cooler parts of the fuel, followed by secondary reactions, can produce tar.

(5) Autocatalytic secondary pyrolysis reactions proceed, while primary pyrolytic reactions (item 2, above) simultaneously occurs in competition.

(6) Further thermal decomposition, reforming, water gas shift reactions, radicals recombination, and dehydrations can also occur, which are a function of the process's residence time/temperature/pressure profile.

2.3.1 Types of Pyrolysis

Pyrolysis process can be further divided into conventional pyrolysis and fast pyrolysis depending on the heating rate and residence time that are used. Table 2.3 and 2.4 shows the classification and product distribution for biomass pyrolysis processes, respectively.

2.3.1.1 Conventional Pyrolysis

Conventional pyrolysis may also be termed “slow pyrolysis”. This type of pyrolysis has been mainly used for the production of charcoal that applied for thousands of years. Slow pyrolysis is characterized by slow heating rate (less than 10^{o}C/s) and long residence times of gas and solids. The temperature is up to approximately 500°C (Chiaramontia et al, 2007). The release of vapors products do not occur as rapidly as in the fast pyrolysis. Thus, components in the vapor phase continue to react with each other, resulting in the formation of char and additional liquid.

2.3.1.2 Fast Pyrolysis

Fast pyrolysis is a high-temperature process in which biomass is rapidly heated in the absence of oxygen. Biomass decomposes to generate vapors, aerosols, and some charcoal-like char. Fast pyrolysis heating rate is 100°C/s, or even 10,000°C/s and vapour residence time is normally less than 2 second (Jain, Sharma, and Singh, 1996). At higher fast pyrolysis temperatures, the major product is gas. Rapid heating and rapid quenching maximize pyrolysis liquid products, which condense before further reactions break down the higher-molecular-weight species into gaseous products. A dark brown liquid is formed after cooling and condensation of the vapors. Heating value of this liquid is approximately half of that of conventional fuel oil. Fast pyrolysis processes produce 60-75 wt% of liquid bio-oil, 15-25 wt% of solid char, and 10-20 wt% of non-condensable gases, depending on the feedstock used.

Table 2.3 Pyrolysis methods and their variants (Energy Information Administration, n.d.)

Pyrolysis Technology	**Residence Time**	**Heating Rate**	**Temperature (°C)**	**Main Product**
Carbonization	Days	Very slow	400	Charcoal
Conventional	5-30 min	Low	600	Oil, gas, char
Fast	0.5-5 s	Very high	650	Bio-oil
Flash-liquid	< 1 s	High	<650	Bio-oil
Flash-gas	< 1 s	High	<650	Chemicals-gas
Ultra	< 0.5 s	Very high	1000	Chemicals-gas
Vacuum	2-30 s	Medium	400	Bio-oil
Hydro-pyrolysis	<10 s	High	<500	Bio-oil
Methanol-pyrolysis	< 10 s	High	>700	Chemicals

Table 2.4 Biomass Pyrolysis Products (Bridgewater, 2004)

Types of pyrolysis	**Pyrolysis Products (wt%)**		
	Liquid	**Char**	**Gas**
Fast Pyrolysis Moderate temperature (~ 500^{o}C), short hot vapour residence time (< 2 s)	75 Mostly organics	12	13
Slow pyrolysis (Carbonization) Low-moderate temperature, long residence times	30 Mostly water	35	35
Gasification High temperature (> 800^{o}C), long vapour residence time	5 Tar	10	85

2.3.2 Pyrolysis Parameters

Pyrolysis of biomass is complex functions of the experimental conditions, under which the pyrolysis process proceeds. The most important factors, which affect the yield and composition of the volatile fraction liberated, are heating rate, particle size, temperature, holding time, pressure, biomass species, and reactor configuration.

2.3.2.1 The Effect of Heating Rate

Hayakiri – Acma, Yaman and Kucukbayrak (2006) studied the effect of heating rate on the mass losses of rapeseed by using the derivative thermogravimetric analysis profiles. The important differences on the pyrolytic behavior of rapeseed are observed when heating rate was changed from 5 to 50 K/min at a constant pyrolysis temperature of 1273 K. The mass losses of rapeseed were also increased with the increasing of heating rate. However, Tsai, Lee, and Chang (2006) found that heating rate higher than 100^{o}C/min had relatively small influence on the product yield from pyrolysis process of rice straw, sugarcane basgasses, and coconut shell in a fixed - bed when pyrolyzing at 500^{o}C and holding time of 1 min.

2.3.2.2 The Effect of Particle Size

Heat can be distributed more uniformly if the particle size is sufficiently small (Acıkgoz, Onay, and Kockar, 2004). Thus, the decrease in particle size leads to more open pores, giving an increase in the sample specific surface area and specific pore volume, and hence is beneficial to volatile matter release (Keliang, Wenguo and Changsui, 2007). Increasing in particle size led to decrease in char yield but the oil yield was not much affected.

2.3.2.3 The Effect of Final Temperature

The final temperature affects the physical characteristics of biomass. Several researchers found that pyrolysis temperature was the main factor for the sample weight loss. The chemical bond becomes weaker and gets broken at a higher temperature. Char yield significantly decreased as the final pyrolysis temperature was raised from 400 to 700 ^{o}C. However the weight loss rate of the samples changed little when the final pyrolysis temperature was over 500^{o}C. This temperature is also the minimum required for the char to have a microporous structure. The oil yield also increased as the pyrolysis temperature was raised from 400^{o}C to a level of 500-550^{o}C. At the higher pyrolysis temperature of under 700^{o}C a decrease in the oil yield was observed, because of the secondary volatiles decomposition at temperatures above 500°C (Acıkgoz et al., 2004). The composition of the liquid product depended on the final temperature. Furthermore, gas yield significantly increased as the final pyrolysis temperature was raised from 350 to 700°C. Using this condition, the yields of the CO_2, CO and hydrocarbon gas were found to increase with increasing the final pyrolysis temperature (Aguado, Olazar, San Jośe, Aguirre and Bilbao, 2000)

2.3.2.4 The Effect of Holding Time

Tsai et al. (2006) investigated the influence of the holding time on the product yield of rice straw, bagasse and coconut shell in a fixed - bed reactor. Experimental data showed that for holding time longer than 2 minutes, yields of pyrolysis products remained almost unchanged at pyrolysis temperature of 500°C. On the other hand, the holding time appeared to have a significant effect on the pyrolysis product yield when the holding time is shorter than 2 minutes.

2.3.2.5 The Effect of Pressure

The effect of pressure on the yields of natural coke pyrolysis was investigated by Keliang et al., (2007). The studies were preformed in a pressurized thermogravimetric analyzer. Their results show that at pyrolysis temperatures lowers than 400°C the pressure range from 0.1 – 2.0 MPa has less effect on pyrolysis solid yields, while its effect becomes stronger when the pyrolysis temperature is higher.

2.3.2.6 The Effect of Raw Materials

Types of raw material has an effect on the yield of pyrolysis product. Tsai et al. (2006) showed that the char yield of rice straw and bagass were lower than the char yield of coconut shell at the same operating condition. On the other hand, yields of the oil product from the three precursors were similar. In addition, liquid product calorific value was found to depend on the type of biomass precursor.

2.3.2.7 The Effect of Inert Gas Flow Rate

The product yields of pyrolysis are related to the flow rate of sweep gas. Acıkgoz et al. (2004) found that the liquid product yield tended to increase upon increasing the inert gas flow rate from 50 to 100 cm^3/min for the fast pyrolysis of linseed in a fixed – bed reactor at 500^{o}C, the heating rate of 300^{o}C/min and the average particle size of 0.6 mm. However, the increase in the sweep gas flow rate above 100 cm^3/min decreased the oil yields to a level less than the oil yields obtained with a sweep gas flow rate of 50 cm^3/min. They have argued that there might be an insufficient cooling in the system at the sweep gas flow rate higher than 100 cm^3/min. Furthermore, the sweep gas flow rate did not show a significant change in the char and water yield.

2.3.3 Pyrolysis Kinetic Models

The rate at which the various fractions are released is termed the kinetics of devolatilization, or kinetics of pyrolysis. Nevertheless, devolatilization is not just a chemical process but it involves phase changes, mass, and heat transfers. Thus, rigorously speaking, the term kinetics to describe pyrolysis is just a crude approximation of reality. Therefore, it is not surprising to find models representing devolatilization with a wide range of precision when compared against the real process.

Due to the complexity and variation in composition of lignocellulosic materials, together with a large number of complex reactions involved in the pyrolysis process, it is difficult to obtain an exact model of the pyrolysis mechanism and of the effect of the various pyrolysis parameters involved. Several research groups have shown that the most significant parameters in biomass pyrolysis are temperature, particle size, biomass composition and heating conditions. Different classes of mechanisms were proposed for the pyrolysis of wood and other cellulosic materials. The models can be classified into two categories: one-step (global) models and combination of series and parallel reactions model.

2.3.3.1 Global Models

Global kinetic model, also called single-step model, is the simplest level of kinetic model to describe the thermal decomposition of biomass. Many investigators (Zabaniotou and Damartzis, 2007, Safi, Mishra and Prasad, 2004, Kim and Agblevor, 2007 and Jain et al., 1996) determined the biomass pyrolysis kinetic parameters by using this single-step model. They assumed that the volatile release can be represented by a single overall reaction, for example,

$$\text{Biomass} \xrightarrow{k} \text{Volatiles} + \text{Char} \tag{2.1}$$

where the conversion by pyrolysis depends on the residual mass and on the temperature according to the following rate equation;

$$\frac{d\alpha}{dt} = kf(\alpha) \tag{2.2}$$

The function f(α) depends on the reaction mechanism of the pyrolysis, and k is the rate constant and defined by the following Arrhenius equation.

$$k = A\exp\left(-\frac{E}{RT}\right) \tag{2.3}$$

The symbol α represents the conversion of the convertible part of the biomass, defined as

$$\alpha = \left(\frac{W_o - W}{W_o - W_f}\right) \tag{2.4}$$

where parameters W_o, W and W_f are the initial, actual and final weights of the sample, respectively. A is the pre-exponential or frequency factor, E is the activation energy of the decomposition reaction and R and T are the universal gas constant and the absolute temperature, respectively. Substituting k from equation 2.3 into 2.2 gives

$$\frac{d\alpha}{dt} = A\exp\left(-\frac{E}{RT}\right)f(\alpha) \tag{2.5}$$

For the single reaction pyrolysis model with a reaction order of n, the rate of conversion can be described by

$$\frac{d\alpha}{dt} = A\exp\left(-\frac{E}{RT}\right)(1-\alpha)^n \tag{2.6}$$

where (1−α) represents the remaining portion of the convertible part of the solid and n is the reaction order of pyrolysis. For the constant heating rate,β, the correlation between the temperature T and time t can be described by

$$\frac{dT}{dt} = \beta \tag{2.7}$$

The rate of conversion at a constant heating rate then can be expressed as

$$\frac{d\alpha}{dT} = \frac{A}{\beta}\exp\left(-\frac{E}{RT}\right)(1-\alpha)^n \tag{2.8}$$

or

$$\frac{d\alpha}{(1-\alpha)^n} = \frac{A}{\beta}\exp\left(-\frac{E}{RT}\right)dT \tag{2.9}$$

Equation (2.9) is a general rate equation and used for the determination of reaction kinetic parameters. Solutions of this equation have been suggested in different ways. On integrating the following relation, one obtains

$$\int_0^{\alpha}\frac{d\alpha}{(1-\alpha)^n} = \frac{A}{\beta}\int_0^{T}\exp\left(-\frac{E}{RT}\right)dT \tag{2.10}$$

The right hand side of equation 2.10 has no exact solution and several approximate solutions have been proposed. This equation has been used to determine the order of reaction (n), energy of activation (E) and the pre-exponential factor (A). The energy of activation for wood and other constituents of biomass reported by various investigators are given in Table 2.5.

2.3.3.2 Combination of Series and Parallel Reactions Model

One-step global model is a simplified mechanistic model. This model does not take into account the existence of several possible pyrolysis reactions. Thus, many research groups have considered the pyrolysis phenomena as consisting of a combination of series and parallel reaction schemes. Zabaniotou et al. (2007) investigated the kinetic models for fast pyrolysis of olive kernel by considering the pyrolysis as a parallel reaction with the secondary interactions being negligible. Manya et al. (2003) studied the thermal decompositions of sugarcane bagasse and waste wood by using thermogravimetic analysis. Three – pseudocomponents kinetic model was adopted in their work. The assumption of three-pseudocomponents is consistent with the lignocellulosic composition of biomass, namely cellulose,

Table 2.5 Kinetic parameters of thermal degradation of biomass from TG curve under non-isothermal conditions obtained by the global kinetic model.

Biomass	**Heating rate (K/min)**	**Kinetic Parameters**		
		n	**E (kJ/mol)**	**A (s^{-1})**
Pine needles$^{(1)}$	5	0.50	98.46	1.69×10^5
Palm shell$^{(2)}$	5	1.02	54.1	7.45×10^3
Avicel Cellulose $^{(3)}$	5	1.00	244	-

$^{(1)}$ Safi et al., 2004, $^{(2)}$ Guo and Lua, 2001, $^{(3)}$ Manya, Velo and Puigjaner, 2003 hemicellulose and lignin. Moreover, some research groups are also interested in the thermal decomposition kinetic models of co-biomasses (Aboulkas, El - Harfi, El - Bouadili, Benchanaa, Mokhlisse and Outzourit, 2007).

As an example, a modification of the Kilzer–Broido pyrolysis model based on the combination of series and parallel reaction was made by Agrawal in 1988 (Capart, Khezami and Burnham, 2004). The schematic representation of the pyrolysis reaction of this model is shown in Equation 2.11.

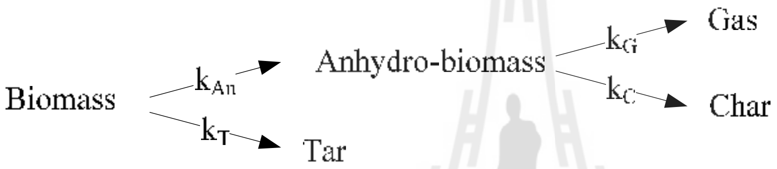

(2.11)

The first order reaction hypothesis was assumed for all of the reactions considered. The mass balance equations for the degradation of biomass for the modified Kilzer–Broido model are

$$\frac{dW_B}{dt} = -(k_T + k_{An})W_B = -k_1 W_B \tag{2.12}$$

$$\frac{dW_T}{dt} = -k_T W_B \tag{2.13}$$

$$\frac{dW_{An}}{dt} = k_{An} W_B - (k_G + k_C) W_{An} = k_{An} W_B - k_2 W_{An} \tag{2.14}$$

$$dW_G = k_G W_{An} \tag{2.15}$$

$$dW_C = k_C W_{An} \tag{2.16}$$

where

k_1 = $k_T + k_{An}$

k_2 = $k_G + k_C$

k_T = Tar formation rate constant

k_{An} = Anhydro-biomass formation rate constant

k_C = Char formation rate constant

k_G = Gas formation rate constant

W_B = Weight of biomass

W_{An} = Weight of anhydro-biomass

W_T = Weight of tar

W_G = Weight of gas

W_C = Weight of char

If R is the weight of residue at time t, the following relationship can be obtained:

$$R = W_B + W_{An} + W_C \tag{2.17}$$

To solve the set of differential equations above, the initial and final boundary conditions are as follows:

Initial boundary condition (t = 0):

$W_B = W_{B,0}$

$R = R_{B,0}$

and $W_{An} = W_T = W_G = W_C = 0$

Final boundary condition ($t \rightarrow \infty$):

$W_B = W_{An} = 0$

$W_T = W_{T,\infty}$

$W_G = W_{G,\infty}$

$W_C = W_{C,\infty}$

and $R = W_{C,\infty}$

Integrating the above equations using these boundary conditions, gives

$$W_B = W_{B,0}e^{-k_1t} \tag{2.18}$$

$$W_T = \frac{k_T W_{B,0}}{k_1}(1-e^{-k_1t}) \tag{2.19}$$

$$W_{An} = \frac{k_{An} W_{B,0}}{k_1 - k_2}(e^{-k_2t} - e^{-k_1t}) \tag{2.20}$$

$$W_G = \frac{k_G k_{An} W_{B,0}}{(k_1 - k_2)k_1k_2}\left[(k_1 - k_2) + k_2e^{-k_1t} - k_1e^{-k_2t}\right] \tag{2.21}$$

$$W_C = \frac{k_C k_{An} W_{B,0}}{(k_1 - k_2)k_1k_2}\left[(k_1 - k_2) + k_2e^{-k_1t} - k_1e^{-k_2t}\right] \tag{2.22}$$

If $t \rightarrow \infty$, $W_{T,\infty}$, $W_{G,\infty}$ and $W_{C,\infty}$ can be written as

$$W_{T,\infty} = \frac{k_T W_{B,0}}{k_1} \tag{2.23}$$

$$W_{G,\infty} = \frac{k_G k_{An} W_{B,0}}{k_1 k_2} \tag{2.24}$$

$$W_{C,\infty} = \frac{k_C k_{An} W_{B,0}}{k_1 k_2} \tag{2.25}$$

By substituting W_B, W_{An} and W_C in Equation 2.17 with these relationships and rearranging the equation, the following equation can be finally obtained,

$$\frac{R - R_\infty}{W_{B,0}} = \left[1 - \frac{k_{An}}{k_1 - k_2} + \frac{k_C k_{An}}{(k_1 - k_2)k_1}\right] e^{-k_1 t} + \left[\frac{k_{An}}{k_1 - k_2} - \frac{k_C k_{An}}{(k_1 - k_2)k_2}\right] e^{-k_2 t} \tag{2.26}$$

The negative slopes in the initial and final stage of a graphical plot between $\ln\left(\frac{R - R_\infty}{W_{B,0}}\right)$ versus time are k_1 and k_2, respectively. It was found by Conesa et al. in 1995 that the modification of Kilzer-Broido model can give better representation of the experimental data of cellulose pyrolysis.

2.3.3.3 The Two-Parallel Reactions Model

This kinetic model considers pyrolysis as a parallel reaction of two biomass components and the secondary interactions were assumed negligible. The reaction mechanism is represented as follows.

$$\text{Biomass} \xrightarrow{\qquad} \text{Volatile 1 + Volatile 2 + Char} \tag{2.27}$$

$$M_1 \xrightarrow{k_1} \text{Volatile 1 + Char} \tag{2.28}$$

$$M_2 \xrightarrow{k_2} \text{Volatile 2 + Char} \tag{2.29}$$

where k_1 and k_2 are the rate constant of each reaction. The residual weight fraction of char components are defined as follows,

$$\alpha = \frac{M_o - M_f}{1 - M_f}; \quad \alpha_1 = \frac{M_1 - M_{1,f}}{1 - M_f}; \quad \alpha_2 = \frac{M_2 - M_{2,f}}{1 - M_f} \tag{2.30}$$

where

M_f = the final mass fraction of solid char

$M_{1,f}$ and $M_{2,f}$ = the final mass fraction of first and second components

M = mass fraction of total residual weight at time, t

M_1 = mass fraction of residual weight of component 1 at time, t

M_2 = mass fraction of residual weight of component 2 at time, t

$M = M_1 + M_2$

$M_f = M_{1,f} + M_{2,f}$

The decomposition rate reaction of equation 2.28 and 2.29 are expressed as

$$\frac{d\alpha_1}{dt} = -A_1 \exp\left(-\frac{E_1}{RT}\right)\alpha_1 \qquad (2.31)$$

$$\frac{d\alpha_2}{dt} = -A_2 \exp\left(-\frac{E_2}{RT}\right)\alpha_2{}^n \qquad (2.32)$$

where; A = pre-exponential factor

E = activation energy

R = universal gas constant

T = absolute temperature

n = decomposition reaction order

t = time

For the constant heating rate, $\beta = \frac{dT}{dt}$, equation 2.31 and 2.32 are in the form,

$$\frac{d\alpha_1}{dT} = -\frac{A_1}{\beta} \exp\left(-\frac{E_1}{RT}\right)\alpha_1 \qquad (2.33)$$

$$\frac{d\alpha_2}{dT} = -\frac{A_2}{\beta} \exp\left(-\frac{E_2}{RT}\right)\alpha_2{}^n \qquad (2.34)$$

Rearranging Eq. 2.33 and 2.34 and integrating to obtain

$$\int_{a}^{\alpha_1} \frac{d\alpha_1}{\alpha_1} = -\frac{A_1}{\beta} \int_{0}^{T} \exp\left(-\frac{E_1}{RT}\right) dT \tag{2.35}$$

$$\int_{b}^{\alpha_2} \frac{d\alpha_2}{\alpha_2{}^{n}} = -\frac{A_2}{\beta} \int_{0}^{T} \exp\left(-\frac{E_2}{RT}\right) dT \tag{2.36}$$

The parameter a and b are initial values of α_1 and α_2, respectively. They indicate the initial weight fractions of component 1 and 2 in the starting raw material. They are assumed constant and depend only on the characteristics of the raw material. The relationship between a and b is expressed as,

$$a + b = 1 \tag{2.37}$$

An exponential term on the right-hand side of Eq. 2.35 and 2.36 can be expressed in an asymptotic series and the higher order terms were neglected. The integration yields the following expression (Guo and Lua, 2001).

$$\frac{A_i}{\beta} \int_{0}^{T} \exp\left(-\frac{E_1}{RT}\right) dT = \frac{A_i R T^2}{\beta E_i} \left[1 - \frac{2RT}{E_i}\right] \exp\left(-\frac{E_i}{RT}\right) \tag{2.38}$$

Combining Equation (2.38) with Equation (2.35) and Equation (2.36) and after integrating the left – hand side term, we obtain

$$\alpha_1 = \exp\left[-\frac{A_1RT^2}{\beta E_1}\left(1-\frac{2RT}{E_1}\right)\exp\left(-\frac{E_1}{RT}\right)+\ln(a)\right] \tag{2.39}$$

$$\alpha_2 = \exp\left[\frac{(n-1)A_2RT^2}{\beta E_2}\left(1-\frac{2RT}{E_2}\right)\exp\left(-\frac{E_2}{RT}\right)+b^{(1-n)}\right]^{\frac{1}{1-n}} \tag{2.40}$$

Finally, the total residual fraction of the remaining mass at any temperature is

$$\begin{aligned}\alpha &= \alpha_1 + \alpha_2 \\ &= \exp\left[-\frac{A_1RT^2}{\beta E_1}\left(1-\frac{2RT}{E_1}\right)\exp\left(-\frac{E_1}{RT}\right)+\ln(a)\right] \\ &\quad +\exp\left[\frac{(n-1)A_2RT^2}{\beta E_2}\left(1-\frac{2RT}{E_2}\right)\exp\left(-\frac{E_2}{RT}\right)+b^{(1-n)}\right]^{\frac{1}{1-n}}\end{aligned} \tag{2.41}$$

The unknown parameters of the model including A_1, E_1, A_2, E_2, n, a and b are determined by a non – linear fitting of the experimental data. The best fit of the model to experimental data is obtained by minimizing the sum of square of relative error defined as,

$$\mathrm{SSRE} = \sum\left(\frac{\alpha_{\exp} - \alpha_{\mathrm{model}}}{\alpha_{\exp}}\right)^2 \tag{2.42}$$

The symbols $\alpha_{\exp}$ and α_{model} represents the experimental and calculation values of the residual weight fraction, respectively.

2.3.3.4 The Three – Pseudocomponent Model

The model was proposed based on the assumption that the biomass consists of three – pseudocomponents: cellulose, hemi cellulose and lignin. The pyrolysis rate is described by

$$\frac{d\alpha}{dt} = \sum_{i=1}^{3} c_i \frac{d\alpha_i}{dt} = \sum_{i=1}^{3} c_i A_i \exp\left(-\frac{E_i}{RT}\right) f(\alpha_i) \tag{2.43}$$

where the parameter c_i is the coefficient which expresses the contribution of the partial processes to the overall mass loss. Subscript i indicates the i component.

The kinetic equation that was used for the pyrolysis of each pseudo – component is expressed as

$$\frac{d\alpha_i}{dt} = A_i \exp\left(-\frac{E_i}{RT}\right)(1-\alpha_i)^{n_i} \tag{2.44}$$

For the constant heating rate, β, equation (2.44) can be written as

$$\beta \frac{d\alpha_i}{dT} = A_i \exp\left(-\frac{E_i}{RT}\right)(1-\alpha_i)^{n_i} \tag{2.45}$$

For $n_i = 1$

$$\frac{d\alpha_i}{dT} = A_i \exp\left(-\frac{E_i}{RT}\right) \exp\left\{-\frac{A_i}{\beta} \exp\left(-\frac{E_i}{RT}\right) dT\right\} \tag{2.46}$$

For $n_i \neq 1$

$$\frac{d\alpha_i}{dT} = A_i \exp\left(-\frac{E_i}{RT}\right)\left\{\left(\frac{(n_i - 1)A_i}{\beta}\int_{To}^{T}\exp\left(-\frac{E_i}{RT}\right)dT\right) + 1\right\}^{n_i/(1-n_i)} \tag{2.47}$$

where $\alpha_i = \dfrac{(M_o - M_t)}{(M_o - M_f)}$

Parameter M_o, M_t and M_f are initial mass, mass at reaction time t and final mass, respectively.

The unknown parameters of the model are determined by fitting the model equation with the experimental data by employing non – linear square fitting. The best fit was obtained by minimizing the following objective function,

$$\mathrm{Fit} = 100\frac{\left(\sum\left[\left(\frac{d\alpha}{dt}\right)^{exp} - \left(\frac{d\alpha}{dt}\right)^{calc}\right]^2\right)^{1/2}}{\left(-\frac{d\alpha}{dt}\right)^{exp}_{max}} \tag{2.48}$$

2.3.4 Products of Biomass Pyrolysis

Biomass pyrolysis product consists of gas, condensable liquid and solid. Most of products from the thermal processes are potential fuels. The distribution and properties of the various products vary depending upon the pyrolysis conditions, such as feedstock material, time, temperatures and reactor system. The properties of the various pyrolysis products are now briefly presented.

2.3.4.1 Gas Product

Gas products from the pyrolysis of biomass may be considered to be a binary mixture of primary and secondary gases. The primary gases are formed during the formation of char and the secondary gases occur after the secondary cracking of organic volatile matters. The main gaseous compositions by thermal pyrolysis process consist of carbon monoxide, carbon dioxide, hydrogen and methane. Gas calorific values are dependent on the proportional ratio of each gas components. For convenience, gases can be grouped according to their calorific values (see Table 2.6). These gases can be used for feed drying, heating process, and power generation, etc.

2.3.4.2 Liquid Product

Pyroligneous liquor are aqueous and non-aqueous mixtures which are condensed and collected from a pyrolysis step. Water and organic compounds are the main compositions in an aqueous liquid, while tar and oil can be found in the non-aqueous liquid. Pyroligneous liquid is very complex in composition and has a calorific value in the range of 10-30 MJ/kg. The calorific value of this product is considerably decreased by the presence of water. Tars and oils in the non-aqueous fraction have a higher calorific value, but their yields are often low when a biomass feedstock is used, and they are difficult to handle. The chemical components in biomass tars are listed in Table 2.7. Pyroligneous liquor can be used as a fuel if the water content is sufficiently low. Special storage and piping are required to prevent the corrosiveness from its acidity. It is also difficult to atomize when compared to normal fuel oils. Blending the pyrolysis liquid with hydrocarbon oils in a burner is possible but the two fuels are not fully miscible.

2.3.4.3 Solid Product

Solid is one of the major pyrolysis products and is referred to as “Char”. At the optimal pyrolysis conditions, the solid product yield is approximately 25 - 30%wt, based on dry weight of biomass, with its calorific value approaching the value of 32.8 MJ/kg.

Table 2.6 Groups of gas products (The Watt Committee on Energy, n.d.)

Calorific value	Main Components	Typical Production Process
Low calorific value gas (approx. 3-4 MJ/m^3)	$N_2 + CO + H_2$	Air-blown gasifier
Medium calorific value gas (approx. 10-20 MJ/m^3)	$CO + H_2$	Pyrolysis, steam reforming, oxygen-blown gasifier
High calorific value gas (33-42 MJ/m^3)	CH_4	Hydrogasification and hydrogeneration

Table 2.7 The chemical components in biomass tars (Bain, 2004)

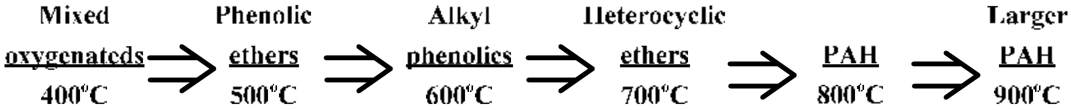

Conventional FlashPyrolysis (450 - 500°C)	**Hi-Temperature FlashPyrolysis (600 - 650°C)**	**Conventional SteamGasification (700 - 800°C)**	**Hi-Temperature SteamGasification (900 - 1000°C)**
Acids Aldehydes Ketones Furans Alcohols Complex Oxygenates Phenols Guaiacols Syringols Complex Phenols	Benzenes Phenols Catechols Naphthalenes Biphenyls Phenanthrenes Benzofurans Benzaldehydes	Naphthalenes Acenaphthylenes Fluorenes Phnanthrenes Benzaldehydes Phenols Naphthofurans Benzanthracenes	Naphthalene* Acenaphthylene Phenanthrene Fluoranthene Pyrene Acephenanthrylene Benzanthracenes Benzopyrenes 226 MW PAHs 276 MW PAHs*
*At the highest severity, naphthalenes such as methylnaphthalene are stripped to simple naphthalene.			

2.4 Spouted Bed

The words spouted bed and spouting were first coined by Mather and Gishler in 1955 (Yang, 2003) at the Nation Research Council of Canada during the development of a technique for drying wheat. The first extensive assimilation of the literature came from the publication of spouted beds by Mathur and Epstein in 1974 (Yang, 2003). The first commercial spouted bed units were installed in Canada for drying peas, lentils and flax in 1962. Since then, spouted beds have been used for many different processes such as evaporative crystallization, solid blending, cooling, coating and granulation. Nowadays, these applications are already commercialized in drying of granular materials, drying of suspension and solutions, tablet coating, cooling of fertilizers, and charcoal activation.

A classical and conventional spouted bed is shown in Figure 2.6. The fluid is supplied through a central nozzle. If the fluid velocity is high and the bed is short enough, the fluid stream will push through the bed as a spout, as shown in Figure 2.6 (a). The spouting fluid will entrain the solid particles at the spout – annulus interface and form a fountain above the bed. The spouting fluid will also leak through the spout-annulus interface into the annulus to provide aeration for the particles in the annulus. The spouted bed is usually constructed as a cylindrical vessel with a conical bottom as shown in Figure 2.6 (b) to eliminate the stagnant region. Spouting in a conical vessel has also been employed. Solid particles can be continuously fed into a spouted bed through the concentric jet or into the annulus region and continuously withdrawn from the annulus region, just as in a fluidized bed. Some of the key features of gas-spouted and gas-fluidized beds are presented in Table 2.8 for comparison (Cui and Grace, 2008).

Table 2.8 Significant differences between gas-spouted beds and gas-fluidized beds.

Aspect	**Fluidized bed**	**Spouted bed**
Mean particle size	~0.03-3 mm; usually < 1mm	~0.6-6 mm; usually > 1 mm
Particle size distribution	Usually broad	Usually narrow
Pressure drop/height within the bed	96-100% of that needed to support the particles, i.e. ~$(\rho_p - \rho_s)g(1-\varepsilon)$	Less than ~ 75% of that needed to support the weight of the particles, i.e. < 0.75 × $((\rho_p - \rho_s)g(1-\varepsilon)$
Pressure drop across entry orifices	Usually 30-50% of that across the bed	As small as possible consistent with satisfying the other constraints, e.g. orifice dia. < 25 mean particle dia.
Axial gradient of pressure	Virtually independent of height in the column	Varies with height
Temperature gradient	Very uniform temperature over entire fluidized bed region	Significant temperature gradients both axially and radially

Table 2.8 Significant differences between gas-spouted beds and gas-fluidized beds (Continued).

Aspect	**Fluidized bed**	**Spouted bed**
Column geometry	Usually cylindrical columns	Usually diverging conical base with or without cylindrical portion above
Orifice diameter	No restriction	Must not exceed 25 mean particle diameters
Orifice number density and configuration	Large number of orifices (typically > 100 per square meter). Many geometries. No constriction needed at the entrance	Usually for orifice multiple spoutings, small number density of orifices (typically no more than ~10-50 per square meter). It is helpful to have a constriction right at the entrance.
Orifice orientation	Most frequently horizontal, downward facing or oblique with downwards component, but may also be upwards-facing	Always upward-facing.
Superficial gas velocity	Broad range, typically $(U-U_{mf}) = 0.2\text{-}10$ m/s	More limited range, typically 1.1-1.8 U_{ms}

Table 2.8 Significant differences between gas-spouted beds and gas-fluidized beds (Continued).

Aspect	Fluidized bed	Spouted bed
Orifice feed system	Windbox (sometimes called plenum chamber) feeds all orifices	Separate gas supply and control of each orifice
Gas motion	Less ordered; depends on flow regime and specific geometry	Outwards from the spouts into the dense phase, except just above inlet
Particle motion	Complex flow regimes and particle motion. Region surrounding the gas entry orifices is usually fluidized with few particle-particle contacts	Systematic circulation patterns, up the spout and slowly downward in the annulus. Annulus is in moving packed bed flow with substantial particle-particle contacts
Particle segregation	Very little segregation providing that particles are well fluidized	Significant segregation according to both size and density of particles

Table 2.8 Significant differences between gas-spouted beds and gas-fluidized beds (Continued).

Aspect	**Fluidized bed**	**Spouted bed**
Attrition	Normally little except in cyclone or jet regions	Significant in spout region and in fountain above
Bed depth	Broad range of depths, e.g. from 0.1 to 20 m dense bed depth	More limited range of depths, usually between 0.2 and 2.0 m
Orifice velocity variation	Some variation with time across each individual orifice as bubbles from and leave the orifice or jet	Essentially steady as flow is controlled to each hole from an upstream valve
Internals	Common in fluidized bed processes	Rare in spouted bed process, except for some use of draught tubes and heat transfer coils

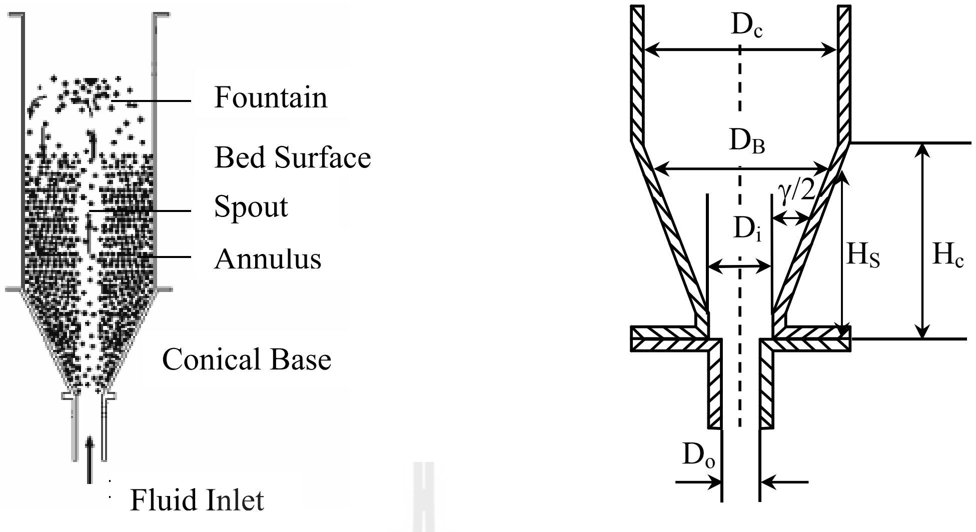

(a) (b)

Figure 2.6 (a) A classical and conventional spouted bed (Cui and Grace, 2008) and (b) Geometric factor of the contactor (San José et al., 2005)

Not all bed particles are spoutable. For beds with the ratio of nozzle diameter to column diameter D_i/D_c, above a certain critical value, there is no spouting regime. In this case, the bed will transfer from the fixed bed directly into the fluidized state with increasing gas velocity. To achieve a stable non-pulsating spouted bed, the nozzle-to-particle-diameter ratio, D_i/d_p, should be less than 25 or 30 (Yang, 2003). There exists also the minimum spouting velocity and the maximum spoutable bed height requirements in a spouted – bed operation.

According to Epstein and Grace in 1977 (Yang, 2003), the Mathur-Gishler equation shown below remains the simplest equation to estimate the minimum spouting velocity, accurate to within 15% for cylindrical vessels (D_c) up to about 0.5 m.

$$(U_{ms})_{0.5} = \left(\frac{d_p}{D_c}\right)\left(\frac{D_i}{D_c}\right)^{1/3} \sqrt{\frac{2gH_s(\rho_p - \rho_f)}{\rho_f}}, \quad D_c < 0.5 \text{ m} \tag{2.49}$$

where

$(U_{ms})_{0.5}$ = minimum spouting velocity for cylindrical vessel up to about 0.5 m (m/s)

d_p = particle size diameter (m)

D_i = nozzle diameter (m)

D_c = cylindrical vessel diameter (m)

g = acceleration of gravity (m/s^2)

H_s = static bed height (m)

ρ_p = particle density (kg/m^3)

ρ_f = fluid density (kg/m^3)

For non-spherical particles, the diameter, d_p, to be used in Equation (2.49) should be the diameter of a sphere with equal volume for closely sized near-spherical particles or the volume – surface mean diameter should be employed. For prelate spheroids, the smaller of the two principal dimensions is best used as the particle diameter in Equation (2.49). San José, Olazar, Peńas, Arandes, Bilbao (1995) used this equation to study the hydrodynamics of the shallow spouted beds in a conical spouted bed. For cylindrical vessels larger than 0.5 m the proposed correlation is

$$U_{ms} = 2.0D_c(U_{ms})_{0.5}, \ D_c > 0.5 \text{ m} \tag{2.50}$$

The Mathur and Gishler equation under – predicted the U_{ms} by about 50% for the heavy steel balls and about 39.5% for the larger glass beads. The deviation is smaller, about 26% for the small glass beads. This corresponds to a U_{ms} dependence of gas density of $\rho_f^{-0.36}$ for the steel balls and large glass beads and of $\rho_f^{-0.22}$ for the small glass beads. Thus, for correct prediction of the density effect on U_{ms}, the exponent on ρ_f in the Mathur and Gishler equation should have different values, depending on the particle Reynolds number (Anabtawi et al., 1988b, quoted in Yang, 2003).

San José, Olazar, Aguado and Bilbao (1996) studied the influence of the conical section geometry on the hydrodynamics of the shallow spouted beds. The contactor angle (γ), air inlet diameter (D_o) and particle size (d_p) had an influence on the bed regimes. The operation in the spouted bed for the larger base angle is more stable than the small base angle. Limitation of the operation in any case is the maximum spoutable bed height that causes the slugging, spout blockage (choking) and fluidization of the particles on the upper surface of the cylindrical section. A dilute zone is generated in the spouted bed above the cylindrical section when a large velocity was used. A smaller D_o/D_i ratio should be used for the larger particle size. The instability problem was observed for particle with d_p = 6 mm. In this case, the stable regime is obtained over a wide range of values of the stagnant bed height and air velocity for the smaller particle size. Furthermore, their results showed that the influence of the contactor angle is significantly less than the particle diameter variation.

Yang (2003) reported that the maximum spoutable bed height decreased with increasing in particle size for particle size larger than a critical particle size. The correlation equation of a critical particle size was proposed by Anabtawi (1998). This equation is only good for gas – solid spouting and is not applicable to liquid – solid spouting. For the liquid – solid spouting, the maximum spoutable bed height decrease with the increase in particle size for all cases. For gas – solid spouting, the critical particle diameter is usually in the range of 1.0 to 1.5 mm.

The bed voidage at minimum spouting is a basic parameter for the calculation of the minimum contactor volume needed for treating a given amount of solid and, in general, for the design of the operation or process to be carried out. The correlation proposed for the calculation of the bed voidage at minimum spouting was proposed by San José et al. (1996). The calculation and experimental values of the bed voidage at minimum spouting was reported by San José et al. (1996). The decrease in bed voidage with increasing stagnant bed height is significant in the cone section when the stagnant bed height reaches the cylinder section; the bed voidage increases slightly with the increase in stagnant bed height. In 1978, Lim and Mathur suggested that the voidage in the spout decreases from 1 at the spout inlet almost linearly with increasing in height until it reaches around 0.7 at the top of the spout. Models are available for the prediction of the voidage distribution for both the annulus and spout regions (Yang, 2003).

The correlation for the calculation of the total pressure drop and the maximum pressure drop of the bed was proposed by San José et al. (1996) and their experimental results showed that the total pressure drop increased with increasing of stagnant bed height for all the contactor – particle systems. The total pressure drop increased with the particle diameter and decreased with the inlet diameter. Furthermore, their results suggested that the influence of the particle diameter was more significant than the those of other parameters. For the maximum pressure drop, it was found that the maximum pressure drop increased more than proportionally with the stagnant bed height. The maximum pressure drop increased as the particle diameter was increased, whereas it decreased with the increase of contactor inlet diameter. The effect of the contactor angle is less important than that of the aforementioned variables. As the cone angle was increased, the maximum pressure drop was found to decrease slightly.

2.5 Conical Spouted Beds

The first study of conical spouted beds was started by Russiun researcher in 1960s. Their investigations were focused on the determination of various parameters at stable spouting condition, including stable minimum spouting velocity, the maximum pressure drop and the pressure drop as a function of flow velocity (Wang, 2006). Schematic diagram of a conical spouted bed is shown in Figure 2.7. There are three regions in the spouted bed: spout, annular and fountain. The central core is called spout. Annulus denotes the peripheral annular region in the bed. The mushroom-shaped zone above the level of the annulus is called fountain (Cui and Grace, 2008).

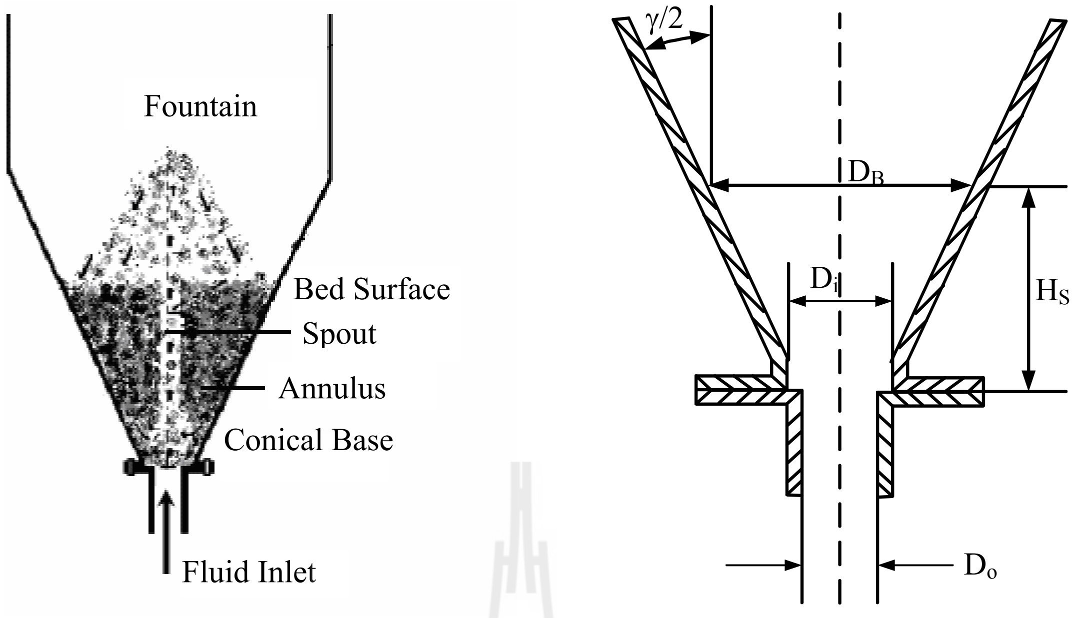

(a)

(b)

Figure 2.7 (a) A classical conical spouted bed (Wang, 2006) and (b) Geometric factors of the contactor.

The expansion state of conical spouted bed have been determined in details from a typical diagram of the relationship between the total bed pressure drop of a conical spouted bed and the superficial gas velocity, as typically shown in Figure 2.8 (Wang, 2006). Four operation regimes (Figure 2.9) upon increasing gas velocity can be distinguished, including fixed bed regime, stable spouting regime, transition regime, and jet-spouting regime, respectively.

Fixed bed or static packed bed regime (Figure 2.9 (a)) occurs at low flow rates where the gas passes up through the bed without particle disturbing. The pressure drop rises with gas flow rate to the maximum pressure drop. Then, the pressure drop decreases with further increasing of the gas flow rate until the incipient spouting point was reached, which indicates the state of stable spouting (Figure 2.9 (b)).

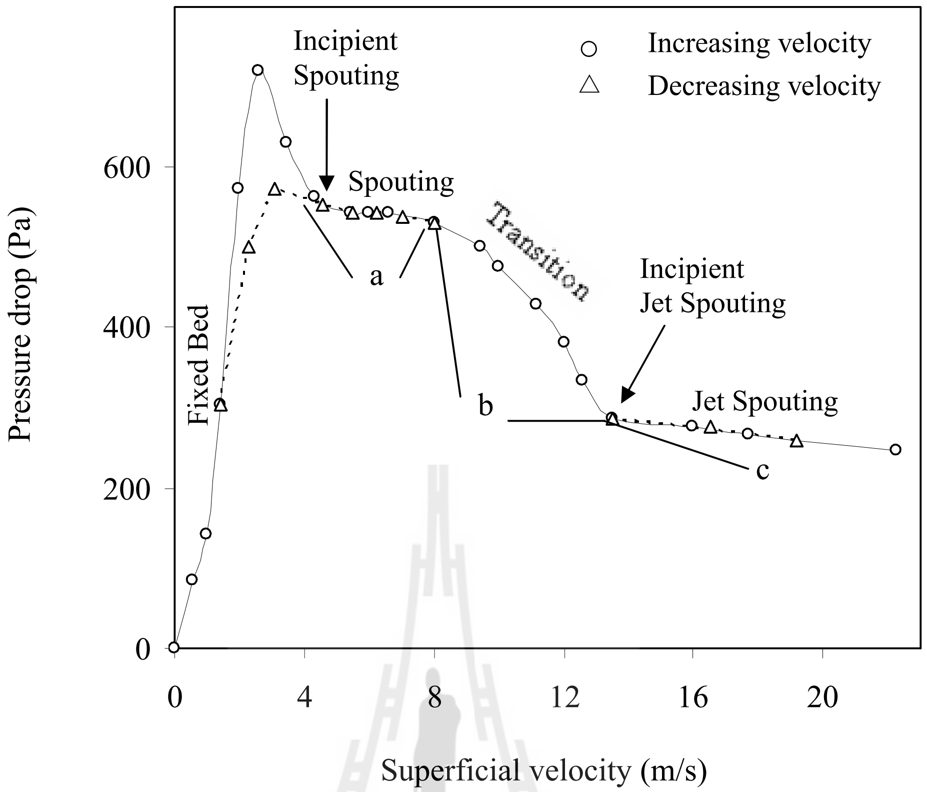

Figure 2.8 Typical pressure drop-flow rate curves (Wang, 2006).

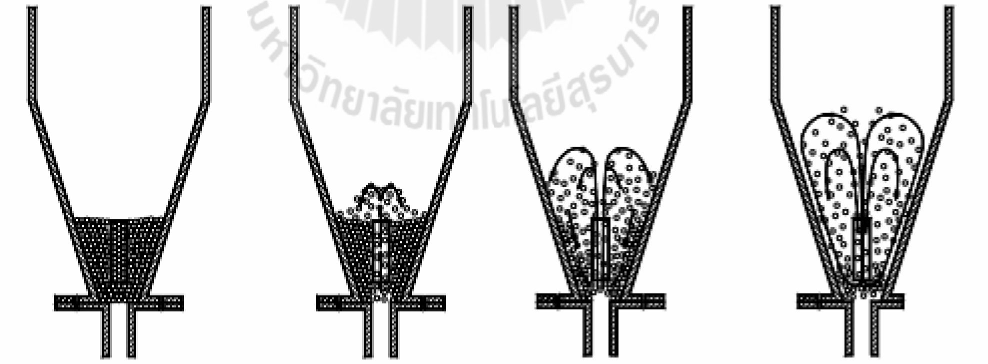

(a) (b) (c) (d)

Figure 2.9 Solid flow outline: (a) Fixed bed regime, (b) spouted bed regime, (c) transition regime, and (d) jet - spouted bed regime (Yang, 2003).

The internal cavity now elongates into an internal spout in this regime. Transition regime comes into effect when the end of stable spouting was reached. At this stage both annular and spout zones become progressively diffused and the pattern of particle movement as in Figure 2.9 (c) is obtained. Jet – spouting regime (Figure 2.9 (d)) occurs when the bed passes through a transition state until it reaches a new regime with different hydrodynamic characteristic and the bed voidage becomes almost uniform throughout. This regime stays stable with further increase in velocity, with a constant value of pressure drop.

Olazar and coworkers (1992) studied the design, operation, and performance of a conical spouted bed and found that the conical spouted bed is especially useful for hard – to – handle solids that are irregular in texture or sticky. The conical spouted bed exhibits pronounced axial and radial voidage profiles that are quite different from the cylindrical spouted beds (Yang, 2003).

2.5.1 Minimum Spouting Velocity

The determination of minimum spouting velocity of a conical spouted bed (U_{ms}) was proposed by Olazar et al. (1992). The results were obtained with materials such as glass beads or other materials of similar density and covered a wide range of geometric factors (angle, gas inlet diameter, contactor base diameter) and experimental conditions (particle size, stagnant bed height, relative velocity over that of minimum spouting velocity). The following correlation for predicting U_{ms} in terms of Reynolds number was proposed,

$$(\mathrm{Re})_{D_{o,ms}} = 0.126\mathrm{Ar}^{0.5}\left(\frac{D_B}{D_o}\right)^{1.68}\left[\tan\left(\frac{\gamma}{2}\right)\right]^{-0.57} \tag{2.51}$$

where $(\mathrm{Re})_{D_{o,ms}}$ is the Reynolds number of minimum spouting velocity, defined as

$$(\mathrm{Re})_{D_{o,ms}} = \frac{\rho_f D_o U_{ms}}{\mu_f} \tag{2.52}$$

where ρ_f is the fluid density($\left(\mathrm{kg/m^3}\right)$and μ_f is the fluid viscosity $\left(\mathrm{kg/m-s}\right)$. The expression of Archimedes modulus $\left(\mathrm{Ar}\right)$ is expressed as

$$\mathrm{Ar} = \frac{g d_p^3 \rho_f \left(\rho_s - \rho_f\right)}{\mu_f^2} \tag{2.53}$$

Sari, Kulah, and Koksal (2012) investigated the hydrodynamics of conical spouted bed for high density particles. Their measurements were performed in three 15 cm ID full circular with different cone angle ($\gamma = 30^o$, 45^o, 60^o) and one half circular conical spouted ($\gamma = 30^o$) with yttria – stabilized zirconia particles ($d_p = 0.5$ and 1.0 mm, $\rho_p = 6050$ kg/m^3). The results showed that the minimum spouting velocity increased with increasing cone angle, particle diameter and static bed height. Minimum spouting velocity values obtained from the full and half bed experiments gave a maximum 15% difference.

2.5.2 Bed Voidage along the Spout Axis

The bed voidage (ε) along the spout axis at r = 0 was found to be parabolic and dependent on the system variables (San José, Olazar, Alvarez, Izquierdo, and Bilbao 1998) as follows.

$$\varepsilon(0) = 1 - E\left(\frac{z}{H}\right)^2 \tag{2.54}$$

where E is an epical parameter varying between 0.3 and 0.6 and is empirically correlated by

$$E = 1.20\left(\frac{D_B}{D_o}\right)^{-0.12}\left(\frac{H_S}{D_i}\right)^{-0.97}\left(\frac{U}{U_{ms}}\right)^{-0.7}\gamma^{-0.25} \tag{2.55}$$

where H_o is the height of the stagnant bed and

$$D_B = D_i + 2H_S \tan\left(\frac{\gamma}{2}\right) \tag{2.56}$$

2.6 References

Aboulkas, A., El - Harfi, K., El - Bouadili, A., Benchanaa, M., Mokhlisse, A., and Outzourit, A. (2007). Kinetics of co-pyrolysis of tarfaya (morocco) oil shale with high-density polyethylene. **Oil shale.** 24 (1): 15-33.

Acıkgoz, C., Onay, O., and Kockar, O.M. (2004). Fast pyrolysis of linseed: product yields and compositions. **Journal of Analytical and Applied Pyrolysis.** 71: 417- 429.

Aguado, R., Olazar, M., San Jośe, M.J., Aguirre, G., and Bilbao, J.(2000). Pyrolysis of sawdust in a conical spouted bed reactor-Yields and product composition. **Ind. Eng. Chem. Res.** 39: 1925-1933.

Bain, R.L. (2004). **National Renewable Energy Laboratory**. **Operated for the U.S. Department of Energy by Midwest Research Institute • Battelle 2004**. Available: www.msenergy.ms.

BRIDGWATER, V. (2004). **Biomass fast pyrolysis.** Review paper. 8 (2): 21-49.

Capart, R., Khezami, L., and Burnham, A. K. (2004). Assessment of Various Kinetic Models for the Pyrolysis of a Microgranular Cellulose. **Thermochemica Acta.** 417: 79–890.

Chaplin, M. (n.d.)**. Water Structure and Science: Cellulose.** Available: http://www.lsbu.ac.uk/ water/hycel.html.

Chiaramontia, D., Oasmaab, A., and Solantaustab, Y. (2007). Power generation using fast pyrolysis liquids from biomass. **Renewable and Sustainable Energy Reviews.** 11: 1056–1086.

Cui, H., and Grace, J.R. (2008). Spouting of biomass particles: A review. **Bioresource Technology.** 99(10): 4008 – 4020.

Energy Information Administration. (n.d.). Office of Coal, Nuclear, Electric and Alternative Fuels.

Haykiri – Acma, H., Yaman, S., and Kucukbayrak, S. (2006). Effect of heating rate on the pyrolysis yields of rapeseed. **Renewable Energy.** 31: 803 – 810.

Grønli, M., Antal, M. J., and Va´rhegyi, G. (1999). A Round-Robin Study of Cellulose Pyrolysis Kinetics by Thermogravimetry. **Ind. Eng. Chem. Res.** 38: 2238-2244.

Guo, J., and Lua, A.C. (2001). Kinetic study on pyrolysis process of oil-palm solid waste using two-step consecutive reaction model. **Biomass and Bioenergy.** 20: 223-233.

He, B.B., McDonald, A.G. (n.d.). **Thermochemical Processes for Biomass Conversion**. Available: http://www.webpages.uidaho.edu/~bhe/biorefinery/4.pdf.

Hu, S., Jess, A., and Xu, M. (2007). Kinetic study of Chinese biomass slow pyrolysis: Comparison of different kinetic models. **Fuel.** 86(17 – 18): 2778 – 2788.

Jain, A.K., Sharma, S.K., and Singh, D. (1996). Reaction kinetics of paddy husk thermal decomposition. **Energy Research Center Panjab University** .India. Available:http://ieeexplore.ieee.org/iel3/4058/12000/00561172.pdf?arnumber=561172.

Keliang, P., Wenguo, X., and Changsui, Z. (2007). Investigation on pyrolysis charateristic characteristic of natural coke using thermogravimetric and Fourier-transform infrared method. **Journal of Analytical and Applied Pyrolysis.** 80: 77-84.

Kim, S.S., Agblevor, F.A. (2007). Pyrolysis characteristics and kinetics of chicken litter. **Waste Management.** 27: 135-140.

Luangkiattikhun, P., Tangsathitkulchai, C., and Tangsathitkulchai, M.(2007). Non-isothermal thermogravimetric analysis of oil-palm solid wastes. **Bioresource Technology.** Article In Press.

Manya, J. J., Velo, E., and Puigjaner, L. (2003). Kinetics of biomass pyrolysis: a reformulated three-parallel-reactions model. **Ind. Eng. Chem. Res.** 42: 434-441.

Maschio, G., Lucchesi, A., and Koufopanos, C. (1994). Study of kinetic and transfer phenomena in the pyrolysis of biomass particles. **Advances in thermochemical biomass conversion.** Volume 2. Chapman&Hall. New York. Edited by A.V. Bridgwater.

Miller, B.R. (n.d.). **Structure of Wood**. http://www.fpl.fs.fed.us/documnts/fplgtr/fplgtr113/ch02.pdf.

Olazar, M., San José, M.J., Aguayo, A.T., Arandes, J.M., and Bilbao, J. (1992). Stable Operation Conditions for Gas – Solid Contact Regimes in Conical Spouted Beds. **Ind. Eng. Chem. Res.** 31: 1784 – 1791.

Properties of wood. (n.d.). **Chemical composition of wood.** Available: http://www.paperonweb.com/wood.htm.

San José, M.J., Olazar, M., Peńas, F.J., Arandes, J. M. and Bilbao, J. (1995). Correlation for calculation of the gas dispersion coefficient in conical spouted beds. **Chemical Engineering Science.** 50 (13): 2161-2172.

San José, M.J., Olazar, M., Aguado, R., and Bilbao, J. (1996). Influence of the conical section geometry on the hydrodynamics of shallow spouted beds. **The Chemical Engineering Journal.** 62: 113-120.

San José, M.J., Olazar, M., Alvarez, S., Izquierdo, M.A., and Bilbao, J. (1998). Solid cross – flow into the spout and particle. **Chemical Engineering Science.** 53 (20): 3561-3570.

San José, M.J., Olazar, M., Alvarez, S., Orales, A., and Bilbao, J. (2005). Spout and Fountain Geometry in Conical Spouted Beds Consisting of Solids of Varying Density. **Ind. Eng. Chem. Res.** 44: 193–200.

Safi, M.J., Mishra, I.M., and Prasad, B. (2004). Global degradation kinetics of pine needles in air. **Thermochemica Acta.** 412: 155–162.

Sari, S., Kulah, G., and Koksal, M. (2012). Characterization of gas – solid flow in conical spouted beds operating with heavy particles. **Experimetal Thermal and Fluid Science.** 40: 132 – 139.

Smith, H. (n.d.). **The molecular biology of plant cells.** Available: http://ark.cdlib.org/ark:/13030/ft796nb4n2/.

The Watt Committee on Energy. (n.d.). Report No. 5. **Energy from the Biomass.** A series of papers presented to Watt Committee Consultative Council and since extended for publication, with the verbal and written discussion.

Tsai, W.T., Lee, M.K., and Chang, Y.M. (2006). Fast pyrolysis of rice straw, sugarcane bagasse and coconut shell in an induction-heating reactor. **Journal of Analytical and Applied Pyrolysis.** 76: 230-237.

Wikipedia The Free Encyclopedia. (n.d.). Available: http://en.wikipedia.org/wiki/Lignin.

Wooten, J.B., Seeman, J. I., and Hajaligol, M. R. (2004). Observation and Characterization of Cellulose Pyrolysis Intermediates by 13C CPMAS NMR. A New Mechanistic Model. **Energy Fuel**.18 (1): 1 – 15.

Yang, W.C. (2003). Handbook of Fluidization and Fluid – Particle System. Headquarters. New York.

Yang, H., Yan, R., Chen, H., Lee, D. H., and Zheng, C. (2007). Characteristics of hemicellulose, cellulose and lignin pyrolysis. **Fuel.** 86: 1781–1788.

Zabaniotou, A., Damartzis, T. (2007). Modelling the intra-particle transport phenomena and chemical reactions of olive kernel fast pyrolysis. **Journal of Analytical and Applied Pyrolysis.** 80: 187-194.

Wang, Z. (2006). **Experimental studies and CFD simulations of conical spouted bed hydrodynamics.** Thesis. The University of Britis Columbia.

CHAPTER III

BIOMASS PYROLYSIS IN A FREE FALL REACTOR

3.1 Abstract

Pyrolysis of biomass including palm shell, palm kernel, and cassava pulp residue was studied in a free fall reactor. The effects of pyrolysis temperature, sample particle size, and sweeping gas flow rate on the product distribution and kinetic parameters were investigated. The biomass precursors were pyrolyzed in a reactor under a constant flow of N_2. A higher temperature and smaller particle size increased the gas yield but decreased the char yield. Cassava pulp residue gave more volatiles and less char than palm kernel and palm shell. Increasing of sweeping gas flow rate in the range of 100 – 200 cm^3/min gave increased liquid yield and less gas yield. The two - parallel reaction model was introduced to simulate the pyrolysis kinetics of the three biomass precursors studied based on the weight loss of the solid product. Kinetic prediction by the two – parallel reactions model agreed very well with the experimental data for all biomass precursors studies under all pyrolysis conditions.

3.2 Introduction

Biomass – based fuels are non – fossil and renewable and are regarded as CO_2 neutral since biomass assimilates carbon dioxide from the atmosphere during growth period. Wood will remain one of the resources of renewable energy for the need of mankind for unpredictably long period of time. The relatively large amount of biomass used for energy generation in the developing countries comes from wood and traditional fuels. Wood and charcoal are historically used earlier than petroleum. Nowadays, biomass is becoming increasingly important as a renewable source of energy. The primary biomass fuel is wood waste, however, bagasses, straw, rice hull, shell hulls, and biomass grown as a fuel crop as well as other agriculture crops are becoming more popular. The chemistry of biomass is complicated but the major components which can be isolated by analytical methods are cellulose, hemicelluloses, lignin, organics extractive, and inorganic materials (Chiaramontia, Oasmaab and Solantaustab, 2007). Biomass is confined to use on site or a short distance off-site due to the low bulk density of it. This is the reason why it is difficult to transport and use biomass in many applications without substantial modification. When considering biomass as a fuel, the final goal is to convert the biomass into energy. Currently, there are several processes to convert biomass into energy such as, fermentation and thermal decomposition. On the basis of the end products, thermal decomposition can be classified as (1) direct combustion (2) gasification and (3) pyrolysis (Chiaramontia et al., 2007). The first kind of thermal decomposition, direct combustion, is the most straightforward method from which a complete oxidation process and heat is a primary objective. The second type of thermal decomposition, gasification is a partial oxidation process in the presence of an external supply of oxidizing agent, for example, air, pure oxygen or steam. Combustible gases including methane, carbon monoxide, and hydrogen are major products of gasification which can be primarily used either directly as fuel gas or used as synthesis gas for further conversion to a liquid fuel or a number of chemical products. The last process of thermal decomposition is pyrolysis which is the thermal decomposition of material in the absence of oxygen. During the pyrolysis, a substantial weight loss occurs due to devolatilization and decomposition of molecules. The products obtained are in the form of gas, liquid and the remaining solid called char.

Based on the pyrolysis time and heating rate the pyrolysis process can be classified into conventional and fast or flash pyrolysis. Conventional pyrolysis may also be termed “slow pyrolysis”. This type of pyrolysis is defined as the one which occurs under a slow heating rate (less than 10^{o}C/s), slow heat transfer rate in the reaction zone, and long mean residence time (Jain, Sharma and Singh, 1996). Normally, conventional pyrolysis has been used mainly for charcoal production. Conversely, fast or flash pyrolysis is a thermal decomposition process that occurs at a high heating rate and short mean residence time. Heating rate of flash pyrolysis is around 100^{o}C/s, or even 10,000^{o}C/s and the mean residence time is normally less than 2 seconds (Jain et al., 1996). Flash pyrolysis process generally produces 45-75 wt% of liquid, 15-25 wt% of solid and 10-20 wt% of non-condensable gases, depending on the feedstock used and pyrolysis conditions.

Generally, solid, liquid and gas products are of prime interest for used as a primary fuel. Furthermore, solid product for pyrolysis process can be utilized as a sorbent precursor. Nevertheless, several researchers (Acıkgoz, Onay, and Kockar, 2004, and Tsai, Lee, and Chang, 2007) have focused on investigating the effect of pyrolysis condition on maximizing the yield of pyrolytic liquids which have the potential to replace depleting petroleum oil reserves and as chemicals feedstocks. However, the liquid product from thermal decomposition process is composed of a large number of oxygenated compounds. The oil is combustible but its fuel properties do not conform to the standards of petroleum based fuels. It is therefore necessary to be upgraded along with some form of pretreatment before it can be used in any combustion systems. Due to the numerous utility of pyrolysis products as mentioned above, the work is focused on the biomass flash pyrolysis process to maximize the yield of liquid product.

In this work, a free fall reactor is proposed for the study of biomass flash pyrolysis. The primary purpose of this study is to gather information on – flash pyrolysis of isolated biomass particles that will help better understand the subsequent study on biomass pyrolysis in a conical spouted – bed reactor. A free fall reactor has been widely used in laboratory studies on flash pyrolysis because it provides high heating rate. Determinations of mass balance and mean residence time in this type of reactor are simple and straightforward (Lehto, 2007). Moreover, the mean residence time in this type of reactor can be moderately controlled (Lehto, 2007). Further, the single biomass decomposition kinetic parameters can be conveniently examined by using pyrolysis results from the free fall reactor.

When heated in the absence of oxygen, material undergoes a series of complex chemical changes. The nature of these changes and distribution and amounts of pyrolysis products depend on the type of materials, temperature, heating rate, and particle size. It is difficult to obtain an exact model of the pyrolysis mechanism. Proper design of such a reactor requires the understanding of mechanisms and kinetics of biomass pyrolysis. Several investigators have studied the pyrolysis of biomass and reported overall product yields (Ozlem, and Kockar, 2006), heat effects (Sezer, et al. 2008), and weight loss at different pyrolysis temperatures (Yang et al. 2006). However, a few kinetic data are available on the formation rates of the various pyrolysis products. Due to the large number of complex reactions involved in the pyrolysis process and the effect of the various pyrolysis parameters, different model approaches have been proposed for the pyrolysis of wood and other cellulosic materials such as the global kinetics model (Safi, Mishra, and Prasad, 2004), the Brodi-Shafizadeh model (Nagranad, 1997), the two-parallel reactions model (Luangkiattikhun, Tangsathitkulchai, and Tangsathitkulchai, 2007) and the three-pseudo component model (Hu, Jess and Xu, 2007). In this study, the two-parallel reaction model was adopted and used to describe the pyrolysis mechanism. According to Luangkiattikhun et.al (2007), the prediction by the two–parallel reactions model gave excellent fitting with the experimental data of all palm solid wastes under the pyrolysis condition investigated.

3.3 Models of Pyrolysis Kinetics

There are several models that have been proposed to describe the pyrolysis kinetics of biomass. However, since the two main components of biomass are holocellulose and lignin, it seems logical to adopt the two – parallel reaction model in analyzing the kinetics of biomass pyrolysis in the present work. The schematic representation of the pyrolysis reaction is shown according to Equations (3.1) – (3.3)

$$\text{Biomass} \xrightarrow{k} \text{Volatiles 1} + \text{Volatiles 2} + \text{Char} \tag{3.1}$$

$$W_1 \xrightarrow{k_1} \text{Volatiles 1} + \text{Char} \tag{3.2}$$

$$W_2 \xrightarrow{k_2} \text{Volatiles 2} + \text{Char} \tag{3.3}$$

where k_1 and k_2 are the rate constant of each reaction. The residual weight fraction of char components are defined as $\alpha = 1 - \frac{W_f}{W_O}$, where W_f is the final sample weight, and W_O is the initial dry sample weight.

The basic assumptions used in deriving the pyrolysis kinetic equations are that the reaction can be described by an n^{th} – order rate equation and there are no secondary reactions among the evolved gaseous products. Therefore, the decomposition kinetic reaction of Equation (3.2) and (3.3) can be written as:

$$\frac{d\alpha_1}{dt} = -A_1 \exp\left(-\frac{E_1}{RT}\right)\alpha_1^{n_1} \tag{3.4}$$

$$\frac{d\alpha_2}{dt} = -A_2 \exp\left(-\frac{E_2}{RT}\right)\alpha_2^{n_2} \tag{3.5}$$

where α_1 and α_2 are the residual weight fraction of the first and second components, A is the pre-exponential constant, E is the apparent activation energy, T is the absolute temperature, and R is the gas constant. The time variable (t) in Equation (3.4) and (3.5) can be transformed into the reactor length (L) by applying Stokes' law for calculating terminal velocity $\left(v_s\right)$ under laminar flow regime, as shown in Equation (5.6). Thus,

$$v_S = \frac{dL}{dt} = \frac{gd_p^2(\rho_S - \rho_f)}{18\mu_f} \tag{3.6}$$

By combining Equations (3.4) and (3.5) with Equation (3.6), we obtain the rate expressions in terms of reactor length, as shown in Equation (3.7). It is further assumed that (i) ρ_S is constant, (ii) d_p is constant (no particle shrinkage), (iii) Reynolds number is relatively small so that the flow is in the laminar regime, and (iv) temperature of the particle is basically equal to the temperature of the surrounding fluid, so that heat transfer resistance inside the particle can be neglected.

$$\frac{d\alpha_1}{\alpha_1{}^{n_1}} = A_1 \exp\left[\frac{-E_1}{RT}\right]\left[\frac{18\mu_f}{gd_p^2(\rho_s - \rho_f) - 18\mu_f v_f}\right]dL \tag{3.7a}$$

$$\frac{d\alpha_2}{\alpha_2{}^{n_2}} = A_2 \exp\left[\frac{-E_2}{RT}\right]\left[\frac{18\mu_f}{gd_p^2(\rho_s - \rho_f) - 18\mu_f v_f}\right]dL \tag{3.7b}$$

where μ_f is fluid viscosity (N.s/m^2), v_f is the initial fluid velocity calculated from the fluid superficial velocity (m/s), ρ_f is the fluid density (kg/m^3), ρ_s is the density of the solid particle (kg/m^3), g is the acceleration of gravity (m/s^2), d_p is the average diameter of solid particle (m). The temperature zones inside the reactor are displayed in Figure 3.1 which indicates that the reactor can be divided from the top of reactor into three consecutive regions: (i) preheating zone, (ii) heated zone and (iii) cooling zone. Therefore, the kinetic rates of reaction for the first and second component in the three zones of the reactor can be written as:

1. Preheating zone (Zone 1)

1st component: $$\frac{d\alpha_1}{\alpha_1^{n_1}} = \left[\frac{18\mu_{f,1}A_1}{gd_p^2(\rho_s-\rho_{f,1})-18\mu_{f,1}v_{f,1}}\right]\int_{0}^{0.45}\exp\left[\frac{-E_1}{RT_1(L)}\right]dL \tag{3.8}$$

2nd component: $$\frac{d\alpha_2}{\alpha_2^{n_2}} = \left[\frac{18\mu_{f,1}A_2}{gd_p^2(\rho_s-\rho_{f,1})-18\mu_{f,1}v_{f,1}}\right]\int_{0}^{0.45}\exp\left[\frac{-E_2}{RT_1(L)}\right]dL \tag{3.9}$$

2. Heated zone (Zone 2)

1st component: $$\frac{d\alpha_1}{\alpha_1^{n_1}} = \left[\frac{18\mu_{f,2}A_1}{gd_p^2(\rho_s-\rho_{f,2})-18\mu_{f,2}v_{f,2}}\right]\int_{0.45}^{0.60}\exp\left[\frac{-E_1}{RT_2}\right]dL \tag{3.10}$$

2nd component: $$\frac{d\alpha_2}{\alpha_2^{n_2}} = \left[\frac{18\mu_{f,2}A_2}{gd_p^2(\rho_s-\rho_{f,2})-18\mu_{f,2}v_{f,2}}\right]\int_{0.45}^{0.60}\exp\left[\frac{-E_2}{RT_2}\right]dL \tag{3.11}$$

3. Cooling zone (Zone 3)

1st component: $$\frac{d\alpha_1}{\alpha_1^{n_1}} = \left[\frac{18\mu_{f,3}A_1}{gd_p^2(\rho_s-\rho_{f,3})-18\mu_{f,3}v_{f,3}}\right]\int_{0.60}^{1.10}\exp\left[\frac{-E_1}{RT_3(L)}\right]dL \tag{3.12}$$

2nd component: $$\frac{d\alpha_2}{\alpha_2^{n_2}}=\left[\frac{18\mu_{f,3}A_2}{gd_p^2(\rho_s-\rho_{f,3})-18\mu_{f,3}v_{f,3}}\right]\int_{0.60}^{1.10}\exp\left[\frac{-E_2}{RT_3(L)}\right]dL \qquad (3.13)$$

The weight fractions of biomass components during pyrolysis (α_1 and α_2) in Equation (3.8) to (3.13) were solved by numerical method using the classical Fourth - Order Runge-Kutta algorithm. The initial weight of the first and second components (α_1 and α_2 at t = 0) is designated as *a* and *b* and the sum of the two numbers equals to unity. The final weight of residue leaving one zone will be the initial weight for the next adjacent zone. To simplify the calculation, fluid properties that appear in the kinetic rate equations were kept constant at the average temperature of that zone. $T_1(L)$ and $T_3(L)$ are the temperatures at the exit of the preheating and cooling zone of the reactor, respectively, which depend on the reactor length. The estimation of these temperatures at various positions along the reactor was obtained from the measured reactor temperature profile as shown in Figure 3.2. The temperature of the heated zone (T_2) is considered constant and its value was also derived from the reactor temperature profile. The kinetic parameters of the model (n, A and E) were determined by using the nonlinear least square (NLS) algorithm to minimize the objective function defined as: $\text{O.F.}=\sum_{i=1}^{N}(w_{cal,i}-w_{exp,i})^2$, where $w_{exp,i}$ and $w_{cal,i}$ represent the experimental and calculated mass fraction. Subscript i denotes the discrete values of w, and N is the number of data points used in the least-squares fitting.

3.4 Research Methods

3.4.1 Feedstock Preparation and Characterization

The pyrolysis tests were carried out with three types of biomass: palm shell (PS), palm kernel (PK), and cassava pulp residue (CPR). These materials were first crushed by a jaw crusher, and then screened to obtain the average screen size in the range of 0.18 to1.55 mm. The materials were then dried at 110°C for 24 hours in an oven to remove the excess moisture. Also, the material characterization was made for the proximate and ultimate analysis. Proximate analysis of biomass precursor was evaluated by following ASTM method which gives the following information: (1) moisture content (ASTM D2867 – 95), (2) volatile matter (VM) (ASTM D5832 – 95), (3) ash (ASTM D2866 – 94) or inorganic material left behind when all organic substances have been burned off and (4) fixed carbon (FC) which is defined by %FC = 100 - [%Moisture + %VM + %Ash]. Ultimate analysis was used to determine carbon, nitrogen, hydrogen, oxygen, and sulfur content. The analysis was performed by CHNS/O analyzer (Perkin Elmer PE2400 Series II). The true densities of dried biomass precursor were characterized by using a pycnometer analyzer (AccuPyc 1330 Micromeritics) with helium being used as the displacement fluid. In addition, thermal decomposition of biomass precursors was evaluated by a thermo – gravimetric analyzer (SDT 2960 simultaneous DSC – TGA model, TA instruments) which is one of the most widely used techniques to measure the weight loss of a material as a function of increasing temperature and time. In this analysis, biomass sample approximately 10 mg of 0.18 mm particle size was placed in a silica-alumina pan and then put in the microbalance installed in the reactor chamber. Purified nitrogen gas (99.99% purity) was fed into the reactor chamber as the purge gas to provide an inert atmosphere for pyrolysis and to remove any gaseous and condensable products evolved. The furnace was heated at a constant heating rate of 10^{o}C/min from ambient temperature to a set temperature of 900^{o}C. The sample mass was monitored and recorded continuously by microbalance as a function of temperature and time.

3.4.2 Pyrolysis Experiments

The pyrolysis of biomass samples was performed in a stainless steel free fall reactor at different pyrolysis conditions. The reactor with a length of 110 centimeter, inner diameter of 4.1 centimeter was inserted in a vertical electrically heated tube furnace (Carbolite, UK) of the same length with a central heated zone of 15 centimeter. Figure 3.3 shows the experimental set – up of the pyrolysis study. During the pyrolysis, nitrogen gas (99.5% purity) was continuously supplied in the downward direction through a reactor from a gas cylinder and its flow rate was regulated and measured by a pressure regulator and a rotameter. Details of operating conditions employed for each biomass was shown in Table 3.1. An adjustable screw feeder was used for continuous feeding of the biomass sample from the top of the reactor. The solid product after pyrolysis was collected in a bottom solid collector. Pyrolysis tests were carried out at various temperatures to obtain information on biomass weight loss. The pyrolysis vapor flew through a condenser to collect the liquid product. The condenser operated at – 10^{o}C using a temperature controlled water bath filled with a glycerin – water mixture. The solid product and the liquid product in the condenser were collected and weighed and the respective product yields based on the initial biomass feed were determined. Finally, gas yield was calculated by mass balance, knowing the yields of total collected solid and liquid products.

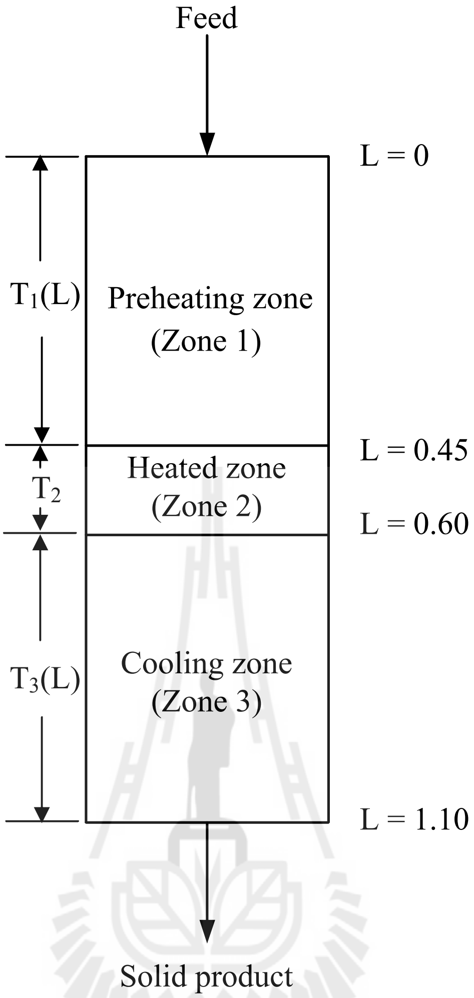

Figure 3.1 Schematic diagrams of each zone in a free fall reactor unit.

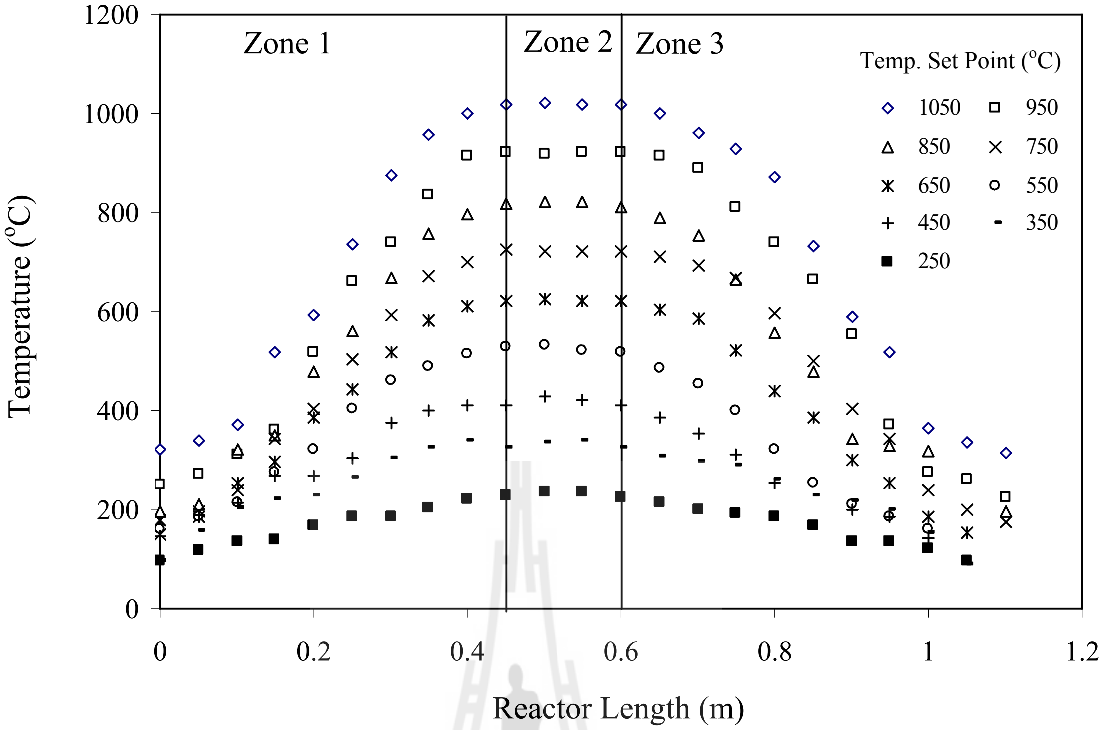

Figure 3.2 Temperature profile in a free fall reactor.

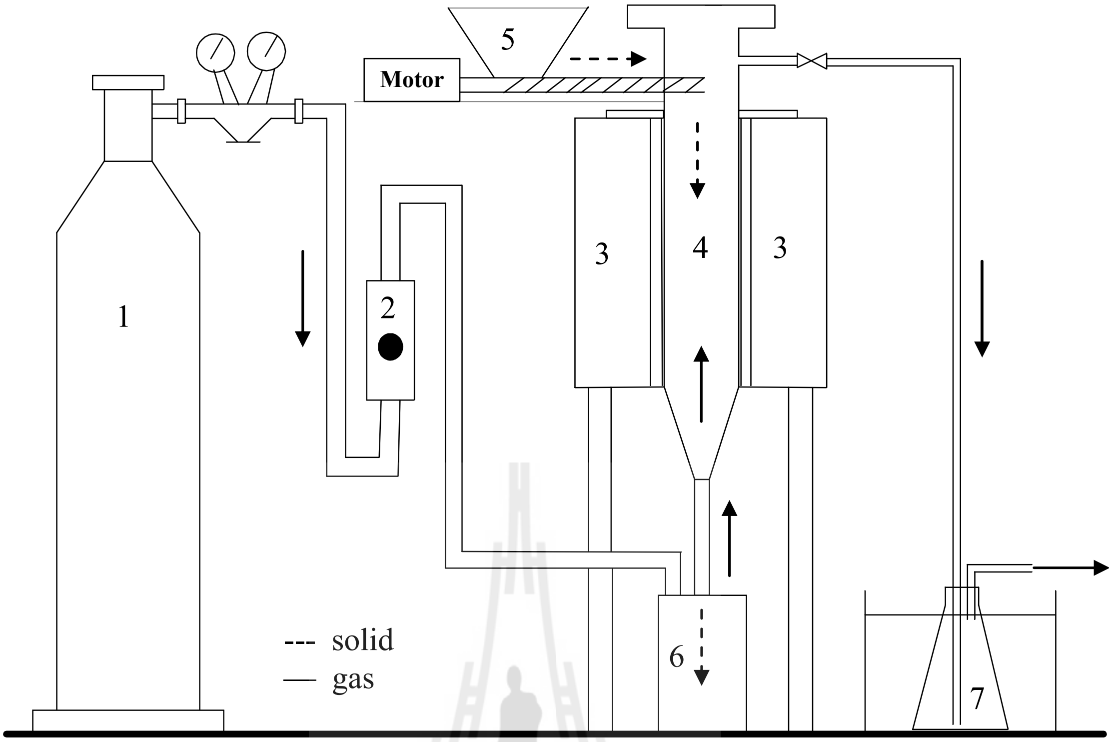

(1) Nitrogen tank cylinder
(2) Flow meter
(3) High temperature vertical tube furnace
(4) Stainless steel free – fall reactor
(5) Raw material feeder
(6) Solid product collector
(7) Condenser

Figure 3.3 Schematic diagram of the free fall reactor unit.

Table 3.1 Pyrolysis operating conditions

Biomass	Tempertue (^oC)	Inert gas flow rate (cm^3/min)	Average Particle Size (mm)	Biomass Feed Rate (g/min)
PS	250-1050	200	0.18-1.55	0.6
PK	250-1050	200	0.28	0.6
CPR	250-1050	200	0.28	0.6

PS = Palm Shell, CPR = Cassava Pulp Residue, PK = Palm Kernel

3.5 Results and Discussion

3.5.1 Biomass Properties

Table 3.2 presents the proximate and ultimate analysis of the biomass precursors. It is seen that the biomass sample contains more than 70% of volatile matters. The high volatile matter found in the samples suggests the high potential of this residue for energy production by pyrolysis (Wu, Dai, Shiraiwa, Sheng and Fu, 1999). High levels of volatile matter result in more liquid and gas fuel to be obtained from the pyrolysis process. The fixed carbon content is the carbon found in the biomass that is left after volatile matters are driven off and it is used as an estimate of the amount of solid product left after the pyrolysis of biomass (Hutagalung, 2008). The fixed carbon reported in Table 3.2 indicates that the solid yield of pyrolysis from palm shell is higher than those of palm kernel and cassava pulp residue. Table 3.2 indicates that the carbon content of biomass precursor varied from 41.27 to 47.91%. Generally, higher carbon content leads to a higher heating value of combustion (Demirbas, 2007), thus making these biomass to be good precursors for energy production. The data also indicate that sulfur content in biomass precursors is

Table 3.2 Proximate and ultimate analysis of oil-palm shell, oil-palm kernel and cassava pulp residue

Biomass	**Ultimate analysis (%wt)**					**Proximate analysis**			**Bulk density$^{(1)}$ (g/cm^3)**
	C	**H**	**N**	**S**	**O**	**Volatile**	**Fixed carbon**	**Ash**	
PS	47.91	5.83	0.76	0.32	42.28	72.56	25.97	1.47	0.65
PK	41.27	5.77	2.93	0.06	44.11	79.68	16.78	3.54	0.61
CPR	42.46	6.01	0.39	0.07	49.64	83.86	12.12	4.02	0.31

(1) Particle size of 1.55 mm

much lower than most typical fossil fuels (bituminous coal 0.5 – 1.5%, typical distillate oil 0.2 – 1.2%) (Miller, n.d.). This suggests that thermal decomposition of biomass should give lower emission than fossil fuel. The reason that biomass fuels are almost devoid of sulfur and coupled with low ash content, make biomass a highly desirable fuel from the standard point of pollution control cost. In addition, the composition of ash which contains alkaline metals (e.g. Na, K, Mg, Ca) can react with the released sulfur dioxide. Overall, the use of biomass as a fuel creates less environmental problems. The true densities of the three biomasses indicate that particles of palm shell are more densely packed than those of palm kernel and cassava plum residue, respectively.

3.5.2 Thermal Behavior of Biomass

In this work TGA is used an analytical technique to study the thermal decomposition of biomass sample in an inert atmosphere of N_2. The results of TGA analysis are displayed in Figure 3.4 which show the weight loss curves (TG) and derivative thermogravimetric (DTG) evolution profiles, respectively, as a function of temperature. As can be observed, the cassava pulp residue started to decompose first

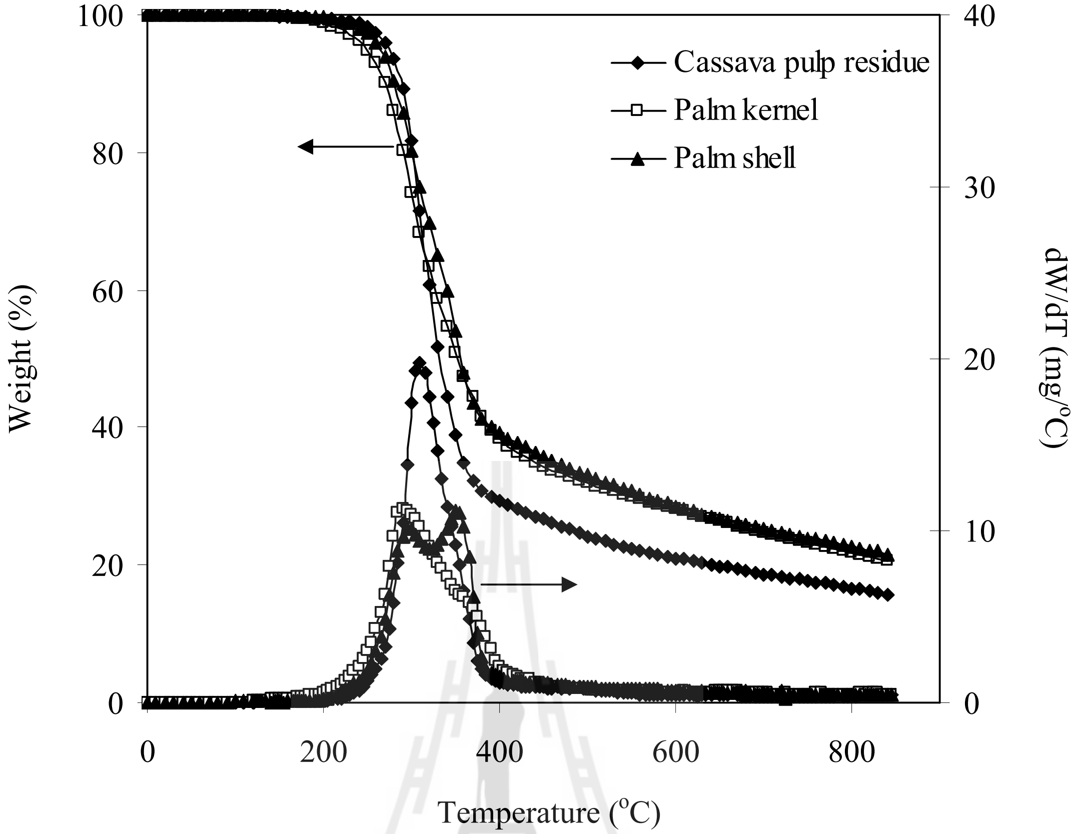

Figure 3.4 TG and DTG data of palm shell, palm kernel and cassava pulp residue.

followed by palm kernel and palm shell. Thermal decomposition of the biomass started at approximately 250^{o}C, possibly by the liberation of inherent moisture. Then it was followed by a major loss of weight where the main devolatilization occurs at approximately 250 ~ 400^{o}C. In the temperature range of 200 - 400^{o}C differences in weight loss behavior for the three samples exist: cassava pulp residue and palm kernel showed one DTG peak while palm shell exhibited two peaks. This is attributed to the differences in the cellulosic composition of the biomass and the pyrolysis behavior of each biomass component. Typically, hemicellulose decomposition occurs over the temperature of 200-260^{o}C (Prins, Ptasinski, and Janssen., 2006), cellulose between

240-350^{o}C (Wooten, Seeman, and Hajaligol, 2004), and lignin decomposes when heated over the range 280-500^{o}C (Prins et al., 2006).

3.5.3 Pyrolysis in a Free Fall Reactor

The effect of pyrolysis temperature, particle size, biomass type and sweep gas flow rate on the product yields of biomass pyrolysis is discussed first. On studying the effect of pyrolysis temperature and particle size, the experiments were conducted on palm shell with nine different final pyrolysis temperatures (heated zone temperature) and six different particle size ranges under a fixed sweep gas flow rate of 200 cm^3/min. The next set of experiments was performed for different precursors under a fixed sweep gas flow rate of 200 cm^3/min and particle size of 0.28 mm. For the effect of sweep gas velocity, the experiments were carried out at 100, 200 and 400 cm^3/min of inert gas velocity with varying final temperatures for a fixed particle size of 0.28 mm and with only one types of biomass precursor of palm shell.

Figure 3.5 shows the final solid, liquid, and gas yield from palm shell pyrolysis expressed as the fraction of the initial sample weight for different particle sizes and pyrolysis temperatures. For all particle sizes the solid yields continuously decreased as the temperature was increased (see Figure 3.5 (a)). At high pyrolysis temperature, the solid yields tended to become constant close to the value of 15% except for particle sizes greater than 0.36 mm and the highest conversion is achieved for the smallest biomass particle. The following observations can be drawn regarding the thermal decomposition behavior: (i) thermal decomposition of the biomass sample started at approximately 250^{o}C and essentially completed at approximately 950^{o}C for particle size between 0.18 – 0.28 mm, (ii) thermal decomposition of the biomass sample started at approximately 450^{o}C and essentially completed at approximately

950°C for the particle size of 0.36 mm, and (iii) for the average particle size larger than 0.36 mm (0.51 and 1.55 mm in this case), the thermal decomposition started at temperature higher than 450°C and requires temperature higher than 1000°C in order to complete the decomposition. It is noted from Figure 3.5 (a) that at a fixed pyrolysis temperature, the solid yield increased with increasing in particle size. This can be explained by the fact that a larger size particle has greater temperature gradient due to the longer heat diffusional path. This effect leads to a lower average particle temperature and hence giving less solid conversion by the pyrolysis reaction. As a result, to cover a wide range of solid yield or solid conversion for large particle size, it is necessary to extend the length of heated zone of the reactor to allow sufficient time for more solid decomposition.

During pyrolysis the solid phase is decomposed into liquid and gas causing structural changes. Figure 3.5 (b) shows the effect of palm shell particle size and pyrolysis temperature on the yields of liquid product. The liquid yield increased with increasing of the pyrolysis temperature and pass through a maximum at temperature around 650°C for particle size of 0.18 mm and at 750°C for particle size in the range of 0.23 – 0.36 mm. For particle size larger than 0.36 mm, the liquid yield tended to increase with increasing pyrolysis temperature but showed no existence of the optimum temperature. The decrease in liquid yield and increase in gas yield (see Figure 3.5 (c)) above the optimum pyrolysis temperature are probably due to the decomposition of some liquid vapors in the gas product. It is also noted that there was no liquid product being obtained from the pyrolysis of the largest size of 1.55 mm at the temperature below 1000°C. From Figure 3.5(c), it is seen that higher pyrolysis temperature and small particle size led to more volatilization resulting in higher yield

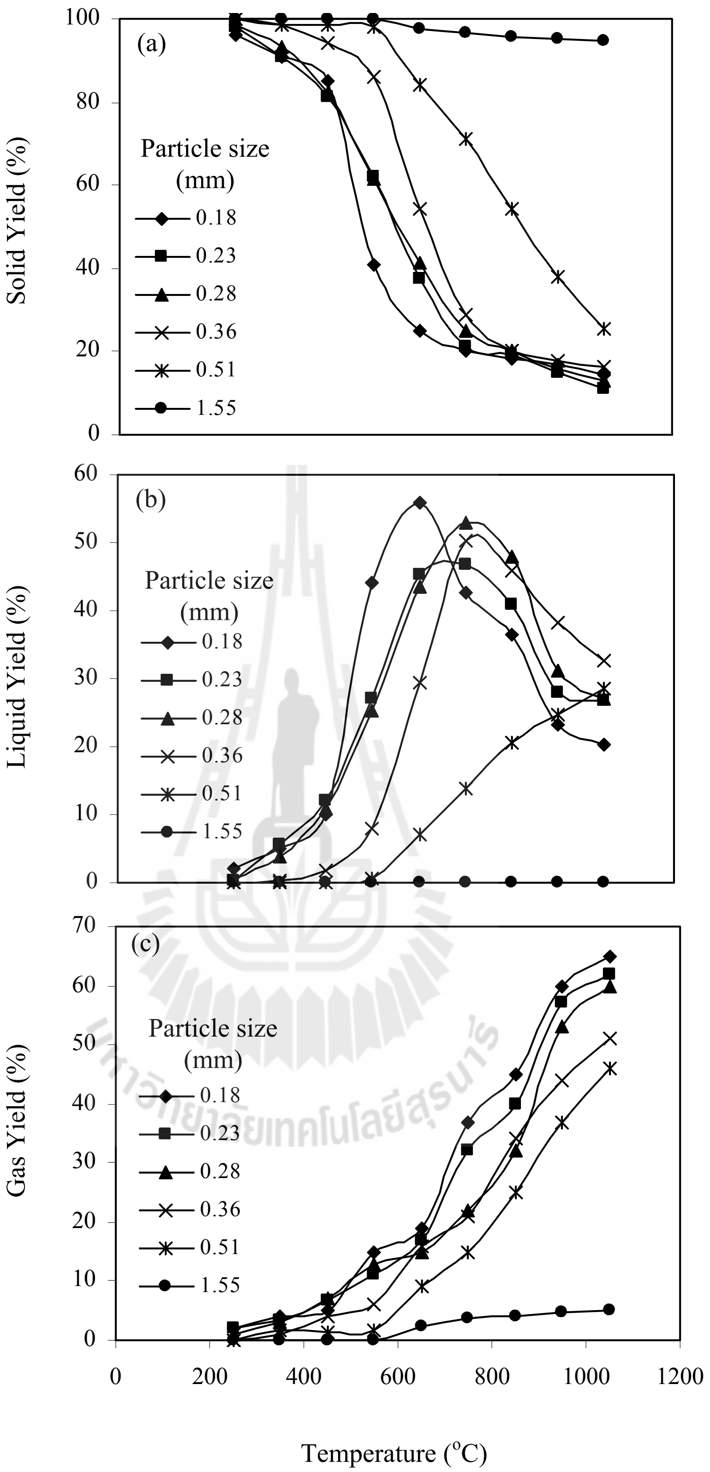

Figure 3.5 Effect of particle size and pyrolysis temperature on (a) solid yield, (b) liquid yield and (c) gas yield (Palm shell feed rate 0.6 g/min and sweep gas flow rate 200 cm^3/min).

of gaseous products. The increase in gaseous products is believed to be predominantly due to secondary cracking of the pyrolysis vapors at higher temperatures (Mohan et al., 2006). At high temperatures both the rate of primary pyrolysis and the rate of thermal cracking of tar to gaseous products are expectedly high. A smaller particle is more favorable for higher gas yield. The heating rate and heat flux are higher in small particles than in the larger particles. Therefore, in the smaller particle the produced gas leaves the particle faster than from large particles and hence increasing the residence time of gas in the reactor (Zanzi, Sjöström, and Björnbom, 1995). This observation agrees with the work of Wei et al. (2006) who studied the effect of particle size on products distribution from pyrolysis of pine sawdust and apricot stone in a free fall reactor at 800°C. They reported that decreasing of biomass particle size contributes to an increase in the gas yields.

Figure 3.6(a) shows the solid yields of biomass pyrolysis derived from palm shell, palm kernel and cassava pulp residue at various pyrolysis temperatures. The cassava pulp residue started to decompose at a lower pyrolysis temperature than palm kernel and palm shell. These results are also consistent with the results from the TGA analysis (Figure 3.4). The decomposition of these three biomasses started at the temperature near 250°C and completed at the temperature about 950°C which is higher than the temperature in TGA. This may be due to the difference in the heat transfer history of the two systems. The rate of decomposition was more rapid in the range of 250°C to 750°C. Increasing of pyrolysis temperature above this range exerts less effect on the decomposition rate of biomass precursor because biomass precursor now contains less volatile contents. It is also found that the thermal decomposition behavior of biomass was consistent with the value of volatile matter. Biomass with a high volatile matter can be easily decomposed by heating than that with lower volatile matter. Therefore, cassava pulp residue which has the highest amount of volatile matter (83.86 wt%) could decompose more readily than palm kernel (79.62 wt%) and palm shell (72.56 wt%), respectively. The yield of liquid product (Figure 3.6 (b)) was found to increase with pyrolysis temperature to give a maximum value at around 400^{o}C for cassava pulp residue and 520^{o}C for palm shell and palm kernel and then decreased with increasing pyrolysis temperature. It appears that a fairly sharp optimum temperature exists at which maximum yield of liquid product was achieved is probably due to a more drastic cracking of the selected biomass precursor at that temperature. The decrease in liquid yields and increase in gas yields above the optimum temperature (see Figure 3.6(c)) are probably due to secondary cracking of the pyrolysis vapor at relatively high temperatures (Ozlem and Koçkar, 2006). However, the secondary decomposition of the char at higher temperatures may also give non – condensable gaseous product (Patrick and Williams, 1996). In addition, Figure 3.6(c) shows the gas yield to increase over the whole temperature range and the pyrolysis of cassava pulp residue gave higher gas product than palm kernel and palm shell. This is probably due to the differences of cellulosic components of these biomasses. The cellulose and hemicellulose components of biomass are mainly responsible for the volatile portion of the pyrolysis products while lignin is the main contributor to the formation of char (Ozlem and Koçkar, 2006).

Pyrolysis of palm shell biomass at different N_2 gas flow rate was studied under pyrolysis temperature range of 250 to 1050°C, average particle size of 0.28 mm, and at biomass feed rate of 0.6 g/min. Results in Figure 3.7 indicate the effect of sweeping gas flow rate (100 – 400 cm^3/min) on the pyrolysis product yields. Sweep gas flow rate through the reactor affects the contact time between primary vapors and hot char and also affects the degree of secondary char formation (Zaror, Hutchings, Pyle and Stiles and Kandiyoti, 1985). When the flow of N_2 gas was increased from 100 – 200 cm^3/min, the liquid yield increased while the gas yield decreased. Increasing the flow of N_2 gas causes the rate of removal of pyrolysis vapour products from the hot zone. It is noted that, N_2 gas flow seems to have no definite effect on the solid yield. As reported in the literature (Ozlem and Koçkar, 2006), sweep gas flow rate greater than 100 cm^3/min had no significant effect on the solid and liquid product yields. It is probable that the sweep gas flow rate of 100 cm^3/min is enough to remove the pyrolysis volatile products from the heated zone.

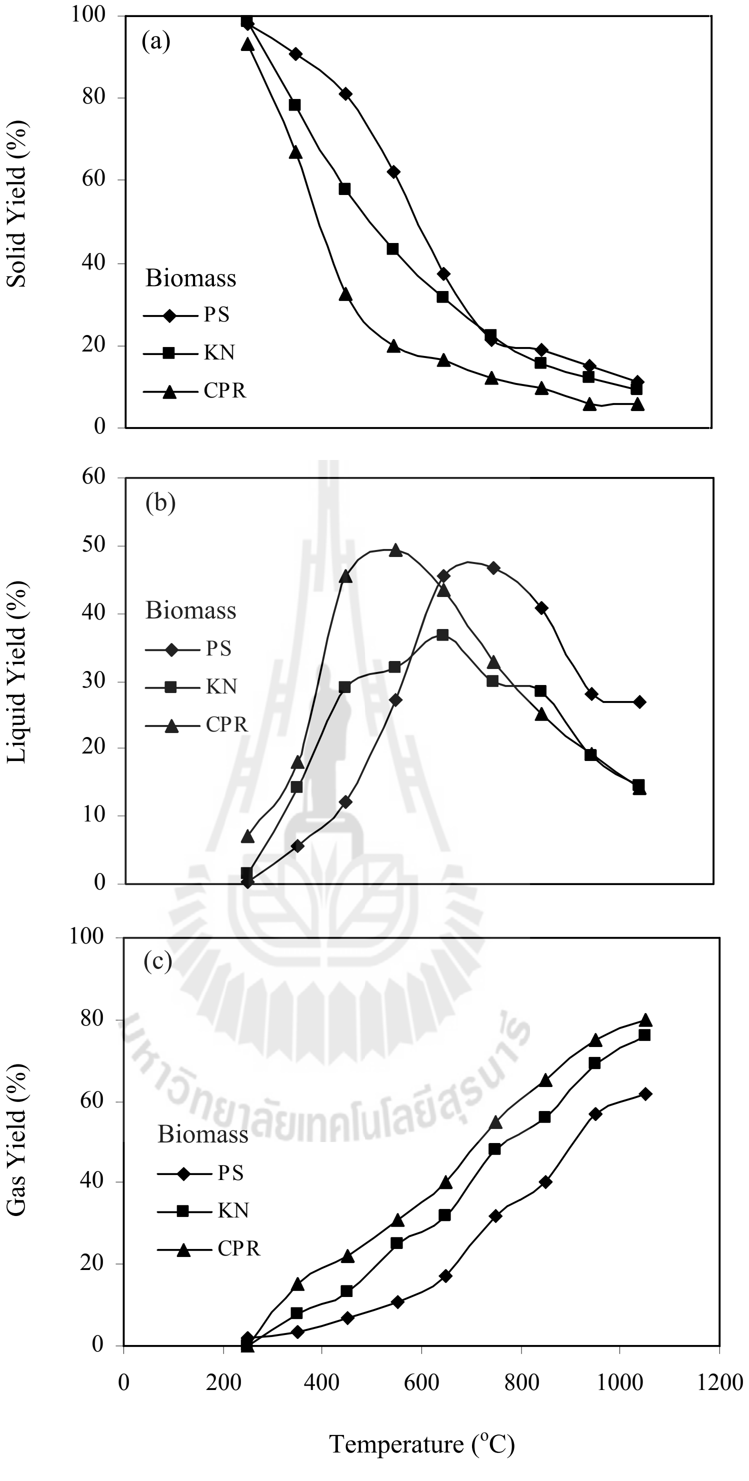

Figure 3.6 Effect of biomass type and pyrolysis temperature on (a) solid yield, (b) liquid yield and (c) gas yield (Biomass feed rate 0.6 g/min, sweep gas flow rate 200 ml/min and particle size of 0.28 mm).

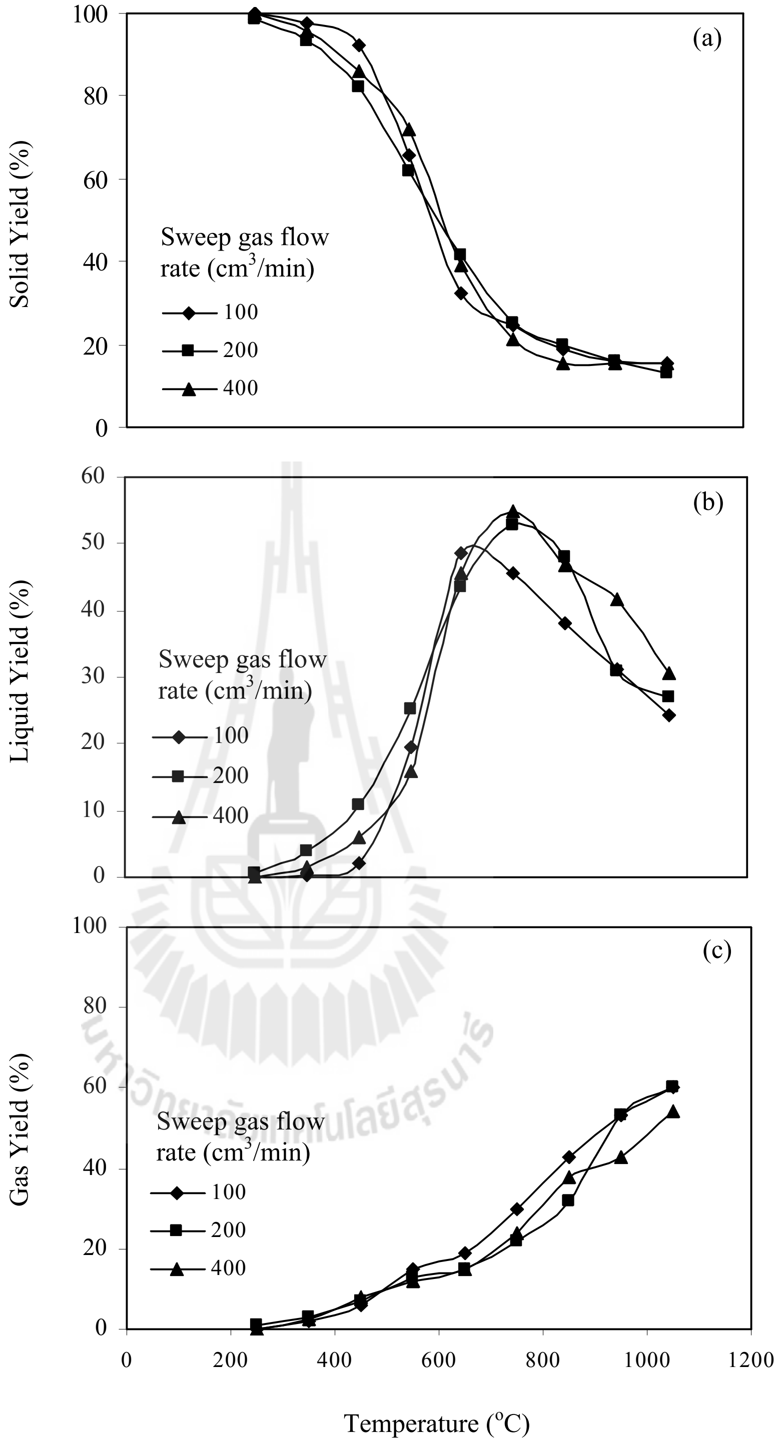

Figure 3.7 Effect of sweep gas flow rate and pyrolysis temperature on (a) solid yield, (b) liquid yield and (c) gas yield (Palm shell feed rate 0.6 g/min and particle size 0.28 mm).

3.5.4 Kinetics of Biomass Pyrolysis

Figure 3.8 and 3.9 compares the calculated and experimental solid yields as a function of heated zone temperature showing the effects of particle size and type of biomass, respectively. The results show a satisfactory agreement between the experimental data and the model prediction in this study. The kinetic parameters (E, A and n), maximum error, and correlation coefficient calculated from the model are summarized in Table 3.3. It was found that for almost all conditions, the value of the correlation coefficients by the model was higher than 0.98 except for palm shell of particle size 1.55 mm. This proves that the kinetic model proposed in this study can be used to describe the mass loss behaviors within acceptable accuracy, except for a relatively large size particle.

Generally, the apparent activation energy, pre – exponential constant and reaction order are three important parameters from the point of view of the evaluation of stability and compatibility for energetic material. Activation energy may also be defined as the minimum energy required to start a chemical reaction. The high value of activation energy indicates that the chemical reaction requires a large amount of energy to initiate the reaction. As is evident from Table 3.3, the activation energy of the second component (E_2) appears to have lager values than those of the first component (E_1). This indicates that the second component requires a larger amount of energy to initiate the pyrolysis reaction than that of the first component. In addition, the larger value of *a* in comparison with that of *b* indicates that the decomposition of palm shell and palm kernel are mainly contributed by the first component. However, the results further indicate that the decomposition of cassava pulp residue is mainly contributed by the second component because of the larger value of *b*.

Table 3.3 shows that the pre-exponential constants (A_1 and A_2) of both components also tended to increase with increasing particle size of palm shell except A_2 for the largest size of 1.55 mm. However, no clear correlation exists between the reaction order (n) and the particle size. Generally, the kinetic parameters of pyrolysis should be constant and independent of particle size if the process is a true purely kinetic control. The reason of this inconsistency should result from the influence of heat and mass transfer limitations. It is noted that a mathematical model in this work is based on the assumption of pure kinetic control without the effects of heat and mass transfer resistance and drag coefficient was also assumed constant.

The variation of solid yield of different biomass precursors as a function of pyrolysis temperature is illustrated in Figure 3.9. Over the pyrolysis temperature range studied, the solid yield of cassava pulp residue was lower than the solid yields of palm kernel and palm shell. This indicates that cassava pulp residue decomposed faster than both palm kernel and palm shell. These results are consistent with the lower values of E_1 and E_2 calculated from the model. Evidently, reaction with high activation energy will proceed slower than that with lower activation energy. Furthermore, an endothermic reaction was assumed for all pyrolysis reactions in this work which reflects the positive sign for the activation energy.

Based on the obtained kinetic parameters, the predicted profiles of solid yield versus the length of a free – fall reactor are presented in Figure 3.10. As seen, palm shell (0.28 mm in size) starts to decompose in the first zone and appears to reach the completion of devolatilization in the second zone of the reactor. Also, the decomposition of biomass precursor does not occur at a relatively low pyrolysis temperature of 250°C. At this temperature the weight loss of only 1 wt% is found.

In addition, knowing the average mean residence time of the biomass precursor in the reactor would also indicate whether such a reactor length is reasonable. However, the calculation of the actual mean residence time is very complex and was not attempted here. The properties of biomass particles (e.g., particle size and particle density) continuously change during the pyrolysis process. Instead, the mean residence time was approximately estimated by using Stokes'law, $v_S = \frac{dL}{dt} = \frac{gD_p^2(\rho_S - \rho_f)}{18\mu_f}$. Also, the mean residence time can be calculated by the integral solution of Stokes'law equation, $t = \frac{18\mu_f L}{gD_p^2(\rho_S - \rho_f)}$. Table 3.4 summarizes the mean residence time of palm shell at various particle sizes in the reactor at different pyrolysis temperatures. It is observed that particle size and temperature influence the mean residence time of biomass precursor in a reactor. The calculation results show that the mean residence time decreases with increasing in particle size. It is noted that the mean residence time should have a limited effect on the heat transfer by radiation from the surface of reactor to the biomass particle. Heat transfer by radiation could not occur for a short mean residence time. From the calculation results in Table 3.5, the mean residence time of small particle in the reactor is longer than the larger particle. Therefore, the decomposition of the smaller particles was greater as compared to the larger particles. Pyrolysis temperature exerts an influence on the mean residence time of biomass in a reactor particularly on a mean residence time of a small particle. Mean residence time appears to increase with increasing pyrolysis temperature for each particle size. Large particle has a very short mean residence time in a reactor because it can move significantly faster than a smaller particle. This is the reason that the decomposition did not occur at a low pyrolysis temperature for a large particle size.

Table 3.6 presents the mean residence time for each biomass at various pyrolysis temperatures. At the same pyrolysis temperature, cassava pulp residue showed the longest mean residence time in the reactor. This calculation results are consistent with the experimental results that the solid yields of cassava pulp residue was lower than those of palm kernel and palm shell.

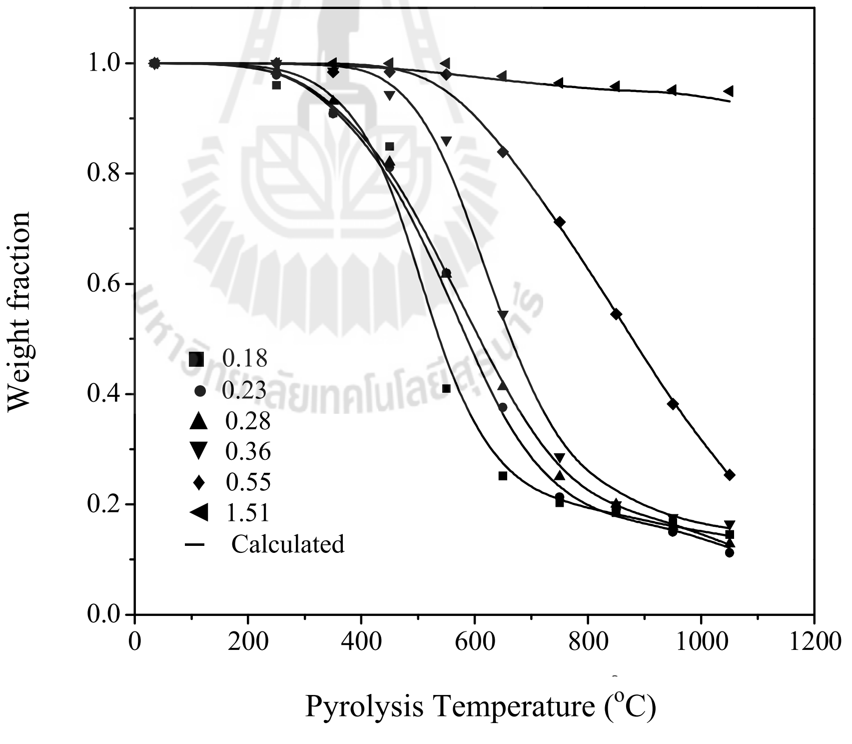

Figure 3.8 Weight fraction of solid product pyrolysis of palm shell in a free fall reactor at different pyrolysis temperature for various particle sizes (N_2 flow rate 200 cm^3/min).

Table 3.3 Kinetic parameters of the two-parallel reaction model of various biomasses in a free fall reactor.

Biomass	**Size (mm)**	**a**	**A_1 (s^{-1})**	**E_1 (kJ/mol)**	**n_1**	**b**	**A_2 (s^{-1})**	**E_2 (kJ/mol)**	**n_2**	**Max. error (%)**	**Correlation Cofficient (R^2)**
PS	0.18	0.7	1.94×10^4	74.88	1.57	0.3	4.39×10^6	76.47	7.65	4.21	0.9951
	0.23		1.28×10^5	71.60	5.22		4.70×10^6	118.11	1.85	8.67	0.9970
	0.28		1.28×10^5	70.36	5.15		4.70×10^6	116.84	2.17	1.73	0.9996
	0.36		2.20×10^5	95.46	1.78		5.50×10^6	78.69	7.15	4.83	0.9974
	0.51		1.00×10^6	100.61	5.63		1.31×10^7	147.02	2.02	1.84	0.9986
	1.55		1.20×10^7	41.66	32.47		2.53×10^5	305.92	2.00	1.96	0.8630
PK	0.28	0.54	2.58×10^5	66.45	2.52	0.46	5.80×10^6	109.87	4.46	4.40	0.9995
CPR	0.28	0.38	2.28×10^5	64.26	2.63	0.62	5.90×10^6	81.05	4.76	8.90	0.9800

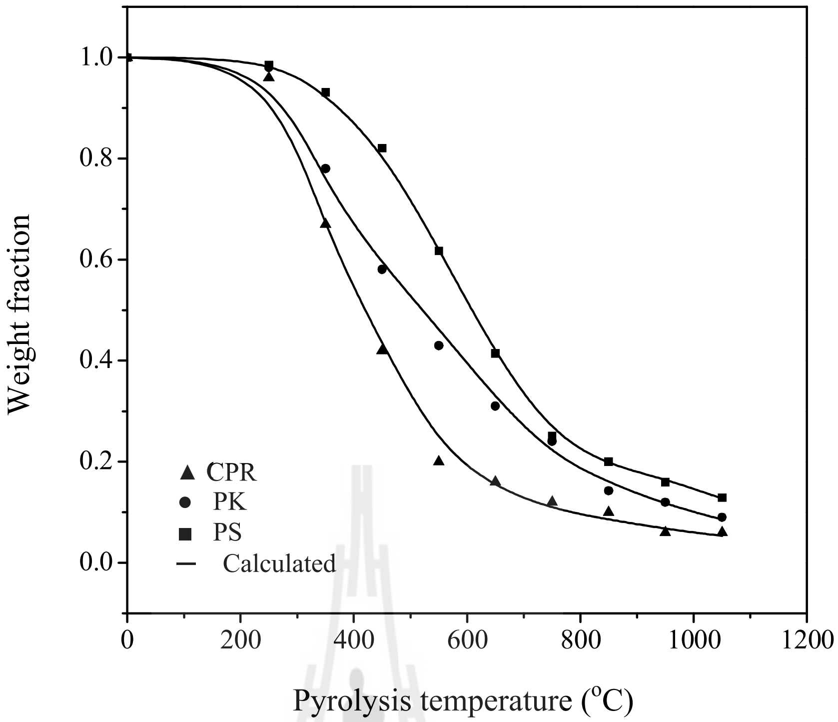

Figure 3.9 Weight fraction of solid product pyrolysis in a free fall reactor at different pyrolysis temperature for various biomass types (particle size 0.28 mm and N_2 flow rate 200 cm^3/min).

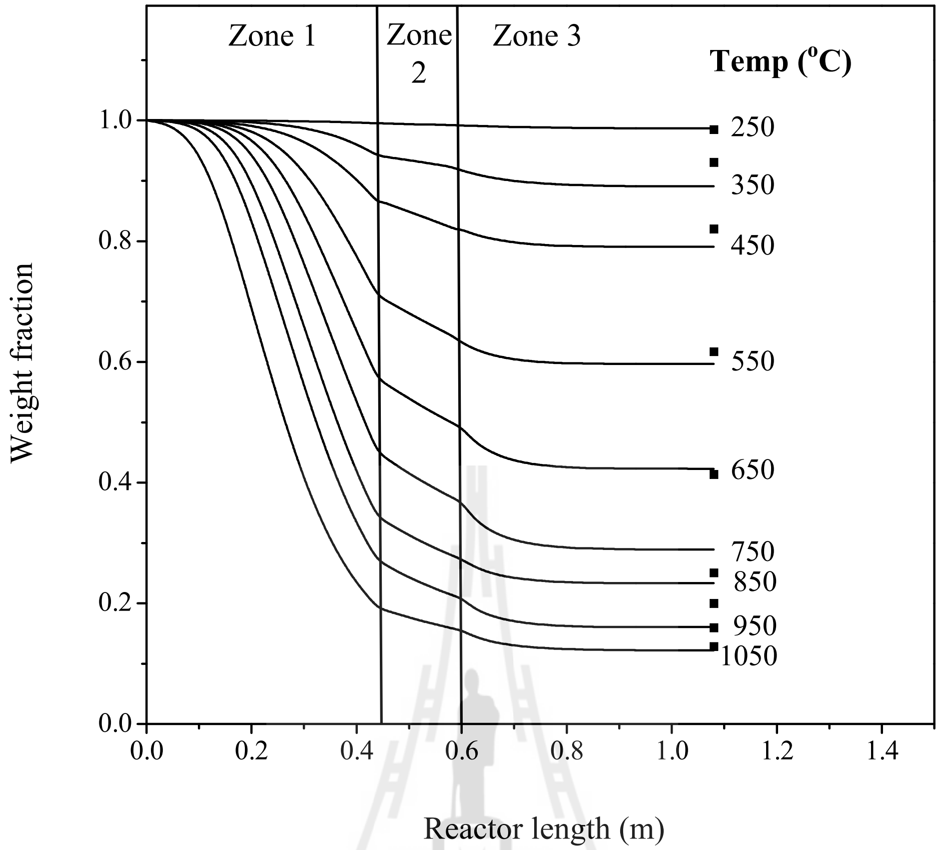

Figure 3.10 Weight fraction of solid product pyrolysis from the simulation program for palm shell at the average particle size of 0.28 mm and N_2 flow rate 200 cm^3/min (line is a simulation and dot is an experimental data).

Table 3.4 Calculated mean residence time of palm shell in a reactor at various pyrolysis temperatures and particle sizes.

Temperature (^oC)	Mean residence time (second)			
	0.18 mm	**0.28 mm**	**0.51 mm**	**1.55 mm**
250	1.40	0.54	0.17	0.02
350	1.61	0.64	0.19	0.02
450	2.04	0.85	0.20	0.02
550	4.17	1.19	0.22	0.02
650	7.49	1.92	0.23	0.03
750	9.81	3.28	0.25	0.03
850	11.58	4.53	0.26	0.03
950	13.78	5.29	0.26	0.03
1050	16.06	7.55	0.28	0.03

Table 3.5 Calculated mean residence time of various biomasses in a reactor under the same pyrolysis condition.

Temperature (^oC)	Mean residence time (second)		
	PS	**PK**	**CPR**
250	0.54	0.56	0.56
350	0.64	0.80	1.06
450	0.85	1.15	1.95
550	1.19	1.63	3.88
650	1.92	2.42	5.97
750	3.28	3.80	8.31
850	4.53	5.24	10.41
950	5.29	7.05	12.75
1050	7.55	10.07	16.61

3.6 Conclusions

Pyrolysis of three types of biomass precursors, including cassava pulp residue, palm shell, and palm kernel were investigated in a laboratory free fall reactor, consisting of three consecutive zones of preheating zone (Zone I), constant temperature heated zone (Zone II) and cooling zone (Zone III). The following conclusions can be drawn from this study.

- The char yield of cassava pulp residue, palm shell, and palm kernel decreased with increasing pyrolysis temperature.
- Pyrolysis temperature had no significant effect on the yield of char, gas, and liquid product when the particle size of palm shells was larger than 1.55 mm.
- The yield of liquid products increased significantly with increasing pyrolysis temperature and then decreased when the pyrolysis temperature reached the optimum value.
- Sweeping gas flow rate had no significant effect on the yield of char.
- Type of biomass precursor had a significant effect on the pyrolysis yield and pyrolysis product distribution.
- The two – parallel reaction model gave a good fitting with the experimental data for all biomass precursors under all pyrolysis conditions investigated.
- Biomass precursor started to decompose in the first zone and reached the completion in the second zone of the reactor.
- The mean residence time of larger particle size is shorter than the small size particle. At the same pyrolysis temperature, cassava pulp residue showed the longest mean residence time in the reactor.

3.7 References

Acıkgoz, C., Onay, O., and Kockar, O.M. (2004). Fast pyrolysis of linseed: product yields and compositions. **Journal of Analytical and Applied Pyrolysis.** 71: 417- 429.

Alves, S.S., and Figueiredo, J.L. (1988). Pyrolysis kinetics of lignocellulosic materials by multistage isothermal thermogravimetry. **Journal of Analytical and Applied Pyrolysis.** 13: 123 – 134.

Branca, C., and Di Blasi, C. (2003). Kinetics of the isothermal degradation of wood in the temperature range 528 – 708 K. **Journal of Analytical and Applied Pyrolysis.** 67: 207 – 219.

Chiaramontia, D., Oasmaab, A., and Solantaustab, Y. (2007). Power generation using fast pyrolysis liquids from biomass. **Renewable and Sustainable Energy Reviews.** 11: 1056–1086.

Demirbas, A. (2004). Combustion characteristics of biomass fuels. **Progess Energy Combustion Science.** 30: 219 – 230.

Grønli, M.G., Várhegyi, G., and Di Blassi, C.(2002). Thermogravimetric analysis and devolatilization kinetics of wood. **Industrial and Engineering Chemistry Research.** 41: 4201 – 4208.

Hu, S., Jess, A., and Xu, M. (2007). Kinetic study of Chinese biomass slow pyrolysis: Comparison of different kinetic models. **Fuel.** Available online 26 March 2007.

Hutagalung, M. (2008). Understanding coal analysis. **Majari Magazine** [On – line]. Available:http://majarimagazine.com/2008/06/understanding-coal-sample-analysis/

Jain, A.K., Sharma, S.K., and Singh, D. (1996). Reaction kinetics of paddy husk thermal decomposition. **Energy Research Center Panjab University** .India. Available:http://ieeexplore.ieee.org/iel3/4058/12000/00561172.pdf?arnumber =561172.

Lehto, J. (2007). Determination of kinetic parameters for Finish milled peat in conditions similar reactor and optical measurement techniques. **Fuel.** 85: 1656- 1663.

Luangkiattikhun, P., Tangsathitkulchai, C., and Tangsathitkulchai, M. (2007). Non-isothermal thermogravimetric analysis of oil-palm solid wastes. **Bioresource Technology.**

Mohan, et al. (2006). Pyrolysis of Wood/Biomass for Bio –oil: A Critical Review. **Energy & Fuels.** 20: 848 – 889.

Nugranad, N. (1997). **Pyrolysis of biomass.** Thesis. University of Leeds Department of Fuel and Enegy.

Ozlem, O., and Koçkar, O. M. (2006). Pyrolysis of rapeseed in a free fall reactor for production of bio-oil. **Fuel.** 85; 1921-1928.

Patrick, A.H., and Williams, T.P. (1996). Influence of temperature on the products from the flash pyrolysis of biomass. **Fuel.** 75(9): 1051 – 1059.

Prins, M.J., Ptasinski, K. J., and Janssen, F.J.J.G. (2006). Torrefaction of wood. Part 1. Weight loss kinetics. **Journal of Analytical and Applied Pyrolysis.** 77:28 - 34.

Safi, M.J., Mishra, I.M., and Prasad, B. (2004). Global degradation kinetics of pine needles in air. **Thermochimica Acta.** 412: 155–162.

Sezer, M., et al. (2008). Flash pyrolysis of Silopi asphaltite in a free - fall reactor under vacuum. **J. Anal. Appl. Pyrol.** doi: 10.1016/j.jaap.2008.01.003

Tsai, W.T., Lee, M.K., and Chang, Y.M. (2007). Fast pyrolysis of rice husk: Product yields and compositions. **Bioresource Technology.** 98: 22–28.

Wei et al. (2006). Characteristics of fast pyrolysis of biomass in a free fall reactor. **Fuel Processing Technology.** 87: 863 – 871.

Wu, Q., Dai, J., Shiraiwa, Y., Sheng, G., and Fu, Jiamo. (1999). A renewable energy source – hydrocarbon gases resulting from pyrolysis of the marine nanoplanktonic alga *Emiliania huxleyi*. **Journal of Applied Phycology**. 11: 137 – 142.

Wooten, J.B., Seeman, J. I., and Hajaligol, M. R. (2004). Observation and Characterization of Cellulose Pyrolysis Intermediates by 13C CPMAS NMR. A New Mechanistic Model. **Energy&Fuel; AN AMERICAL CHEMICAL SOCIETY JOURNAL.** 18.

Yang, H. et al. (2006). Pyrolysis of palm oil wastes for enhanced production of hydrogen rich gases. **Fuel Processing Technology.** 87: 935–942.

Zanzi, R., Sjöström, K., and Björnbom, E. (1995). Rapid pyrolysis of bagasse at high temperature. In **proceedings of the third Asian – Pacific international symposium on combustion and energy utilization** 1995 (pp. 211 – 215). Hong Kong:The Hong Kong Polytechnic University.

Zaror, C.A, Hutchings, I.S., Pyle, D. L., Stikes, H. N., and Kaydiyoti, R. (1985). Secondary char formation in the catalytic pyrolysis of biomass. **Fuel.** 64(7): 990 – 994.

CHAPTER IV

HYDRODYNAMIC STUDY OF A CONICAL SPOUTED BED SYSTEM

4.1 Abstract

Hydrodynamic behavior of a conical spouted bed system was studied by using air as a spouting fluid and oil palm shell particles as a disperse solid. The effects of initial static bed height, air superficial velocity and geometric factors including air inlet diameter and conical base angle on minimum spouting velocity, pressure drop across the bed, and expanded bed height were investigated experimentally. The minimum spouting velocity was found to increase with increasing of static bed height, gas inlet diameter, conical base angle, and particle size. The increasing in particle size led to the pressure drop increasing for all air inlet diameters and conical base angles. On the contrary, the pressure drop decreased with the increase of air inlet diameter for all static bed height, particle size diameter and conical spouted bed geometry. In addition, simulation of spouted bed behavior for air - palm shell particles was also performed by using the commercial CFD package software (ANSYS CFX 10.0). The simulated results were validated by comparison with those obtained from experiments under similar conditions. It was found that the minimum spouting velocity predicted from CFD simulation agreed very well with the experimental results. However, the pressure drop across the bed, and expanded bed height predicted from CFD

simulation differed greatly from experimental results. Moreover, the simulated results also indicated a significant decrease in the minimum spouting velocity when the bed temperature was increased.

4.2 Introduction

A spouted bed is a kind of high – performance reactor for contacting fluid and solid particles. This technology has been applied to a wide variety of chemical processes such as drying, coating, and gasification. According to Salam and Bhattacharya (2006), the difference between fluidized bed and spouted bed lies in the dynamic behavior of the solid particles. In a fluidized bed, air is passed through a uniform distributor plate to float the particles which move up and down in groups. In a spouted bed, air enters the bed through a small orifice at the center of a conical or flat base, instead of a uniform distributor, resulting in a systematic cyclic pattern of solid movement inside the bed. The hydrodynamic features of a spouted bed are significantly different from those of a fluidized bed. Compared with the fluidized bed, a spouted bed has several advantages, such as high efficiency of gas – solid contact, large capacity for handling coarse particles, stable operation over a wide range of gas flow rates, small pressure drop, and low air flow rate (Gong, Hu, and Li, 2006 and Olazar, San José, Aguayo, Arandes, and Bilbao, 1992). According to San José et al. (2005a) a spouted bed can be applied for irregular texture, fine particles, and those with a wide size distribution and sticky solids, whose treatment is difficult using other kinds of gas-solid contactors. The stability of the spouting regime depends on particle and fluid properties as well as the configuration and column dimensions geometry (Mathur and Epstein, 1974). The minimum spouting velocity is an important parameter for the proper design and scaling up of spouted beds. This parameter depends on a specific system having different bed dimensions, and particle and spouting gas properties. A crucial parameter that limits the scaling up of spouted beds is the ratio between the inlet diameter and particle diameter. The inlet diameter should be less than 20-30 times the average particle diameter in order to achieve spouting stability (Altzibar et al., 2009).

In recent years, a number of researches have been dedicated to spouted beds with new geometries such as conical shape. The hydrodynamics of conventional (conical – cylindrical) spouted beds have been extensively investigated (Wang, et al., 2001 and Duarte, Olazar, Murata, and Barrozo 2009). Conical spouted bed allows for strong gas – solid contact and stable operation over a wide range of gas flow rate. Thus, conical spouted beds are suitable for operating in a state of transition between the high voidage bed and diluted spouting bed regimes (Duarte, et al., 2008). They are also well suited for some applications that cannot be normally achieved in conventional spouted beds, such as particles with irregular texture or wide range of particle size distribution (San José et al, 2005a). As a result, a conical spouted bed can be equally applied in the pyrolysis process particularly for solids of irregular shape (Olaza, et al., 2005, Aguado, et al., 2002, and San José et al, 2005b).

Studies of numerical simulation techniques and computational fluid dynamics (CFD) have become popular in the field of gas – solid two-phase flow (TFM) and also the chemical kinetic characterization in several types of chemical reactors. The main advantage of numerical simulation is that the effect of a wide range of flow properties can be conveniently studied. Moreover, CFD is now an established engineering design tool that can provide the complete information required for the design and scale up of equipments and processes throughout the engineering profession, with the cheapest cost and short design time. Papadikis, Gerhauser and Bridgwate (2009), have applied CFD in a fluidized bed reactor, to understand the convective heat transfer to the surface of the particle of an in – flight cellulosic particle for a fast pyrolysis process.

According to Lettieri et al., (2003), CFD models for gas – solid flow can be divided into two groups, the Lagrangian – Eulerian models and Eulerian – Eulerian models. The Lagrangian approach describes the solid phase at the particle level and the gas phase as a continuum. The Eulerian – Eulerian approach, on the other hand, is based on the two – fluid model (TFM) that treats each phase as an interpenetrating continuum. Most of the fluidization modeling using TFM is based on applying granular kinetic theory to describe the characteristics of the particle phase. Duarte, Murata, and Barrozo (2005), applied the CFD to investigate the hydrodynamic behavior of a gas - solid flow in a conventional spouted bed. Their results showed that the CFD simulation gave a good agreement with the experimental data. Hence, in this work the CFD based on the two – fluid model was introduced to understand the hydrodynamic behavior of a conical spouted bed by using the commercial CFD simulation package ANSYS CFX 10.0. The effect of conical spouted reactor geometry, particle size, initial static bed height, and air inlet diameter on the minimum spouting velocity was investigated. As already noted, minimum spouting velocity is an important parameter used for the proper design and scale - up of a spouted bed system. Also, the comparison of numerical results with corresponding experimental data was made to validate the applicability of the numerical flow model. Furthermore, the results of hydrodynamic behavior in this chapter can be applied to a hydrodynamic design and specifying the pyrolysis condition for a conical spouted reactor as reported in chapter 5.

4.3 Research Methods

4.3.1 Hydrodynamics of a Conical Spouted Bed

Hydrodynamic study of a conical spouted bed was performed in a small-scale unit fabricated from a 2 mm thick transparent polyvinyl chloride (PCV) sheet and the oil palm shell particles were employed as the dispersed solid phase. Figure 4.1 and Table 4.1 show, respectively, the geometry and dimensions of the laboratory conical spouted bed column used in this study. Open U-tube manometer containing mercury was used to determine the static pressure of the spouted bed. In this work, three different inclination base angles ($\gamma = 28$, 45 and 60^{o}) were tested. The effect of particle size (1.09 – 2.18 mm) and the initial bed height (5 – 9 cm) on the minimum spouting velocity of palm oil shell in a conical spouted bed were investigated. In running the test, air flow rate was gradually increased until a steady spouting was achieved. After that, the air flow rate was gradually reduced until the observed spouting just collapsed. The minimum spouting velocity (U_{ms}) was determined and recorded at this point. Bed pressure drop and expanding bed height were also measured during the increasing air flow rate from fixed bed to fully spouting state, as well as during the decreasing air flow rate step.

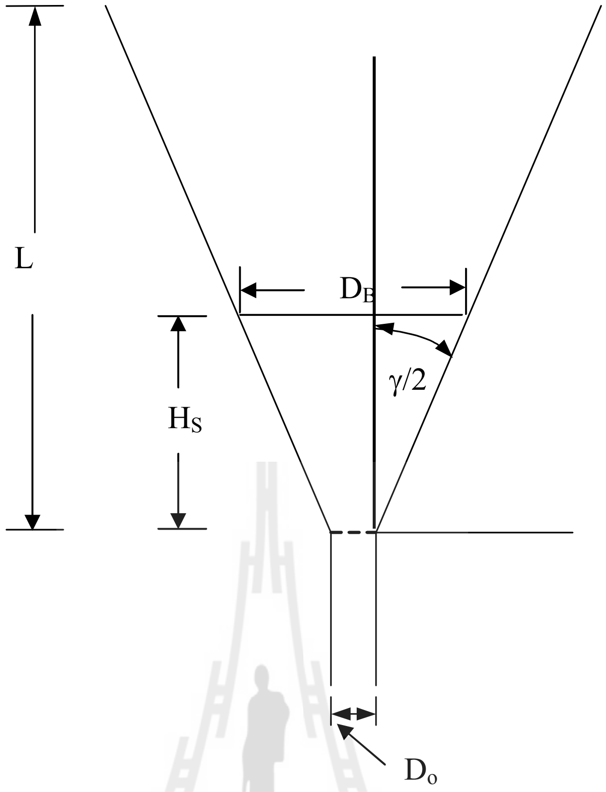

Figure 4.1 Schematic diagram of a conical spouted bed column

Table 4.1 Spouted bed dimensions and conditions for hydrodynamic study of a conical spouted bed at room temperature.

Geometric factor	Size
air inlet diameter (D_o), mm	4 – 12
conical base angle (γ)	28, 45 and 60^o
column length (L), cm	60
static bed height (H_s), cm	5-10
particle size (d_p), mm	1.09 - 2.18

4.3.2 CFD Simulation of Conical Spouted Bed Hydrodynamics

The aim of this section is to apply CFD simulation technique to simulate the hydrodynamic behavior of a conical spouted bed under conditions similar to those obtained from the experimental study. The CFD simulation of spouted bed hydrodynamics was achieved using the commercial CFD package ANSYS CFX 10.0. The computational program is based on the general description of the Eulerian multiphase model. The conservation equations can be derived by ensemble averaging the local instantaneous balance for each phase. The mean and fluctuating velocity of solid particle are described by the kinetic theory of granular flow (KTFG) (Lun, Savage, Jeffey and Chepurnity 1984; Gidaspow, 1994).

The mass conservation equations for fluid and solid phase are represented by the following equations:

$$\frac{\partial}{\partial t}\alpha_f + \nabla.(\alpha_f \vec{v}_f) = 0 \tag{4.1}$$

$$\frac{\partial}{\partial t}\alpha_s + \nabla.(\alpha_s \vec{v}_s) = 0 \tag{4.2}$$

where α_f and α_s are the volume fractions of fluid and solid phase, respectively, and $\vec{v}_f$ and $\vec{v}_s$ are the velocities of fluid and solid phases, respectively. The gas volume V_f is defined by

$$V_f = \int_V \alpha_f dV_f \tag{4.3}$$

The conservation of the gas and solids momentum is given by the following equations:

For the gas phase g:

$$\frac{\partial}{\partial t}(\alpha_f\rho_f\vec{v}_f)+\nabla.(\alpha_f\rho_f\vec{v}_f\vec{v}_f)=-\alpha_f\nabla P-\nabla P_f+\nabla.\overline{\overline{\tau}}_f+\varepsilon_f\rho_f\vec{g}_f+K_{fs}(\vec{v}_s-\vec{v}_f) \qquad (4.4)$$

For the solid phase s:

$$\frac{\partial}{\partial t}(\alpha_s\rho_s\vec{v}_s)+\nabla.(\alpha_s\rho_s\vec{v}_s\vec{v}_s)=-\alpha_s\nabla P-\nabla P_s+\nabla.\overline{\overline{\tau}}_s+\varepsilon_s\rho_s\vec{g}_s+K_{fs}(\vec{v}_s-\vec{v}_f) \qquad (4.5)$$

where ρ_f is density of the gas phase, P is the static pressure shared by all phase, $\overline{\overline{\tau}}$ is the gas phase stress – strain tensor, $\vec{g}$ is the gravitational acceleration, K_{fs} is the momentum exchange coefficient between the fluid phase f and the solid phase s, ρ_s is the density of the solid, $\overline{\overline{\tau}}_s$ is the solid phase stress – strain tensor, and P_s is the solid pressure.

The interphase momentum transfer between gas and solid phases is one of the dominant forces in the gas and solid phase momentum balances and represented by a drag force. Numerical correlations for calculating the momentum exchange coefficient of gas - solid systems have been reported by Gidaspow (Duarte et al., 2008). The solid – fluid exchange coefficient K_{sf} is expressed in the following form:

$$K_{sf} = \frac{3}{4} \frac{C_D \alpha_s \alpha_f \left| \vec{v}_s - \vec{v}_f \right|}{d_s} \alpha_f^{-2.65} \tag{4.6}$$

where the drag coefficient, C_D, is expressed by

$$C_D = \begin{cases} \frac{24}{\alpha_f Re_P} \left[1 + 0.15 \left(\alpha_f Re_P \right)^{0.687} \right] & \text{for } Re_P < 1000 \\ \\ 0.44 & \text{for } Re_P > 1000 \end{cases} \tag{4.7}$$

and the particle Reynolds number is defined as

$$Re_P = \frac{\rho_g U d_P}{\mu} \tag{4.8}$$

where U is a slip velocity.

The set of governing equations are solved by a finite control volume method, and the following initial and boundary conditions, and some specific simulation parameters were employed in the CFD simulation program.

(1) The system was assumed to consist of static bed of spherical palm shell particles with solid volume fraction of 0.6.

(2) The initial system pressure is set to be constant at 1.0 atm.

(3) At the entrance:

- the gas flows only in the axial direction with zero velocity gradient

- the inlet velocities of the solids are zero

(4) At the outlet: the velocity gradients for the two phases along the axial direction are zero and the column is exposed to ambient pressure.

(5) On the wall: a no – slip boundary condition was assumed for both gas and solid phase.

(6) Gidaspow drag force and solid pressure model (Ding and Gidaspow, 1990) are provided in the simulation program.

(7) The k – Epsilon model (Jones and Launder, 1972) for turbulence flow is used in this work.

The grid used in the computational domain was generated by using commercial engineering CAD software, ANSYS Workbench 10.0 and it is shown in Figure 4.2. The time steps of 10^{-5} sec were used for the computation in this section. The required simulation parameters including geometric factors, properties of solid (disperse) and fluid phases (continuous) are listed in Table 4.2. The simulation was performed for air inlet velocity varying in the range of 0 – 2 times the minimum spouting velocity. The expected results generated from CFD simulation are concentration profile of gas and solid phases, and the minimum spouting velocity.

The simplified flow sheet for the simulation algorithm is shown in Figure 4.3. The calculation procedure commences by setting the initial and boundary conditions, such as turbulence kinetic energy and turbulence eddy dissipation and restitution coefficient. The initial guesses of these system variables are given automatically by the computer program. Then, the conservation equation of momentum is first solved using Semi-Implicit Method for Pressure-Linked Equations-Consistent (SIMPLEC) algorithm (Versteeg and Malalasekera, 1995).

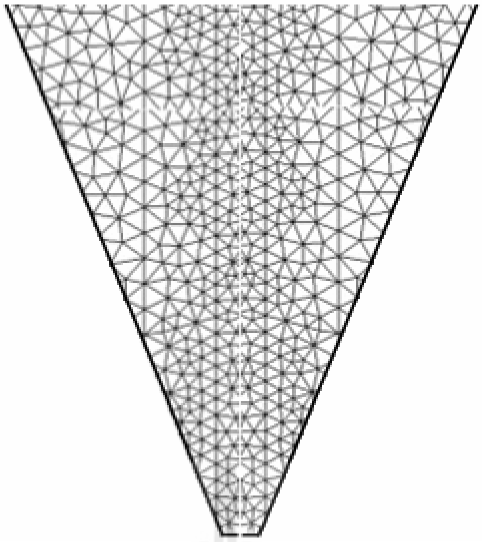

Figure 4.2 Numerical grids of spouted bed used in CFD simulation.

Table 4.2 Simulation parameters for CFD simulation of a conical spouted bed system.

Parameters	**Description**	**Value**
ρ_P (kg / m^3)	Solid density	1427
ρ_f (kg / m^3)	Air density (35^{o}C)	1.2278
μ_f (kg / m.s)	Air viscosity (35^{o}C)	1.9×10^{-5}
D_P (mm)	Particle diameter	1.09 – 2.5
e_{RC}	Particle restitution coefficient	0.90
$x_{P,Max}$	Maximum particle packing volume fraction	0.60
H_S (cm)	Static bed height	5 – 9
D_o (cm)	Inlet air diameter	0.7
γ	Conical base angle	45 and 60^o

Then, the conservation equation of mass is solved to obtain volume fraction (α_f and α_s) and mass flow rates for both phases. Finally, other governing equations are then solved, including turbulence model, drag force model, and KTGF model to obtain the other remaining system variables. The convergence or final steady-state criterion of simulated system is achieved by considering the RMS of residual values of the governing equations used in CFD simulation. This residual is caused by the truncated error of the numerical computation and the differences of computed values resuting from the iteration scheme. All the RMS of residual values of all physical parameters (such as velocity components, particle concentration, pressure, etc.) are set as 10^{-5}. This means that if the RMS of residual value is lower than 10^{-5}, the iteration is considered convergent or the steady-state condition is achieved. The RMS of residual is calculated from the following equation:

$$\text{RMS of Residual } \langle r_{rms} \rangle = \sqrt{\frac{1}{n}\sum_{i=1}^{n} r_i^2} \tag{4.9}$$

where r_i is the residual value collected from n control volume of all numerical grids.

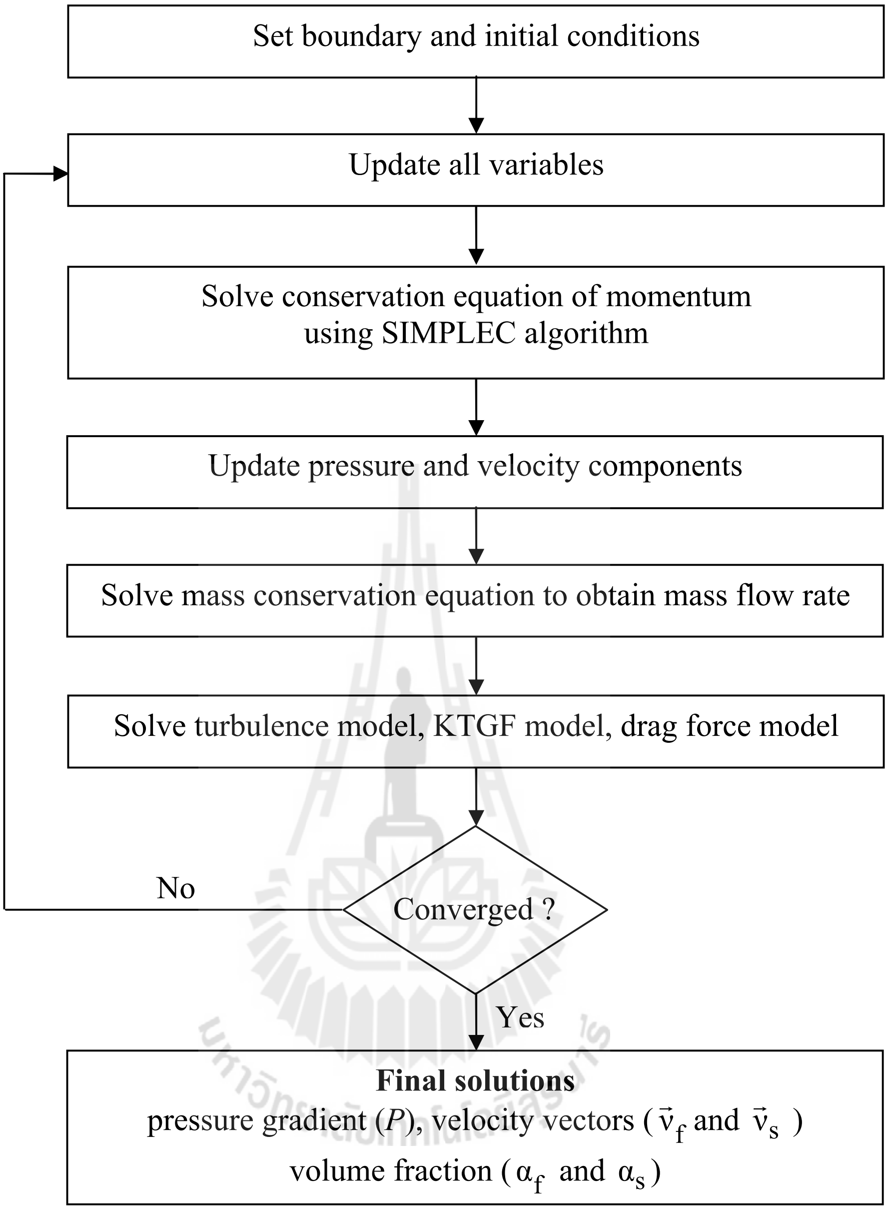

Figure 4.3 Flow sheet of the CFD simulation algorithm.

4.4 Results and Discussion

The effect of particle size, static bed height, air inlet diameter and conical base angle on the experimentally measured minimum spouting velocity is reported in this section. This information is required for the design, and operation of a conical spouted bed system for studying biomass pyrolysis as presented in the next chapter.

4.4.1 Hydrodynamic Study of a Conical Spouted Bed

The general characteristic of pressure drop variation in the bed with increasing air velocity is illustrated in Figure 4.4. These results are generated from the conical spouted bed with a contactor geometry of D_o = 6.0 mm, $\gamma = 45^o$ and for a bed consisting of palm oil shell of particle diameter 1.09 mm and initial static bed height of 8.0 cm. The results show that the behavior of pressure drop – air flow rate curve is similar to that reported by Wang (2006) who studied the hydrodynamics of glass bead of 1.16 mm in a conical spouted bed. The air superficial velocity shown in the figure was calculated based on cross – sectional area of air inlet diameter. The bed height can be reported either as height of dense solid bed (H_B) or total height of spouted bed ($H_T = H_B + H_F$) for increasing air flow, where H_F represents the height of solid fountain measured from the surface of the dense solid phase.

It can be observed that at low air velocity, pressure drop across the bed increased linearly with the increase of air velocity. The air flow upward through the bed without disturbing the particle with the pressure drop reaching maximum around point B. This point represents the boundary between a fixed bed and a transition region. Beyond point B, the whole bed was in the state of transition. The internal cavity elongated into an internal spout. The pressure drop now decreased with the increase of the superficial air velocity until point C was reached, which indicates the onset of stable spouting. Further increasing of air velocity from point C on will affect only the fountain height (H_T) with no consequent effect on the dense bed height (H_B) and pressure drop across the bed. The minimum spouting velocity was determined by observing the bed during the decreasing of gas velocity. During this period the bed remained in the spouting state until point C* was reached and the spouting state changed from stable spouting into the fixed bed region. This observed transitional point was regarded in this work as the minimum spouting velocity, U_{ms}. A further slight decreasing of gas velocity will cause the spout to collapse and the bed pressure started to increase abruptly to point B^*. After this point, the pressure drop decreased with decreasing air velocity. For each run, the pressure drop at each air velocity was measured for at least 3 times and the average was taken as the representative pressure drop at that velocity.

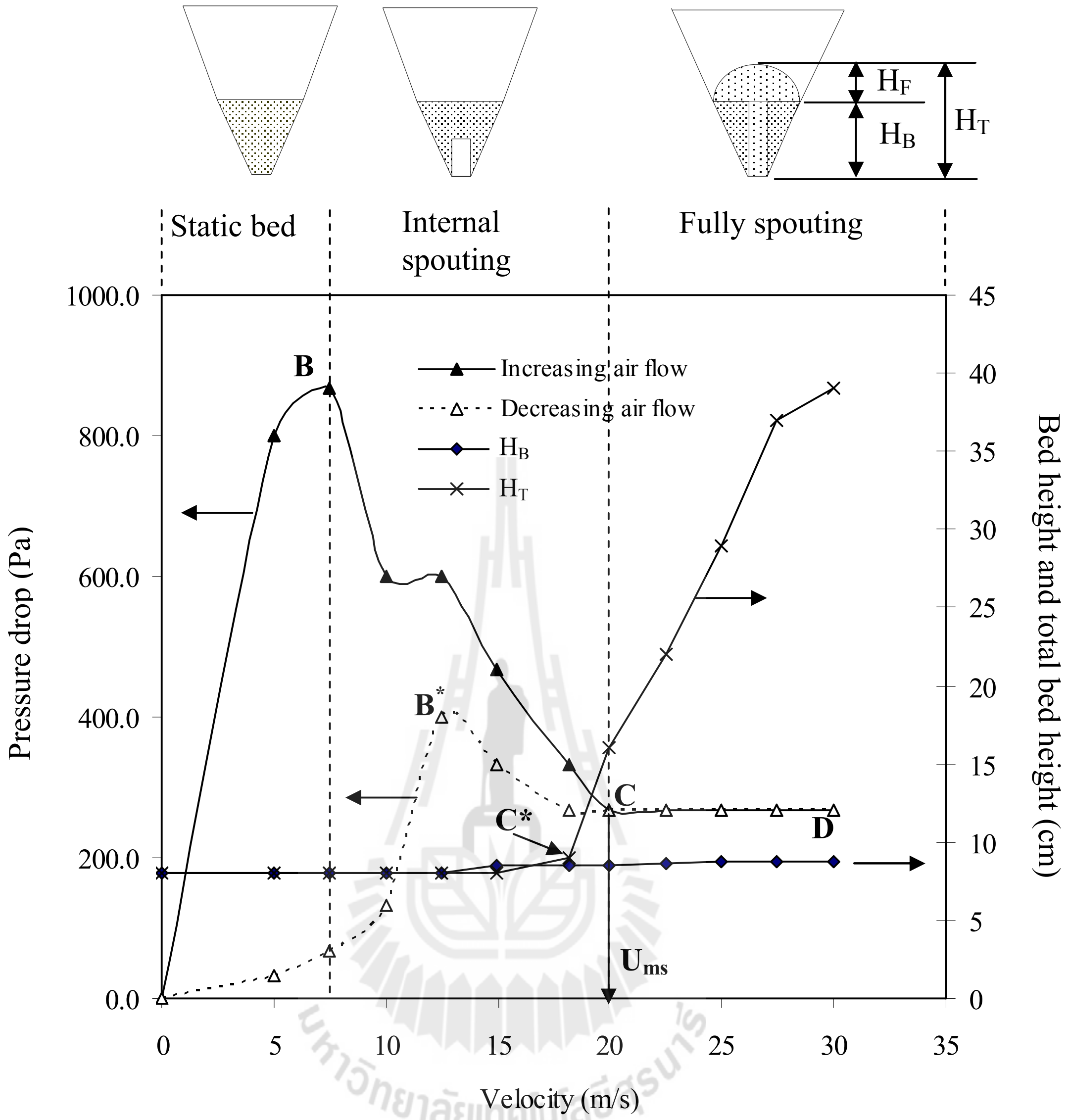

Figure 4.4 Pressure drop-flow rate diagram and bed height of a conical spouted bed for $D_o = 6.0$ mm, $d_p = 1.09$ mm, $\gamma = 45^o$, and $H_S = 8.0$ cm.

The effects of particle size (d_p), air inlet diameter (D_o), static bed height (H_S) and conical base angle (γ) on the minimum spouting velocity are shown in Figures 4.5 and 4.6. The results clearly indicate that the minimum spouting velocity increased with increasing of particle size for given contactor geometry and static bed height. Similar observations are also reported in the literature (Salam and Bhattacharya, 2006) for a cylindrical spouted bed for a central jet and circular slit distributors. The force required to push the particle moving upward in the spouting core is increasing when the particle size is increased and thus the lift force can be increased only by the increasing of the air flow rate. In addition, increasing of particle size leads to higher porosity and less frictional resistance for gas flowing through the packed bed, thus resulting in higher spouting gas velocity. Figure 4.5 further shows that for a given static bed height and particle size, the minimum spouting velocity tended to increase with the increase of conical base angle. As the conical base angle of the spouted bed is increased, the cross – sectional area of the top bed surface will be increased as compared with a smaller conical base angle. As a result of this effect, more fluid is required to fluidize the particles, leading to an increasing of minimum spouting velocity. In addition, more palm shell particles can be loaded into the column when the conical base angel is increased for a given initial static bed height. This increasing in the number of particles then necessitates the need to increase air supply to lift up the whole bed particles.

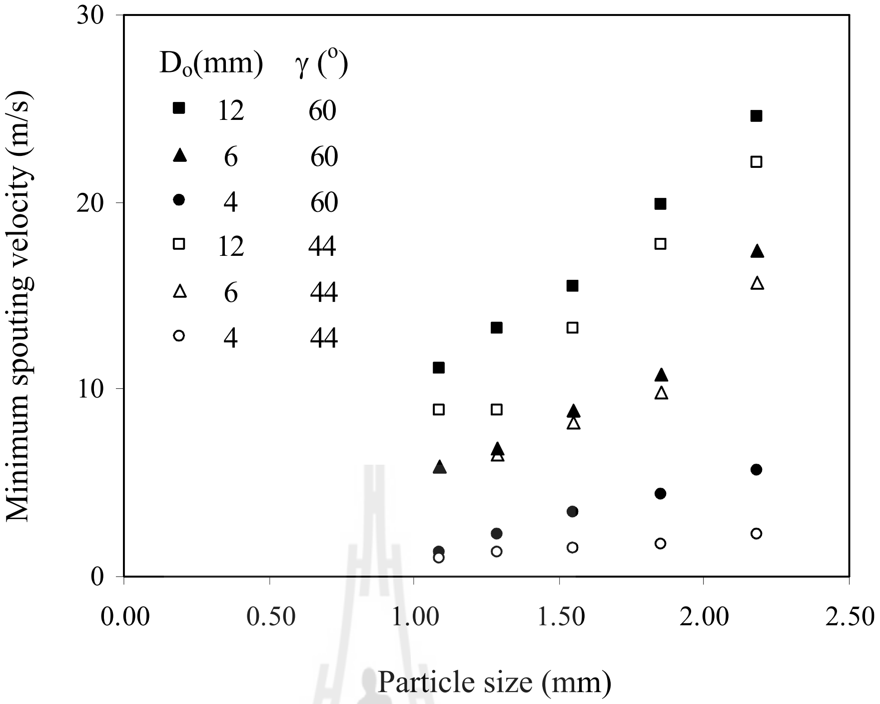

Figure 4.5 Effect of particle size, air inlet diameter (D_o), conical base angle (γ) and particle size on minimum spouting velocity for static bed height of 5 cm.

Figure 4.6 presents the effect of the initial static bed height for a given air inlet diameter and conical base angle. The increasing in static bed height leads to the increasing in the cross – sectional area of the top bed surface (D_B), thus increasing in interface area between spouting core and annulus zone and increasing in the number of particles. The expansion of the interface area is the reason for the increasing of gas leaking from spouting core to annulus zone through that interface. Thus, higher gas flow rate must be required to compensate for gas leakage to maintain spouting state of the solid bed. For these reasons the increasing of static bed height will lead to the consequent increase of minimum spouting velocity for a given spouted bed geometry.

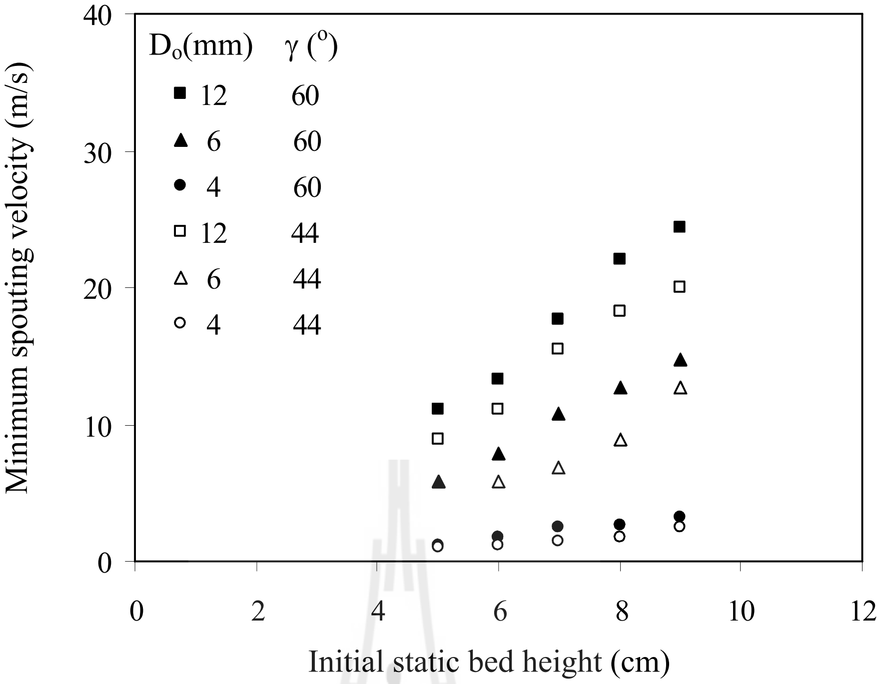

Figure 4.6 Effect of initial static bed height, air inlet diameter (D_o) and conical base angle (γ) on minimum spouting velocity for d_p = 1.09 mm.

As evident from Figure 4.5 and 4.6, the minimum spouting velocity (U_{ms}) was found to increase with the increase in the air inlet area (increasing D_o). For a given particle size, larger size of spout core is expected when the gas inlet diameter is increased. Therefore, higher gas flow is required to maintain the same velocity in spouting the bed.

As described in the experimental section, three different conical base angles were tested in this work. The results show that the bed particles were not spoutable when a minimum conical base angle of 28° was employed. The bed just transformed from the packed state directly into the fluidized state with increasing gas flow rate. San Jose et al. (1995) reported that the operation in the spouted bed for a larger base angle is more stable than the small angle. According to Yang (2003), for the bed with the ratio of nozzle diameter to column (D_o/D_c) above a certain critical value, there is no spouting regime and the bed transforms from the fixed bed into the fluidized state when the gas velocity is increasing.

Several correlations for calculating the minimum spouting velocity of a spouted bed have been reported. Mathur and Gisher (1995) proposed the simplest equation to calculate the minimum spouting velocity, with accuracy being within 15% for cylindrical vessel, D_c, up to about 0.5 m. Since the structure of conical spouted bed in Figure 4.2 is different form the conventional cylindrical spouted bed, it is necessary to modify the equation of Mathur and Gisher for correlating our results. In this work, the cylindrical vessel column diameter (D_c) is replaced by the diameter of the top bed surface (D_B) in the Mather and Gisher equation. This diameter directly affects the amount of particles loaded into the column, which affects the value of U_{ms}. The follwing modified Mather and Gisher equation is represented as,

$$U_{ms}=\left(\frac{d_p}{D_B}\right)\left(\frac{D_o}{D_B}\right)^{1/3}\sqrt{\frac{2gH_S\left(\rho_p-\rho_f\right)}{\rho_f}} \tag{4.10}$$

where the original equation of Mathur and Gisher for the cylindrical spouted bed is

$$U_{ms}=\left(\frac{d_p}{D_c}\right)\left(\frac{D_o}{D_c}\right)^{1/3}\sqrt{\frac{2gH_S\left(\rho_p-\rho_f\right)}{\rho_f}} \tag{4.11}$$

The comparison between minimum spouting velocity obtained from experimental determination and that calculated from the modified expression in Equation (4.10) was performed and it was found that Equation (4.10) gave poor prediction with the maximum deviation up to 80%. Therefore, it was considered that Equation (4.10) was not suitable for the prediction of minimum spouting velocity for a conical spouted bed studied in this work.

Olazar and coworker (1992) proposed the correlation for predicting minimum spouting velocity of a conical spouted bed (Equation (2.51)) in form of Reynolds number, geometric parameters and the Archimedes modulus. By fitting the experimental data with Equation (2.51), the computation results indicate that the correlation proposed by Olazar and coworker (1992) improved the prediction but still with large deviation of up to 45%. Therefore, it was decided to propose a more suitable correlation to improve the accuracy of predicting minimum spouting velocity for air – palm shell particle system. Abdul Salam and Bhattacharya (2006) reported that the correlation in Equation (4.12) for a cylindrical spouted bed showed a good agreement between the experimental and predicted values, with accuracy to be within 20%.

$$U_{ms} = \lambda\left(2gH_B\right)^k \left(\frac{d_p}{D_c}\right)^{\alpha} \left(\frac{D_o}{D_c}\right)^{\beta} \left(\frac{H_B}{D_c}\right)^{\gamma} \left[\frac{\rho_p - \rho_f}{\rho_f}\right]^{\delta} \tag{4.12}$$

By substituting D_c with D_B in Equation (4.12), the following equation can be written as:

$$U_{ms} = \lambda\left(2gH_B\right)^k \left(\frac{d_p}{D_B}\right)^{\alpha} \left(\frac{D_o}{D_B}\right)^{\beta} \left(\frac{H_B}{D_B}\right)^{\gamma} \left[\frac{\rho_p - \rho_f}{\rho_f}\right]^{\delta} \tag{4.13}$$

where λ, k, α, β, γ and δ are constant parameters and can be estimated by fitting Equation (4.13) with the experimental data. The parameters of the model were determined by using the non – linear least square (NLS) algorithm to minimize the objective function defined as:

$$\text{O.F.} = \sum \left(U_{ms,exp} - U_{ms,cal} \right)^2 \tag{4.14}$$

where $U_{ms,exp}$ and $U_{ms,cal}$ are the experimental and calculated minimum spouting velocities, respectively. The fitting results gave the constants as $\lambda = 1.04$, $k = 4.79$, $\alpha = 1.34$, $\beta = 1.80$, $\gamma = -4.06$, and $\delta = 1.40$, leading to the following final proposed equation,

$$U_{ms} = 1.04 \left(2gH_B \right)^{4.79} \left(\frac{d_p}{D_B} \right)^{1.34} \left(\frac{D_o}{D_B} \right)^{1.80} \left(\frac{H_B}{D_B} \right)^{-4.06} \left[\frac{\rho_p - \rho_f}{\rho_f} \right]^{1.40} \tag{4.15}$$

The comparison between the measured and the calculated minimum spouting velocity is summarized in Table 4.3. Although, the prediction results still show relatively large deviation up to 30% for some operating conditions and the standard error of estimate was found to be 12.7% but the overall prediction had improved considerably. Thus it is fair to infer that Equation (4.15) is suitable for the calculation of the minimum spouting velocity of the conical spouted bed studied in this work. Figure 4.7 illustrates the comparison between the experimental and predicted values of the minimum spouting velocity and about 90% of the predicted values are within ±20% of deviation line.

The results of the bed pressure drop corresponding to stable operation at the minimum spouting velocity are shown in Figure 4.8. For all air inlet diameter (D_o) and conical base angle (γ), the pressure drop increased with the particle size as shown in Figure 4.8 (a) and (b). Besides, there was a tendency for the bed pressure drop to decrease with increasing air inlet diameter for all stagnant bed heights, and particle sizes. Also, the bed pressure drop shows a slight decrease when the base angle is increased. As shown in Figure 4.8 (a) and (b), the influence of the particle size appears to be more pronounced than the effects of base angle and air inlet diameter. The results of bed pressure drop in this work are consistent with those of San José et al., (1996). Considering the measured bed pressure drop data, the conical base angle of 60^o and the air inlet diameter of 6 mm are considered to be suitable for the construction of a conical spouted bed reactor for pyrolysis study, to be reported in the next chapter. The reasons are that the pressure drop is lower than that of the 45^o base angle for all of stagnant bed height, particle diameter and air inlet diameter, and the increasing of air inlet diameter from 6 mm to 12 mm does not show a significant effect on the bed pressure drop.

Table 4.3 Minimum spouting velocity (U_{ms}) of conical spouted bed (experimentally determined) for various geometric factors, particle sizes and static bed heights and U_{ms} calculated from Equation (4.15).

Air inlet diameter (D_o, mm)	**Base angle (γ)**	**Particle size (d_P, mm)**	**Static bed height (H_s, cm)**	**Min. spouting velocity (U_{ms}, m/s)**		**%Error**
				Exp.	**Cal. (Eq. (4.15))**	
4	45	1.09	5	0.98	1.06	-8.16
			6	1.23	1.42	-15.45
			7	1.47	1.81	-23.13
			8	1.72	2.23	-29.65
			9	2.46	2.69	-9.35
		1.29	5	1.23	1.33	-8.13
		1.55		1.47	1.71	-16.33
		1.85		1.72	2.16	-25.58
		2.18		2.21	2.69	-21.72
6	45	1.09	5	8.84	6.62	25.11
			6	11.05	8.46	23.44
			7	15.47	10.72	30.70
			8	18.20	13.36	26.59
			9	20.00	13.13	34.35
		1.29	5	6.48	6.62	-2.16
		1.55		8.24	8.46	-2.67
		1.85		9.82	10.72	-9.16
		2.18		15.72	13.36	15.01
12	45	1.09	5	8.84	8.92	-0.90
			6	11.05	11.60	-4.98
			7	15.47	14.56	5.88
			8	18.20	17.77	2.36
			9	20.00	21.22	-6.10
		1.29	5	8.84	11.17	-26.36
		1.55		13.26	14.28	-7.69
		1.85		17.68	18.10	-2.38
		2.18		22.11	22.55	-1.99

Table 4.3 Minimum spouting velocity (U_{ms}) of conical spouted bed (experimentally determined) for various geometric factors, particle sizes and static bed heights and U_{ms} calculated from Equation (4.15) (continued).

Air inlet diameter (D_o, mm)	Base angle (γ)	Particle size (d_P, mm)	Static bed height (H_s, cm)	Min. spouting velocity (U_{ms}, m/s)		%Error
				Exp.	Cal. (Eq. (4.15))	
4	60	1.09	5	1.23	1.43	-16.26
			6	1.72	1.93	-12.21
			7	2.46	2.45	0.41
			8	2.7	3.05	-12.96
			9	3.19	3.74	-17.24
		1.29	5	2.21	1.79	19.00
		1.55		3.44	2.29	33.43
		1.85		4.42	2.9	34.39
6	60	1.09	5	5.89	5.26	10.70
			6	7.86	6.95	11.58
			7	10.81	8.82	18.41
			8	12.77	10.96	14.17
			9	14.74	13.5	8.41
		1.29	5	6.88	6.59	4.22
		1.55		8.84	8.43	4.64
		1.85		10.81	10.68	1.20
12	60	1.09	5	11.05	11.52	-4.25
			6	13.26	15.07	-13.65
			7	17.68	19.17	-8.43
			8	22.11	23.44	-6.02
			9	24.32	28.26	-16.20
		1.29	5	13.26	14.43	-8.82
		1.55		15.47	18.45	-19.26
		1.85		19.9	23.38	-17.49

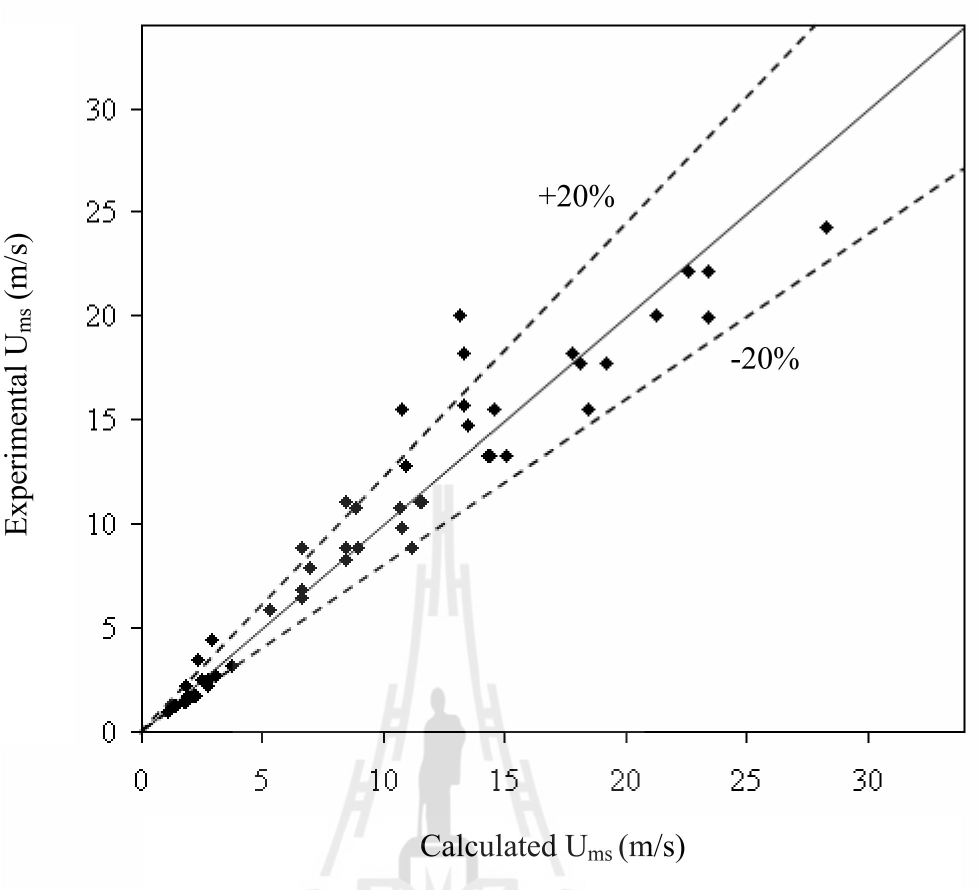

Figure 4.7 Comparison of experimental and calculated minimum spouting velocities by Equation (4.15).

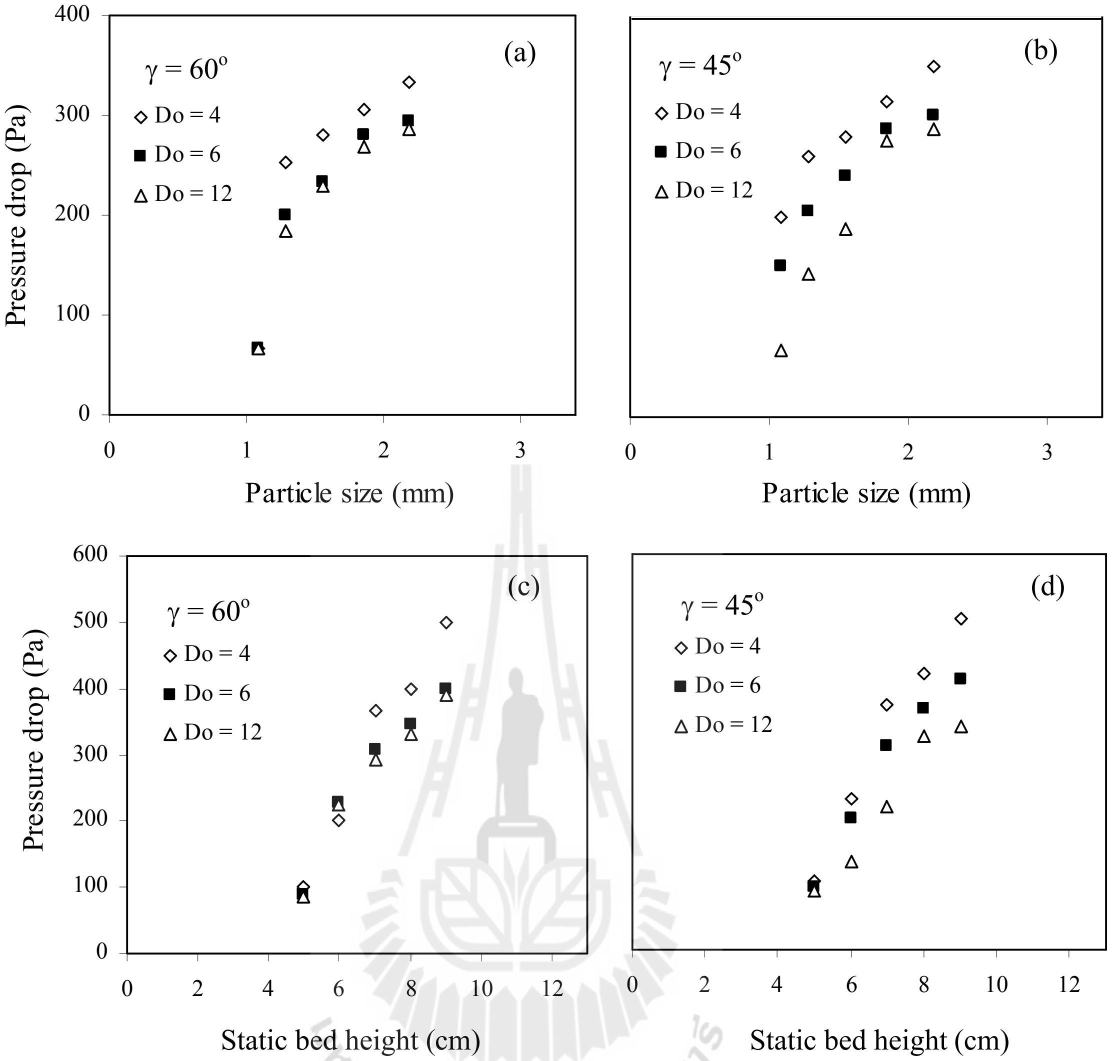

Figure 4.8 Effect of stagnant bed height, air inlet diameter and particle size diameter, air inlet diameter on the bed pressure drop at U_{ms} of a conical spouted bed.

4.4.2 Hydrodynamics Study of Conical Spouted bed by CFD Simulation

Figure 4.9 shows the circulating pattern of particle motion in the conical spouted bed obtained from the CFD simulation. The arrow symbols present the moving direction and velocity magnitude of palm oil shell particle inside the bed. It is noted that the particles move upward in the spout core region until they reach the top of fountain and then raining downward onto the annulus surface. Then, the particles move downward in the annulus region and again swept up into the core zone. The circulation flow pattern of the particles from the simulation agrees considerably well with those reported by Gryczka, et al., (2008). The several regions of different particle motion can be identified by analyzing the velocity vector map appearing in Figure 4.9. The spout flow regime is characterized by a vertical particle motion from the bottom of the column to the top with particles moving at high velocities and conveyed upward in the core region. In the annulus zone, the particles move downwards due to gravity, thus the particle velocities are much lower than in the spout regime. For the fountain regime, the particles are separated towards the annulus zone and also in the vicinity of apparatus wall, following by the downward movement within the annulus regime.

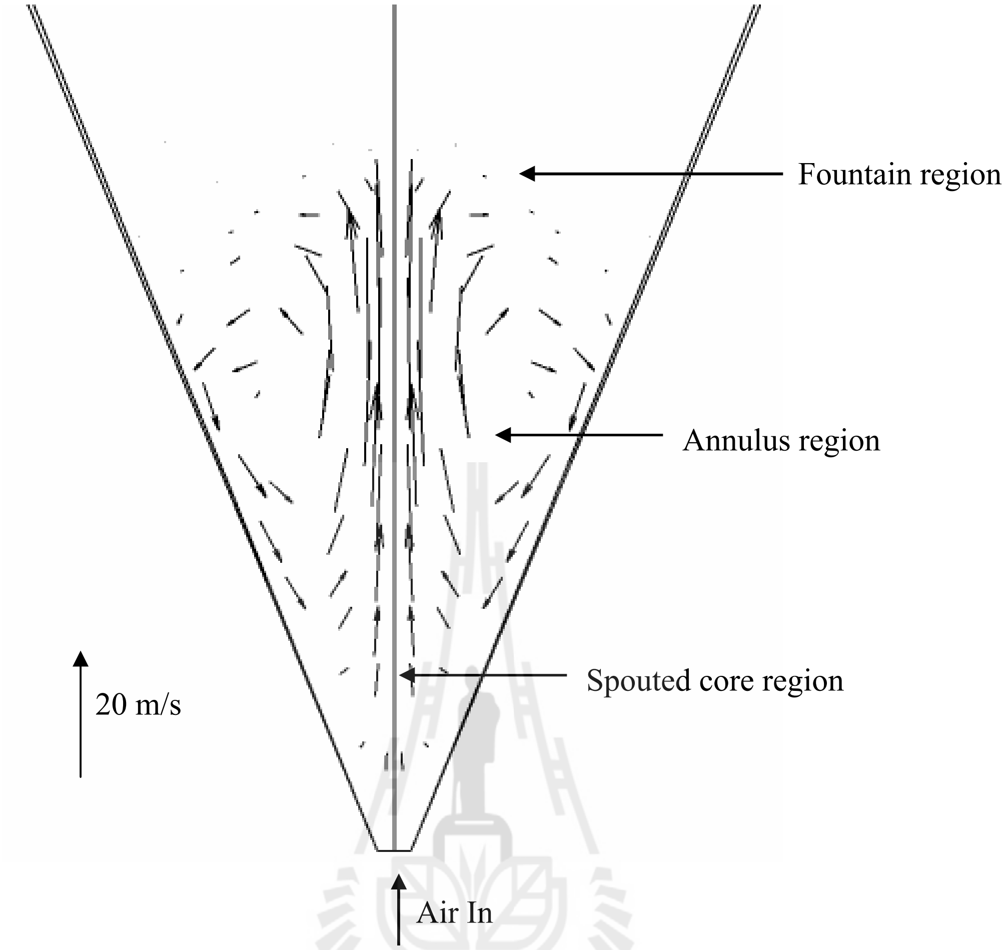

Figure 4.9 Simulated trajectory for particle motion in a conical spouted bed at air velocity of 1.0 U_{ms} (d_p = 1.08 mm, $\gamma = 45^o$, H_S = 8 cm, D_o = 6 mm and U_{ms} = 17.5 m/s).

The radial velocity profile of the palm shell particle at different static bed heights for the air velocity of 1.0U$_{ms}$ is shown in Figure 4.10. The particle velocities have their maxima at the central core of the bed and decrease to a minimum at the spout – annular interface. The results are consistent with the earlier research (Du, Bao, Xu and Wei, 2005 and Duarte et al., 2009) that reported on the hydrodynamic behavior of air – solid in cylindrical spouted beds by using CFD model.

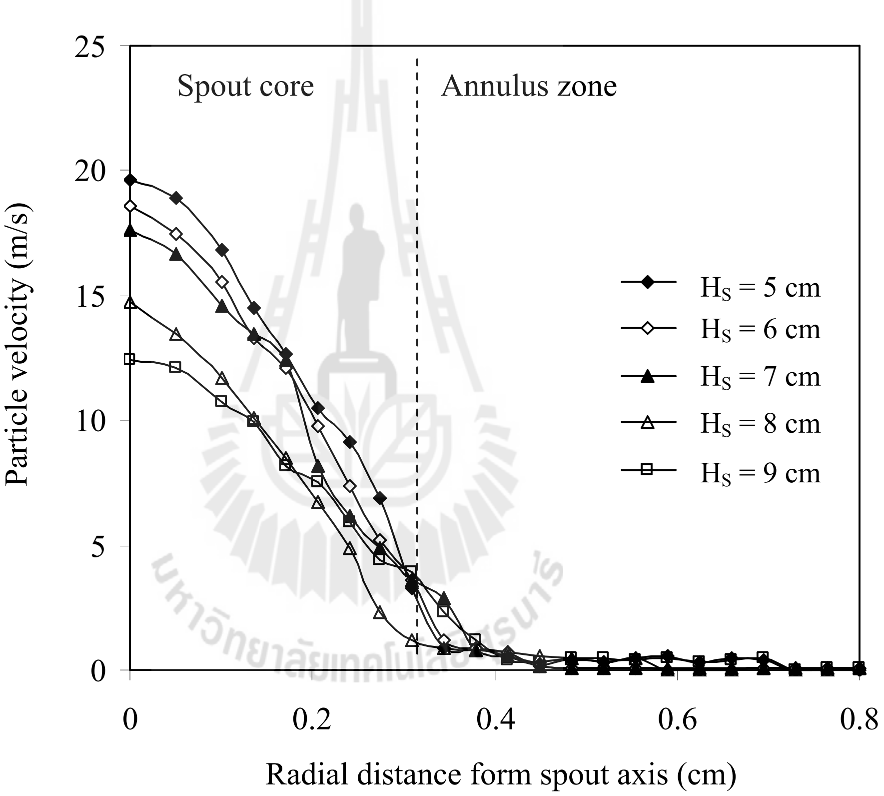

Figure 4.10 Radial velocity profile of palm shell particle at different static bed heights for air inlet velocity of 1.0U$_{ms}$ (d_p = 1.08 mm, $\gamma = 45^o$, D_o = 6 mm).

Figure 4.11 illustrates the redial velocity profiles of particles in the spouting and annular regions at different spouting gas velocities. As expected, the particle velocity in the spouting region increases with increasing spouting gas velocity. However, in the annular region the particle velocity does not vary markedly with increasing spouting velocity in this work. This behavior agrees with the predicted CFD result reported by Zhonghua and Mujumdar (2007). They employed the CFD modeling to simulate the flow behavior of gas – particle system in a cylindrical spouted bed.

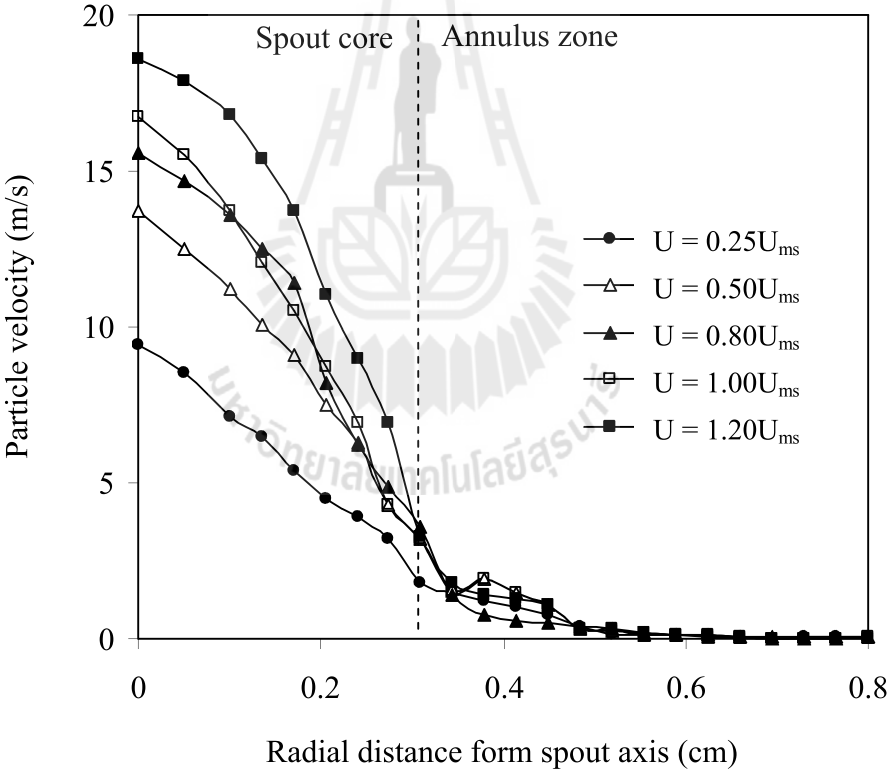

Figure 4.11 Radial velocity profile of palm shell particles at different spouting air velocities (d_p = 1.08 mm, $\gamma = 45^o$, D_o = 6 mm, H_S = 8.0 cm and U_{ms} = 17.5 m/s).

Figure 4.12 presents typically the variation of solid volume fraction in a conical spouted bed at increasing air velocity from fixed - bed to fully spouting regimes. The results obtained by simulation are qualitatively similar to those observed experimentally. In the fixed- bed regime, at air velocity around 0.25 U_{ms} an internal cavity starts to develop around the inlet region. As the flow rate is increased, the height of the hollow internal spout tends to elongate and reaches the top surface. The minimum spouting condition can be determined from a visual analysis of the simulated results when the height of the hollow internal spout just reaches the top surface as indicated in Figure 4.12 (e). Table 4.4 compares the experimental and the CFD simulation results of the minimum spouting velocity. The simulation results indicate that the simulation underpredicts the measured data for all cases. The maximum deviation between the experimental and simulated minimum spouting velocity is 10.57%. With this error limit, it is logical to infer that the CFD simulation is able to predict the minimum spouting velocity for the conical spouted bed under varied conditions with reasonable accuracy. This difference is probably caused by the assumptions of spherical shape and uniform particle size used in the CFD model. For actual system, the particles are irregular in shape with distribution of size which can affect the behavior of gas and solid interaction. The inter – locking of solid particle determined by packing condition could hinder the free movement of solid particles. Therefore, higher gas flow is required to overcome this increased frictional forces between particles in the real system.

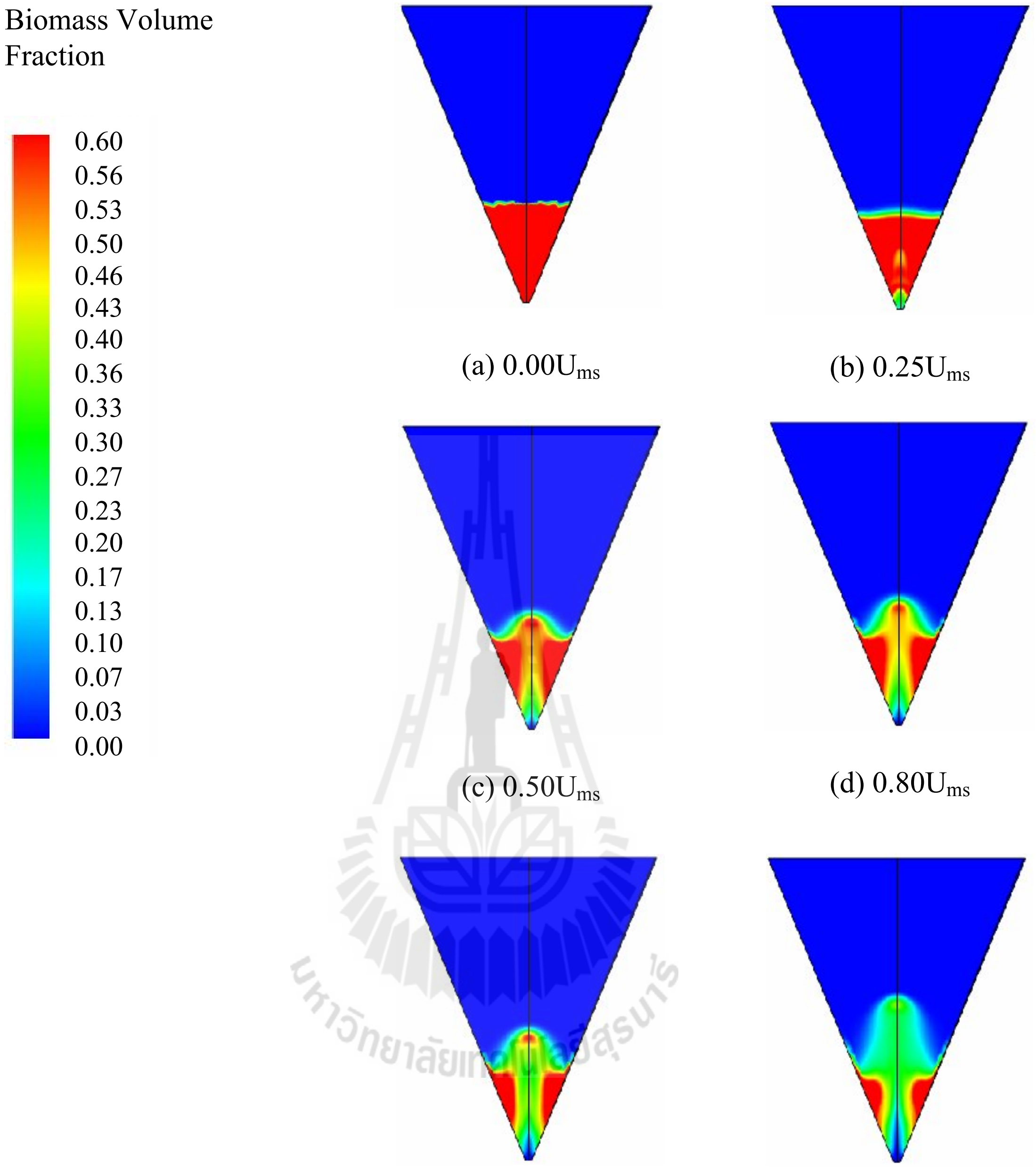

(a) $0.00U_{ms}$ (b) $0.25U_{ms}$

(c) $0.50U_{ms}$ (d) $0.80U_{ms}$

(e) $1.00U_{ms}$ (f) $1.20U_{ms}$

Figure 4.12 Solid volume fraction profiles for conical spouted bed with oil palm shell (d_p = 1.08 mm, $\gamma = 45^o$, H_S = 8 cm, D_o = 6 mm, U_{ms} = 17.5 m/s).

Table 4.4 Minimum spouting velocity (U_{ms}) of conical spouted bed (experimentally determined) for various geometric factors, particle sizes and static bed heights and U_{ms} calculated from CFD simulation.

Air inlet diameter (D_o, mm)	Base angle (γ)	Particle size (d_P, mm)	Static bed height (H_s, cm)	Min. spouting velocity (U_{ms}, m/s)		%Error
				Exp.	CFD Cal.	
4	45	1.09	5	0.98	0.9	8.16
			6	1.23	1.1	10.57
			7	1.47	1.4	4.08
			8	1.72	1.7	1.74
			9	2.46	2.4	4.47
		1.29	5	1.23	1.1	8.94
		1.55		1.47	1.4	4.08
		1.85		1.72	1.7	1.74
		2.18		2.21	2.2	2.71
6	45	1.09	5	8.84	8.7	2.15
			6	11.05	11.0	0.90
			7	15.47	15.0	3.04
			8	18.20	17.5	3.80
			9	20.00	19.8	1.00
		1.29	5	6.48	6.4	1.23
		1.55		8.24	8.0	2.91
		1.85		9.82	9.5	3.26
		2.18		15.72	15.5	1.40
12	45	1.09	5	8.84	8.5	3.85
			6	11.05	10.9	1.36
			7	15.47	14.8	4.33
			8	18.20	17.9	1.65
			9	20.00	19.5	2.50
		1.29	5	8.84	8.5	3.85
		1.55		13.26	13.0	1.96
		1.85		17.68	17.2	2.71
		2.18		22.11	21.5	2.76

Table 4.4 Minimum spouting velocity (U_{ms}) of conical spouted bed (experimentally determined) for various geometric factors, particle sizes and static bed heights and U_{ms} calculated from CFD simulation (continued).

Air inlet diameter (D_o, mm)	Base angle (γ)	Particle size (d_P, mm)	Static bed height (H_s, cm)	Min. spouting velocity (U_{ms}, m/s)		%Error
				Exp.	CFD Cal.	
4	60	1.09	5	1.23	1.2	2.44
			6	1.72	1.7	1.16
			7	2.46	2.4	2.44
			8	2.7	2.5	7.41
			9	3.19	2.9	9.09
		1.29	5	2.21	2.1	4.98
		1.55		3.44	3.1	9.88
		1.85		4.42	4.1	7.24
6	60	1.09	5	5.89	5.5	6.62
			6	7.86	7.5	4.58
			7	10.81	10.5	2.87
			8	12.77	12.5	2.11
			9	14.74	13.5	8.41
		1.29	5	6.88	6.5	5.52
		1.55		8.84	8.5	3.85
		1.85		10.81	10.5	2.87
12	60	1.09	5	11.05	10.5	4.98
			6	13.26	12.5	5.73
			7	17.68	17.5	1.02
			8	22.11	21.5	2.76
			9	24.32	23.5	3.37
		1.29	5	13.26	13.0	1.96
		1.55		15.47	15.0	3.04
		1.85		19.9	19.5	2.01

The simulated results on total bed heights (H_T) and dense bed height (H_B) of a conical spouted bed as a function of air flow rate are shown in Figure (4.13). The CFD simulation shows the similar predictive trend for the total bed height and dense bed height as compared to the corresponding experimental results. However, the simulation values of both H_T and H_B from the simulating results were lower than the experimental values, particularly for the total bed height. The large deviation of the simulated fountain height is probably due to the quality (number and shape) of numerical grids mesh, the chosen set of model parameters such as the drag model, particle restitution coefficient, the maximum particle packing, the time step interval and under – relaxation factor. According to Wang et al., (2001), the quality of numerical grids and time step are important parameters for determining the magnitude of round-off error occurring in the numerical calculation during simulation task. Moreover, the total bed height increases approximately linearly with the air velocity when the air velocity is higher than the minimum spouted velocity for both of the experiment and simulation. However, the deviation of total bed height between simulation and experiment seems to increase with increasing air velocity when air velocity higher than the minimum spouting velocity. This may be due to the limitation of CFD program and the set of model parameters. Also, the result shows a small difference of the dense bed height between simulation and experiment. It is probably that the size of numerical grids mesh used in the calculation is rather small near an entrance of the gas. In this work, the data of solid bed voidage and velocity profile of the fluid and dispersed solid were not presented because the most important parameter that is necessary for the design and scale up of spouted bed equipment is the minimum spouted velocity. However, the total bed height is also important for determining the overall height of the column required. Also, the predicting of the total bed heights with CFD in this work may not be appropriate, because of the large deviation of the calculation.

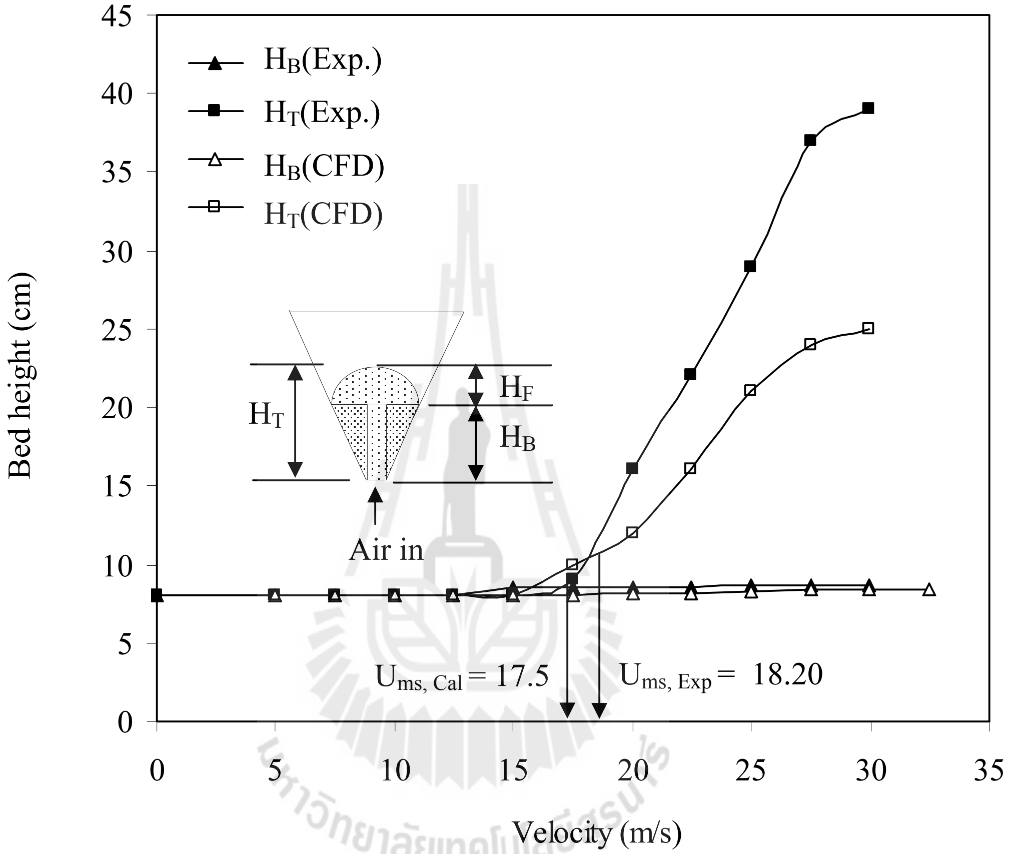

Figure 4.13 Comparison of experimental and CFD simulated results of bed height in conical spouted bed for D_o = 6.0 mm, d_p = 1.09 mm, $\gamma = 45^o$, and H_S = 8.0 cm.

Figure 4.14 compares the experimental and simulated pressured drop – air velocity curves of a conical spouted bed. The pressure drop – flow rate diagram from the simulation shows different behavior from that observed experimentally. At the air velocity lower than 5.0 m/s, the calculated pressure drop increases linearly with air flow rate. With increasing air flows through the simulated spouted bed at the velocity higher than 5.0 m/s, the internal cavity starts to elongate and increases in length as the air flow is increased. The elongation of the internal cavity causes the decreasing of pressure drop across the bed. The size of internal cavity becomes larger when the air flow is increased and the fully spout state was finally observed when the air velocity approaches the value of about 18m/s. At higher air flow rate, the pressure drop across the bed becomes constant. The pressure drop across the bed of simulated results for decreasing air flow is the same with the increasing step of air flow. On the other hand, the experimental pressure drop increases with increasing of air flow from 0 – 5 m/s without disturbing the bed. The pressure drop continues to increase further until the maximum value at air velocity of 8.5 m/s is attained. At this point, the bed starts to expand and suddenly transforms into the spout state, giving a reduction in pressure drop. Pressure drop across the bed continues to decrease with increasing air velocity from 8.5 m/s to 20 m/s and then the pressure drop becomes constant. As shown in Figure 4.14, the calculated pressure drop value lie somewhat between the experimental values of increasing and decreasing the air velocity. The large deviation between the experimental and simulated pressure drop results could come from the limitation of CFD model to simulate the actual behavior of particle in the internal spouting region.

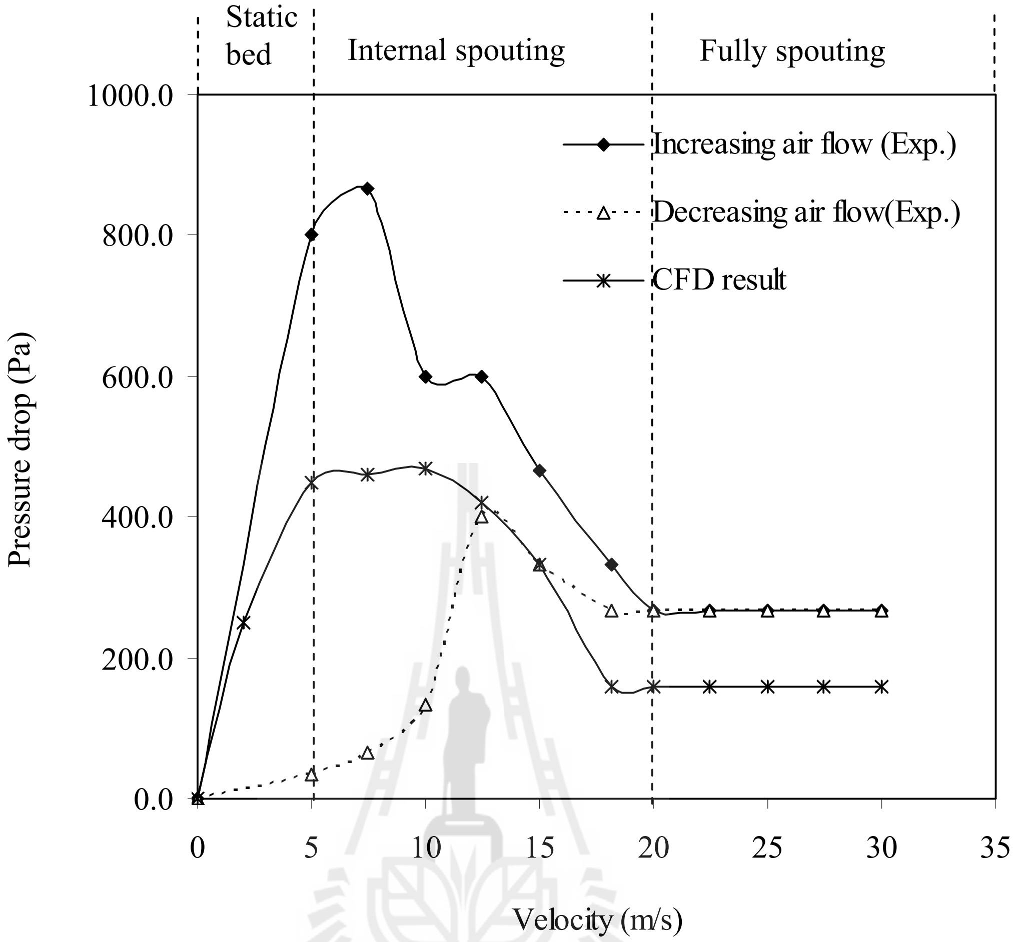

Figure 4.14 The experimental and CFD simulated results of pressure drop-flow rate diagram and bed height of conical spouted bed for D_o = 6.0 mm, d_p = 1.09 mm, $\gamma = 45^o$, and H_S = 8.0 cm.

The simulated results of minimum spouting velocity of nitrogen – solid flow are shown in Table 4.5. The effects of the reactor temperature, geometric factor, particle size and static bed height on minimum spouting velocity were studied. As already mentioned, the results of the hydrodynamic study in this chapter will be used for the design and specifying the operating condition of a conical spouted bed reactor in Chapter 5 which is operated at higher temperature. Therefore, it is necessary to investigate the effect of reactor temperature on the minimum spouting velocity.

The simulated results in Table 4.5 indicate that increasing of reactor temperature leads to a significant decrease in the minimum spouting velocity. Since the increase in reactor temperature mainly causes an increase in gas velocity, gas viscosity and gas volume and these in turn increase the momentum transfer from the gas to the solids (Pannala, Syamlal and O'Brien, 2011). Therefore, the gas mass flow (at room temperature) required for initiating the onset of spouting thus decreases as the reactor temperature is increased. Using nitrogen as the disperse fluid at the temperature of 35°C shows a slight increase in the minimum spouting velocity when comparing with air.

Table 4.5 Effect of operating temperature on the minimum spouting velocity (U_{ms}) of conical spouted bed for various geometric factors, particle sizes and static bed heights from CFD simulation of nitrogen – solid flow.

Air inlet diameter (D_o, mm)	**Base angle (γ)**	**Particle size (d_p, mm)**	**Static bed height (H_s, cm)**	**Min. spouting velocity* (U_{ms}, m/s)**					
				35 °C**	**350 °C****	**450 °C****	**550 °C****	**650 °C****	**750 °C****
6	60	1.09	5	6.0				1.4	
		1.29	5	8.3				1.7	
		1.55	5	15.5				4.2	
			6					4.4	
			7					4.7	
			8					4.9	
			9					5.2	
		2.18	5	12.7	5.0	4.2	3.7	3.3	3.0
4	60	2.18	5	16.0	5.1	4.0	3.9	3.7	3.4

*minimum spouting velocity at the inlet nozzle (room temperature of 35°C)

**Conical spouted bed reactor temperature

4.5 Conclusions

In this chapter, the effects of conical spouted bed geometry, particle size and initial static bed height on the minimum spouting velocity were studied both by experimentation and by the application of commercial CFD simulation package ANSYS CFX 10.0. The methodology used in CFD simulation was validated by comparison with experimental data obtained from a small scale spouted – bed unit, using a palm shell as a disperse particle phase. The following conclusions can be drawn from this study.

- From the experimental results of hydrodynamic study of a conical spouted bed, the minimum spouting velocity was found to increase with increasing initial static bed height, gas inlet diameter, conical base angle, and particle size.

- The increasing in particle size led to the pressure drop increasing for all air inlet diameters and conical base angles. In contrast, the pressure drop decreased with increasing air inlet diameter for all stagnant bed height, and particle size diameter. The increasing of a conical base angle led to a slight decrease in the bed pressure drop.

- Increasing of air inlet diameter form 6 mm to 12 mm exerted no significant effect on the pressure drop across the conical spouted bed.

- The modified Mather and Gisher equation for predicting the minimum spouting velocity of a conical spouted bed for air – palm shell system was proposed in this work as

$$U_{ms} = \left(\frac{d_p}{D_B}\right)\left(\frac{D_o}{D_B}\right)^{1/3} \sqrt{\frac{2gH_S\left(\rho_p - \rho_f\right)}{\rho_f}}$$

and was found to give maximum deviation from experimental results up to 80%.

- The final correlation for minimum spouting velocity for air – palm shell system was proposed as the following,

$$U_{ms} = 1.04\left(2gH_B\right)^{4.79}\left(\frac{d_p}{D_B}\right)^{1.34}\left(\frac{D_o}{D_B}\right)^{1.80}\left(\frac{H_B}{D_B}\right)^{-4.06}\left[\frac{\rho_p - \rho_f}{\rho_f}\right]^{1.40}$$

The predictive capability was improved by this proposed equation giving about 30% maximum deviation.

- The hydrodynamic behavior of conical spouted bed was studied using the commercial CFD simulation package ANSYS CFX 10.0. The CFD simulation result of minimum spouting velocity showed satisfactory agreement with the experimental by measured results.

- The simulated results also indicated that increasing the reactor temperature from room temperature to 750°C caused a decrease in the minimum spouting velocity by about fourfold.

4.6 References

Aguado, R., et al. (2002). Kinetic Study of Polyolefin Pyrolysis in a Conical Spouted Bed Reactor. **Ind. Eng. Chem. Res.** 41: 4559 – 4566.

Altzibar, H., et al. (2009). Hydrodynamics of Conical Spouted Beds Using Different Types of Internal Devices. **Chemical Engineering Technology.** 32: 463-469.

Ding, J. and Gidaspow, D. (1990). A bubbling fluidization model using kinetic theory of granular flow. **AIChE Journal** 36: 523-538.

Du, W., Bao, X., Xu, J., and Wei, W. (2005). Computaional fluid dynamics (CFD) modeling of spouted bed: Assessment of drag coefficient correlation. **Chemical Engineering Science.** 61: 1401 – 1420.

Duarte, C.R., Olazar, M., Murata, V.V., and Barrozo, M.A.S. (2009). Numerical simulation and experimental study of fluid – particle flows in a spouted bed. **Power technology.** 188(3): 195 – 205.

Duarte, C. R., Murata, V. V., and Barrozo, M. A. S. (2005). A study of the fluid dynamics of the spouted bed using CFD. **Brazilian Journal of Chemical Engineering.** 22(2): 263 – 270.

Gidaspow, D. (1994). **Multiphase flow and fluidization : Continuum and kinetic theory descriptions**. Boston: Academic Press.

Gong, X., Hu, G., and Li, Y. (2006). Hydrodynamic Characteristics of a Novel Annular Spouted Bed with Multiple Air Nozzles. **Ind. Eng. Chem. Res.** 45: 4830 – 4836.

Gryczka, O., et al. (2008). Characterization of pneumatic behavior of a novel spouted bed apparatus with two adjustable gas inlets. **Chemical Engineering Science.** 63(3): 791 – 814.

Jones, W.P. and Launder, B.E. (1972). The prediction of laminarization with a two equation model of turbulence. **International Journal of Heat and Mass Transfer** 15: 301-314.

Lettieri, et al. (2003) CFD Simulations of Gas Fluidized Beds Using Alternative Eulerian – Eulerian Modelling Approaches**. International Journal of Chemical Reactor Engineering.** 1: 1 – 19.

Lun, C.K.K., Savage, S.B., Jeffey, D.J. and Chepurnity, N. (1984). Kinetic theories for granular flow: inelastic particles in Couette flow and slightly inelastic particles in general flow field. **Journal of Fluid Mechanics** 140: 223-256.

Mathur, K.B., and Epstein, N. (1974). **Spouted Beds.** Academic Press, New York.

Olaza, M, et al. (2005). Kinetics of Scrap Tire Pyrolysis in a Conical Spouted Bed Reactor. **Ind. Eng. Chem. Res.** 44: 3918 – 3924.

Olazar, M., San José, M.J., Aguayo, A.T., Arandes, J.M., and Bilbao, J. (1992). Stable Operation Conditions for Gas – Solid Contact Regimes in Conical Spouted Beds. **Ind. Eng. Chem. Res.** 31: 1784 – 1791.

Pannala, S., Syamlal, M., and O'Brien, J. T. (2011). **COMPUTATIONAL GAS – SOLIDS FLOWS AND REACTING SYSTEMS: Theory, Methods and Practice.** IGI Glogal. United State of America.

Papadikis, K., Gerhauser, H., and Bridgwate, A. V. (2009). CFD modeling of the fast pyrolysis of an in – flight cellulosic partical subjected to convective heat transfer. **Biomass and Bioenergy.** 33(1): 97 – 107.

Salam, P. A., and Bhattacharya, S. C., (2006). A comparative hydrodynamic study of two types of spouted bed reactor designs. **Chemical Engineering Science.** 61: 1946 – 1957.

San José, M.J., Olazar, M., Aguado, R., and Bilbao, J. (1996). Influence of the conical section geometry on the hydrodynamics of shallow spouted beds. **The Chemical Engineering Journal.** 62: 113-120.

San José, M. J., et al. (2005a). Influence of the particle diameter and density in the gas velocity in jet spouted beds. **Chemical Engineering and Processing.** 44: 153 – 157.

San José, M. J., et al. (2005b). Local porosity in conical spouted beds consisting of solids of varying density. **Chemical Engineering Science.** 60: 2017 - 2025.

Wang, Z., et al. (2001). Study on the Hydrodynamics of a Spouting – Moving Bed. **Ind. Eng. Chem. Res.** 40: 4983 – 4989.

Wang, Z. (2006). **Experimental studies and CFD simulations of conical spouted bed hydrodynamics.** Thesis. The University of Britis Columbia.

Yang, W.C. (2003). Handbook of Fluidization and Fluid – Particle System. Headquarters. New York.

Zhonghus, W., and Mujumdar, S.A. (2007). CFD modeling of the gas – particle flow behavior in spouted bed. **Powder Technology.** 183(2): 260 – 272.

CHAPTER V

PALM SHELL PYROLYSIS IN A CONICAL SPOUTED BED REACTOR

5.1 Abstract

In this work, palm shell was pyrolyzed in a batch and continuous conical spouted bed to investigate the effect of pyrolysis temperature and time, particle size, and static bed height on the product yields and kinetic parameters. The optimal pyrolysis condition given from the batch operation was selected for the continuous runs where the only effect of pyrolysis temperature was studied. To achieve the stable spouting operation, palm shell was pyrolyzed in a reactor using nitrogen gas flowing at 1.2U_{ms}. From the experimental results it was found that pyrolysis temperature and time showed a significant effect on the pyrolysis product yields, while particle size and static bed height exerted no significant effect. For the continuous spouted bed mode, the maximum liquid yield of 65 wt% was obtained from palm shell pyrolysis at 650^{o}C, palm shell feed rate of 5 g/min, particle size of 1.55 mm and N_2 flow rate of 9.6 L/min. The bio – oil from palm shell is less attractive to use as a direct fuel, due to its high water contents, low in calorific value and high acidity. The derived solid product (char) gave a high calorific value of 30.78 MJ/kg and a reasonably high BET surface area of 220 m^2/g. On gas composition, carbon monoxide and carbon dioxide gas were the dominant components in the gas product. The production yields

predicted using the competitive model showed good agreement with the experimental results.

5.2 Introduction

The pyrolysis liquid product or bio – oil contains many chemical compounds with different functional groups and molecular weights, such as aldehydes, phenols and their derivatives, furans and other mixed oxygenates acids and alcohols (Czernik and Bridgwater, 2004). Distribution of pyrolysis products depends on such operating conditions as types of feedstock and reactor, reaction time, pyrolysis temperature and sweeping gas flow rate (Bridgwater, 2000). To obtain the high liquid yield the pyrolysis conditions require high heating rate, moderate temperature (450 – 550^{o}C) and short vapor product residence time. A longer residence time favors secondary reactions such as thermal cracking, repolymerization, and recondensation and hence minimizes the liquid yield (Ozlem, Kockar, 2006). Generally, fast pyrolysis processes produce 60 – 75 wt% of liquid bio-oil, 15-25 wt% of solid char, and 10-20 wt% of non-condensable gases, depending on the pyrolysis conditions. Liquid product is considered a very promising fuel because it can be easily transported, burnt directly in thermal power stations, and can be further used as a chemical feed stock to produce many valuable chemical species (Goyal, Seal and Saxena, 2008). For these reasons, considerable research effort has recently been focused on flash pyrolysis to produce liquid product (bio –oil) with high yield.

Several researchers examined the most suitable pyrolysis conditions in many types of pyrolysis reactors, including fixed bed reactors (Azduwin, Ridzuan, Hafis and Amran, 2012), packed bed reactors (Yang, 2007), fluidized-bed reactors (Wang et al., 2005), and conical-cylindrical spouted bed reactors (Tsai, Lee and Chang, 2007). Compared to the fluidized bed, the conical spouted bed has a lower operating pressure drop and can handle particles with a wide size range or density distribution without segregation. The vigorous contact between phases and the collision between particles in the spout and fountain avoid defluidization problems, which take place in the fluidized bed due to the agglomeration of solid particles. Also, the conical spouted bed reactor has the following further advantages over conventional spouted beds (cylindrical with conical base): simpler design because no distributor plate is needed, lower pressure drop, cyclic circulation of the particles make it suitable for sticky or irregular shape particles, high heat and mass transfer between gas and solid whose circulation is mainly counter – current, and short gas residence time. For these reasons a conical spouted bed is proposed for the study of flash pyrolysis of biomass in the present work.

In this study the flash pyrolysis of palm shell was investigated in the batch and continuous reactor. In particular, the influence of final pyrolysis temperature and time, particle size range and bed height on the product yields was studied. In addition, the pyrolysis oil obtained under the condition producing maximum liquid product yield was characterized, using chromatographic and spectroscopic techniques, to determine its potential use as a source of renewable fuel and chemical feedstock.

5.3 Research Method

5.3.1 Feedstock Preparation and Characterization

The pyrolysis test was carried out with palm shell particles. Palm shell was first crushed by a jaw crusher, and then screened to obtain the average screen sizes of 1.09 to 2.18 mm, the same size range as used in Chapter 4. The sized particles were then dried at 110°C for 24 hours in an oven to remove the excess moisture and then kept for further characterization and pyrolysis study. Material characterization method and their results were previously described and presented in Chapter 3.

5.3.2 Pyrolysis Experiments

Both batch and continuous pyrolysis of palm shell samples were performed in a stainless steel conical spouted bed reactor at different pyrolysis conditions. Based on the hydrodynamic study presented in the previous chapter, a laboratory conical spouted bed unit was designed and constructed. The reactor was made from a stainless steel pipe with the following geometries: air inlet diameter (D_o) 6 mm, thickness 2 mm, height 60 cm, and the cone angle (γ) of 60^o. According to the hydrodynamic behavior reported in Chapter 4, for the cone angle (γ) of 60^o the pressure drop across the bed is lower than that with cone angle (γ) of 45^o for a given air inlet diameter, static bed height and particle size. The increasing of air inlet diameter in the range of 6 to 12 mm did not seem to have an important effect on the pressure drop across the bed. However, the nozzle – to – particle ratio (D_o/d_p) should be less than 25 – 30 to achieve a stable non – pulsating spouted bed (Yang, 2003). Therefore, a very small particle size can be performed when choosing air inlet diameter of 6 mm. Also, the total bed height results in Chapter 4 indicated that the reactor height higher than 50 cm should be recommended. The reactor was inserted in an electric heated furnace which was constructed specifically for the experiments in this section. Figure 5.1 shows the experimental set – up of the pyrolysis unit and details of operating conditions are listed in Table 5.1. In this study, the pyrolysis experiments were carried out at operating spouting velocity of $1.2U_{ms}$ by using nitrogen (99.5% purity) as a medium gas for all tests. The flow rate of N_2 was controlled by a rotameter and was preheated before entering the reactor. According to Bridgewater (1997), the spouting is better defined and stable when the ratio of spouting velocity (U_s) to minimum spouting velocity (U_{ms}) is in the range of 1.1 – 1.3. The pressure drop across the bed was measured at position P_1 as shown in Figure 5.1.

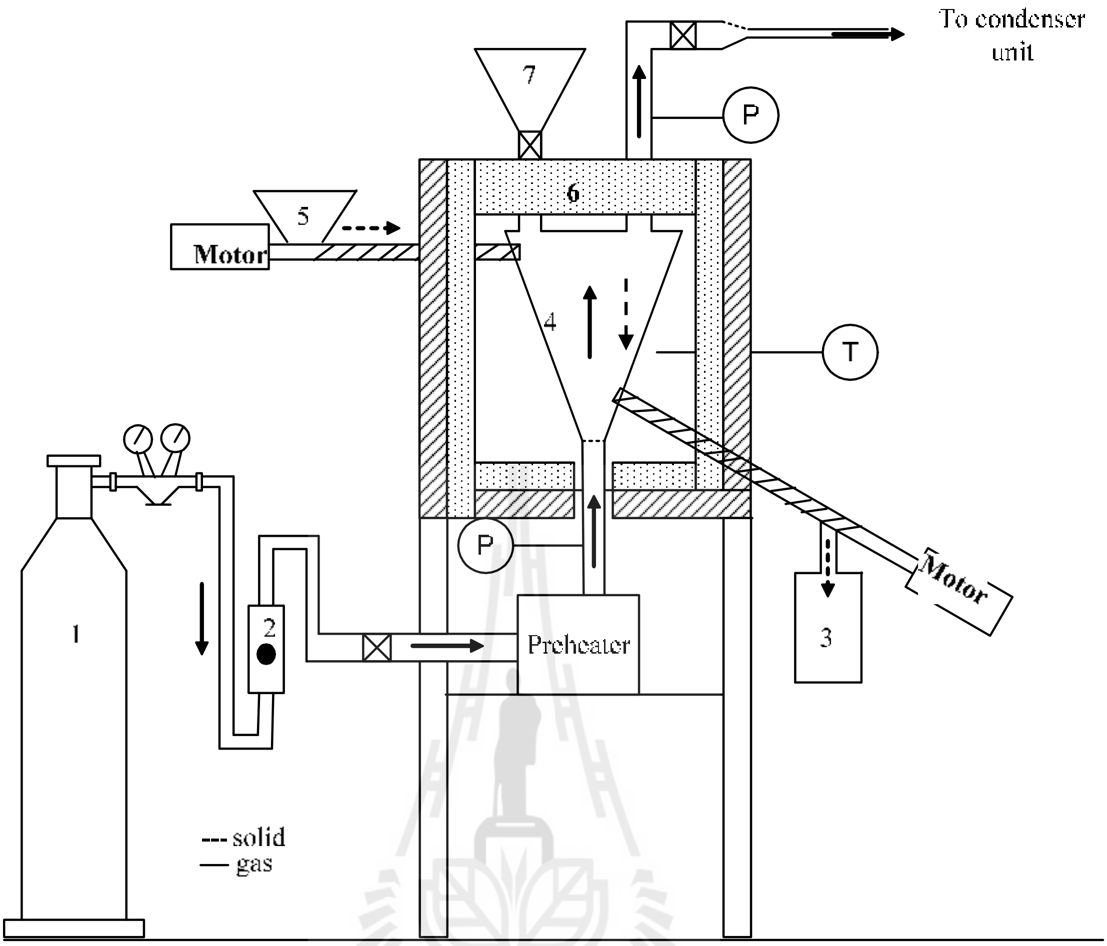

- (1) Nitrogen tank cylinder
- (2) Flow meter
- (3) Solid product collector
- (4) Stainless steel conical bed reactor
- (5) Raw material feeder for continuous operation
- (6) High temperature furnace
- (7) Raw material feed hopper for batch operation

Figure 5.1 Schematic diagram of the conical spouted bed reactor unit.

Table 5.1 Experimental conditions for batch and continuous pyrolysis of palm shell in a conical spouted bed.

Sys-tem	Particle Size (mm)	Bed height (cm)	Temp. (^oC)	Minimum spouting velocity (m/s)	Superfical velocity (m/s)	N_2 supply (L/min)	Time (min)
Batch	2.18	5	350	5.0	6.0	10.2	5
			450	4.2	5.0	8.5	
			550	3.7	4.4	7.5	
			650	3.3	4.0	6.7	
			750	3.0	3.6	5.1	
	2.18	5	650	3.7	4.0	6.7	5
							10
							15
							20
							30
							45
	1.09	5	650	1.4	1.68	2.8	15
	1.29	5	650	1.7	2.04	3.5	15
	1.55	5	650	4.2	5.0	8.5	15
		6		4.4	5.3	9.0	
		7		4.7	5.6	9.6	
		8		4.9	5.9	10.0	
		9		5.2	6.2	10.6	
	1.55	5	450	4.9	5.9	10	15
			550	4.8	5.8	9.8	
			750	3.7	4.5	7.7	
Continuous	1.55	5	450	4.9	5.9	10.0	-
			550	4.8	5.8	9.8	
			650	4.7	5.6	9.6	
			750	3.8	4.5	7.7	

5.3.2.1 Batch Experiment

The effects of pyrolysis temperature and time, particle size, and bed height on the product yield and distribution of palm shell pyrolysis were studied in the batch mode from which the optimized condition was identified and used for running the continuous tests.

The first series of experiments were carried out to determine the effect of the pyrolysis temperature on pyrolysis yields in a batch type process. The reactor temperature was heated from room temperature to the desired temperature and hold at that point for 60 minutes. Next, 70 g of palm shell particles (2.18 mm in size) was charged into a conical spouted bed reactor. The pyrolysis temperature was varied from 350 to 750^{o}C, holding pyrolysis time for 5 min and 1.2U_{ms} of N_2 flow rate (see Table 5.1). The pyrolysis vapor flew through a –10^{o}C condenser to condense and collect the liquid product. The condenser operated by using a glycerin – water mixture filled in a temperature controlled water bath. The solid product and liquid product in the condenser were collected and weighed. The respective product yields based on the initial palm shell feed were determined. Also, the gas yield was calculated by mass balance, knowing the yields of total collected solid and liquid products.

The second series of experiments were performed, also in the batch mode, to investigate the effect of pyrolysis time on the pyrolysis yield. The experiments were conducted with seven different pyrolysis time varying from 5 to 45 min with constant pyrolysis conditions of 650^{o}C, 6.7 L/min of N_2 flow rate, 70 g of palm shell and 2.18 mm particle size.

The third series of experiments were carried out to study the effect of particle size on the product yields. The experiments were performed by changing five different particle sizes with constant running conditions of 650°C, 6.7 L/min of N_2 flow rate, 70 g of palm shell and 15 min pyrolysis time.

The last part of experiments of batch pyrolysis was to study the effect of bed height on the product yield by varying palm shell weight of 90, 120, 150 and 200 g, corresponding to bed heights of 6, 7, 8, and 9 cm, respectively. For all those runs, the pyrolysis temperature, particle size, pyrolysis time and N_2 flow rate were kept constant at 650°C, 1.55 mm, and 15 min and $1.2U_{ms}$ respectively.

The required reactor temperature was set and monitored by a furnace temperature controller from which its temperature was calibrated with K – type chromel/alumina thermocouple. The pressure drop across the bed was measured by means of a U – tube mercury manometer.

5.3.2.2 Continuous Experiment

Based on the results from batch experiments, the maximum liquid product yield was achieve with particle size of 1.55 mm, bed height of 5 cm and at pyrolysis temperature of 650°C, and this set of condition was introduced for the continuous process. The continuous operation was first carried out by feeding 5 g/min palm shell to the reactor for 15 min without discharging to set up the initial static bed height of 5 cm inside the reactor. After that, the solid screw feeder was turned on to convey the solid into the reactor. The pyrolyzed solid product was withdrawn from the reactor by a screw feeder and collected in a bottom collector. The pyrolysis vapor flowed through a –10°C condenser to collect the liquid product. The condenser operated by using a glycerin – water mixture filled in a temperature controlled water bath. The stability of process was followed by monitoring the pressure and temperature. In this experiment only the effect of temperature was investigated.

5.3.3 Analysis of Pyrolysis Products

5.3.3.1 Liquid Product

Liquid products collected from palm shell pyrolysis were analyzed for physicochemical properties. The water in the bio –oil was removed by isotropic distillation with toluene (Baker and Elliott, 1988 quoted in Froment, Delmon and Grange, n.d.). A chemical analysis of dewatered bio – oil was determined by gas chromatography. Due to the presence of a wide range of chemical components with different properties and a wide variety of compound polarities and molecular weight, the fractionation of bio –oil sample through multi – step extraction or column separation into different fractions prior to the chemical analysis was necessary. The dewatered bio –oil was first fractionated by silica – gel column chromatography and followed by GC analysis. The dewatered bio –oil of 2 ml was mixed with 1 g of silica gel (100 – 200 mesh) under ultrasonic irradiation. Then the mixture was transfered into a packed column of 2 cm inside diameter. Next, fractionation of bio –oil was performed using pentane (40 ml), toluene (40 ml), diethyl ether (40 ml) and methanol (40 ml) to obtain aliphatic aromatic, oxygenated and polar fractions, respectively. After that, each eluted fraction was concentrated to have a volume of 2 ml and further analyzed by gas chromatography (Varian CP - 3800) equipped with a capillary coated with VF – 5MS (30 m × 0.39 mm, and 0.25 μm film thickness).

Functional group compositional analysis of the liquid products was carried out using Fourier transform infra-red spectrometry (Nicolet Impact). A small amount of bio – oil was mixed with potassium bromide (KBr) powder and pressed into a disc and then the spectrum of the sample was taken.

In addition, the bio – oil derived under the optimal pyrolysis conditions giving the maximum bio –oil yield was also analyzed for their chemical properties, calorific value (ASTM D240 – 92), density (Gay – Lussac bottle), viscociry (ASTM D445 – 96), and water by the Karl Fischer Titration.

5.3.3.2 Solid Product

The solid product derived from pyrolysis of palm shell was characterized for elemental analysis (CHNS/O analyzer, Perkin Elmer PE2400 series II). Proximate analysis, consisting of moisture content (ASTM D2867 – 95), volatile content (ASTM D5832 – 95), ash content (ASTM D2866 -94) and fixed carbon content by different methods. Furthermore, true density and porous properties analysis by using He pycnometer (Accupyc 1330 Mocrimeritics) and Autosorb – iQ (Quantachrome) respectively.

5.3.3.3 Gas Product

The gas product was characterized by a gas chromatograph (Varian CP -3800) equipped with a thermal conductivity detector (TCD). A capillary coated with CP - Carboplot (27.5 m × 0.53 mm, and 0.25 μm film thickness) was used for the analysis of H_2, O_2, N_2, CO and CH_4.

5.3.4 Kinetic Model of Palm Shell Pyrolysis

Pyrolysis is a very versatile process, and different operating strategies may be established in order for the products obtained to be used in many applications. The modeling of pyrolysis reaction is extremely complicated because several components are decomposed simultaneously. Kinetic knowledge of pyrolysis process is essential for the determination of the optimum conditions for maximization of a given product and for the design and simulation of the pyrolysis system. Therefore, different classes of mechanism were proposed for the biomass pyrolysis. A general concern in the measurement of pyrolysis kinetics is the exclusion of heat transport limitation. Global kinetic model is the simplest level of kinetic model to describe the thermal decomposition of biomass pyrolysis. However, the model proposed is based on the assumption of a single overall reaction. Thus, the global kinetic model cannot calculate the pyrolysis product yields simultaneously. The competing reaction model of Thurner and Mann (1981) is one of the most classical models for wood pyrolysis, consisting of secondary reactions lumped with primary reactions over a narrow temperature range, representing by three competitive reactions. The schematic representation of the pyrolysis reaction of this model is shown in Equation (5.1). The first – order pyrolysis reaction was assumed for all of the reactions considered.

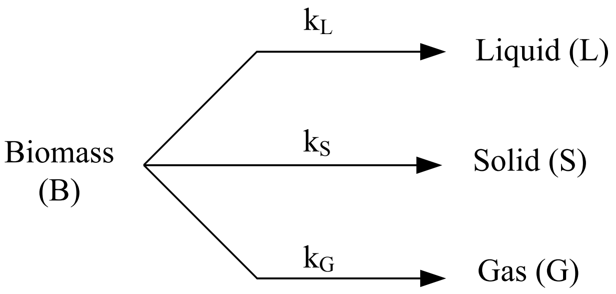

(5.1)

The mass balance equations for the degradation of biomass for the competing reaction model are as follows.

$$\frac{dW_B}{dt} = -(k_L + k_S + k_G)W_B = -k_B W_B \tag{5.2}$$

$$\frac{dW_L}{dt} = k_L W_B = A_L \exp\left(-\frac{E_L}{RT}\right) W_B \tag{5.3}$$

$$\frac{dW_S}{dt} = k_S W_B = A_S \exp\left(-\frac{E_S}{RT}\right) W_B \tag{5.4}$$

$$\frac{dW_G}{dt} = k_G W_B = A_G \exp\left(-\frac{E_G}{RT}\right) W_B \tag{5.5}$$

where;

$$k_B = k_L + k_S + k_G$$

k_L, k_S and k_G = liquid, solid and gas formation rate constant, respectively

W_B, W_L, W_S and W_G = final weight of biomass precursor, and liquid, solid and gas products, respectively

A_L, A_S and A_G = pre-exponential constant of liquid, solid and gas, respectively

E_L, E_S and E_G = activation energy of liquid, solid and gas formation, respectively

The weight of each product of biomass pyrolysis can be solved by numerical method. In this work, numerical method using classical Fourth – Order Runge – Kutta algorithm was employed. The kinetic parameters of the model (A, E) were determined by using the nonlinear least square (NLS) algorithm to minimize the objective function defined a $\mathrm{O.F.} = \sum_{i=1}^{N} (w_{cal,i} - w_{exp,i})^2$, where $w_{cal,i}$ and $w_{exp,i}$ represent the calculated and experimental final weight, respectively. Subscript i denotes the discrete values of w, and N is the number of data points used in the least-squares fitting. According to Elordi and coworker (2007), the prediction by the competing reaction model gave a good agreement with the experiment data for pyrolysis of high density polyethylene under the pyrolysis conditions investigate. Therefore, in this work, the competing reaction model was adopted and used to describe the biomass pyrolysis mechanism in a conical spouted bed.

5.4 Results and Discussion

5.4.1 Palm Shell Pyrolysis in a Conical Spouted Bed Reactor

The effect of pyrolysis temperature, particle size, pyrolysis time and bed height on the product yields and properties of palm shell pyrolysis in a batch conical spouted bed was studied. On studying the effect of pyrolysis temperature and time in batch mode, the experiments were conducted with five different pyrolysis temperatures and six different pyrolysis times for a given particle size and bed height. The next set of experiment was performed for different particle sizes under a fixed pyrolysis temperature and time, and bed height. For the effect of bed height, the experiments were carried out by varying bed height from 5 – 9 cm. at a given pyrolysis conditions. The results of pyrolysis product yields under various conditions are shown in Table 5.2.

5.4.1.1 Effect of Pyrolysis Temperature

Figure 5.2 shows the effect of pyrolysis temperature on the product yields of palm shell pyrolysis in the batch conical spouted reactor. The experiments were conducted at a constant average particle size of 2.18 mm, bed height 5.0 cm (20 grams of palm shell), pyrolysis time 5 min and nitrogen flow rate at $1.2U_{ms}$ for each pyrolysis temperature (see Table 5.1). The solid yield derived from pyrolysis of palm shell decreased sharply from 350 to 650°C, and dropped slightly at pyrolysis temperatures above 650°C. This is to be expected because the rate of devolatilization increases with increasing pyrolysis temperature. Similar observation was reported by Tsai et al. (2006) who investigated the effect of pyrolysis temperature (400 – 800°C) on the pyrolysis product yields and their chemical compositions from coconut shell using a lab – scale fast pyrolysis system. As the temperature was increased from 350 to 750°C, the solid yield dropped from 61 to 29 wt%. This decrease in solid yield was reflected in the increase in liquid and gas yields. Over the temperature range from 350 to 750°C, the liquid yield increased from 29 wt% to the maximum yield of 52 wt% at pyrolysis temperature 750°C. Figure 5.2 shows that liquid product yield increased slightly from 50 to 52 wt% when the pyrolysis temperature was increase from 650 – 750°C. Therefore, it can be concluded that the optimum pyrolysis temperature for the production of bio- oil should be at 650°C. Previous workers (Tsai et al, 2006) found that the optimum pyrolysis temperature for maximizing the oil yield lies in the temperature range between 500 –

Table 5.2 Product yields from various pyrolysis condition in a conical spouted bed reactor.

System	Particle Size (mm)	Bed height (cm)	Temp. (^oC)	Time (min)	Product yields (%)		
					Solid	Liquid	Gas
Batch	2.18	5	350	5	61	30	9
			450		50	36	14
			550		46	39	15
			650		31	50	19
			750		29	52	19
	2.18	5	650	5	46	35	19
				10	43	40	17
				15	31	50	19
				20	33	51	16
				30	30	52	18
				45	30	51	19
	1.09	5	650	15	29	52	19
	1.29	5	650	15	29	53	18
	1.55	5	650	15	28	55	17
		6			27	54	19
		7			28	55	17
		8			27	53	20
		9			29	52	19
	1.55	5	450	15	45	45	9
			550		35	53	12
			750		25	61	14
Continuous	1.55	5	450	-	59	29	12
			550		47	42	11
			650		22	65	12
			750		22	64	14

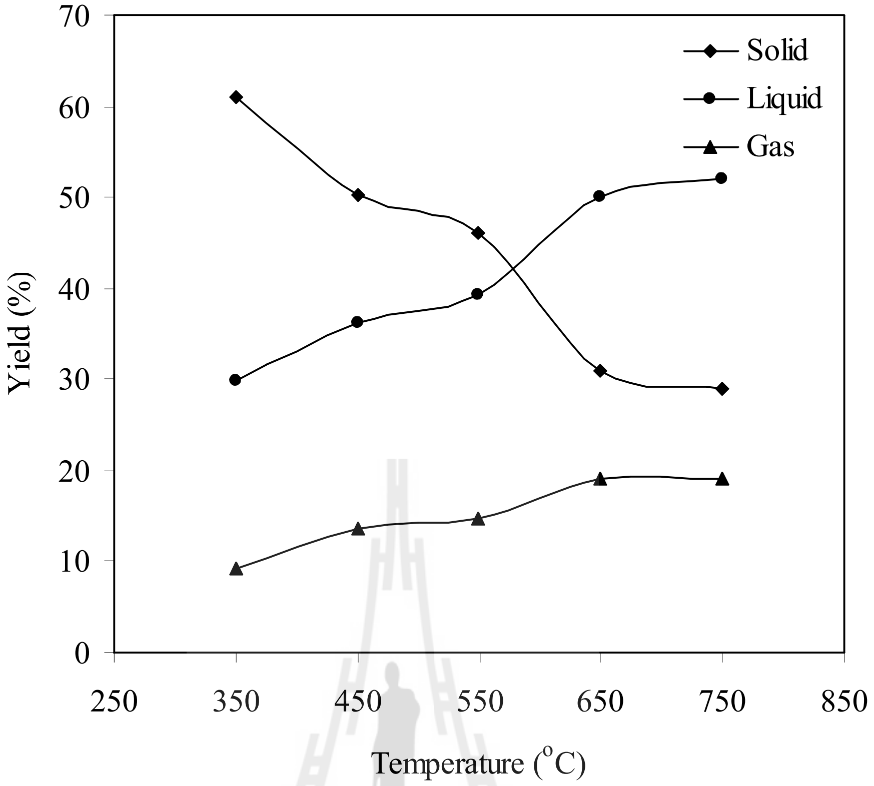

Figure 5.2 Effect of pyrolysis temperature on product yields for batch spouted bed reactor (average particle size 2.18 mm, pyrolysis time 5 min and bed height of 5.0 cm).

650°C depending on the type of biomass precursor. It is seen from Figure 5.2 that the gas yield increased over a narrow range from 9 to 19% when the pyrolysis temperature was increased from 350 to 750°C. Similar results with different biomass samples were also obtained in the previous investigators (Uzun, Pütün, and Pütün, 2006). They found that the gas yield increased when the pyrolysis temperature was raised from 400 – 700°C for soybean cake pyrolysis in a fixed bed reactor.

5.4.1.2 Effect of Pyrolysis Time

To determine the effect of pyrolysis time on the yields of pyrolysis products, the experiments were conducted at 5, 10, 15, 20, 30 and 45 min, under constant pyrolysis temperature of 650^{o}C, 6.7 L/min of N_2 flow rate, 5.0 cm. of bed height and average particle size of 2.18 mm in a batch conical spouted bed reactor. The obtained results are shown in Figure 5.3 and it seems that the holding time plays a somewhat important role on the pyrolysis product yields. As the pyrolysis time was increased from 5 to 30 min, the solid yield decreased from 46 to 30 wt% and approached an almost constant value at longer pyrolysis times. The maximum yield of liquid product (51 wt%) was obtained at 20 min of pyrolysis time. The liquid yields increased steadily with pyrolysis time from 5 – 15 min, and became almost constant at longer times.

The experimental results in Figure 5.2 and 5.3 indicate that increasing in pyrolysis temperature and time did not greatly affect the gas yield as compared to liquid and solid yields. It is probable that the N_2 flow rate used in this work is high enough to remove the vaporized products from the pyrolysis zone hence, hence help minimizing the possible secondary reactions for producing additional gas product (Uzun et al., 2006).

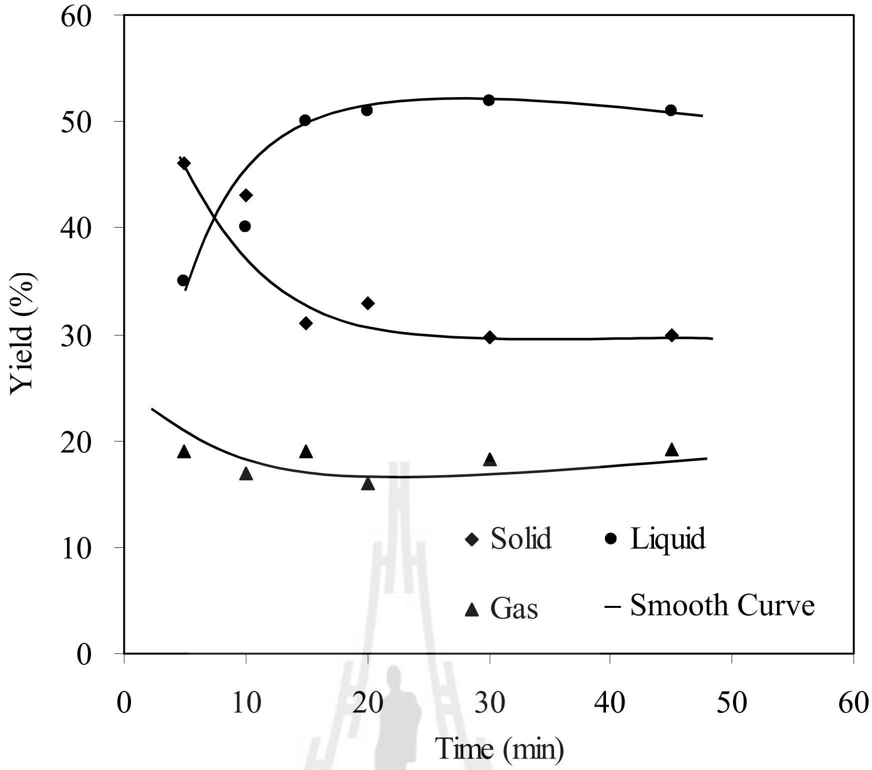

Figure 5.3 Effect of pyrolysis time on product yields (pyrolysis temperature 650^{o}C, 6.7 L/min of N_2 flow rate, 5.0 cm. of bed height and average particle size of 2.18 mm).

5.4.1.3 Effect of Particle Size

The effect of particle size in the range of 1.05 – 2.18 mm on product yields was studied at 650^{o}C, constant pyrolysis time of 15 min, N_2 flow rate of 1.2 U_{ms}, and bed height of 5.0 cm. The experimental results are given in Figure 5.4. There was almost no significant effect of particle size on the pyrolysis yields for the selected particle size range. The maximum liquid yield of 53.5 wt% was achieved with particle size of 1.55 mm and slightly decreased when the particle was larger than 1.55mm. This result agrees with the work of Uzun et al. (2006). They reported that there was no significant effect of particle size on pyrolysis in the selected ranges of 1 – 4 mm for fast pyrolysis of soybean cake. Their experiments were conduced at pyrolysis temperature of 550^{o}C with a constant heating rate of 300^{o}C/min and sweeping gas velocity of 100 cm^3/min. Also, Encinar, Gonzalez and Conzalez (2000) found a similar trend when they performed the pyrolysis of C. cardunculus in a fixed bed reactor at 800^{o}C, nitrogen flow rate of 200 cm^3/min, initial sample weight of 5 g, and particle size range from 0.43 – 2.00 mm. The increasing of particle size range from 1.05 to 1.55 mm exerted small effect on the solid and gas yield. The solid yield showed an increase when using a particle size larger than 1.55 mm, while the gas yield gave the opposite trend. As reported by Onay and Koçkar (2001) particle size range of 1.0 – 2.0 mm is sufficiently small so that it can be heated uniformly throughout. In addition the hot char is known to be catalytically active (Bridgwater, Meier, and Radlein, 1999). The vapors coming from a particle interior have to penetrate through a thicker char layer for a large particle size. This process may cause more severe a secondary cracking of vapor. Moreover, a larger particle size could lead to a slower heating rate in particle interior and longer residence time. These two factors could result in the decrease of liquid and gas yield, and a consequent increase of solid yield with larger particle size.

5.4.1.4 Effect of Bed Height

To determine the effect of bed height on the yields of pyrolysis product, a set of experiments were performed at five static bed height of 5 – 9 cm. For this set of experiment, the pyrolysis temperature and time, and particle size were kept constant at 650^{o}C, 15 min, and 1.55 mm, respectively. The product yields from the pyrolysis process with respect to the variation static bed height are given in Figure 5.5. For the increasing of static bed height from 5 to 9 cm, the liquid yield appeared to decrease slightly, while the solid and gas yields remained relatively constant. The maximum liquid yield of 55 wt% was obtained at static bed height of 7 cm, whereas solid and gas yields of approximately 29 and 19 wt%, respectively, could be derived at the same bed height. From these results, it is reasonable to conclude that the static bed height had insignificant effect on the product yields of spouted – bed pyrolysis.

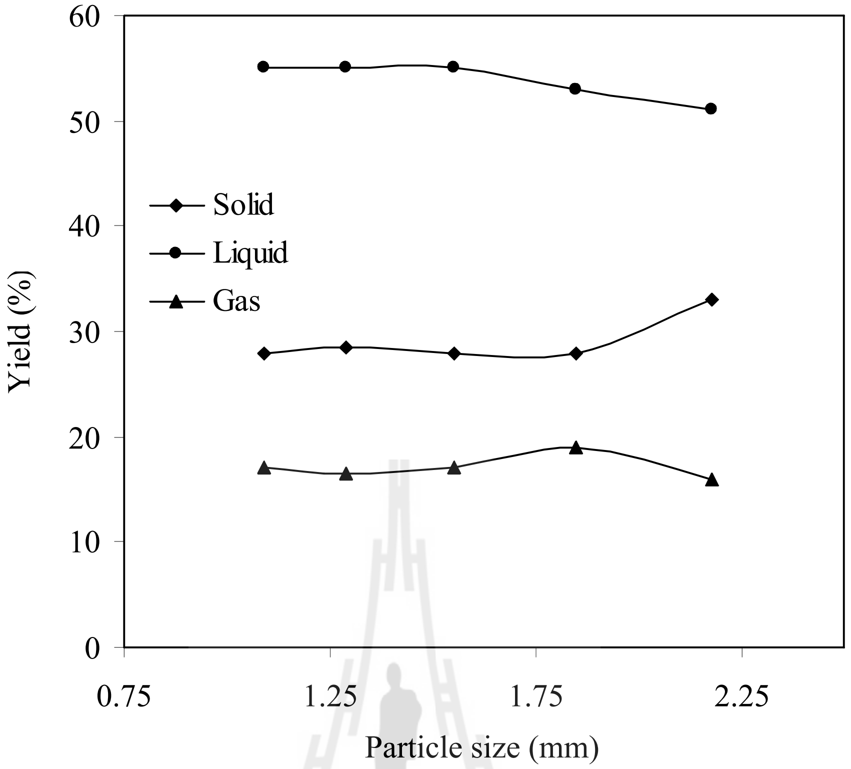

Figure 5.4 Effect of particle size on pyrolysis product yields of batch conical spouted bed (pyrolysis temperature 650°C, N_2 flow rate 6.7 L/min, bed height 5.0 and pyrolysis time of 15 min).

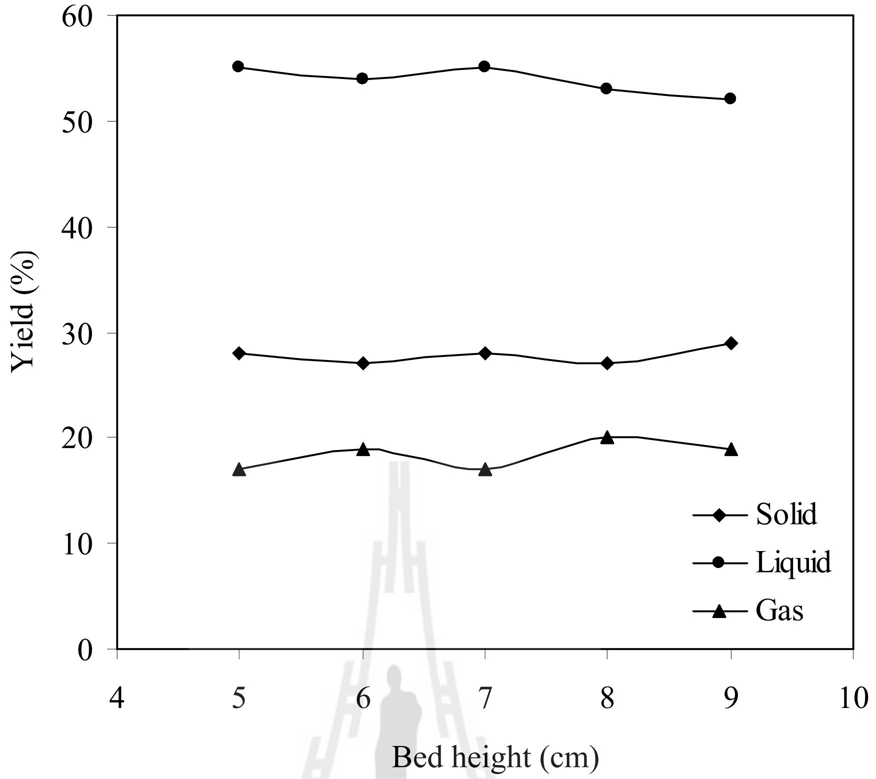

Figure 5.5 Effect of static bed height on product yields (pyrolysis temperature 650^{o}C, particle size of 1.55 mm and pyrolysis time of 15 min).

Figure 5.6 compares the effect of pyrolysis temperature on product yields from batch and continuous process at the same pyrolysis conditions of particle size (1.55 mm) and static bed height (5 cm). The pyrolysis time of batch operation is 20 minutes. Based on the mean residence time of plug flow reactor equation, the mean residence time of continuous run in this work is approximately 5 minutes. The results indicate that both operations gave approximately the same trend and magnitude of gas yield when the pyrolysis temperature was increased from 450 to 750^{o}C. Liquid and solid yields from both processes also show a similar trend tendency concerning the effect of temperature; liquid product yield increased with pyrolysis temperature and became constant at the optimal temperature of 650^{o}C. The maximum liquid yields of 60 wt% and 65 wt% are realized for batch and continuous runs, respectively. Furthermore, the solid yield was found to decrease with increasing pyrolysis temperature for both processes.

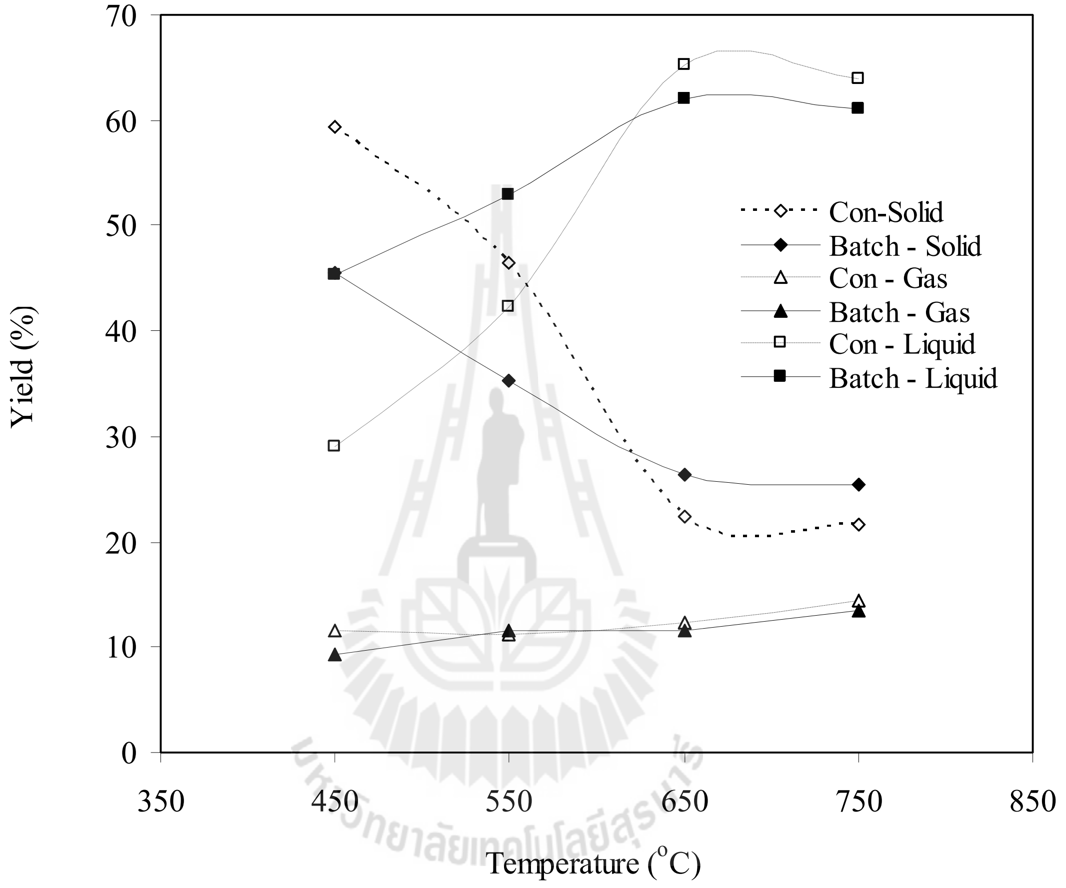

Figure 5.6 Comparison between batch and continuous process on product yields (particle size of 1.55 mm, bed height 5 cm and 20 min pyrolysis time for batch mode).

5.4.1.5 Properties of Pyrolysis Products

Some properties of crude bio - oil derived from batch and continuous operations at pyrolysis temperature 650°C are shown in Table 5.3. Crude oil had opaque dark color and gave the single phase chemical solution. Generally, bio – oil and water can mix to form a single phase chemical solution but the phase separation can occur when the water content exceeds about 30 to 45 wt% (Yaman, 2004). Crude bio – oil from batch and continuous runs of palm shell pyrolysis show similar physical properties. Density of crude bio – oil at 40°C is 1.05 – 1.10 g/cm^3. It is denser than that of diesel fuel (0.78 g/cm^3) and heavy fuel oil (0.85 g/cm^3). The crude bio – oil shows relatively low viscosity characteristic of 3.2 – 3.7 cP at 40°C. The low viscosity is associated with the high value of water content (53 – 55 wt%) present in the crude bio –oil. Generally, the water content in bio – oil mainly derived from the decomposition of lignin – derived materials (Abnisa, Wan Daud, Husin and Sahu, 2011). The crude bio – oil shows a high acid level, pH at room temperature is 2.75 – 2.83. It has been reported that bio –oil with low pH are very corrosive to the metals (Hu, Xu, Hu, Pan and Jiang, 2012). The corrosiveness of bio –oils is more severe when the water content is high and also when bio – oils are used at a high temperature (Czernic, 1999). In addition, removing of water from the crude bio –oil gave rise to an increase in calorific value from 5.4 to 34.7 MJ/kg. According to these results, the removal of water from bio –oil still gives calorific value lowers than that of commercial diesel oil fuel (45.0 MJ/kg). Several physical properties of bio – oil obtained from this experiment agrees with the work of Abnisa et al., (2011). They studied the effect of temperature, sweeping gas flow rate, particle size and holding time on the optimization of production of bio-oil from palm shell. Their experiments

Table 5.3 Physical and chemical properties of bio – oil from batch and continuous pyrolysis in a conical spouted bed, and pyrolysis in a free fall reactor of palm shell.

Properties	**Batch Run**$^{(1)}$	**Continuous Run** $^{(2)}$	**Free fall Reactor**$^{(3)}$	**Fluidized Bed**$^{(4)}$
Viscosity at 40^o (cP)	3.7	3.2	3.5	3.2
Density at 30^oC (g/cm^3)	1.05	1.10	1.16	1.05
pH	2.75	2.83	2.67	2.50
Calorific value (MJ/kg)	5.6 (35.1*)	5.2 (34.2*)	5.8 (35.3*)	6.58
Water Contents (wt %)	53	55	51	53

*Water removed

$^{(1)}$ Particle size of 1.55 mm, time 20 min, temperature 650^oC and N_2 flow rate of 9.8 L/min

$^{(2)}$ Particle size of 1.55 mm, feed rate 5 g/min, temperature 650^oC and N_2 flow rate of 9.8 L/min

$^{(3)}$Particle size of 0.18 mm, feed rate 0.6 g/min, temperature 650^oC and N_2 flow rate of 200 cm^3/min

$^{(4)}$ Abnisa et al., (2001)

were conducted in a fluidized – bed reactor and the maximum yield of bio –oil (47.3 wt%) can be obtained at pyrolysis temperature 500^oC, 2 L/min of sweeping gas, 60 min holding time, 150 g of palm shell feeding, and 1.7 – 2.0 mm average particle size range. Moreover, the experimental results in Table 5.3 indicate that several physical properties of bio – oil obtained from a free fall reactor agree with the properties of bio –oil from conical spouted bed pyrolysis. According to the experimental data of palm shell pyrolysis in a free fall reactor as reported in Chapter 3, the maximum liquid yield of 57 wt% was derived from palm shell pyrolysis at 650^oC, palm shell feed rate of 0.6 g/min, and sweeping gas flow rate 200 cm^3/min).

The spectrum of the crude bio –oil from batch and continuous conical spouted bed and a free fall reactor at pyrolysis temperature of 650°C are given in Figure 5.7 and the functional group compositional analysis for the pyrolysis oil is presented in Table 5.4. The analysis was carried out using KBr pellet. The O – H stretching vibrations between 3200 cm^{-1} and 3400 cm^{-1}of the bio –oils indicates the presence of phenols and alcohols. The C – H stretching vibrations between 2800 cm^{-1} and 3000 cm^{-1} and C – H deformation vibrations between 1350 cm^{-1} and 1450 cm^{-1} indicate the presence of alkanes group. The C = O stretching vibrations between of 1680 cm^{-1} and 1750 cm^{-1} are compatible with the presence of ketones, quinines, and aldehyde group. The absorbance peaks between 1500 cm^{-1} and 1645 cm^{-1} represent C = C stretching vibration which is indicative of alkenes. Also, aromatics groups are indicated by the absorption peaks between 690 cm^{-1} and 900 cm^{-1}. The results in Figure 5.7 show that the spectrums of pyrolysis bio – oils from different pyrolysis reactor and conditions display a similar functional group of the chemical compounds.

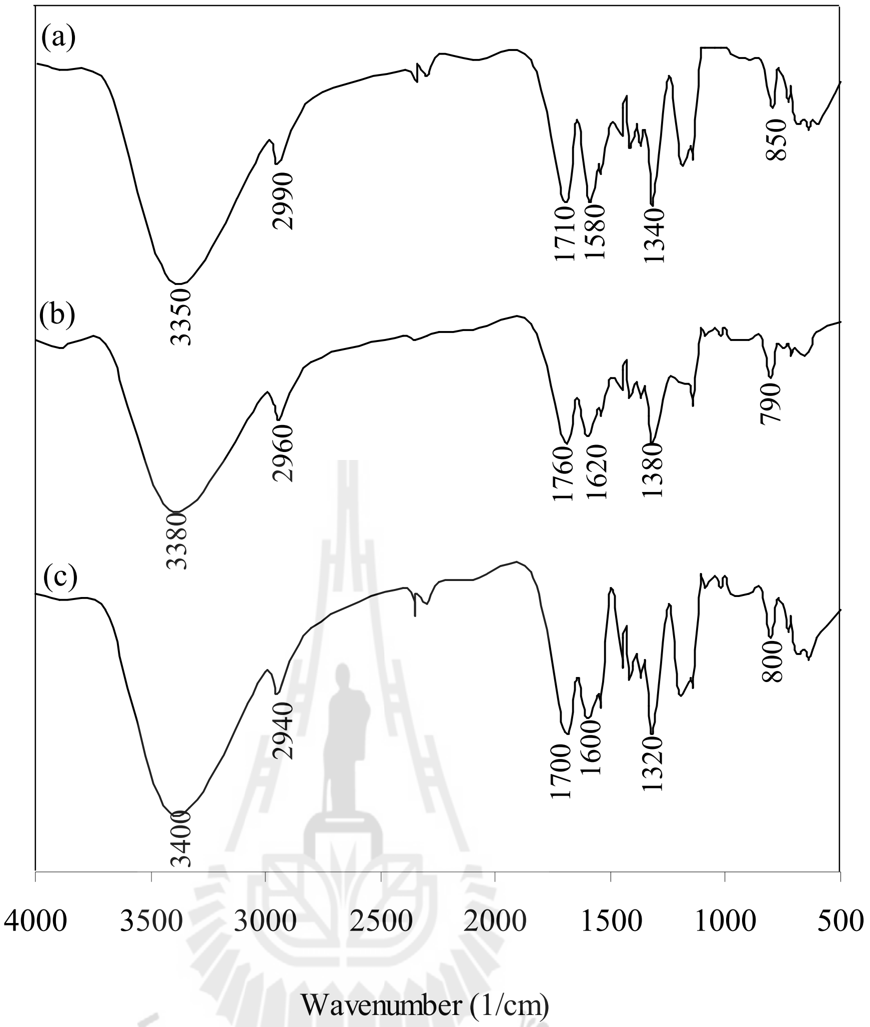

Figure 5.7 FT – IR spectra of bio – oil derived from palm shell pyrolysis of (a) a free fall reactor, (b) a batch conical spouted bed, and (c) a continuous conical spouted bed.

Table 5.4 Functional group composition of bio – oil derived from palm shell pyrolysis.

Groups	Absorbance (cm^{-1})	Class of compounds
O – H	3200 – 3400	Phenols, alcohol
C – H	2800 – 3000	Alkanes
C = O	1680 – 1750	Ketones, quinines, aldehyde groups
C = C	1500 – 1640	Alkenes
C – H	1350 – 1450	Alkanes
O – H	690 – 900	Aromatic groups

GC analysis was carried out on the bio – oil product obtained from batch and continuous conical spouted bed, and a free fall reactor at pyrolysis temperature of 650°C in order to identify and quantify the type of compounds. Table 5.5 shows some chemical compounds present in bio – oil sample obtained from different pyrolysis conditions. The analysis results shows the chemical compounds in bio – oil to consist of alkanes, aromatics, phenol and organic compounds such as furfural. According to the results of Abnisa et al. (2004), the chemical compound in bio –oil obtained for palm shell pyrolysis by using fluidized – bed reactor at 500°C consisted of alkanes, aromatic, phenol derivatives and furfural. Moreover, these chemical compounds are also found in bio-oil from the pyrolysis of rice straw, sugarcane bagasses, and coconut shell in a fixed – bed reactor (Tsai et al., 2006). Also, the chemical concentration of bio-oil from those different pyrolysis conditions did not show a significant different. The derived bio – oil from palm shell fast pyrolysis provides a source of potential chemical feedstocks such as phenol, furfural, benzene, toluene, xylene, styrene, etc. However, due to their presence in low concentrations, the complete separation and purification of each compound pose unacceptable energetic and financial cost. The application in other areas is thus an important alternative consideration. As reported by Czernik and Bridgwater (2004), the use of pyrolytic lignin as phenol replacement in phenol – formaldehyde resins production and glycilaldehyde is also the most active meat browning agent in liquid smoke. Moreover, a potential application of the water - soluble fraction of bio – oil is to use for the production of calcium salts of carboxylic acids that can be used as environmentally friendly road de – icers.

Table 5.6 shows the characteristics of solid product (char) obtained from pyrolysis of palm shell at pyrolysis temperature of 650°C, N_2 flow rate of 9.8 L/min, and particle size 1.55 mm for the continuous run. Bulk density of char is lower than that of the precursor (0.68 g/cm^3), while the true density is higher. Proximate analysis indicates that the main component in char is fixed carbon. It may be that during pyrolysis, hydrogen and oxygen were consumed via reactions of dehydrogenation and deoxygenation to produce CO_2, CO, H_2, H_2O, thus causing the decrease in the molar ratio of H/C and O/C. Calorific values of derived char is comparable to that of coal (~ 35 MJ). Furthermore, porous characteristics of char show char contains mainly microspores which accounts for about 70% of total pore volume.

Table 5.5 Chemical compounds of bio – oil derived from palm shell pyrolysis for different operating conditions.

Chemical	Chemical concentration in bio – oil (wt%)		
	Batch conical spouted bed⁽¹⁾	Continuous conical spouted bed⁽²⁾	Free fall reactor⁽³⁾
n – Octane, C_8	1.768	1.315	2.542
n – Nonane, C_9	0.123	0.089	0.210
n – Decane, C_{10}	0.089	0.076	0.176
n – Undecane, C_{11}	0.056	0.011	0.024
n – Dodecane, C_{12}	0.000	0.005	0.092
n – Tridecane, C_{13}	0.068	0.023	0.014
n – Tetradecane, C_{14}	0.054	0.001	0.037
n – Pentadecane, C_{15}	0.003	0.000	0.067
n – Hexadecane, C_{16}	0.007	0.000	0.025
n – Heptadecane, C_{17}	0.123	0.131	0.154
n – Octadecane, C_{18}	0.067	0.078	0.071
n – Nondadecane, C_{19}	0.235	0.195	0.269
n – Eicosane, C_{20}	0.023	0.000	0.102
Phenol	2.365	2.413	1.987
Furfural	0.721	0.651	0.876
Benzene	0.249	0.350	0.386
Toluene	0.629	0.511	0.712
Xylene	0.254	0.354	0.364
Styrene	0.065	0.082	0.128

(1) Particle size of 1.55 mm, time 20 min, temperature 650°C and N_2 flow rate of 9.8 L/min

(2) Particle size of 1.55 mm, feed rate 5 g/min, temperature 650°C and N_2 flow rate of 9.8 L/min

(3) Particle size of 0.18 mm, feed rate 0.6 g/min, temperature 650°C and N_2 flow rate of 200 cm^3/min

Table 5.6 Properties of chars derived from palm shell pyrolysis at temperature of 650°C, N_2 flow rate of 9.8 L/min, and particle size 1.55 mm for the continuous run of conical spouted bed reactor.

Properties	**Value**
Bulk density (g.cm^3)	0.45
True density (g.cm^3)	1.75
Proximate analysis (Dry basis) (wt%)	
Volatile	18.56
Fixed carbon	71.23
Ash	10.21
Elemental analysis (wt%)	
C	62.23
H	1.25
O	35.05
N	1.47
H/C (mole ratio)	0.24
O/C (mole ratio)	0.42
Calorific Value (MJ/kg)	30.78
Porous characteristics	
BET surface area (m^2/g)	220.15
Micropore area (m^2/g)	170.24
Average pore size (nm)	2.23
Total pore volume (cm^3/g)	0.123
Micropore volume (cm^3/g)	0.085

Typical gas yields and compositions obtained from palm shell pyrolysis at pyrolysis temperature of 650°C, N_2 flow rate of 9.8 L/min, and particle size 1.55 mm for the continuous run are shown in Table 5.7. The gas products consist mainly of CO, CO_2, and CH_4. Hydrogen gas was not detected in the gas compositions. The results show that CO and CO_2 are the dominant components among the others.

5.4.2 Kinetics of Palm Shell Pyrolysis

In this work the experimental data of batch pyrolysis in a conical spouted bed reactor were used to develop a mathematic model to predict product yield and product distribution from flash pyrolysis of palm shell. The kinetic scheme proposed by Thurner and Mann (1981) was adopted for the analysis in this work. The first – order pyrolysis reaction was assumed for all of the reaction considered and the temperature of the particle is basically equal to the temperature of the surrounding fluid, so that heat transfer resistance inside the particle can be neglected. The secondary reactions of pyrolysis are included in the kinetic laws of primary reactions.

Table 5.7 Gas yield of palm shell pyrolysis at pyrolysis temperature of 650°C, N_2 flow rate of 9.8 L/min, and particle size 1.55 mm for the continuous run.

Gas component	**Gas yield (wt%)**
CO	25.21
CO_2	14.20
CH_4	2.43
H_2	not analyzed

Figure 5.8 and 5.9 show the comparison between experimental data and model fitting with the competitive model of Thurner and Mann. Overall, the agreement between experiments and model prediction is considered to be reasonably good. However, the calculated values show excellent agreement with the experimental results at pyrolysis temperature high than 550^{o}C. The predicted data in Figure 5.9 indicate that the pyrolysis reaction completed at 2 min that faster than in the actual process (15 min). As mentioned before, the apparent activation energy and pre – exponential constant are important parameters from the point of view of evaluating the stability and compatibility for energetic material. The frequency factor (A) and activation energy (E) indicate how fast and easy for the pyrolysis reaction to proceed. The minimum energy required to start a chemical reaction can be considered from the value of activation energy. The kinetic parameters, the activation energy (E) and frequency factor (A) determined from the model fitting, are summarized in Table 5.8. The activation energy of gas formation is higher than those of liquid and solid. This indicates that the generation of gas products requires a larger amount of energy than the other products. This result agrees with that of Elordi et al. (2007) who studied the product distribution modeling in the thermal pyrolysis of high density polyethylene in a conical spouted bed. They reported that the activation energy of polyethylene decomposing to gas products is higher than that of liquid and solid product. According to Grønli (1999) who studied the pyrolysis of single – particle of wood in bell – shaped Pyrex reactor found that the decomposition of wood to gas required higher activation energy than liquid and solid product. The frequency factor of gas is higher than solid and liquid, respectively. Generally, the high value of frequency factor and lower activation energy, the faster and easier would be for the pyrolysis reaction to occur. This signifies that the formation of solid should be faster and easier than that of liquid and gas, due to its high frequency factor and lower in activation energy. Considering the kinetic rate at a constant temperature by using the kinetic parameters in Table 5.8, it is discovered that the kinetic rate of solid product is higher than that of liquid and gas, respectively.

Figure 5.10 compares the experimental and calculated solid yields by using the two – parallel reaction model as a function of particle size. The results show a satisfactory agreement between the experimental data and the model prediction in this study. The kinetic parameters (E, A and n), and %error from the model are listed in Table 5.9. The kinetic parameters are relatively constant and independent of particle size. This indicates that internal heat and mass transfer control does not govern the pyrolysis of palm shell in a conical spouted bed reactor. However, these results are quite different from palm shell pyrolysis in a free fall reactor (data in Chapter 3) and thermal gravimetric analyzer (Luangkiattikhun et al. 2007). Furthermore, the results show that the first component having higher activation energy (E_1) than the second component (E_2) could represent the decomposition of the heavier component. The larger value of a in comparison with that of b indicates that the decomposition of palm shell is mainly contributed by the first component. The activation energy (E_1 and E_2) and pre – exponential factor (A_1 and A_2) for palm shell pyrolysis in a conical spouted bed reactor was lower than those of palm shell pyrolysis from a free fall reactor and the thermal gravimetric analyzer.

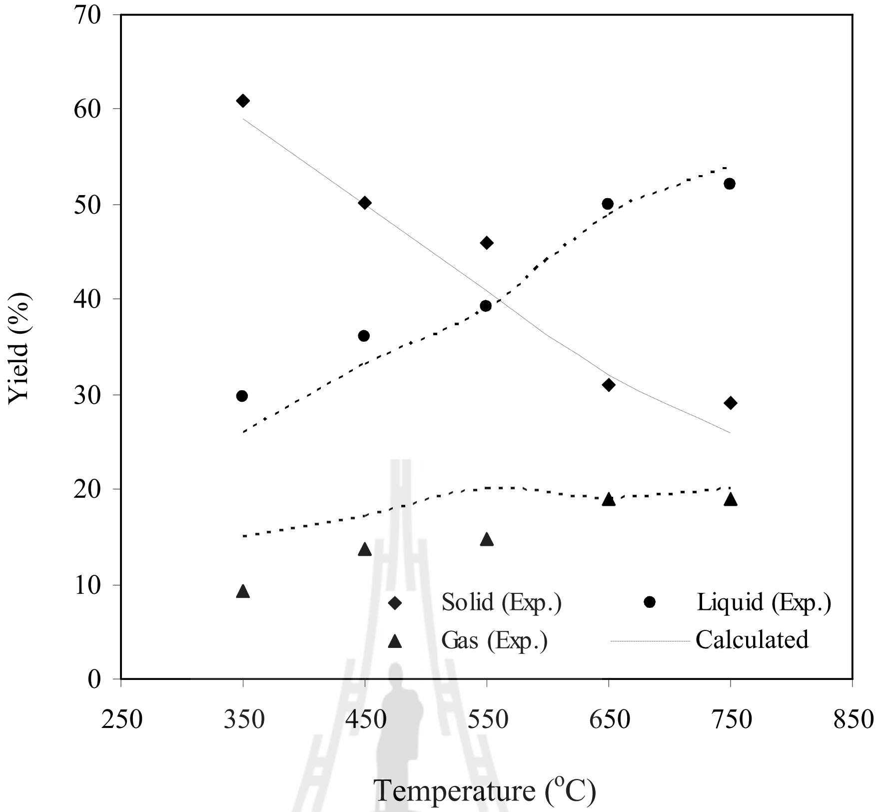

Figure 5.8 Comparison of product yields from experiments and competitive model fitting of palm shell pyrolysis at various temperatures (pyrolysis time 15 min, average particle size 2.18 mm, and bed height of 5 cm).

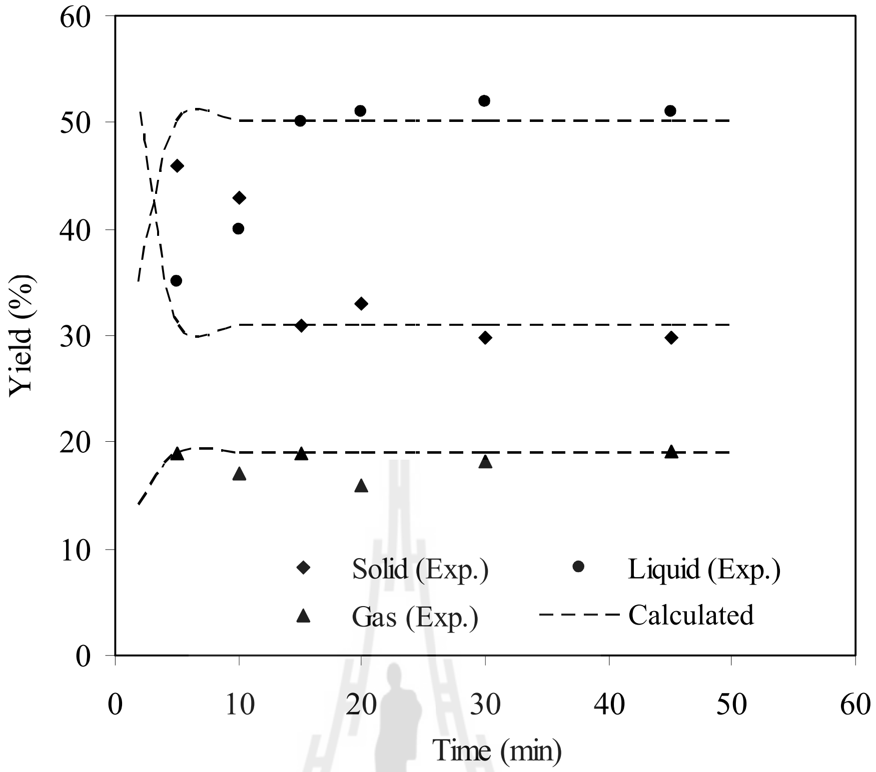

Figure 5.9 Comparison of product yields from experiments and the competitive model fitting of palm shell pyrolysis at various times (pyrolysis temperature 650°C, average particle size 2.18 mm, and bed height of 5 cm).

Table 5.8 Kinetic parameters obtained form competitive model.

Type of product	**Activation Energy, (E) (kJ/mol)**	**Pre-exponential Factor, (A) (1/s)**
Solid	30	1039
Liquid	33	89
Gas	40	1090

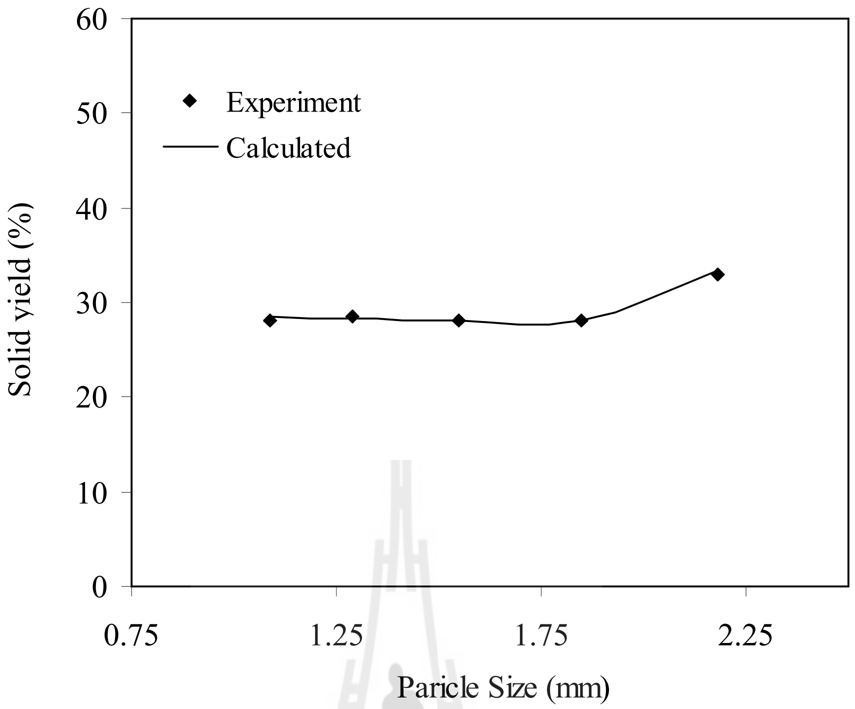

Figure 5.10 Comparison of solid yields from experiments and the two - parallel model fitting of palm shell pyrolysis at various particle size (pyrolysis temperature 650°C, bed height of 5 cm. and pyrolysis time 20 minutes).

Table 5.9 Kinetic parameters obtained form the two - parallel model (pyrolysis temperature 650°C, bed height of 5 cm., and pyrolysis time 20 minutes).

Size (mm)	**a**	**A_1** (s^{-1})	**E_1** (kJ/mol)	**n_1**	**b**	**A_2** (s^{-1})	**E_2** (kJ/mol)	**n_2**	**Error** (%)
1.09	0.7	157	23.7	1.19	0.3	40.2	8.17	1.07	1.78
1.29		157	23.7	1.19		40.2	8.17	1.07	0.77
1.55		157	23.7	1.19		40.2	8.17	1.07	0.53
		1.20×10^{7}(1)	41.66(1)	32.47(1)		2.53×10^{5}(1)	305.92(1)	2.00(1)	1.96(1)
1.85		157	23.8	1.24		40.2	8.17	1.07	0.71
2.18		156	23.9	1.24		40.2	8.17	1.07	1.22
1.40(2)	0.21(2)	1.10×10^{7}(2)	234.4(2)	1.00(2)	0.79(2)	8.66×10^{13}(2)	171.8(2)	4.14(2)	3.11(2)

(1) Pyrolysis of palm shell from a free fall reactor

(2) Pyrolysis of palm shell from TGA (Luangkiattikhun et al. 2007)

5.5 Conclusions

Pyrolysis of palm shell was studied in both batch and continuous conical spouted bed. The following conclusion can be drawn from this study.

- The yield of liquid products tended to increase significantly with pyrolysis temperature and then decreased when the pyrolysis temperature reached to an optimum temperature.
- The solid yield decreased with increasing pyrolysis temperature, while the gas yield gave the opposite trend.
- Particle size and bed height did not appear to show a significant effect on the pyrolysis product yields.
- There was no difference in the gas yield from batch and continuous conical spouted bed when running under similar pyrolysis conditions.
- Both types of batch and continuous operation exerted a significant influence on liquid and solid product yields at the pyrolysis temperatures lower than 550°C.
- Bio – oil from palm shell pyrolysis is less attractive to be used as a direct fuel, due to its high water content and low calorific value.
- FTIR and GC analysis results showed the chemical compounds in bio-oil to consist of alkanes, aromatics, phenol and organic compounds.
- The crude bio-oil shows a high acid level, pH at room temperature is 2.75 – 2.83 for batch and continuous run, respectively.
- The derived solid product (char) had reasonably high calorific value 30.78 MJ/kg comparable to that of coal (~ 35 MJ/kg) and showed reasonable BET surface area of about 220 m^2/g.

- Carbon monoxide and carbon dioxide gas are the dominant components in the gas product.
- The competitive kinetic model of Thurner and Mann gave correct prediction of experimental yields and compositions of pyrolysis products.

5.6 References

Abnisa, F., Wan Daud, W. M. A., Husin, W. N. W, and Sahu, J. N. (2011). Utilization possibilities of palm shell as a source of biomass energy in Malaysia by producing bio – oil in pyrolysis process. **Biomass and Bioenergy.** 35: 1863 – 1872.

Azduwin, K., Ridzuan, K. J. M., Hafis, S. M., Amran, T. A. T. (2012). Slow Pyrolysis of Imperata Cylindrica in a Fixed Bed Reactor. **International Journal of Biology, Ecological and Environmental Sciences**. 1(5): 176 – 180.

Bridgwater, A. V., Peacocke, G. V. C. (2000). Fast pyrolysis process for biomass. **Renewable and Sustainable Energy Reviews.** 4: 1 – 73.

Bridgwater, A. V., Meier, D., Radlein, D. (1999). An overview of fast pyrolysis of biomass. Oganic Geochemistry. 30(12):1479 – 1493.

Bridgewater, A. V. (1997). **Developments in thremochemical biomass conversion**. Volume 2. London: Blakie Academic & Professional. 945 – 959. Boocock DGB, editors.

Czernik, S., and Bridgwater, A. V. (2004). Overview of application of biomass fast pyrolysis oil. **Energy and Fuels.** 18: 590 – 598.

Czernik, S. (1999). **Environment health and safety in Fast pyrolysis of Biomass.** Vol. 1. CPL Press. Newbury. UK. 115 – 118.

Elordi, G., Lopez, G., Olazar, M., Aguado, R and Bibao, J. (2007). Production distribution modeling in the thermal pyrolysis of high density polyethylene. **Journal of Hazardous Materials.** 144: 708 – 714.

Encinar, J. M., Gonzalez, J. F., and Gonzalez, F. (2000). Fiexd –bed pyrolysis of Cynara cardunculus L. Product yields and compositions. **Fuel Processing Technology.** 68: 209 – 222.

Froment, G. F., Delmon, B., and Grange, P. (n.d.). **Hydrotreatment and Hydro - cracking of oil fractions.** ELESEVIER SCIENCE B.V. Netherlands.

Goyal, H.B., Seal, D., and Saxena, R.C. (2008). Bio-fuels from thermo chemical conversion of renewable resources: A review. **Renewable and Sustainable Energy Reviews**.12: 504–517.

Grønli, M., Antal, M. J., and Va´rhegyi, G. (1999). A Round-Robin Study of Cellulose Pyrolysis Kinetics by Thermogravimetry. **Ind. Eng. Chem. Res.** 38: 2238-2244.

Hu, E., Xu, Y., Hu, X., Pan, L., and Jiang, Shaotong. (2012). Corrosion behaviors of metals in biodiesel from rapeseed oil and methanol. **Renewable Energy.** 37(1): 371 – 378.

Luangkiattikhun, P., Tangsathitkulchai, C., and Tangsathitkulchai, M.(2007). Non-isothermal thermogravimetric analysis of oil-palm solid wastes. **Bioresource Technology.** Article In Press.

Onay, O., Koçkar, O. M. (2006). Pyrolysis of rapeseed in a free fall reactor for production of bio – oil. **Fuel.** 85: 1921 – 1928.

Ozlem, O., and Kockar, O. M. 2006. Pyrolysis of rapeseed in a free fall reactor for production of bio-oil. **Fuel.** 85:1921-1928.

Thurner, F., and Mann, U. (1981). **Kinetic Investigation of wood Pyrolysis. Industrial and Engineering Chemical Process Design and Development.** 20: 482 – 488.

Tsai, W. T., Lee, M. K., and Chang, Y. M. (2007). Fast pyrolysis of rice husk: Product yields and compositions. **Bioresource Technology.** 98: 22 – 28.

Tsai, W.T., Lee, M.K., and Chang, Y.M. (2006). Fast pyrolysis of rice straw, sugarcane bagasse and coconut shell in an induction-heating reactor**. J. Anal. Appl. Pyrolysis.** 76:230–237**.**

Uzun, B. B., Pütün, A. E., and Pütün, E. (2006). Fast pyrolysis of soybean cake: Product yields and compositions. **Bioresource Technology.** 97: 569 – 576.

Wang et al. (2005). Biomass pyrolysis in a fluidized bed reactor. Part 2: Experimental validation of model results. Industrial&Engineering Chemistry Research. 44(33). 8786 – 8795.

Yaman, S. (2004). Pyrolysis of biomass to produce fuels and chemical feedstocks. **Energy Conversion and Management.** 45(5): 651 – 671.

Yang, H., Yan, R., Chen, H., Lee, D. H., and Zheng, C. (2007). Characteristics of hemicellulose, cellulose and lignin pyrolysis. **Fuel.** 86: 1781–1788.

CHAPTER 6

LOW TEMPERATURE CATALYTIC GASIFICATION OF COCONUT SHELL FOR THE COMBINED PRODUCTION OF SYNGAS AND ACTIVATED CARBON

6.1 Abstract

Effects of potassium hydroxide additive, reaction temperature, reaction time, and carbonization step on the amount of the gas produced as well as porous properties of the solid products were investigated for the low temperature gasification of coconut shell with carbon dioxide. Results show that the presence of potassium hydroxide had a significant effect on the composition and quantity of gas produced and facilitated the rate of hydrogen and carbon monoxide formation. It has been observed that the total amounts of produced gas, and carbon monoxide were found to increase with increasing gasification temperature. In addition, results indicated that carbonization step can promote the total amount of produced gas, hydrogen and carbon monoxide contents. Furthermore, the extent of porosity development of activated carbon was found to be influenced by the chemical ratio and gasification temperature. The specific surface area was increased as the chemical ratio and gasification temperature were increased. However, the specific surface area decreased

with the increase of gasification time. Finally, the optimum conditions for achieving high hydrogen composition and specific surface area of solid were gasification at 600°C for 60 min with carbonization step and using chemical weight ratio of 3.0. This condition gave the hydrogen composition up to 27.90 wt% of gas produced and specific surface area of activated carbon of 2,650 m^2/g.

6.2 Introduction

Biomass has becomes an interesting alternative choice to substitute the conventional fossil fuels, and more importantly it is a significant renewable energy source. There are several processes to convert biomass into energy such as fermentation, digestion and thermal decomposition. The fermentation and digestion process are relatively slow compared with thermal decomposition. Based on the final products consideration, thermal decomposition can be categorized into (1) combustion, (2) pyrolysis, and (3) gasification.

Gasification is employed to thermally convert biomass into combustible gases called syngas under restricted amount of oxygen and in the presence of an external supply of oxidizing agents such as, pure oxygen, steam, carbon dioxide or carbon monoxide. Produced gases include methane, carbon monoxide, and hydrogen which are the main products of a gasification process that can be used either directly as fuel or as feedstocks for chemical production (e.g. methanol). Gasification process can be achieved in a variety of gasifiers: fixed bed gasifiers (Yin et al., 2012), fluidized bed gasifiers (Yin, Wu, Zheng and Chen, 2002) and spouted bed gasifiers (Slam and Bhattacharya, 2006). However, these technologies are always related to high temperature and pressure with the purpose to enhance the gasification performance.

In terms of energy utilization, it is better to operate the gasification system at a low temperature range and this can be realized by the application of an effective catalyst. Garćia, Salvador, Arauzo and Bilbao (1999) reported that the low temperature catalytic gasification process is a suitable and attractive choice to convert low – calorific value biomass waste into H_2 rich gas and to avoid the ash – related problems at high temperature, such as sintering, agglomeration, decomposition, erosion and corrosion. Various kinds of catalyst have been developed and tested for the gasification process. Several studies have shown that alkali metal salts such as alkali carbonates (Lili, 2011), oxides, hydroxides and chlorides and metal catalyst such as nickel (Sharma, Saito, Nakgawa and Miura, 2007 and Choudhary, Nanerjee and Rajput, 2002) are effective catalysts in gasification. Furthermore, the solid product left from gasification, activated carbon, can be further used as a sorbent material. However, the surface properties of activated carbon from a gasification process will depend on the preparation conditions and type of precursor materials.

Activated carbon, also called activated charcoal, is widely used for purifying polluted air, gases, water, as well as for solvent vapor recovery. Moreover, activated carbon can be used as a catalyst, a catalyst support and for the final stage of cleaning in many processes. One of the most important fields in terms of consumption is in water and water treatment. According to Tseng, Tseng and Wu (2006), activated carbons can also be applied to super capacitors, catalyst supports of fuel cells, safe storage of large quantities of CH_4 or H_2 and even to the field of biomedical engineering. Activated carbon can be produced from a variety of raw materials such as coal, coke, wood and coconut shell. Normally, the production of activated carbon can be conventionally divided into two methods including physical activation and chemical activation method. To obtain activated carbon by using physical activation, the raw material is first carbonized and then partially oxidized with oxidizing gas (steam, CO_2, or air). The aim of the activation step is to develop internal surface area, pore volume and proper pore network suitable for the application in various fields. Chemical activation method is the preparation of activated carbon in the presence of inorganic additives. The temperature used in chemical activation is lower than that in the physical activation process. The chemical agents used are typically acid, strong base or alkali and alkaline earth metal containing substances such as H_3PO_4, KOH , NaOH, $ZnCl_2$ (Uçar, Erdem, Tay and Karagöz, 2009), and K_2CO_3 (Hayashi, Yamamoto, Horikawa, Muroyama and Gomes, 2005). Important parameters that can affect both physical and adsorption characteristics of activated carbon include chemical impregnation ratio, activation time, and activation temperature. In chemical activation process, the weight ratio of the chemical agent and the dry precursor is one of the variables that has a major influence on the final characteristics of activated carbons. According to Gratuito, Panyathanmaporn, Chumnanklang, Sirinuntawittaya and Dutta (2008), the chemical agents used are dehydrating agents that penetrate deep into the structure of the precursor causing tiny pores to develop. The duration of the activation has a profound effect on the development of the carbon's porous networks. The duration time should be long enough to release all the volatile components from the precursor, leading to the basic pore structure development of activated carbon products. However, longer activation time will cause the enlargement of pores at the expense of the surface area. The optimum activation temperature depends on the type of precursor and the chemical agent used. Normally, physical activation method required higher activation temperature than that of chemical activation method to achieve the same surface area.

For these reasons, it was decided to investigate the catalytic gasification of coconut shell with the objective to produce synthesis gas and a high porosity activated carbon at lower activation temperatures. In this work, potassium hydroxide and carbon dioxide gas are employed as a catalyst and gasification oxidizing agent, respectively. Generally, potassium hydroxide is widely used as an activation agent since it can lead to optimal textural and chemical properties of the carbon (Díaz – Terán, M. Nevskaia, Fierro, López – Peinado and Jerez, 2003), although the molecular details of activation mechanism process are not yet fully understood. Huang et al. (2009) have reported the effects of metal catalysts on CO_2 gasification reactivity of biomass char. They found that the CO_2 gasification reactivity of char was improved though the addition of metal catalysts in the order of K>Na>Fe>Mg. Moreover, potassium hydroxide activation creates carbon surface rich in oxygen functional groups that can give further advantages for electrode applications in fuel cells (Lee, Park, Park, Song, 2012 and Hiroyuki, Atsushi and Kouichi, 2000). Therefore, the use of combined potassium hydroxide and carbon dioxide gasification of coconut shell to produce a high heat content fuel and high porosity adsorbent was the main objective of this work.

6.3 Research Methods

This work is focused on studying catalytic gasification of coconut shell for syngas and activated carbon production in a fixed bed reactor. The experimental work consists of the following tasks: (1) the effect of gasification temperature, (2) the effect of alkaline catalyst loading and (3) the effect of oxidizing gas on the product yields and distribution. All research procedures are given in the following section.

6.3.1 Raw Material Preparation

Coconut shell was crushed by a jaw crusher, and screened to obtain an average screen size of 1.41 mm. The obtained sample was then dried at 110°C for 24 hours in an oven to remove excess moisture contained in the raw material and kept for further analysis and experimentation.

6.3.2 Coconut Shell Gasification

Coconut shell is used as a feedstock and potassium hydroxide as a catalyst for the gasification experiments. The experiment was divided into two steps. In the first step or "carbonization step", coconut shell was carbonized in a muffle furnace under the atmosphere of argon (100 ml/min) at 450°C for 60 min and the heating rate of 10°C/min. In the second step or "gasification or activation step", the resulting char from the carbonization step was gasified in a ceramic fixed bed reactor (45 mm inside diameter and 600 mm in length) under the atmosphere of oxidizing gas (50% Ar + 50% CO_2 by volume) The experimental procedure for the gasification study is as follows. Each of the precursors (coconut shell and coconut shell char) was mixed with pellet potassium hydroxide according to the required catalyst to precursor weight ratio by fixing a constant weight of mixture for 10 g. This mixture was dehydrated in a fixed bed reactor at various temperatures (300 – 700°C) for 30 to 180 minutes. Each solid product from this step was rinsed with deionized water to remove any remaining potassium hydroxide and potassium hydroxide derivatives until the pH of rinse water was constant at proximately 7.0, dried at 110°C for 10 – 12 hours and weighed. Finally, this sample was analyzed by an automated surface area analyzer (BELSorp – max) to determine its textural properties. The gas product was continuously collected every 10 minutes in a 10 liters gas sampling bag until no gas product was generated which took about 240 min and analyzed by gas chromatography equipment. Table 6.1 summarizes the experimental conditions used to study the catalytic gasification of coconut shell in this work.

6.3.3 Material Characterization

Physical and chemical properties and chemical analysis of coconut shell, activated carbon, bio-oil and gas products were determined by the following analytical methods.

6.3.3.1 Ultimate Analysis

The coconut shell precursor was analyzed by using CHNS analyzer (TruSpec CHN, LECO). Usually, ultimate analysis involves the determination of carbon, nitrogen, hydrogen, sulfur and oxygen contents.

6.3.3.2 Proximate Analysis

The contents of moisture, volatile matter, fix carbon and ash of biomass precursor was evaluated by using a TGA analyzer (TGA 701, LECO) by following the analytical method ASTM D7582 – 12.

6.3.3.3 Gas Products

The main gas composition including CO, CO_2, H_2, CH_4 and C_3H_8 in the product gases was determined by gas chromatography technique

(Shimadzu, GC – 2014) using thermal conductivity detector (TCD) and flame ionization detector (FID), with helium gas being introduced as the carrier gas.

6.3.3.4 Porous Properties

Specific surface area of activated carbons was determined from the N_2 adsorption isotherm at 77K with an automatic sorption meter (BELSORP-max). Dried activated sample was placed into the sample tube and heated to $300^{o}C$ and evacuated until the pressure became less than 6.7×10^{-7} Pa. The Brunauer – Emmet – Teller (BET) method (Do, 1998) was used to determine an apparent surface area for activated carbon. Total pore volume was estimated by the amount of N_2 adsorbed in liquid state at a relative pressure of 0.95. The t – plot method (Do, 1998) was applied to calculate the micropore volume.

Table 6.1 Experimental conditions for low temperature catalytic gasification of coconut shell.

Sample Code	Step I (carbonization)			Step II (gasification)				
	Temp. (°C)	HT (°C/min)	Time (min)	CR (g/g)	Temp. (°C)	HT (°C/min)	Time (min)	CO_2 (%)
G01	-	-	-	0	600	10	180	50
G02	-	-	-	0.5	600	10	180	50
G03	-	-	-	0.75	600	10	180	50
G04	-	-	-	1.0	600	10	180	50
G05	-	-	-	1.5	600	10	180	50
G06	-	-	-	2.0	600	10	180	50
G07	-	-	-	0.75	300	10	180	50
G08	-	-	-	0.75	400	10	180	50
G09	-	-	-	0.75	500	10	180	50
G10	-	-	-	0.75	600	10	180	0*
G11	450	10	60	2.0	600	10	180	50
G12	450	10	60	2.0	600	10	60	50
G13	450	10	60	2.0	600	10	30	50
G14	450	10	60	3.0	600	10	60	50
G15	450	10	60	4.0	600	10	60	50
G16	450	10	60	4.0	700	10	60	50

*in the atmosphere of inert gas argon

HT = Heating rate

CR = Chemical to biomass weight ratio

Time = Holding time

6.4 Results and Discussion

6.4.1 Raw Material Characterization

Table 6.2 shows the proximate and ultimate analysis of the coconut shell precursors used in this work. It is seen that the coconut shell precursor has high content of volatile matter and low content of ash, nitrogen and sulfur. The low nitrogen content ensures that thermal NO_x formation during the gasification process is insignificant. The low content of sulfur decreases the possibility of acid species formation which can produce acid rain or corrode the metallic part of gasification system. One can see that coconut shell shows a high carbon content (>50%) which makes it suitable to be a good precursor for activated carbon production.

Table 6.2 Proximate and ultimate analysis of coconut shell.

Proximate analysis (wt%)		**Ultimate analysis (wt%)**	
Moisture	2.06	Hydrogen	6.52
Volatile Matter	78.95 (80.61^{db})	Carbon	54.67
Ash	0.31 (0.32^{db})	Nitrogen	0.57
Fix Carbon	18.68 (19.07^{db})	Sulphur	0.02
		Oxygen^{diff}	38.22

^{db} Dry basis
^{diff} Calculated by difference

The gasification of coconut shell using combined potassium hydroxide and carbon dioxide was carried out to study the effect of chemical weight ratio, gasification temperature and carbonization step on the yield and composition of produced gas, and yield and porous properties of solid product or “activated carbon”. The experiments were performed at seven different chemical weight ratios (0.5, 0.75, 1.0, 1.5, 2.0, 3.0 and 4.0) and five gasification temperatures (300, 400, 500, 600 and 700°C).

6.4.2 Effect of Gasification Conditions on the Yield and Composition of the Syngas

In general, the products of thermal decomposition processes consist of gas, solid and liquid. This section presents the results on the composition and yield of syngas during the catalytic gasification of coconut shell with carbon dioxide and potassium hydroxide.

The results on gas yields and compositions under various conditions are shown in Table 6.3. On studying the effect of chemical loading, the amount of the potassium hydroxide catalyst per weight of coconut shell was varied in the range from 0 to 2.0 and the gasification was performed at 600°C for 180 min. It was found that the amount of potassium hydroxide had an important effect on the composition and quantity of gas produced as shown in Figure 6.1. It was discovered that carbon dioxide (43.97 wt%) was the main gas product for the CO_2 gasification without potassium hydroxide, with some amounts of carbon monoxide (16.40 wt%), hydrogen (0.40 wt%), and methane (2.16 wt%) being also detected in the gas product. The composition of propane was not found in the gas product under this condition. It should be noted that the amount of carbon dioxide generated from gasification is determined by the difference between total carbon dioxide output and total carbon dioxide input to the reactor. The total amount of gas product tended to increase with increasing in the chemical weight ratio with the maximum occurring at chemical ratio of 1.5. In addition, gasification by using both of the potassium hydroxide and carbon dioxide seem to promote the generation of hydrogen, carbon monoxide and hydrocarbon gases and also reduced the amount of carbon dioxide generation at the chemical ratio greater than 1.0. The total amount of gas product was reduced approximately 20% when the chemical weight ratio was increased from 1.5 to 2.0. Also, increasing in the amount of potassium hydroxide showed an increase in the hydrogen content in the syngas, with chemical ratio of 2.0 giving the highest generated amount. The maximum generation of hydrogen in the produced gas amounts to 5.2 times higher than the case of without potassium hydroxide. Furthermore, it is interesting to note that the highest amount of carbon monoxide per gram of coconut shell was achieved at the chemical weight ratio of 1.5. Results from the gas analysis indicate that the amount of propane tended to increase with increasing the chemical weight ratio. Although, the propane gas can be generated from gasification but the amount detected is far too small to be significant when compared with the total amount of the gas produced.

Table 6.3 Gas yields and composition from various gasification conditions (see Table 6.1 for gasification conditions).

Sample ID	**Gas yield (%)**	**Gas composition (mmol/g)**					**Gas composition (%wt)**				
		H_2	**CO**	**H_2**	**CO**	**H_2**	**CO**	**H_2**	**CO**	**H_2**	**CO**
G01	26.22	0.53	1.54	2.62	0.00	0.35	0.40	16.40	43.97	0.00	2.16
G02	26.97	1.58	2.19	2.81	0.38	1.12	1.17	22.74	45.85	6.16	6.67
G03	27.22	1.23	2.98	3.56	0.38	0.76	0.91	30.68	57.57	6.12	4.44
G04	28.57	1.25	2.43	4.38	0.57	0.49	0.81	22.06	62.42	8.15	2.56
G05	29.25	3.28	6.24	2.14	0.44	1.22	1.83	48.74	26.26	5.38	5.43
G06	16.15	8.23	0.89	1.18	0.44	0.64	10.20	15.45	32.15	11.85	6.37
G07	9.10	0.88	0.71	1.51	0.00	0.07	1.92	21.76	72.82	0.15	1.15
G08	12.55	1.03	2.43	0.78	0.01	0.03	1.65	54.24	27.36	0.18	0.38
G09	17.17	0.85	4.13	0.69	0.02	0.98	0.99	67.35	17.68	0.46	9.17
G10	17.86	1.23	2.98	3.10	0.38	0.76	0.91	30.70	50.16	6.12	4.44
G11	24.76	22.30	0.32	2.34	0.09	0.72	18.18	3.63	42.04	1.60	4.71
G12	23.23	23.32	0.31	3.00	0.08	0.61	20.29	3.80	57.44	1.48	4.25
G13	23.10	24.80	0.34	3.54	0.07	0.53	21.58	4.19	67.78	1.34	3.69
G14	24.58	27.00	0.16	2.54	0.21	0.57	22.22	1.82	45.97	3.80	3.73
G15	24.89	34.59	0.16	0.13	0.93	0.00	27.90	1.81	2.31	16.50	0.00
G16	24.34	36.52	0.18	0.00	0.30	0.89	29.23	2.03	0.00	5.39	5.75

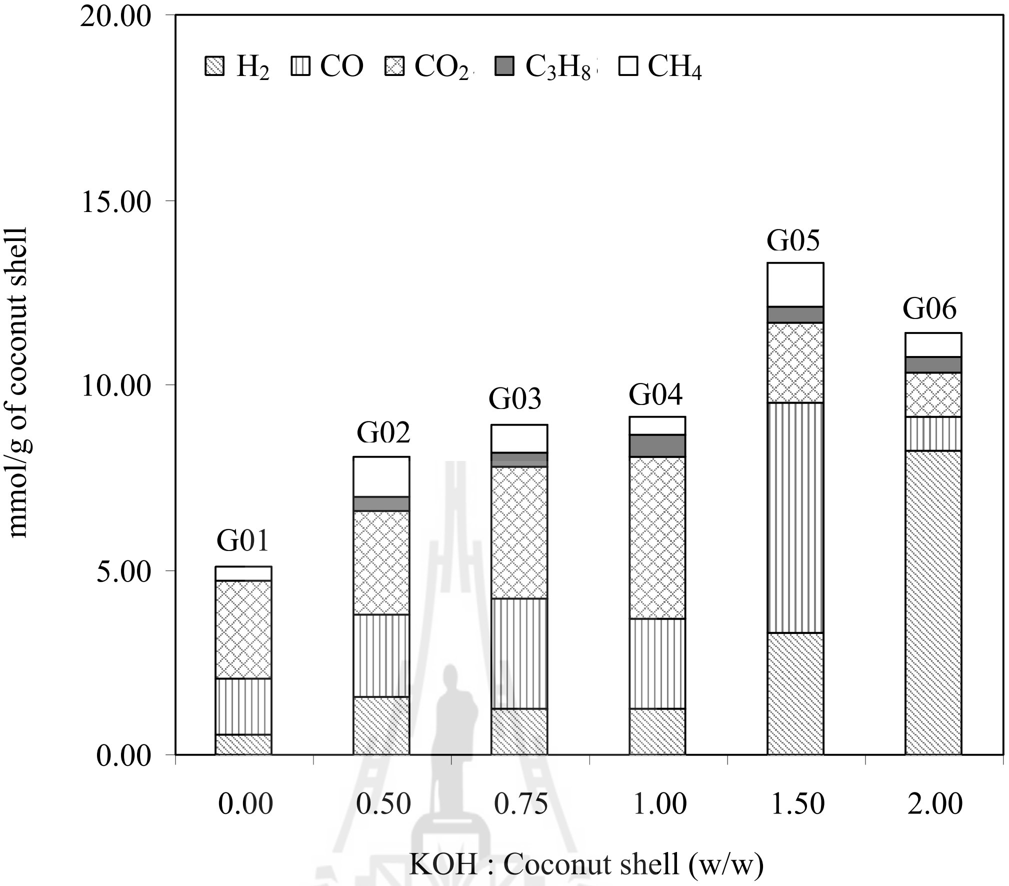

Figure 6.1 Effect of chemical weight ratio on composition of gas products from gasification of coconut shell with CO_2 at 600°C for 180 min.

Figure 6.2 shows the composition and yield of gas products collected during the gasification of coconut shell where the gas sample was periodically collected by using a gas sampling bag from the beginning of gasification (time = 0) until the completion of gasification at 240 minutes. The results indicate that the generation of hydrogen gas started at temperature range of 400 – 500°C when the reaction occurred in the absence of potassium hydroxide (Figure 6.2 (a)) and reduced to the temperature range of 200 – 300°C when the reaction occurred with potassium hydroxide (CR = 0.5 and 2.0). This may be possibly due to the positive effect of potassium hydroxide intercalation reaction that helps produce more hydrogen. Potassium hydroxide can react with disordered or amorphous carbon at high temperatures to form K_2CO_3, K_2O and H_2. The corresponding chemical reaction between potassium hydroxide and carbon material can be represented as in Equation (6.1) (Guo, et al., 2002). Moreover, the experimental results indicate that gasification process is completed at around 1 hr after the gasification temperature has reached to the set point at 600°C.

$$4KOH + C \rightarrow K_2CO_3 + K_2O + 2H_2 \tag{6.1}$$

The effect of gasification temperature on the amount and gas composition for gasification time of 180 min and chemical ratio of 0.75 is shown in Figure 6.3. The total amount of produced gas and carbon monoxide were found to increase with increasing gasification temperature, with the maximum (67.35 wt%, G09) occurring at gasification temperature of 500°C. Also, the component of methane was found at the gasification temperature of 500°C or higher and the component of propane was found only at the highest temperature of 600°C. It can be seen that the occurrence of methane and propane corresponds to the decrease of hydrogen and carbon dioxide at this high temperature condition.

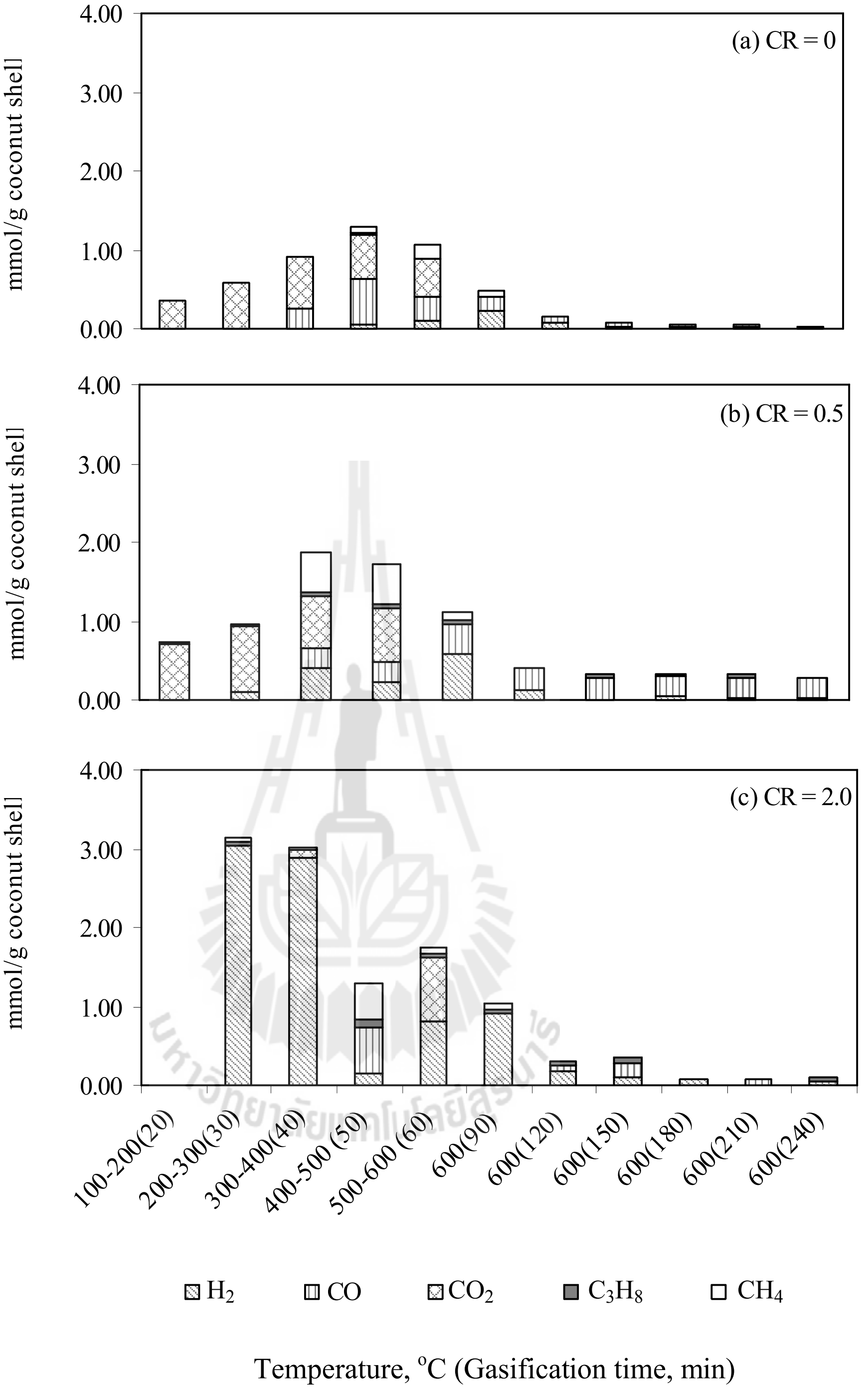

Figure 6.2 Gas composition generated during coconut shell low temperature gasification process at various chemical ratio and under the same gasification conditions.

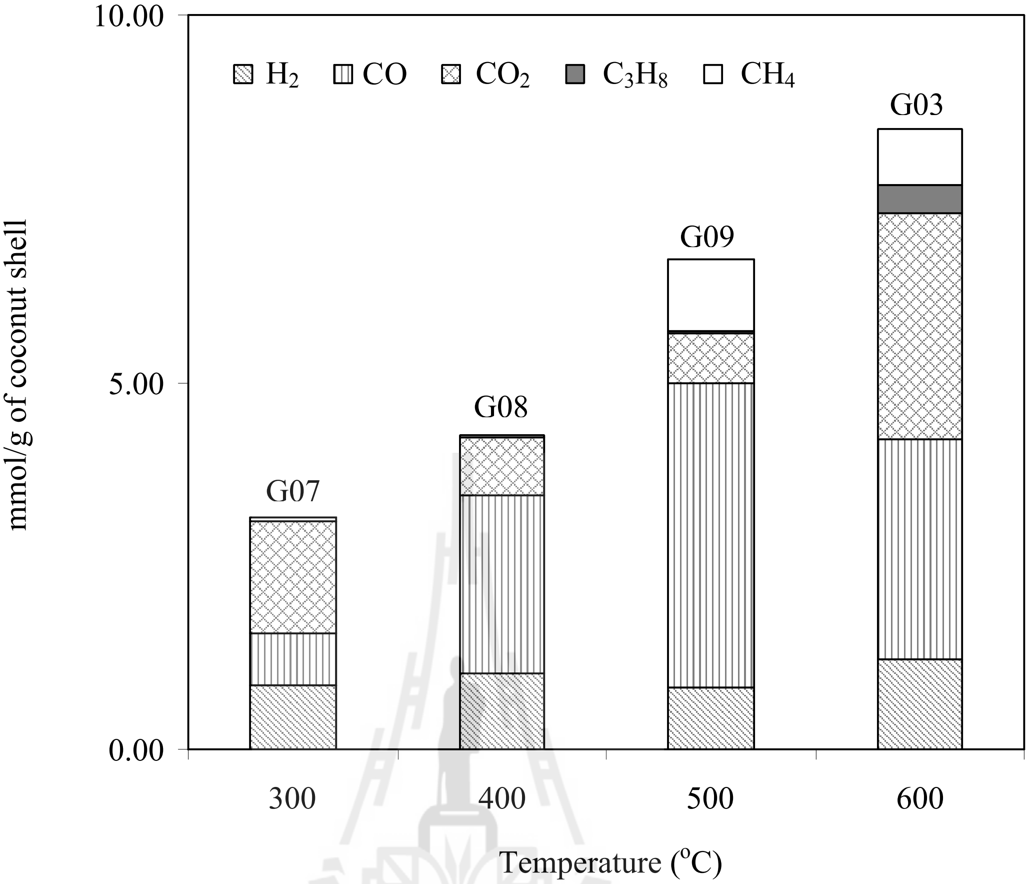

Figure 6.3 Effect of temperature on composition of gas products from gasification of coconut shell for 180 min and chemical ratio of 0.75.

From these obtained results, the gasification schemes for the low – temperature gasification process without a prior carbonization step could be proposed as follows.

1. Gasification with carbon dioxide only:

$$\text{Coconut shell} + CO_2 \rightarrow CO_2 + CO + H_2 + CH_4 \qquad (6.2)$$

2. Gasification with both carbon dioxide and potassium hydroxide:

$$\text{Coconut shell} + CO_2 + KOH \rightarrow K_2CO_3 + K_2O + H_2 + CO + CO_2 + CH_4 \qquad (6.3)$$

Figure 6.4 presents the results of XRD analysis of K_2CO_3 in the final solid product before the washing step. The peak of K_2CO_3 compound at $\theta \approx 32.46^o$ is observed on the intense line of activated carbon samples from coconut shell gasification with only potassium hydroxide and with both carbon dioxide and potassium hydroxide. This indicates that the formation of K_2CO_3 occurs by the reaction of KOH with CO_2 present in the gasification process.

The effect of carbonization step on the gas composition is exhibited in Figure 6.5. In this work, carbonization step or char production was performed prior to gasification in a muffle furnace under argon flow rate of 100 ml/min and temperature of 450°C for 60 min. Figure 6.4 shows the composition of gas products for gasification at 600°C for 180 min and chemical weight ratio of 2.0. It was found that the main gas product of gasification of coconut shell without carbonization step was hydrogen, carbon dioxide and carbon monoxide. However, when incorporating the carbonization step prior to the catalytic gasification. The main gas composition were hydrogen and carbon monoxide, with the amount of hydrogen produced being much higher than the case of without carbonization. Therefore, we can conclude that the carbonization step introduced has facilitated the generation of hydrogen and carbon monoxide during the catalytic gasification of coconut shell. Also, the mechanism of this process is proposed as in Equation (6.4),

$$\text{Char} + \text{KOH} + \text{CO}_2 \rightarrow \text{K}_2\text{CO}_3 + \text{H}_2 + \text{CO} + \text{CO}_2 + \text{CH}_4 \quad (6.4)$$

Considering that the major chemical element of char is a carbon, thus the high production of hydrogen gas may be derived from potassium hydroxide, and possibly carbon dioxide may not participate in this process. Therefore, the reaction mechanism could be represented by

Formation of K_2O:

$$\text{Char (carbon)} + \text{KOH} \rightarrow \text{K}_2\text{O} + \text{H}_2 + \text{CO}_2 + \text{CH}_4 + \text{CO} \quad (6.5)$$

Formation of K_2CO_3:

$$\text{K}_2\text{O} + \text{CO}_2 \rightarrow \text{K}_2\text{CO}_3 \quad (6.6)$$

By combining Equation (6.4) and (6.5), the combined effect of carbon dioxide and potassium hydroxide on the gasification scheme may be as follows.

$$\text{C (char)} + \text{KOH} \rightarrow \text{K}_2\text{CO}_3 + \text{H}_2 + \text{CO}_2 + \text{CO} + \text{CH}_4 \quad (6.7)$$

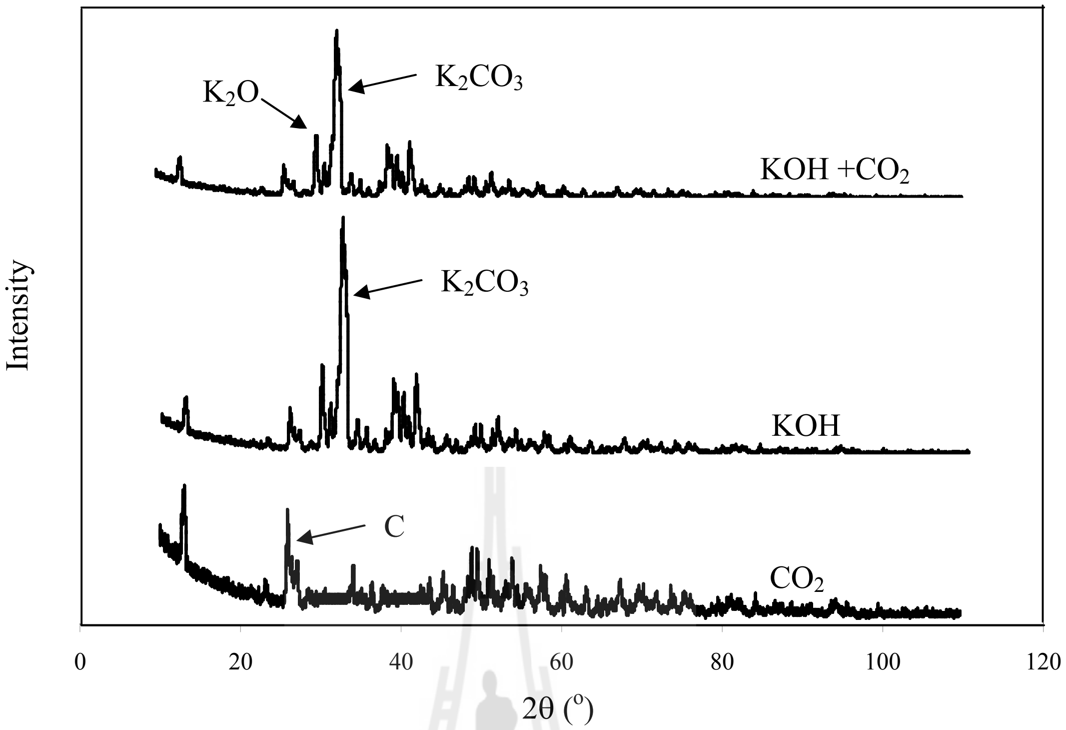

Figure 6.4 XRD patterns of activated carbon from coconut shell by one step gasification method at the same conditions by using different oxidizing agents.

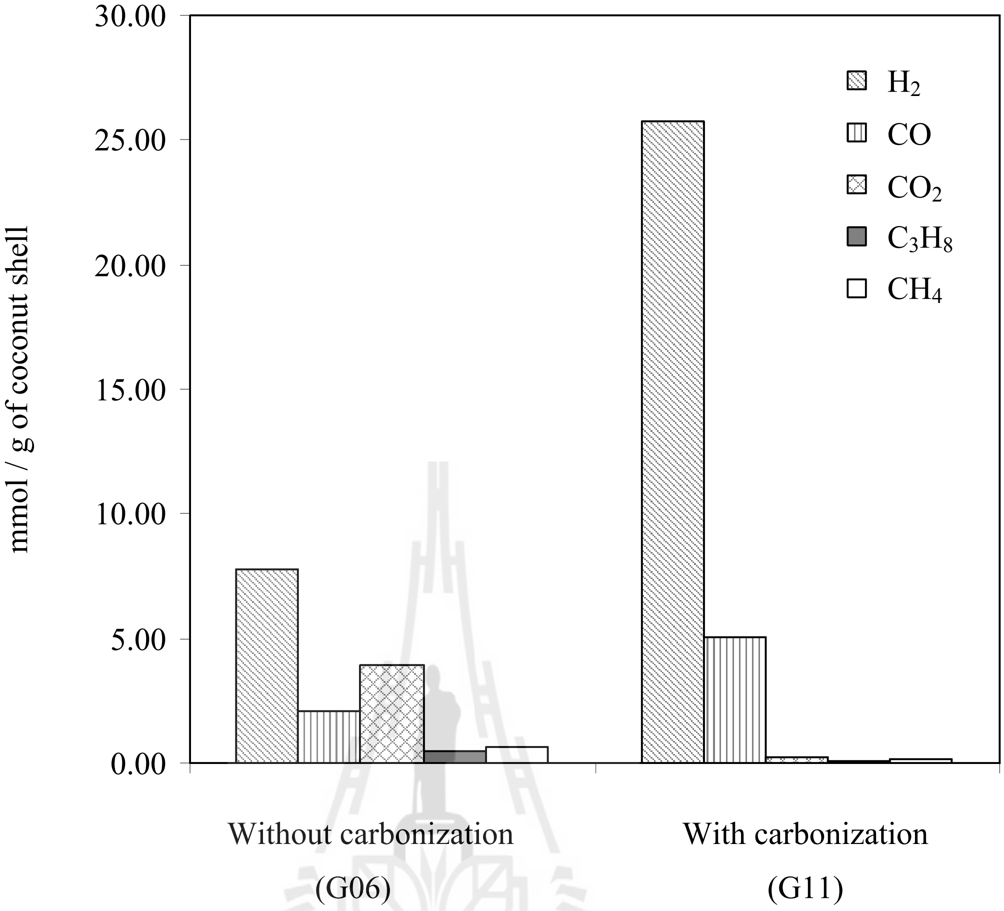

Figure 6.5 Effect of carbonization step on the composition of gas products from gasification of coconut shell with 50% CO_2 at 600°C for 180 min and chemical ratio of 2.0.

Previous results have indicated that relatively large amounts of hydrogen and carbon monoxide were favored by a high chemical ratio and high gasification temperatures (see Figure 6.1 and 6.3). However, the introduction of carbonization step prior to gasification exerted more significant effect on the amount of generated hydrogen and carbon monoxide, as compared with the gasification of raw coconut shell. The effects of chemical ratio and temperature on the yields and composition of produced gas of coconut shell gasification with carbonization step were also investigated and the results are presented as follows.

The effect of chemical ratio on produced gas composition of coconut shell gasification with carbonization step at 600°C for 30 min is shown in Figure 6.6. The increasing of the chemical weight ratio from 2.0 to 3.0 gave slight effect on the total amount of gas generated per gram of char. However, increasing of chemical weight ratio higher than 3.0 showed a reasonable increase of the total amount of gas generated as well as the hydrogen content. The major gas compositions appeared to be hydrogen followed by carbon dioxide. The amount of hydrogen increased with increasing chemical ratio while for carbon dioxide the reverse trend was observed.

Figure 6.7 presents the composition of produced gas from coconut shell gasification with carbonization step when the gasification temperature was increased from 600 to 700°C. The main gas compositions appeared to be hydrogen and followed by traces of methane and propane. The composition of carbon dioxide was not found in the gas product where the gasification temperature was higher than 600°C. It can be seen that the occurrence of methane corresponds to the decrease of carbon dioxide at this high temperature condition (see Table 6.3).

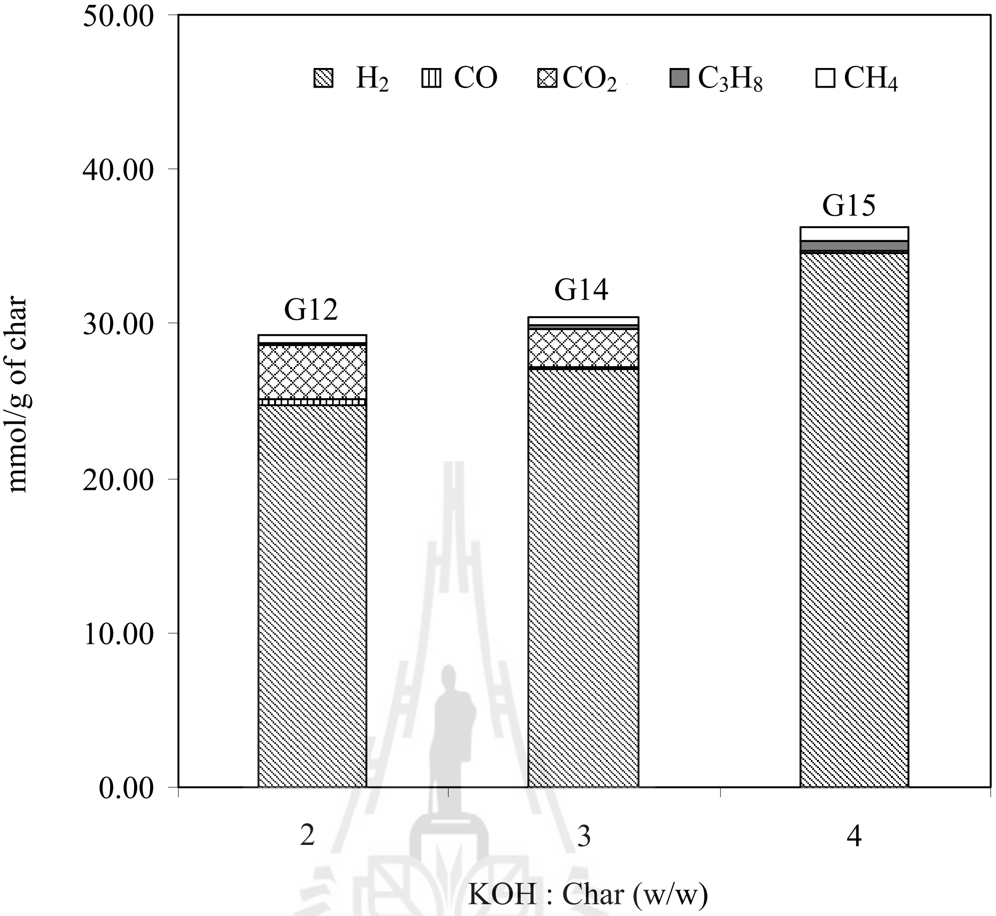

Figure 6.6 Effect of chemical ratio on gas compositions from coconut shell char gasification process with carbonization step with 50%CO_2 at 600°C for 60 min.

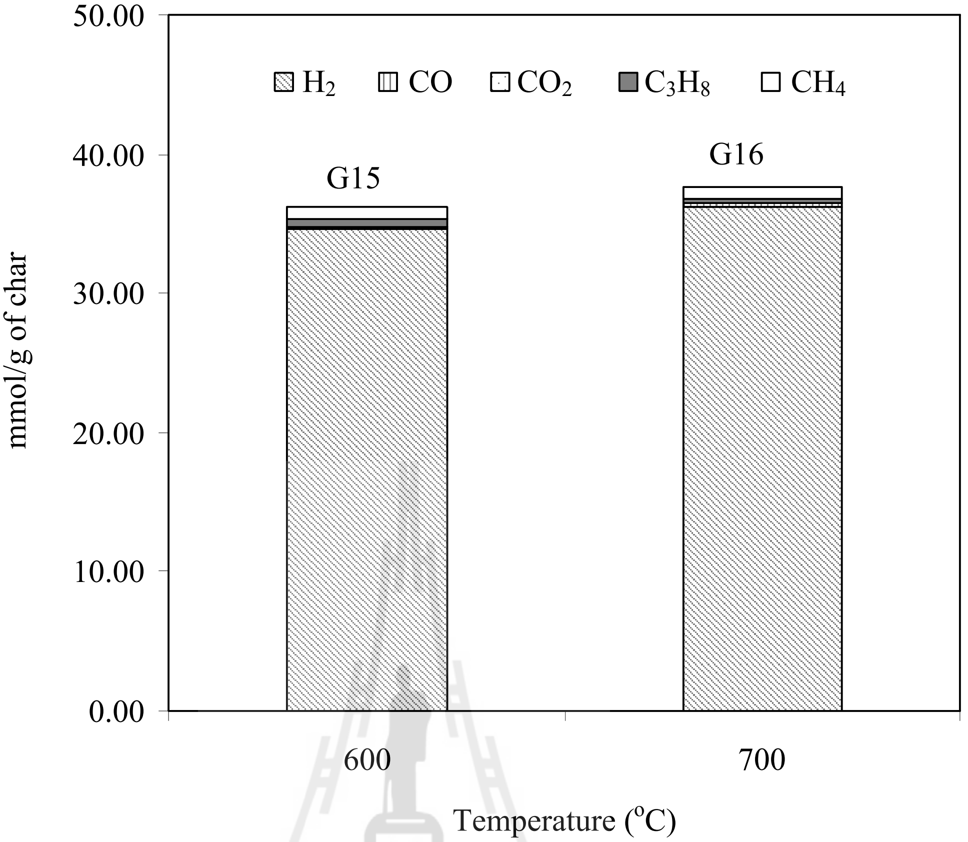

Figure 6.7 Effect of temperature on gas compositions from coconut shell gasification process with carbonization step with 50%CO_2 , chemical ratio of 4.0 and 60 min.

As already mentioned, the products of gasification process are gas, solid and liquid. It is known that potassium hydroxide and carbon dioxide are the most commonly used chemical reagent and oxidizing gas for activated carbon preparation by chemical and physical activation method, respectively. In this work, the combination of potassium hydroxide and carbon dioxide was introduced in the gasification process. Therefore, the effect of gasification conditions on porous properties of solid product is also of interest and is discussed in the next section.

6.4.3 Effect of Gasification Conditions on Porous Properties of Solid Product

In this section the effect of gasification conditions, including chemical ratio, temperatures and carbonization step on the production yields and porous properties of solid product, or so called "activated carbon", will be presented.

The effect of chemical ratio on the yields and porous properties of activated carbon produced by gasification process without carbonization step (only stage II gasification method), and with the combined use of potassium hydroxide and carbon monoxide is listed in Table 6.4 (sample G01 – G16). The ratio of chemical agent and precursor employed for gasification generally depends on the type of precursor and the chemical agent used. Consider first the gasification without carbonization step. The chemical agent ratios between 0 – 2 (sample G01 – G06) were tested to produce high amount of gas and the by product of high porosity activated carbon at fixed activation temperature (600^{o}C), and time (180 min). It was found that the yield of solid product (activated carbon) appeared to decrease from 28.13% to 14.18% when the chemical ratio was increased (see Figure 6.8).

Figure 6.9 presents the N_2 adsorption – desorption isotherms of an activated carbon from coconut shell gasification using different ratios of chemical agent (CR = 0 – 2) at the above gasification conditions. All of N_2 adsorption – desorption isotherms show a similar shape, and they are of type I of the BDDT (Brimauer, Deming, Deming and Teller) classification with a plateau practically parallel to the relative pressure axis and with quite a small hysteresis loop. This indicates that these carbons are essentially microporous with a very low meso – and macro – porosity. These results are consistent with the results of pore volume distribution and the data of an average pore diameter that shown in Figure 6.10 (a) and Table 6.4, respectively. The activated carbon from coconut shell gasification contained mostly micropore volume (more than 90%) and the average pore diameter in the range of 1.85 to 2.75 nm (sample G01 – G06). Also, increasing of chemical agent ratio appears to give activated carbon with smaller average pore size and increasing the proportion of mesopores and macrospores. It was found that the specific surface area of the activated carbon product was increased by about 8.4 times (from 119 to 1000 m^2/g) when gasifying with combined potassium hydroxide and carbon dioxide at the maximum chemical weight ratio of 2.0. However, the specific surface area of solid product obtained by using only potassium hydroxide in the atmosphere of inert gas argon at the gasification temperature of 600^{o}C for 180 min (sample G10, S_{BET} of 591 m^2/g) is just 8% lower than the activated carbon from combined use of potassium hydroxide and carbon dioxide (sample G03). These results indicate that the development of porosity in activated carbon from coconut shell is mainly caused by the action of chemical agent. The experimental results also show that the average pore size of activated carbon obtained from the combined use of potassium hydroxide and carbon dioxide (sample G03; D_p 2.75 nm) is smaller than by activating without potassium hydroxide (sample G10; D_p 3.12 nm). These results are in agreement with the work of Molina , Gonzales, Rodriguez and Sepúlvada (1999) in that the carbon dioxide activation mainly caused the creation of microporosity.

Table 6.4 Yields and porous properties of activated carbon from various preparation conditions (see Table 6.1)

Sample ID	Yield (%)	Surface Area (m^2/g)	Micropore Volume (cm^3/g)	Meso and Macropore Volume (cm^3/g)	Total Pore Volume (cm^3/g)	Micropore Volume (%)	Meso and Macropore Volume (%)	Average Pore Diameter (nm)
G01	28.13	119	0.0633	0.0064	0.0697	90.82	9.18	2.34
G02	25.51	569	0.2544	0.0082	0.2626	96.88	3.12	1.85
G03	25.09	640	0.2950	0.0094	0.3044	96.91	3.09	2.75
G04	23.02	619	0.2839	0.0123	0.2962	95.85	4.15	1.91
G05	18.59	670	0.3267	0.0115	0.3382	96.60	3.40	2.02
G06	14.18	1000	0.4613	0.0351	0.4964	92.93	7.07	1.98
G07	31.10	-	-	-	-	-	-	-
G08	33.86	63.0	0.0519	0.0109	0.0628	82.64	17.36	3.37
G09	32.46	88.7	0.0493	0.0087	0.0580	85.00	15.00	3.25
G10	15.38	591	0.3191	0.0524	0.3715	85.90	14.10	3.12
G11	23.89	921	0.4246	0.0057	0.4303	98.68	1.32	1.87
G12	24.09	1030	0.4626	0.0105	0.4731	97.78	2.22	1.84
G13	24.97	1330	0.6014	0.0169	0.6083	98.86	1.14	1.83
G14	20.96	1710	0.7929	0.0123	0.8052	98.47	1.53	1.88
G15	20.12	2650	1.3128	0.0452	1.3580	96.67	3.33	2.05
G16	18.85	2760	1.4528	0.0321	1.4849	97.84	2.16	2.15

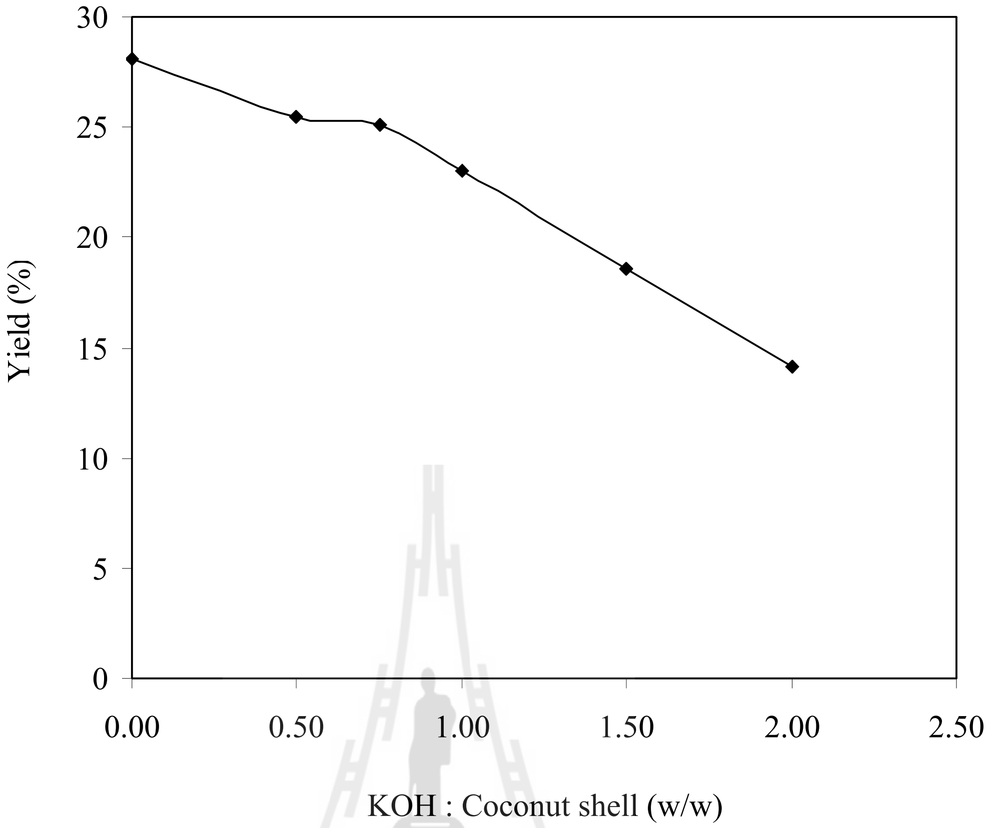

Figure 6.8 Effect of chemical ratio on yield of activated carbon from coconut shell by the combined use potassium hydroxide and carbon dioxide at gasification temperature of 600°C, 180 min, and without carbonization step.

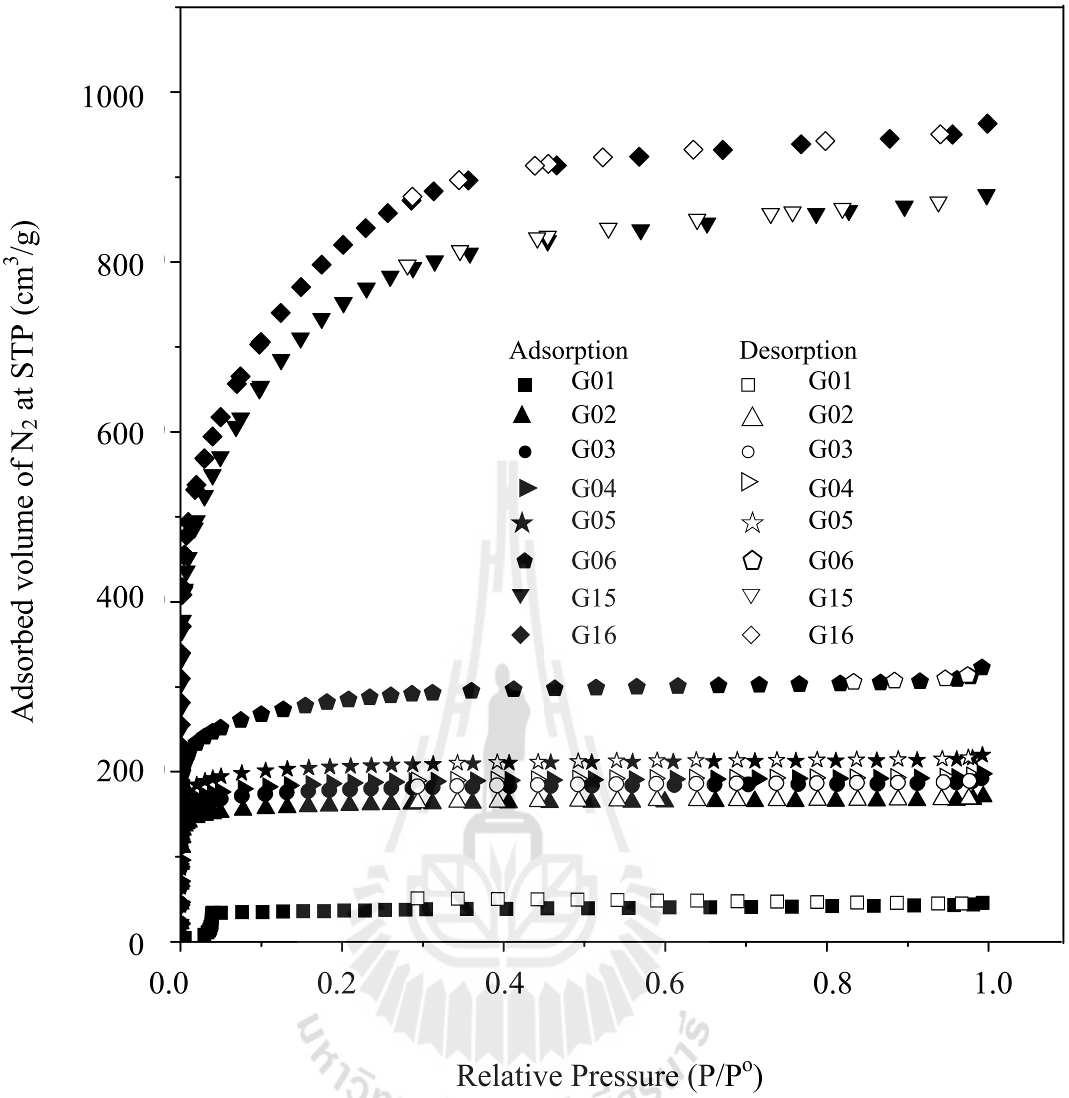

Figure 6.9 Nitrogen adsorption isotherm at 77K of activated carbons produced by combined KOH with CO_2 gasification of coconut shell at various gasification conditions.

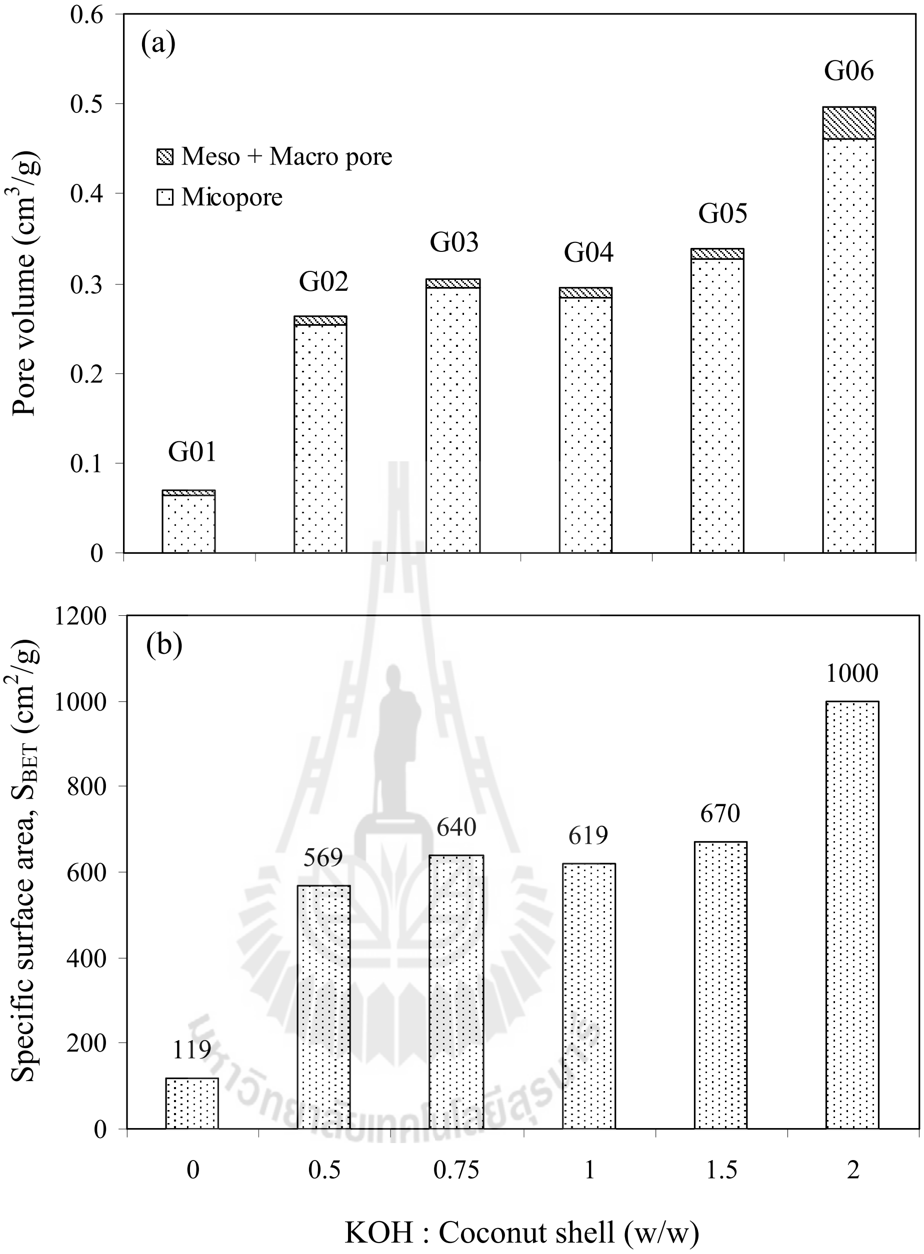

Figure 6.10 Effect of the chemical agent ratio on (a) the pore volume and (b) specific surface area (S_{BET}) of activated carbon from coconut shell gasified with CO_2 at 600°C for 180 min.

As mentioned earlier, the important parameters that affect both physical and adsorption characteristics of activated carbon include chemical impregnation ratio, activation time, and activation temperature. In the previous section, effect of chemical agent ratio on the structural characteristics of activated carbon has been discussed. The effects of activation temperature and time on the surface characteristics of activated carbon will be discussed in this section. In this work, the activation temperature was varied from 300 to 600°C, respectively.

Figure 6.11 demonstrates the effect of activation temperature on the yield and specific surface area of activated carbon from coconut shell gasification without carbonization step (only step II), using the combined potassium hydroxide and carbon monoxide. It can be seen that, higher activation temperature resulted in high specific surface area and lower yields of activated carbon. These results agree with the work of Zou and Han (2001) who reported that the development of porosity was achieved at the activation temperature higher than 500°C. Their activated carbons have been prepared from Chinese coal by chemical activation with potassium hydroxide. Moreover, increasing activation temperature gave a decrease in the average pore size diameter (see G03 and G07 – G09 in Table 6.4 and Table 6.1). As seen from Figure 6.12, the increase in micropore volume can be observed at higher temperatures. The N_2 adsorption isotherms of G03 and G07 to G09 are displayed in Figure 6.13. The N_2 adsorption isotherms indicate that the proportion of micropore was increasing with increasing gasification temperature because of increasing in the adsorbed amount and the Type I isotherm are still observed at a high gasification temperature.

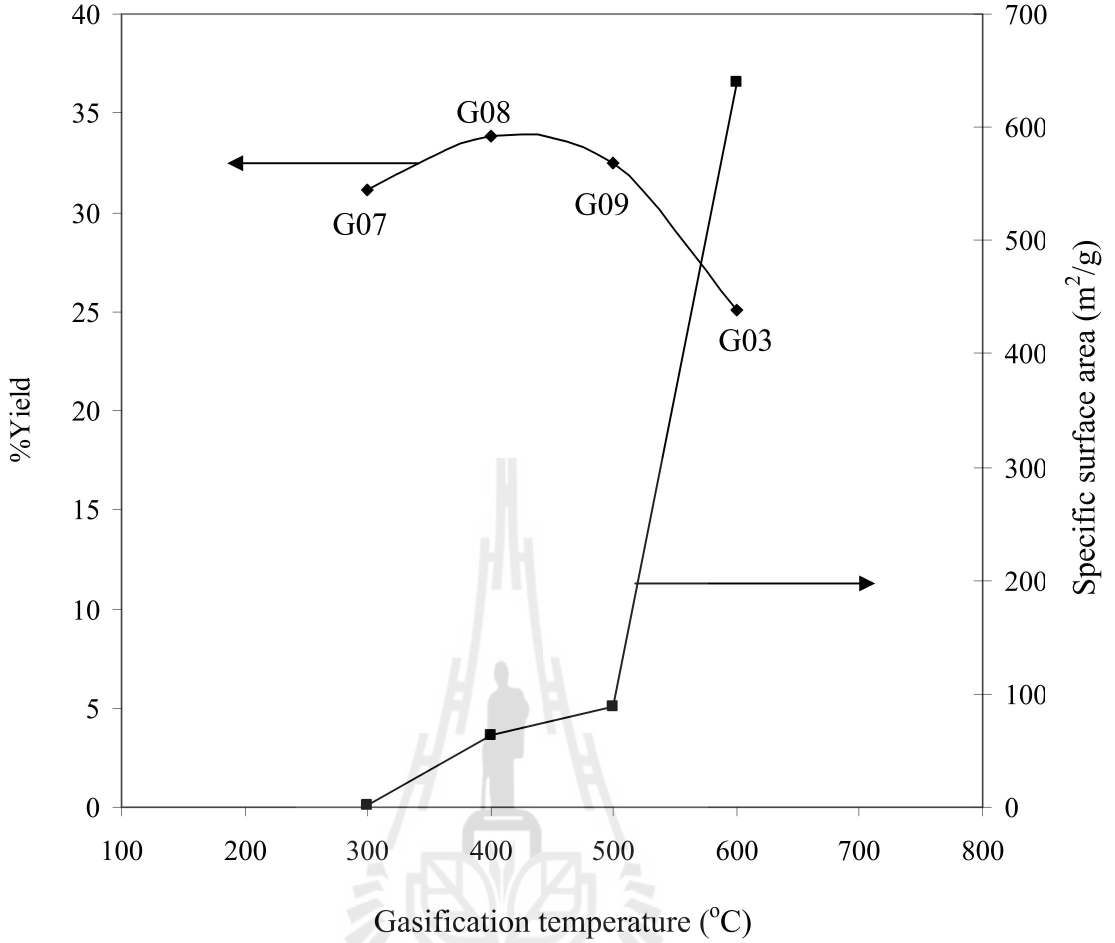

Figure 6.11 Effect of gasification temperature on the specific surface area and yield of activated carbon from coconut shell by the combined use of potassium hydroxide and carbon dioxide at chemical weight ratio of 0.75, 180 min, and without carbonization step.

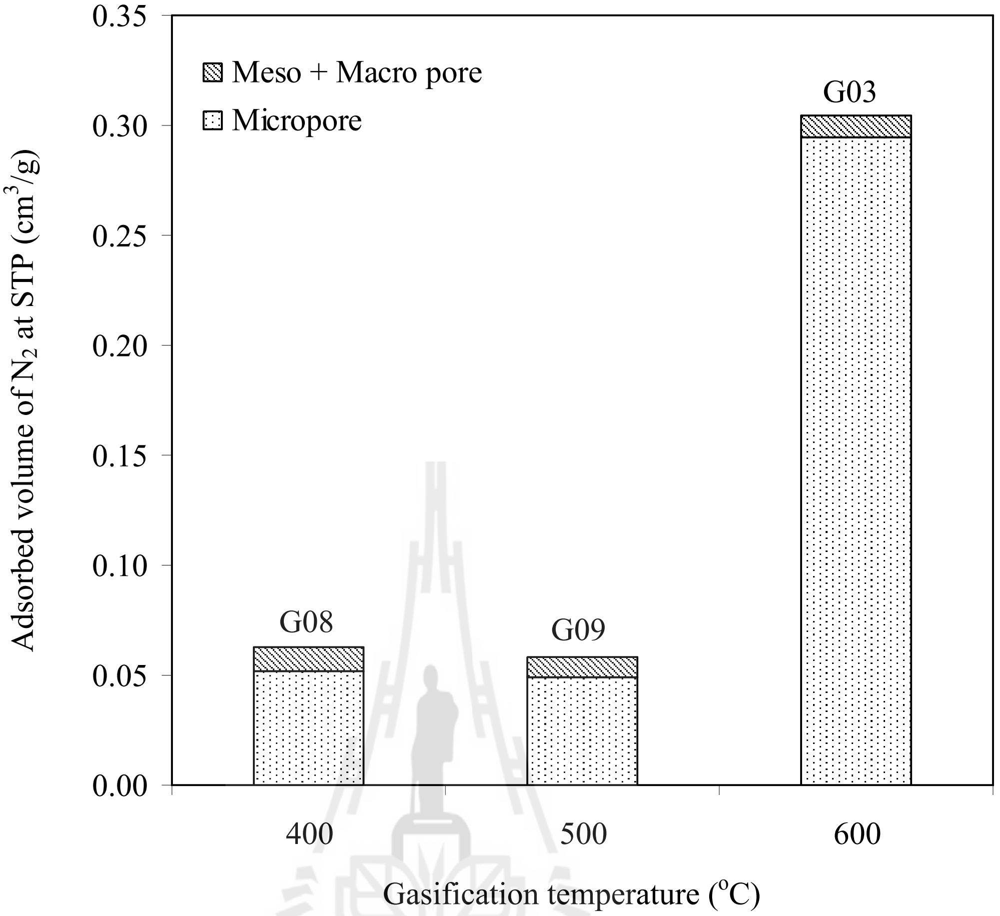

Figure 6.12 Effect of gasification temperature on pore volume distribution of activated carbon from coconut shell by the combined use of potassium hydroxide and carbon dioxide at chemical weight ratio of 0.75, 180 min, and without carbonization step.

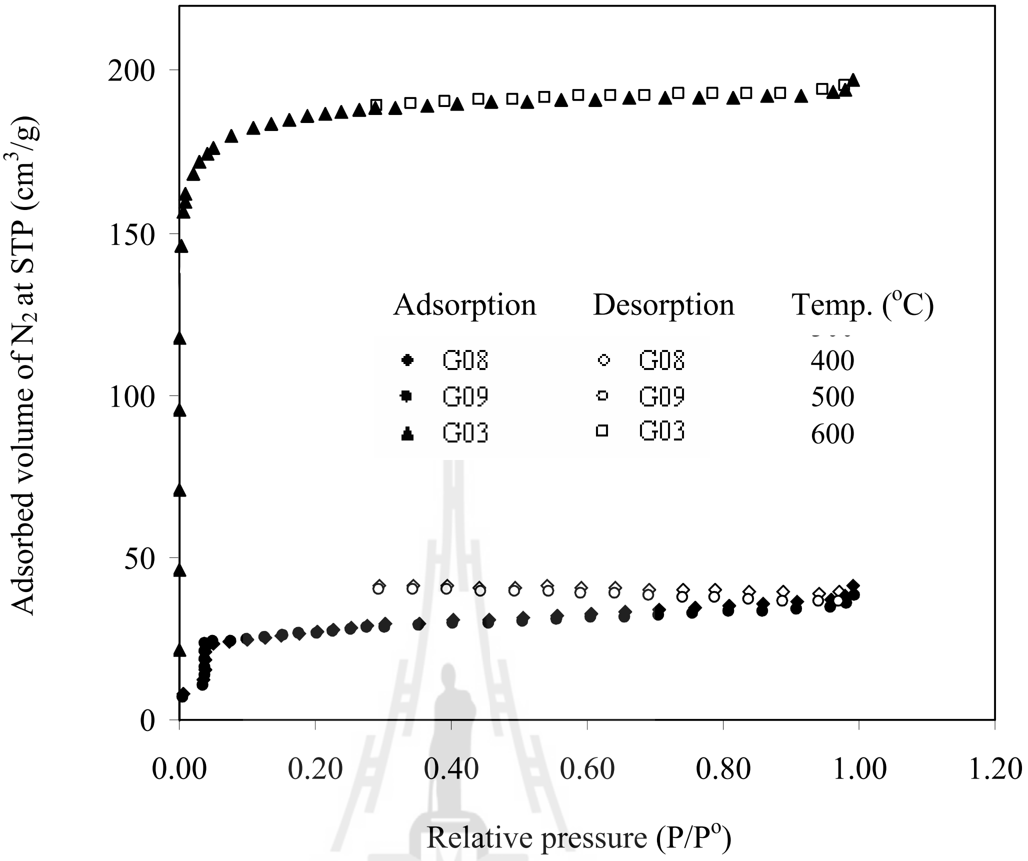

Figure 6.13 Effect of gasification temperature on nitrogen isotherm at 77K of activated carbons from coconut shell by the combined use of potassium hydroxide and carbon dioxide at chemical weight ratio of 0.75, 180 min, and without carbonization step.

When incorporating the carbonization step by heating the biomass in argon flowing at 100 ml/min at 450°C for 60 min, the result showed a slight increase in porosity properties of an activated carbon from gasification process by combination of potassium hydroxide and carbon dioxide (see G06 and G11 in Table 6.4) at gasification temperature of 600°C for 180 min and chemical weight ratio of 2.0. The isotherms of G06 activated carbon shows the same Type I isotherm with a very small hysteresis loop, as compared to that of G11 activated carbon (Figure 6.14). The results in Figure 6.14 indicate that carbonization step did not strongly affect the surface properties of activated carbon, because there are small difference in specific surface area and proportion of porosity of G06 and G11 activated carbons. On the other hand, the incorporation of carbonization step prior to gasification step had an influence on porosity properties of an activated carbon when the gasification time was reduced from 180 min to 30 min at the gasification temperature of 600°C (see G11 - G13 in Table 6.1). Specific surface area of an activated carbon was increased from 962 to 1330 m^2/g when the gasification time was reduced from 180 to 30 min. Furthermore, the experimental results show that the specific surface area of activated carbon was increased by about 1.5 times when increasing the chemical agent /coconut shell char ratio from 3.0 to 4.0 (see G14and G15 in Table 6.4).

Figure 6.16 shows the effect of gasification conditions on specific surface area, yield of hydrogen gas and carbon monoxide gas product. The highest surface area activated carbon (2760 m^2/g) can be achieved from the gasification at temperature of 700°C for 60 min and chemical ratio of 4.0 with carbonization step. It was found that carbonization step promoted the generation of hydrogen gas and appeared to inhibit carbon monoxide formation. The maximum concentration of carbon monoxide of 67 wt% was found at the gasification without carbonization step at 500°C for 180 min and chemical ratio of 0.75. However, the high surface area activated carbon could not be achieved under this gasification condition. Finally, from the experimental results it can be conferred that the optimal condition for achieving high hydrogen composition (27.90 wt%) of produced gas and high specific surface area (2,650 m^2/g) of activated carbon is to run gasification at temperature of 600°C for 60 min, chemical ratio of 4.0 and with the incorporation of carbonization step.

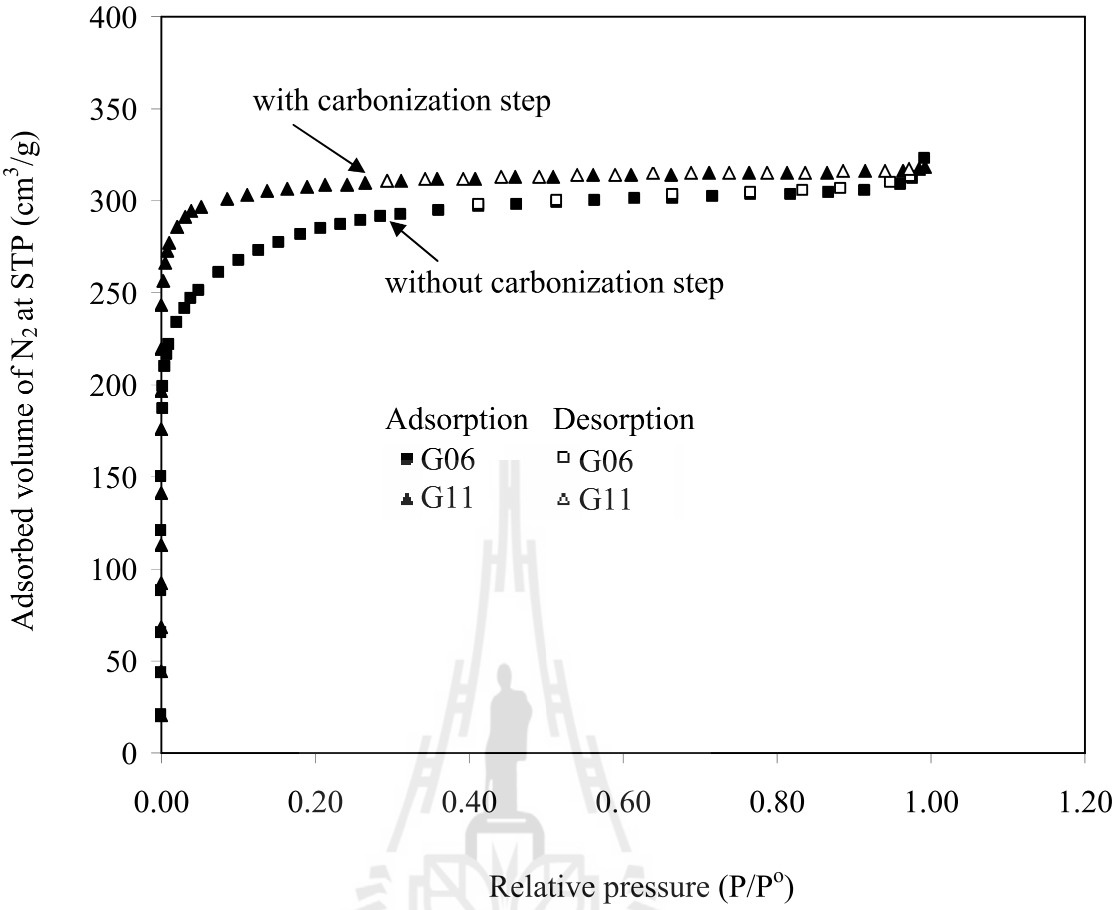

Figure 6.14 Effect of carbonization step on nitrogen isotherm at 77K of activated carbons from coconut shell by combined of potassium hydroxide and carbon dioxide at 600°C for 180 min, and chemical ratio of 2.0.

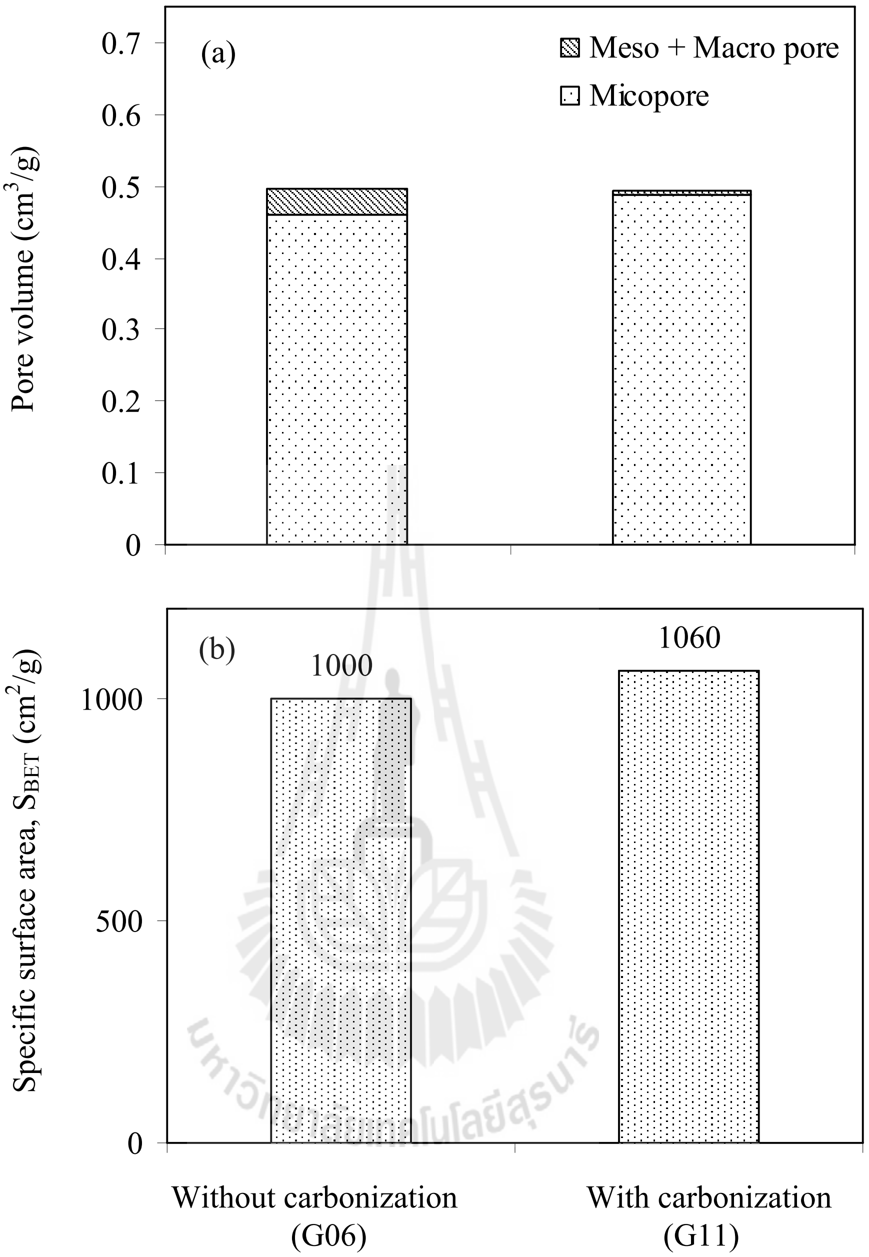

Figure 6.15 Effect of carbonization step on (a) the pore volume and (b) specific surface area (S_{BET}) of activated carbon from coconut shell gasification by combined of potassium hydroxide and carbon dioxide at 600°C for 180 min, and chemical ratio of 2.0.

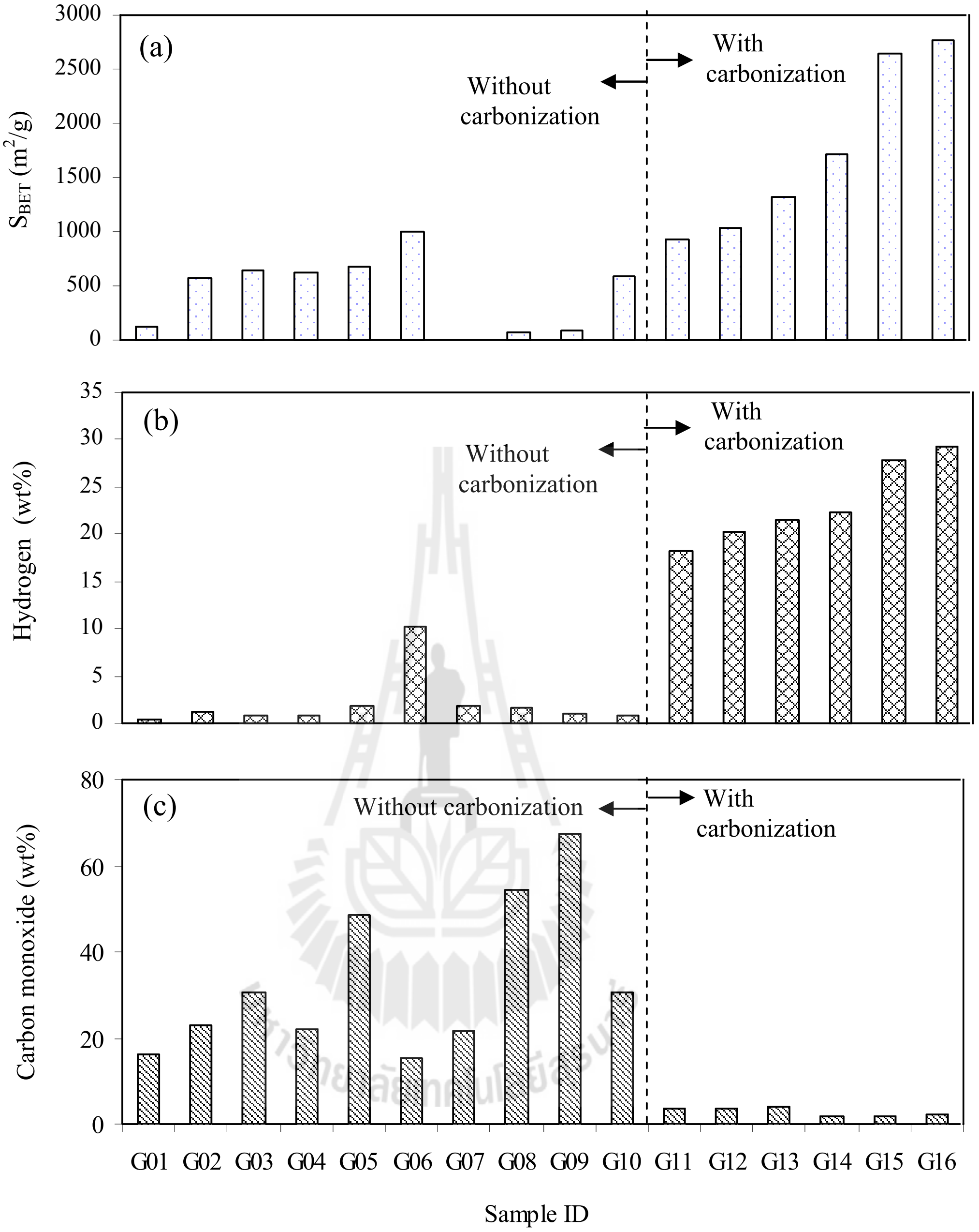

Figure 6.16 Effect of gasification conditions on (a) specific surface are (S_{BET}, m^2/g), (b) hydrogen gas yield (wt%) and (c) carbon monoxide gas yield (wt%).

6.5 Conclusions

In this work, the gasification of coconut shell using combined potassium hydroxide and carbon dioxide was carried out in a fixed bed reactor. It was found that potassium hydroxide catalyst gave favorable effect for low – temperation gasification of coconut shell. The results indicated that catalyst loading and reaction temperature had an important effect on the composition and yield of produced gas. It was observed that the gas yield was decreased with the amount of potassium hydroxide catalyst. Carbon dioxide as well as the main produced gas for coconut shell gasification without potassium hydroxide. Besides, using the potassium hydroxide combined with carbon dioxide promoted the generation of hydrogen and carbon monoxide and appeared to retard the carbon dioxide formation. The formation of hydrogen started at 400 – 500^{o}C for gasification without assisted potassium hydroxide and reduced to 200 – 300^{o}C when the reaction occurred with the presence of potassium hydroxide. The gas yield and content of carbon monoxide, methane and propane were increased with an increase of gasification temperature. In contrast, the amount of hydrogen was decreased with an increase of gasification temperature. It was observed that the occurrence of methane and propane corresponded to the decrease amount of hydrogen and carbon dioxide.

The results indicated that increasing of potassium hydroxide loading and gasification temperature promoted the porosity formation of the solid product. The proportion of micropores was increased with the increase in gasification temperature. The gasification time did not show a significant effect on gas production yield but affect produce gas composition. Furthermore, the carbonization step did not show a significant influence on the porous properties of solid product from the gasification process. The gasification time has no a significant effect on yield of solid product but had an influence on specific surface area of solid product The resultant porous carbons exhibited a high surface area of up to 2,760 m^2 at the gasification temperature of 700°C for 60 min and chemical weight ratio of 4.0 with the incorporation of carbonization. Finally, from the experimental results it can be conclude that the optimal condition for achieving high hydrogen composition (27.90 wt%) of gas produce and high specific surface area (2,650 m^2/g) of activated carbon was gasification temperature of 600°C for 60 min with carbonization step and chemical ratio of 4.0.

6.6 References

Choudhary, V. R., Nanerjee, S., and Rajput, A. M. (2002). Hydrogen from step – wise steam reforming of methane over Ni/ZrO2: factors affecting catalytic methane decomposition and gasification by steam of carbon formed on the catalyst**.** **Applied Catalysis A: General.** 234(1 -2): 259 – 270.

Díaz – Terán, J., Nevskaia, D. M., Fierro, J. L. G., López – Peinado, A.J., and Jerez, A. (2003). Study of chemical activation process of a lignocellulosic material with KOH by XPS and XRD. **Microporous and Mesoporous Material.** 60: 173 – 181.

Do, D. D. (1998). **Adsorption Analysis: Equilibrium and Kinetics.** Imperial College Press.

Garćia, L., Salvador, M.L., Arauzo, J., and Bilbao, R. (1999). Catalyst steam gasification of pine sawdust. Effect of catalyst weight/biomass flow rate and steam/biomass ratio on gas production and composition. **Energy Fuels.** 13: 851 – 859.

Gratuito, M.K.B., Panyathanmaporn, T., Chumnanklang, R.A., Sirinuntawittaya, N., and Dutta, A. (2008). Production of activated carbon from coconut shell: Optimization using response surface methodology. **Bioresource Technology**. 99: 4887 – 4895.

Guo, Y., Yang, Shaofeng, Yu, Kaifeng, Zhao, Jingzhe, Wang Zichen, and Xu, H. (2002). The preparation and mechanism studies of rice husk based porous carbon. **Materials Chemistry and Physics**. 74: 320 – 323.

Hayashi, J., Yamamoto, N., Horikawa, T., Muroyama, K., and Gomes, V. G. (2005). Preparation and characterization of high – specific – area activated carbon from K_2CO_3 – treated waste polyurethane. **Journal of Colloid and Interface Science.** 281(2): 437 – 443.

Huang et al. (2009) Effects of metal catalysts on CO2 gasification reactivity of biomass char. **Biotechnology Advances.** 27(5): 568 – 572.

Hiroyuki, N., Atsushi, S., and Kouichi, M. (2000). High – Capacity Electric Double - Layer Capacitor with High – Density – Activated Carbon Fiber Electrodes. **J. Electrochem. Soc.** 147(1): 38 – 42.

Lee, Y. J., Park, H. W., Park, S., and Song, I. K. (2012). Nono – sized Mn – doped activated carbon aerogel as electrode material for electrochemical capacitor: effect of activation conditions. **J. Nanosci Nanotechnology.** 12(7): 6058 – 64.

Lili, M. et al. (2011). Catalytic effect of alkali carbonate on CO_2 gasification of Pingshuo coal. **Mining Science and Technology (China).** 21: 587 – 590.

Molina- Sabio, M., Gonzales, M.T., Rodriguez, F., and Sepúlvada-Escribano, A. (1999). Effect of steam and carbon dioxide activation in the micropore size distribution of activated carbon. **Carbon.** 34 (4): 505 – 509.

Slam, P. A., and Bhattacharya, S. C. (2006). A comparative study of charcoal gasification in two types of spouted bed reactors. **Energy.** 31: 228 – 243.

Sharma, A., Saito, I., Nakagawa, H., and Miura, K. (2007). Effect of carbonization temperature on nickel crystallite size of Ni/C catalyst for catalytic cydrothermal gasification of organic compounds. **Fuel.** 86(7 – 8): 915 – 920.

Tseng, R. L., Tseng, S. K., and Wu, F. C. (2006). Preparation of high surface area carbons from corncob with KOH etching plus CO2 gasification for the adsorption of dyes and phenols from water. **Colloids and Surfaces A: Physicochem. Eng. Aspects.** 279: 69 - 78.

Uçar, S., Erdem, M., Tay, T., and Karagöz, S. (2009). Preparation and characterization of activated carbon produced from pomegranate seeds by $ZnCl_2$ activation. **Applied Surface Science.** 255(21): 8890 – 8896.

Yin, L. X., Wu, Z. C., Zheng, P. S., and Chen, Y. (2002). Design and operation of a FB gasification and power generation system for rice husk. **Biomass and Bioenergy.** 23: 181 – 187.

Yin, R. et al. (2012). Influence of particle size on performance of a pilot – scale fixed – bed gasification system. **Bioresource Technology.** 119: 15 – 21.

Zou, Y., and Han, B. X. (2001). High – Surface Area Activated Carbon from Chinese Coal. **Energy & Fuels.** 15: 1383 – 1386.

CHAPTER VII

CONCLUSIONS AND RECOMMENDATIONS

7.1 Conclusions

The first part of this thesis work was focused on the systematic study of biomass pyrolysis in a free fall reactor, including palm shell, palm kernel and cassava pulp residues. These precursors are cheap and abundantly available solid wastes from palm-oil milling and cassava factory in Thailand. The influences of pyrolysis temperature, particle size and sweeping gas flow rate on the products distribution and kinetic parameters were investigated. The two-parallel reaction model was employed to describe the kinetic scheme of pyrolysis reaction based on the solid product yield. The second task is the study of hydrodynamic behavior of a conical spouted bed. The influences of the geometric dimensions of spouted bed, initial static bed height, and particle size on the pressure drop across the bed and minimum spouting velocity were explored by the lab scale conical spouted bed and CFD modeling. The results of hydrodynamic behavior from this study can be used for a hydrodynamic design and specifying the pyrolysis condition of a conical spouted reactor. For the next task, the influences of pyrolysis temperate, holding time, particle size, and initial static bed height on the product yield and product distribution were investigated in a conical spouted bed reactor. The final task involved study of low temperature catalytic gasification of coconut shell. In this task the effects of added catalysts, reaction temperature, reaction time, and carbonization step on the amount of the generated gas as well as porous properties of the solid products were simultaneously investigated. The following conclusions can be drawn from the present study.

- From a free fall reactor study, a higher temperature and smaller particle size increased the gas yield and decreased the char yield. Cassava pulp residue gave more volatiles and less char than palm kernel and palm shell. The liquid yield increased with increasing sweeping gas flow rate increasing in the range of 100 – 200 cm^3/min, while the opposite trend was observed for the gas yield. Also, sweeping gas flow rate had no significant effect on the yield of char. The liquid yield increased significantly with increasing pyrolysis temperature and then decreased when the pyrolysis temperature reached the optimum value. Furthermore, the kinetic study of pyrolysis reaction indicated that the two-parallel reactions model was able to describe reasonably well the thermal decomposition of cassava pulp residue, palm shell and palm kernel. In additional, the calculated results showed that the biomass precursor started to decompose in the first zone and reached to complete decomposition in the second zone of the reactor. Finally, the model results proved that the mean residence time of larger particle size is shorter than the smaller size particle at the given pyrolysis temperature with cassava pulp residue showing the longest mean residence time in the reactor.

- The hydrodynamics of a conical spouted bed of air-palm shell particles system was studies as a function of static bed height, gas inlet diameter, conical base angle, and particle size. The increasing in particle size led to the pressure drop increasing for all air inlet diameters and conical base angles. On the contrary, the pressure drop decreased with the increase of air inlet diameter for all static bed height, particle size, and conical spouted bed geometry. By the application of the commercial CFD software package, ANSYS CFX 10.0, the minimum spouting velocity of air predicted from the CFD simulation agreed very well with the experimental results. The predicted hydrodynamic information of pressure drop across the bed, and expanded bed height differed greatly from the experimental results. In addition, CFD simulated results also indicated a significant influence of reactor temperature on the decreasing of the minimum spouting velocity.

- The pyrolysis of palm shell in a batch conical spouted bed reactor, with geometric dimensions: 6.0 mm of gas inlet diameter, 60° for cone angle, 60 cm height and operated at 1.20 times the minimum spouting velocity of $N_{2,}$ showed that pyrolysis temperature and time had a significant effect on the pyrolysis product, while particle size and static bed height had no significant effect on the pyrolysis product yield. The maximum liquid yields of 65 wt% was obtained from palm shell pyrolysis at 650°C, particle feed rate of 5 g/min, particle size of 1.55 mm and N_2 flow rate of 9.6 L/min in a continuous spouted bed mode. The derived bio-oil is less attractive to use as a direct burning fuel, due to its high water content, low in calorific value and high acid value. The solid product gave a high calorific value of 30.78 MJ/kg and reasonably high BET surface area of 220 m^2/g. On gas composition, carbon monoxide and carbon dioxide gas were the dominant component in the gas product. Also, the product yields and composition predicted using the competitive model showed good agreement with the experimental results.

- For the low temperature catalytic gasification of coconut shell in a fixed bed reactor, potassium hydroxide showed a significant effect on the composition and amount of gas product. It also helps to facilitate the rate of hydrogen and carbon monoxide formation. Also, chemical ratio and gasification temperature were found to play an important role in pore development of activated carbon. The optimum gasification conditions to achieve high surface area activated carbon and high hydrogen composition occurred at 600°C gasification temperature for 60 min with provision of carbonization step and using chemical weight ratio of 3.0. The high surface area activated carbon and high hydrogen composition gas obtainable under this gasification condition are 2,650 m^2/g and 27.90 wt%, respectively.

7.2 Recommendations for Future Works

- For the pyrolysis of biomass performed in Chapter 3, the model equation proposed based on the assumption of constant ρ_s and d_p, the gas flow is in the laminar regime and neglecting the heat transfer resistance inside the particle. However, ρ_s and d_p are not constant and their final values depend on the pyrolysis conditions. Therefore, it is interesting to improve the model by taking into consideration these effects.

- For the CFD simulation of hydrodynamic study reported in Chapter 4, the program still gave a good prediction for only a minimum spouting velocity. The predicted hydrodynamic information suggests that the quality of numerical grid used, the adjusting of model parameters, as well as the refining of the governing equations applied (such as drag force model, turbulent model, etc.) should be considered to obtain a better prediction of other hydrodynamic properties such as total bed height, fountain height, and pressure drop across bed. The quality of numerical grid can be improved by reducing the grid size or adjusting grid size distribution in the geometry. Higher quality of numerical grid helps to reduce round-off error occurring in computational procedure.

- The work on biomass pyrolysis in a conical spouted bed reactor was concentrated more on batch operation than on the continuous mode, where only the effect of pyrolysis temperature was studied. Therefore, it is suggested that more experiments be performed to study the influence of varying pyrolysis conditions on the pyrolysis product yield and product distribution for continuous conical spouted bed. The other useful models to predict the pyrolysis product yield and product distribution should be further explored, because of the limitation of the Thurmer and Mann kinetic model.
- For the low temperature catalytic gasification of coconut shell under the combined production of syngas and activated carbon as reported in Chapter 6, the obtained results indicated that carbonization step affect significantly on the porous properties of the activated carbon. It is thus recommended that experiments be performed to study the influence of carbonization conditions (time and temperature) on the porous properties of activated carbon and quality of syngas.
- Because of the limitation of an instrument and research time spent in this work, only a few samples of bio –oil samples were analyzed. Therefore, more samples of bio – oil produced under various pyrolysis conditions should be analyzed to gain more information on the effect of operating conditions on the properties of bio – oil.